

Synthesis of molecular species for nanotechnological applications

Christos Salesiotis

Thesis submitted to the University of Nottingham for the degree of

Doctor of Philosophy

December 2012

Abstract

This thesis details the synthesis of molecular species designed for a variety of nanotechnological applications.

The first chapter gives a brief introduction to nanotechnology and explains the concepts of supramolecular chemistry and self-assembly which are the basis on which this project is built. Special attention is given to non-covalent bonding interactions such as hydrogen-bonding and π-π interactions which drive the formation of complex architectures. The discussion is followed by many examples from the literature describing work that has been accomplished in various fields of supramolecular chemistry.

The second chapter describes the synthesis, characterization and surface deposition studies of 1,4-diphenyl-1,3-butadiyne-3,3'-5,5'-tetracarboxylic acid (DPBDTC). Recent work on surface deposition studies of terphenyl-tetracarboxylic acid (TPTC) has shown the formation of a 2D network that resembles an aperiodic tiling structure that shows orientational order but no translational symmetry. DPBDTC was designed in order to improve the aperiodic characteristics of the network formed. An experimental exploration of the phase space of interacting random tilings was also possible using the network obtained from DPBDTC deposited from nonanoic acid along with networks obtained with different molecules and under different conditions.

The third chapter focuses on the synthesis, characterization and surface deposition studies of a series of porphyrin molecules functionalised with isophthalic acid and ferrocene groups at the meso-positions. The isophthalic acid groups are incorporated to encourage intermolecular interactions while the ferrocene groups are designed as potential carriers of binary information in the form of the redox states of the iron center. The above molecules were designed in order to

study their potential use in molecular memory systems. The series of molecules consisted of porphyrins having the acetylene spacer in various positions. The diethyl-ester protected derivatives of the carboxylic acids and their zinc and magnesium metal complexes were studied using spectroelectrochemistry in order to reveal the qualitative redox properties of these systems.

The fourth chapter discusses the design, synthesis and characterization of a series of metallated homoleptic and heteroleptic dypyrrinato complexes, using the dipyrrin 5-ethynyl-ferrocenyl dipyrrin. These molecules were synthesized with the prospect of validating the role of such complexes as a part of a dye or an electrolyte in dye-sensitized solar cells. Electrochemical and spectroelectrochemical studies in solution were also performed.

Acknowledgements

I wish to deeply thank my supervisor, Professor Neil Champness, for giving me the opportunity to undertake this project. His inspiration, guidance, support and patience were vital for the successful completion of this work.

I would also like to thank our collaborators of the Peter Beton's group from the School of Physics and Astronomy, especially Dr. Andrew Stannard and Dr. Matthew Blunt that undertook most of the surface deposition studies. Many thanks to Dr. Stephen Davies for his precious help in electrochemistry and to Dr. William Lewis for his assistance in solving my crystal structures.

I am deeply grateful to all my labmates that worked with me in B52 lab. Their contribution has been invaluable both in helping me in research-related problems and in making the difficult life in the lab worth experiencing. I would like to thank each and every one of them separately and try to symbolically present and retain my memories of this wonderful place called B52. In particular, I would like to express my gratitude to a very ingenious person, Dr. Stephen Argent, for his invaluable help whenever I needed some, for his patience on our countless arguments and for his marvelous taste in music! I would also like to thank Barry F. Mangham for sharing his awesome and humorous personality and for being the best fumehood-mate I could ever have. I would like to thank Victoria for her sweet hugs, wise Simon for educating me about the conspiracy of conspiracy theorists, Alex for being my hero, Ben and Anna for their lovely banana cakes, Francesco for sharing his sweet soul and spicy fantasy, Harp for breaking the

safety rules with me and Tom for helping me understand the English language better. I would like to give my special thanks to Nassiba for letting me share my mind with hers. Our countless caffeine and nicotine-intoxicated breaks have contributed immensely to this work.

Since everything in life is interconnected, I would like to express my loving thanks to all the people outside of the working environment that contributed to this work by altering and transforming my mind during these four years. I would like to especially thank Nassiba for being the best friend I could ever have, Anja for showing me how to dream again, Henrique and Can for sharing their craziness with me, Karimaki for showing me that "music" is a state of mind, Arianna for allowing me to see that miracle-people truly exist and Ruti for loving me enough to transform England into a sunny paradise.

Finally, I would like to exceptionally thank my family for their encouragement and support throughout the four years of this project. I dedicate this work to my father, who unfortunately is not with us anymore to rejoice with its realization.

Symbols & Abbreviations

^{o}	degrees
~	about
A	hydrogen bond acceptor
Å	Angstrom
at	apparent triplet
$BF_3{\cdot}Et_2O$	boron trifluoride diethyl etherate
bipy	bipyrridine
br	broad (NMR)
C	Celsius
$CHCl_3$	chloroform
cm^3	cubic centimeters
D	hydrogen bond donor
d	days
d	doublet (NMR)
dba	dibenzylideneacetone
DCM	dichloromethane
dd	doublet of doublets (NMR)
DDQ	2,3-Dichloro-5,6-dicyano-1,4-benzoquinone
DFT	Density Functional Theory
DMF	dimethylformamide
DMSO	dimethylsulphoxide

DNA	deoxyribonucleic acid
DPBDTC	1,4-diphenyl-1,3-butadiyne-3,3’-5,5’-tetracarboxylic acid
DSSC	dye-sensitized solar cell
ESI	electrospray ionization
Et_2O	diethyl ether
eV	electronvolt
g	gram
h	hour
HOMO	highest occupied molecular orbital
HOPG	highly oriented pyrolytic graphite
IUPAC	International Union of Pure and Applied Chemistry
J	Joule
K	Kelvin
k_B	Boltzmann's constant
Kcal	kilocalories
LDA	lithium diisopropylamide
LUMO	lowest unoccupied molecular orbital
m	multiplet (NMR)
M	molar
m/z	mass/charge ratio
MALDI	matrix assisted laser desorption ionization
MeCN	acetonitrile
MeOH	methanol

mg	milligram
min.	minute
MLCT	metal to ligand charge transfer
mm	millimeter
mmol	millimole
mol	mole
MS	mass spectrometry
mV	millivolt
NBS	N-bromosuccinimide
nm	nanometer
NMR	nuclear magnetic resonance
p	para-
Ph	phenyl
ppm	parts per million
PTCDI	3,4,9,10-perylene-tetracarboxylic diimide
s	singlet (NMR)
s	second
SCE	saturated calomel electrode
SMM	single molecule magnet
STM	scanning tunneling microscope
T	temperature
t	triplet (NMR)
TBAF	tetrabutylammonium fluoride

THF	tetrahydrofuran
TLC	thin-layer chromatography
TOF	time of flight
TPP	tetraphenyl porphyrin
TPTC	terphenyl tetracarboxylic acid
UHV	ultra high vacuum
UV/Vis	ultraviolet visible

Contents

Chapter 1: Introduction **1**

1.1 Nanotechnology **2**

1.2 Self-assembly **3**

1.3 Intermolecular forces **4**

1.3.1 Hydrogen Bonding 4

1.3.2 π-π interactions 7

1.3.3 Van der Waals interactions 9

1.4 Self assembly on surfaces **9**

1.5 References **13**

Chapter 2: Design, synthesis and characterization of 1,4-diphenyl-1,3-butadiyne-3,3'-5,5'-tetracarboxylic acid for surface deposition studies **16**

2.1 Introduction **17**

2.1.1 Tiling a surface on the nanoscale dimension 17

2.1.2 1,4-diphenyl-1,3-butadiyne-3,3'-5,5'-tetracarboxylic acid 22

2.2 Results and discussion **24**

2.2.1 Synthesis of DPBDTC 24

2.2.2 Surface deposition studies 28

2.2.3 Experimental exploration of the phase space of interacting random tilings 36

2.3 Conclusion 37

2.4 Experimental 39

2.5 References 45

Chapter 3: Design, synthesis and characterization of functionalized porphyrins aiming at applications in molecular memory storage 49

3.1 Introduction 50

3.1.1 Molecular electronics 50

3.1.2 Molecular memories 54

3.2 Synthesis 59

3.2.1 Synthesis of meso-5,15-bis-(isophthalic acid)-10,20-bis(ferrocenyl)-porphyrin 62

3.2.2 Synthesis of meso-5,15-bis-(isophthalic acid)-10,20-bis(ethynylferrocenyl)-porphyrin 67

3.2.3 Synthesis of meso-5,15-bis-(5-ethynylisophthalic acid)-10,20-bis(ferrocenyl)-porphyrin 71

3.2.4 Synthesis of meso-5,15-bis-(5-ethynylisophthalic acid)-10,20-bis-(ethynylferrocenyl)-porphyrin 75

3.3 Crystallographic analysis 80

3.4 Spectroelectrochemistry results 100

3.4.1 Cyclic voltammetry 100

3.4.2 Spectroelectrochemistry 107

3.5 Surface deposition 110

3.6 Conclusion 111

3.7 Experimental 113

3.8 References 141

Chapter 4: Design, synthesis, characterisation and spectroelectrochemical studies of homoleptic and heteroleptic dipyrrin metal complexes 147

4.1 Introduction 148

4.1.1 Dye-Sensitized Solar Cells 148

4.1.2 Dipyrrins 155

4.2 Synthesis 159

4.3 Crystallographic analysis 176

4.4 Cyclic voltammetry measurements 183

4.5 UV-Vis Spectroelectrochemistry 192

4.6 Conclusion 195

4.7 Experimental 198

4.8 References 206

Chapter 1:
Introduction

1.1 Nanotechnology

Nanotechnology is the engineering of functional systems at the atomic or molecular level. Governments around the world spend billions of dollars for its development as it is anticipated that in the future nanotechnology will play a key role in the development of new advanced materials with potential applications in medicine, food, electronics, biomatateriales and energy production. As the name signifies, nanotechnology deals with materials made up from a few molecules with at least one dimension being in the nanoscale range (0.1 to 100 nm).

The very small sizes of these systems give rise to novel properties that are not seen in bulk materials[1]. In order for the supramolecular systems to be able to display device-like properties, their components must be spatially addressed at a molecular scale. For example, they need to be organized at interfaces[2,3], deposited on surfaces[4,5], immobilized inside membranes[6,7] or porous materials[8,9] in order to be able to behave in a coherent manner. In his 1959 lecture[10], Richard P. Feymann declared that 'there is plenty of room at the bottom' thus, giving rise to the idea that atoms could be used to construct nano-scale devices.

Two main methods of fabrication of nano-scale materials have been developed. One of them is the 'top-down' approach, which uses lithography in order to manipulate progressively smaller pieces of matter. This technique has many limitations. One of them is the limit in the final achievable sizes[11] of matter. The alternative strategy that has been developed and continually progressing is the 'bottom up' approach which starts of nano- or sub nanoscale objects (atoms or molecules) to build up nanostructures. This is achieved through intermolecular forces used to drive spatial organization.

1.2 Self-assembly

Self-assembly is the process in which disordered components (i.e. molecules) in a disordered system form an organized structure. This process is directed through local, non-covalent interactions between the components. Self-assembly is a well known phenomenon which is found throughout chemistry. Biological systems, crystal growth[12], the formation of liquid crystals[13], the spontaneous generation of synthetic lipid layers[14] and the alignment of molecules on surfaces[15] are but a few examples. These systems are in thermodynamic equilibrium and they possess an in-built capacity for error-correction. This is a unique property and is very useful especially in the construction of large and complicated systems with increased number of intermolecular contacts.

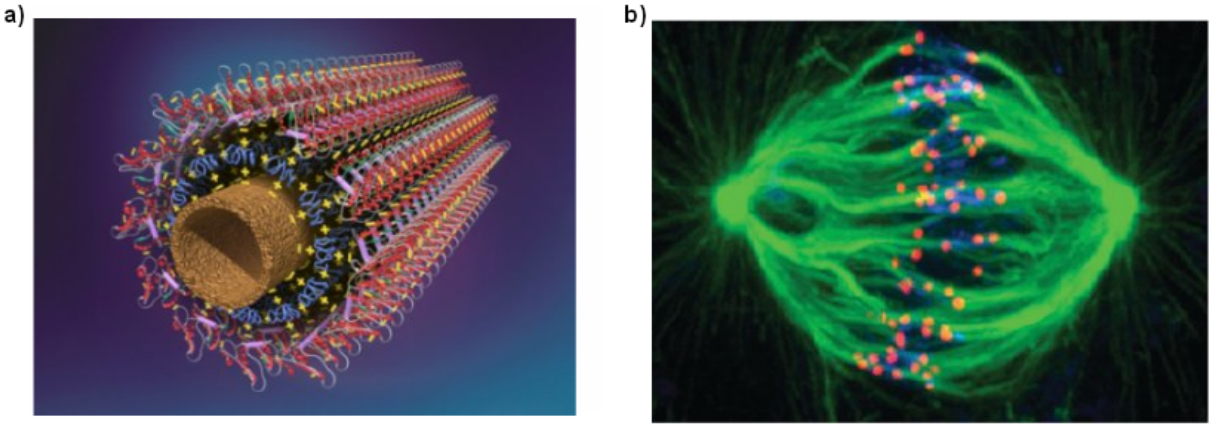


Figure 1.1. Examples of self-assembly a) enzymes self-assembled on carbon nanotubes[37] b) biological self-assembly, mitotic spindle[38].

1.3 Intermolecular forces

1.3.1 Hydrogen Bonding

Hydrogen bonding represents a special type of electrostatic interaction. This term appeared in 1920 to help describe the internal structure of water. A modern definition of a hydrogen bond as described by IUPAC is the following[16]:

> *The hydrogen bond is an attractive interaction between a hydrogen atom from a molecule or a molecular fragment D–H in which D is more electronegative than H, and an atom or a group of atoms A in the same or a different molecule, in which there is evidence of bond formation.*

The atom D where the hydrogen is attached is the hydrogen bond donor (i.e. N, O, S). The atom A is the hydrogen bond acceptor (i.e. N, O, F). Both the donor and acceptor have an electronegative character. The hydrogen is shared between the electron pairs on D and A. The strength of hydrogen bonds varies and a hydrogen bond can be categorized as strong (15 – 40 $Kcal \cdot mol^{-1}$), medium (4-15 $Kcal \cdot mol^{-1}$) or weak (1 – 4 $Kcal \cdot mol^{-1}$)[17]. The distance and the angle between the hydrogen and the acceptor (H…A) are good indicators of the strength of the hydrogen bond. The shorter the distance, the stronger the bond is. Typical hydrogen bonds have a donor-acceptor distance of 2.8 Å. Very strong hydrogen bonds can have a donor-acceptor distance of 2 Å while any distance longer than 3.5 Å would imply a pure dipole-dipole interaction. The D…H…A angle varies between 110^{o} and 180^{o} with the latter being the ideal distance providing the strongest hydrogen bond[18]. Figure 1.2a shows a schematic representation of a hydrogen bond and Figures 1.2b-g show common arrangements of hydrogen bond types.

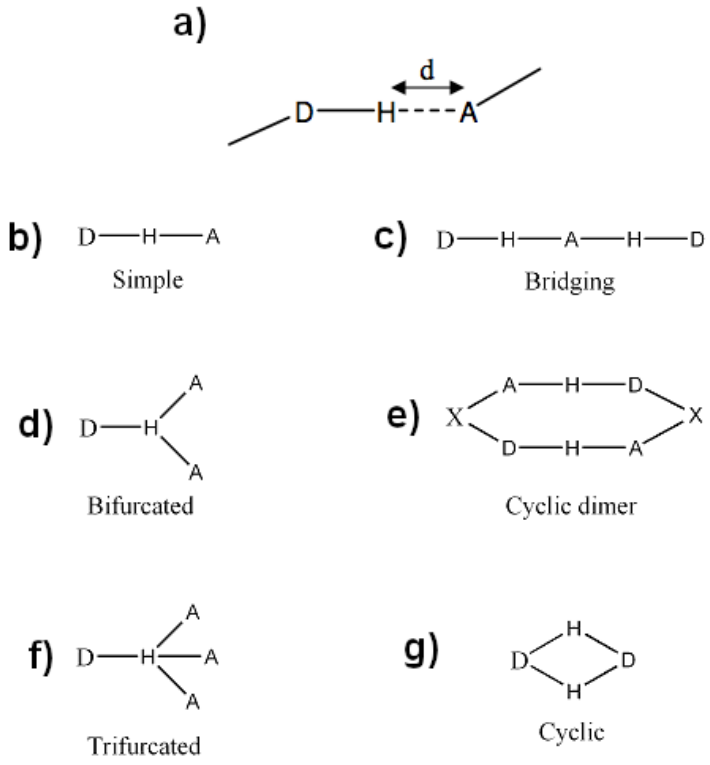


Figure 1.2. a) Schematic representation of a hydrogen bond between an acceptor A and a hydrogen atom of a donor D. The shorter the distance d the stronger the hydrogen bond is. b-g) Common arrangements of hydrogen bond types.

Hydrogen bonds show a high degree of directionality. This makes them ideal candidates for precisely controlling the interactions between supramolecular tectons and advantages over other types of dispersive forces as they are stronger and thoughtful design of the tectons, or building-blocks, can lead to a predictable outcome in the synthesis of a desired molecular architecture. Although the strength of a hydrogen bond is moderate, introduction of many complementary sites can give rise to very strong overall interactions.

Examples of hydrogen bonding can be found in nature and in modern technological applications, for example the hydrogen bonding between water molecules, which is responsible for the high boiling point of water. Another typical example is the double helix of the DNA molecule[19]. The two strands are held together very tightly by the forces produced by millions of hydrogen bonds produced from complementary nucleotides (Figure 1.3). Hydrogen bonds are also found in numerous synthetic polymers. A typical example is Nylon where hydrogen bonding occurs between the carbonyl and amide repeat groups of different chains. This results in adjacent chains being linked together thus affecting the crystallization properties of the material.

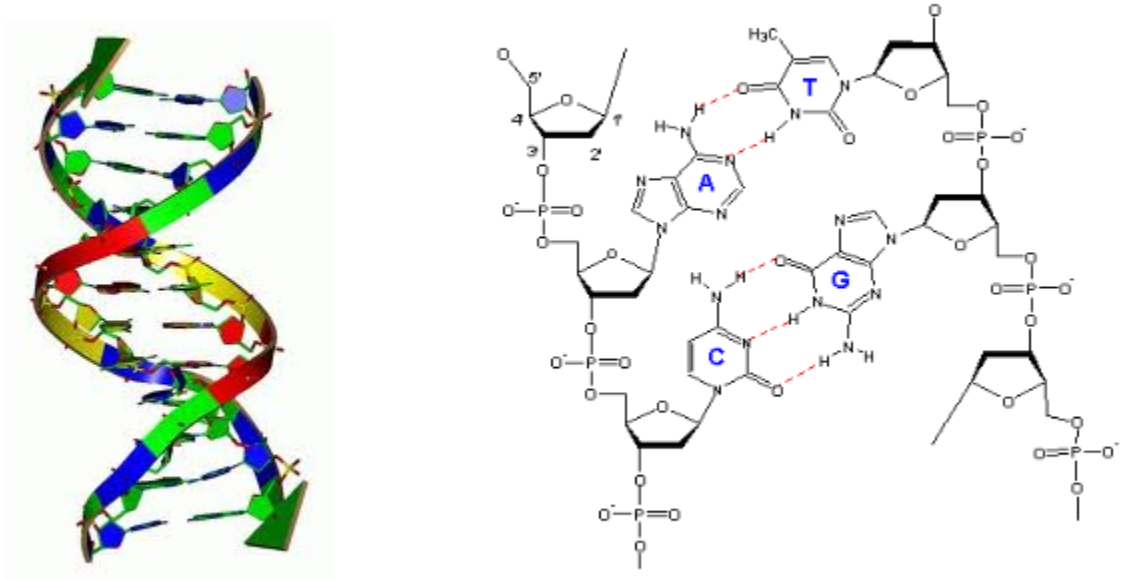


Figure 1.3. Double helix of DNA molecule (left). A schematic representation of the hydrogen bonds formed between the four nucleotides is shown on the right.

1.3.2 π-π interactions

Interactions between the π-systems of molecules are well known. They have been observed in crystal structures, in biological systems such as in stabilization of the helical structure of DNA through vertical π-stacked base-base interactions, in the tertiary structure of proteins, etc[20-23]. Such interactions have also been exploited in many synthetic host-guest systems[24].

Many explanations have been proposed in the past for the occurrence of π-π interactions[29-36]. Solvophobic, electron donor-acceptor and atomic models have been used but none of these models provided satisfactory results. Although high level ab-initio methods[35,36] which include quadrupolar, inductive and short-range interactions between adjacent π-systems have been successfully used to model these interactions, any other simpler model has failed. In 1990 Hunter and Sanders[25] proposed a simple model for treating such interactions. Their model is based upon electrostatic and van der Waals forces. Several conformations have been described such as parallel displaced and T-shaped π-π stacking (Figure 1.4). The strength of π-π stacking is dependent upon many factors such as the π-systems involved, the angle and distance between them and the existence of positive or negative charges. A typical example is the benzene dimmer where the binding energies range between 0.95 and 2.87 kcal/mol depending on the adopted configuration of the benzene rings[39]. These values are comparable to the strength of weak hydrogen bonding.

The main feature of this model is that it considers the σ-framework and the π-electrons separately. The π-clouds show a repulsive force between them. What makes the molecules interact in an attractive manner is the net favorable summation of interactions between the



Figure 1.4. Schematic representation of common π-π interactions. Off-centered parallel displaced conformation (left) and T-geometry arrangement (right).

attraction of the π-system and the σ-framework and the repulsive forces between the two π-clouds.

These non-covalent forces have played a significant role in various supramolecular systems such as efficient host-guest systems and molecular switches in solution (Figure 1.5).

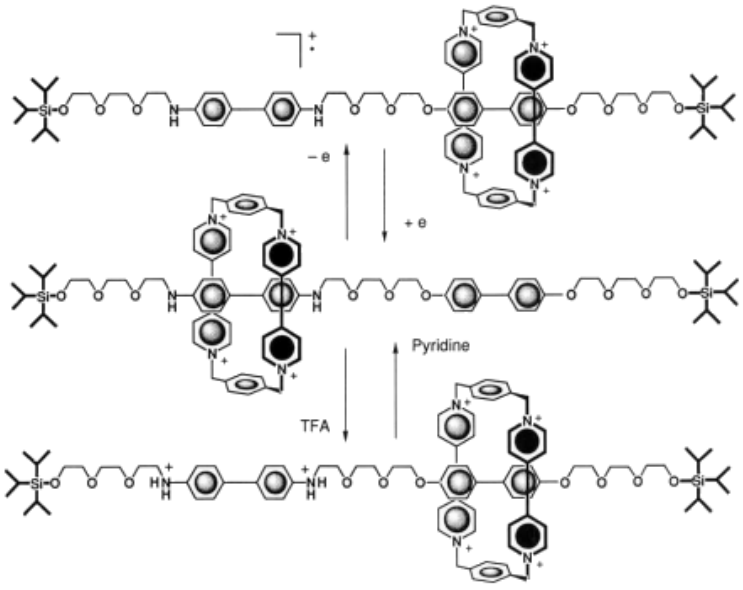


Figure 1.5. A chemically and electrochemically controlled molecular shuttle[36].

1.3.3 Van der Waals interactions

Van der Waals interactions are a collective group of long range inductive and dispersive forces. Inductive forces are attractive and they include permanent dipole-dipole interactions and induced dipole-dipole interactions. Dispersion forces are quantum mechanical in nature and are a product of momentary fluctuations of the electron density within the electron clouds of the molecules. Although these interactions are very weak (typical interactions range from 0.5 to 1.0 kcal/mol per atom pair), they are additive and they can play a significant role when their effect is combined.

1.4 Self assembly on surfaces

The concepts of self-assembly as seen in solution and in the solid state have been applied in order to make supramolecular architectures on surfaces. The development of scanning probe techniques such as scanning tunneling microscopy (STM)[26] have allowed the observation and manipulation of a surface at the molecular, and even atomic, level. This has ignited an interest in the development and observation of systems self-assembled on a surface with potential applications in quantum computing and memory storage.

Ideal candidates to be deposited on surfaces are π-conjugated aromatic systems. Such molecules are adsorbed and sit on the surface in a parallel manner. π-π interactions between the aromatic molecules and the surface[27] can allow the molecules to be adsorbed and at the same time being able to move around thus allowing the peripheral groups to interact with each other.

Functional groups providing hydrogen bonding capabilities have been studied in the past and numerous 2D networks have been formed. Hydrogen bonds are preferred over other intermolecular forces because they provide directionality and a large variety of motifs can be designed and explored experimentally. A typical example is the deposition of trimesic acid on graphite[28]. The carboxylic acid…carboxylic acid hydrogen bonds guide the formation of 2 network types shown in Figure 1.6. Hydrogen bonding interactions between two carboxylic acids lead to the formation of a honeycomb network while hydrogen bonding interactions between 3 carboxylic acids lead to the formation of a flowerlike network. Figure 1.6c-d shows a detailed molecular representation of the hydrogen bonding involved and the formed networks. The emergence of two different network types and the instability of the networks at room temperature signify that the hydrogen bonding ability of the trimesic acid tectons is not always sufficient and other variables such as tecton mobility temperature and type of surface can play a significant role.

The second chapter of this thesis is dedicated to the synthesis of 1,4-diphenyl-1,3-butadiyne-3,3'-5,5'-tetracarboxylic acid (DPBDTC) for surface deposition studies. Theoretical calculations performed by Peter Beton's group from the School of Physics and Astronomy of the University of Nottingham have demonstrated that this molecule could serve as an ideal candidate for the formation of a random rhombus tiling network on a suitable surface. The objective, beyond the actual synthesis, is to deposit DPBDTC to a HOPG surface and quantify the randomness of the network formed thus, verifying the predictions of the aforementioned calculations. There is also a brief presentation of the study of the phase space exploration of interacting aperiodic rhombus tilings that was performed by Peter Beton's group from the School of Physics and Astronomy of

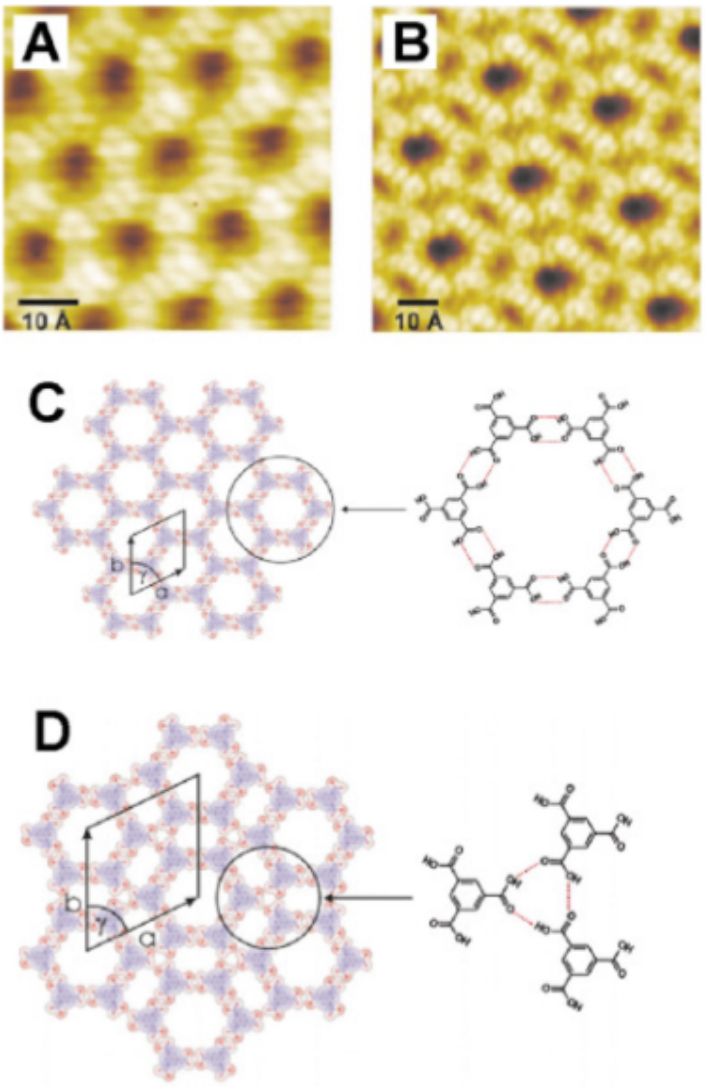


Figure 1.6. a-b) STM images networks formed from trimesic acid absorbed on graphite under UHV conditions[28]. c) Schematic representation of the honeycomb structure of the network showed in (a). d) Schematic representation of the flower-like network structure showed in (b).

the University of Nottingham. The network formed from DPBDTC was considered as a data source in this study.

The third chapter deals with the synthesis of a series of porphyrin molecules bearing ferrocene and isophthalic acid groups at the meso-positions. The aim being to deposit these molecules on a surface and examine the possibility of a two-dimensional network formation. The ferrocene groups can act as information storage centers because the ferrocene iron can exist in two stable redox states thus, offering the possibility of molecular memory storage. Electrochemical and spectroelectrochemical studies were also performed on soluble analogs of the target molecules.

Finally the fourth chapter deals with the synthesis and study of metallated dipyrrinato complexes to be used in dye-sensitized solar cell applications. During the synthesis of the porphyrins discussed in the third chapter, a dipyromethane intermmediate bearing the ethynyl-ferrocene group at the 5-position was thought to act as a ligand for complexes that might be used as dyes or electrolytes in dye sensitized solar cells. Electrochemical and spectroelectrochemical studies have also been performed to gain a better understanding of these ligands.

1.5 References

1 Fritz Allhoff, Patrick Lin, Daniel Moore, *What is nanotechnology and why does it matter?: from science to ethics*, John Wiley and Sons, **2010.**

2. D. E. Lynch, D. G. Hamilton, N. J Calos, B. Wood, J. K. M. Sanders, *Langmuir*, **1999**, *15***,** 5600.

3. C. L. Brown, U. Jonas, J. A. Preece, H. Ringsdorf, M. Seitz, J. F. Stoddart, *Langmuir*, **2000**, *16***,** 1924.

4. M. Cavallini, F. Biscarni, S. Leon, F. Zerbetto, G. Bottari, D. A. Leigh, *Science*, **2003**, *299*, 531.

5. B. Long, K. Niktin, D. Fitzmaurice, *J. Am. Chem. Soc.*, **2003**, *125*, 5152

6. G. Steinberg-Yfrach, P. A. Lidell, S-C. Hung, A. L. Moore, D.Gust, T. A. Moore, *Nature*, **1997**, *385*, 239.

7. I. M. Bennett, H. M. V. Farfano, F. Bogani, A. Primak, P. A. Liddel, L. Otero, L. Sereno, J. J. Silber, A. L. Moore, T. A. Moore, D. Gust, *Nature*, **2002**, *420*, 398.

8. S. Chia, J. Cao, J. F. Stoddart, J. I. Zink, *Angew. Chem. Int. Ed.*, **2001**, *40*, 2447.

9. M. Alvaro, B. Ferrer, H. Garcia, E. J. Palomares, V. Balzani, A. Credi, M. Venturi, J. F. Stoddart, S. Wenger, *J. Phys. Chem. B,* **2003**, *107*, 14319.

10. R. P. Feymann, *The pleasure of finding things out: The Best Short Works Of Richard Feymann,* Ed. J. Robbins, Penguin, London, **2001**.

11. R. F. Service, *Science*, **2001**, *293*, 785.

12. G.R. Desiraju, *The Crystal as a Supramolecular Entity*, **1996**, Wiley, Chichester, UK.

13. P. Espinet, M.A. Esteruelas, L. A. Oro, J. L. Serrano, E. Sola, *Coord. Chem. Rev.*, **1992**, *117*, 215.

14. P.F. Knowles, P.G. Stockley, *Chem. Br.*, **1995**, 27.

15. C.D. Bain, S.D. Evans, *Chem. Br.*, **1995**, 46.

16. E. Arunan, G. R. Desiraju, R. A Klein, J. Sadlej, S. Scheiner, I. Alkorta, D. C. Clary, R. H. Crabtree, J. J. Dannenberg, P. Hobza, H. G. Kjaergaard, A. C. Legon, B. Mennucci, D. J. Nesbitt, *Pure Appl. Chem.,* **2011**, *83*, 1637.

17. G. R. Desiraju, *Acc. Chem. Res.*, **2002**, *35*, 565.

18. T. Steiner, *Angew. Chem. Int. Ed. Engl.*, **2002**, *41*, 48.

19. J.D. Watson, F.H. C. Crick, *Nature*, **1953**, *171*, 737.

20. W. Saenger, *Principles of Nucleic Acid Structures*, Springer-Verlag: New York, **1984**, 132.

21. S. K. Burley, G. A. Petsko, *Adv. Protein Chem.*, **1988**, *39*, 125.

22. L. P. G. Wakelin, *Med. Res. Rev.*, **1986**, *6*, 275.

23. D. Ranganathan, V. Haridas, R. Gilardi,I. L. Karle, *J. Am. Chem. Soc.*, **1998**, *120*, 10793.

24. C. G. Claessens, J. F. Stoddart, *J. Phys. Org. Chem.*, **1997**, *10*, 254.

25. C. A. Hunter, J. K. M. Sanders, *J. Am. Chem. Soc.*, **1990**, *112*, 5525.

26. G. Binnig, H. Rohrer, *Rev. Mod. Phys.*, **1987**, *59*, 615.

27. Alain Rochefort, and James D. Wuest, *Langmuir*, **2009**, *25*, 210.

28. S. Griessl, M. Lackinger, M. Edelwirth, M. Hietschold, W. M. Heckl, *Single Mol.*, **2002**, *3*, 25.

29. H. J. Schneider, K. Philippi, J. Poehlmann, *Angew. Chem. Inr. Ed.*, **1984**, *23*, 908.

30. J. Canceill, L. Lacombe, A. Collet, *J. Chem. Soc. Chem. Comm.*, **1987**, 219-211.

31. B. Askew, P. Ballester, C. Buhr, K. S. Jeong, S. Jones, K. Parris, K. Williams, J. Rebek, *J. Am. Chem. Soc.*, **1989**, *111*, 1082.

32. S. C. Zimmerman, C. M. Vanzyl, G. S. Hamilton, *J. Am. Chem. Soc.,* **1989**, *111*, 1373.

33. T. J. Shepodd, M. A. Petti, D. A. Dougherty, *J. Am. Chem. Soc.*, **1988**, *110*, 1983.

34. A.V. Muehldorf, D. Van Engen, J. C. Warner, A. D. Hamilton, *J. Am. Chem. Soc.*, **1988**, *110*, 6561.

35. J. Langlet, P. Claverie, F. Caron, J. C. Boeuve, *J. Quantum Chem.*, **1981**, *19*, 299.

36. S. L. Price, A. J. Stone, *J. Chem. Phys.*, **1987**, *86*, 2859.

36. A. E. Kaifer, J. F. Stoddart, *Nature*, **1994**, *369*, 133.

37. G.D. Liu, Y.H. Lin, *J. Nanosci. Nanotechnol.*, **2006**, *4*, 948.

38. A. L. Knowlton, J. A. Millet, Regulation of Kinesins in the Mitotic Spindle, *Proquest Umi Dissertation Publishing*, University of Virginia, 2009.

39. C. D. Sherrill, T. Takatani, E. G. Hohenstein, *J. Phys. Chem. A*, **2009**, *113*, 10146.

Chapter 2:

Design, synthesis and characterization of 1,4-diphenyl-1,3-butadiyne-3,3'-5,5'-tetracarboxylic acid for surface deposition studies.

2.1 Introduction

2.1.1 Tiling a surface on the nanoscale dimension

Human societies have always made use of tilings in one form or another. From intricate mosaics to impressive geometric designs covering religious buildings, tiling a surface is a very old practice with high artistic value. Tilings can also be found all around us in nature. The cells in the skin of an onion, the design of a spider's web, the honey comb of a bee and the patches of dried-up mud are typical examples. Tilings of these kinds, often referred as "random tessellations", have been extensively studied because of their relevance to applications in science and engineering. Such applications include cell arrangements in skins and membranes of animals and plants, and image enhancement and coding in communication theory[1].

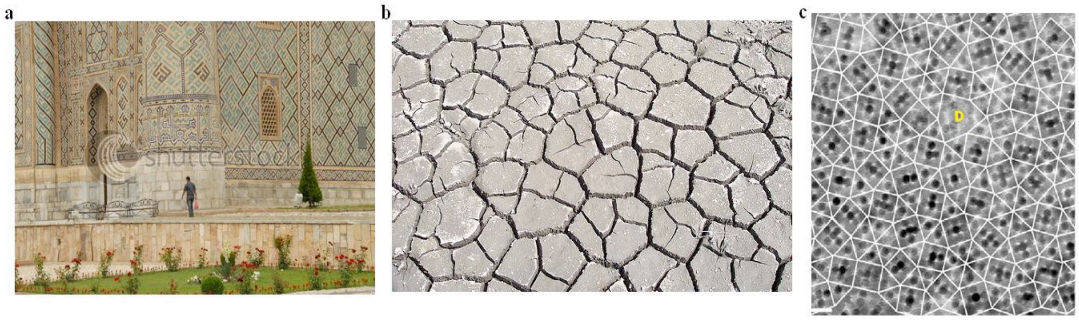


Figure 2.1. a) Tiles in contrasting geometric patterns in an Islamic garden. b) Natural tiling formed of dried-up mud c) Square-triangular tiling overlaid onto the TEM image of a binary quasi-crystal of Fe_2O_3 and gold colloidal sphere nanoparticles[57].

A tiling can be defined as a partition of an infinite space into pieces having a finite number of distinct shapes. Tilings can be divided into two types, periodic and aperiodic depending on whether they show translational symmetry. The mathematical rules of periodic tiling have been extensively studied. Tiling theory can be used to study crystal structure and methods to most efficiently fill a surface or a volume. On the other hand aperiodic tiling was considered a mathematical artefact up until 1982 when the first quasi-crystal was discovered by Dan Shechtman[2]. Since then, quasi-crystals have inspired great interest in aperiodic tiling, which exhibits symmetry that has no translational order[3-6].

The rhombus, with internal angles of 60^{o} and 120^{o} (also known as a Lozenge) can be used to perfectly tile a surface. As shown in Figure 2.2, in these tilings, the rhombus can appear in a

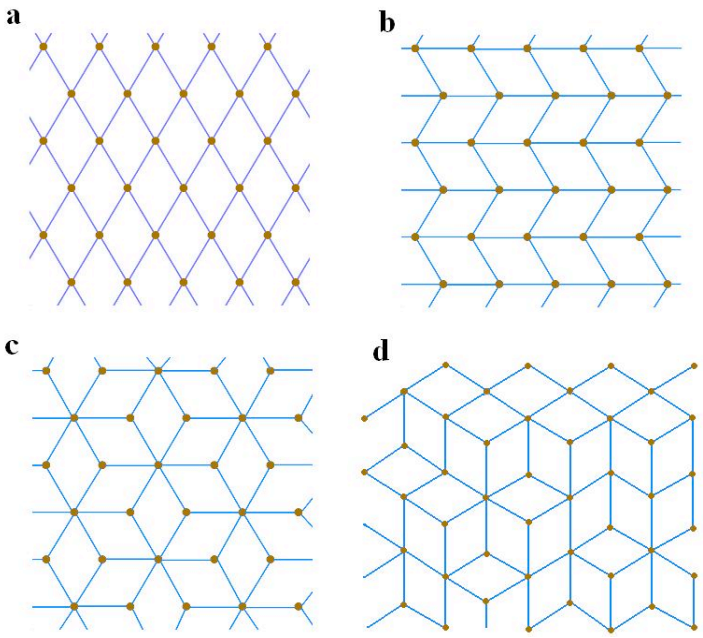


Figure 2.2. Tilings with different arrangement of the rhombi. a) Translational rhombic b) Zig-zag rhombic c) Rhombille d) Aperiodic rhombic arrangement.

plethora of arrangements. Both periodic and random non-periodic tilings are permitted[7,8]. The non-periodic tilings however can be of great interest due to their relevance to mixing algorithms, antiferromagnetism and entropic models of quasi-crystals.

Recently the Champness group, in collaboration with Peter Beton's group from the School of Physics and Astronomy of the University of Nottingham, managed to reproduce the aperiodic rhombus tiling by depositing p-terphenyl-3,5,3',5'-tetracarboxylic acid (Figure 2.3a) on highly oriented pyrolytic graphite (HOPG)[17]. A typical area of the TPTC network absorbed on the HOPG surface is shown in Figure 2.3b. The three phenyl rings that constitute the backbone of the TPTC molecule appear as bright rod-like features in the image. This arrangement is unusual as it shows hexagonal orientational order but no translational symmetry.

Every molecule in this network can be considered as a rhombus tile. Figure 2.3c shows the tiling representation of the scanned area that is shown in Figure 2.3b. Each molecule points along one of the three high symmetry directions and thus, for clarity, each direction on the tiling representation is highlighted with a different rhombus colour. The pores in the molecular network lie at the junctions where the vertices of the rhombi meet. The mapping is possible because the intermolecular bonds between neighbouring molecules are located at the midpoints of the edges of the rhombi (Figure 2.4a). This mapping of the network onto a tiling can make more obvious the absence of translational symmetry.

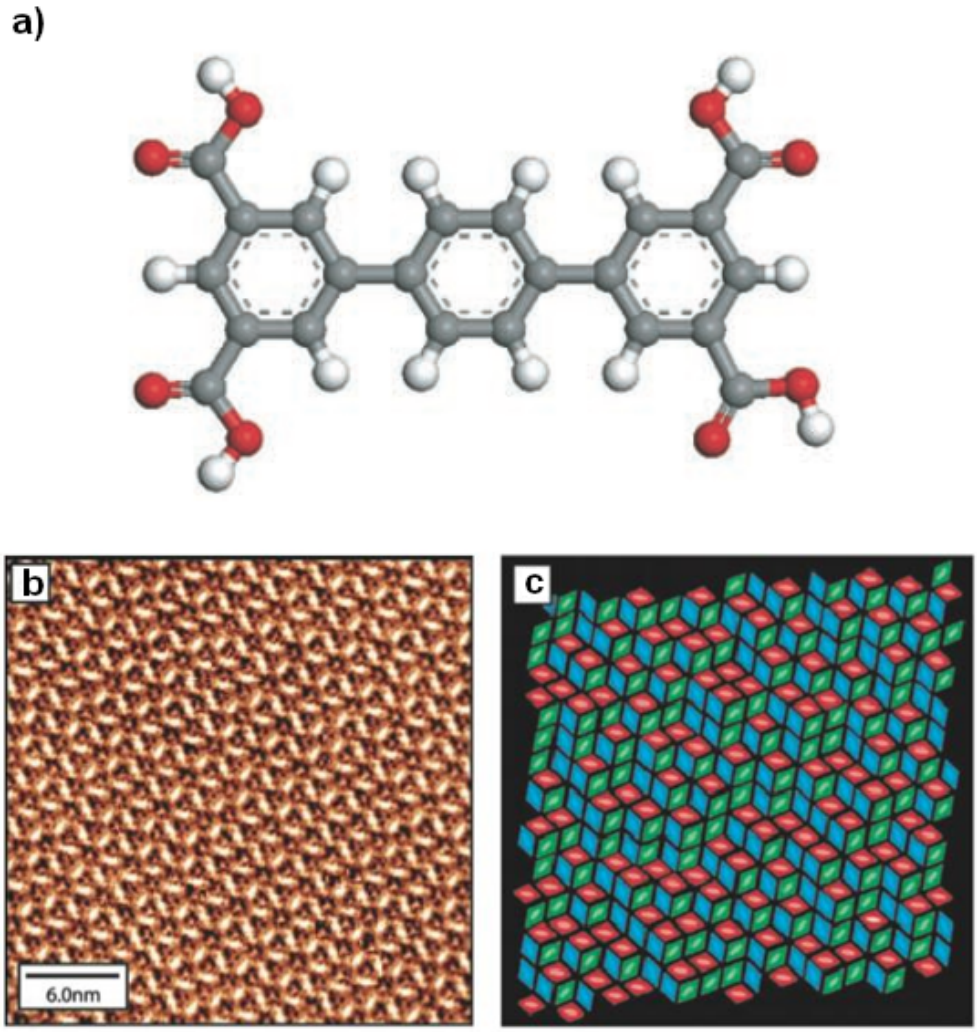


Figure 2.3. a) molecular structure of TPTC. b) STM image of a typical area of the TPTC network at the nonanoic acid/HOPG interface c) Tiling representation of (b). The three different colours represent the three different possible orientations of the rhombi within the tiling.[17]

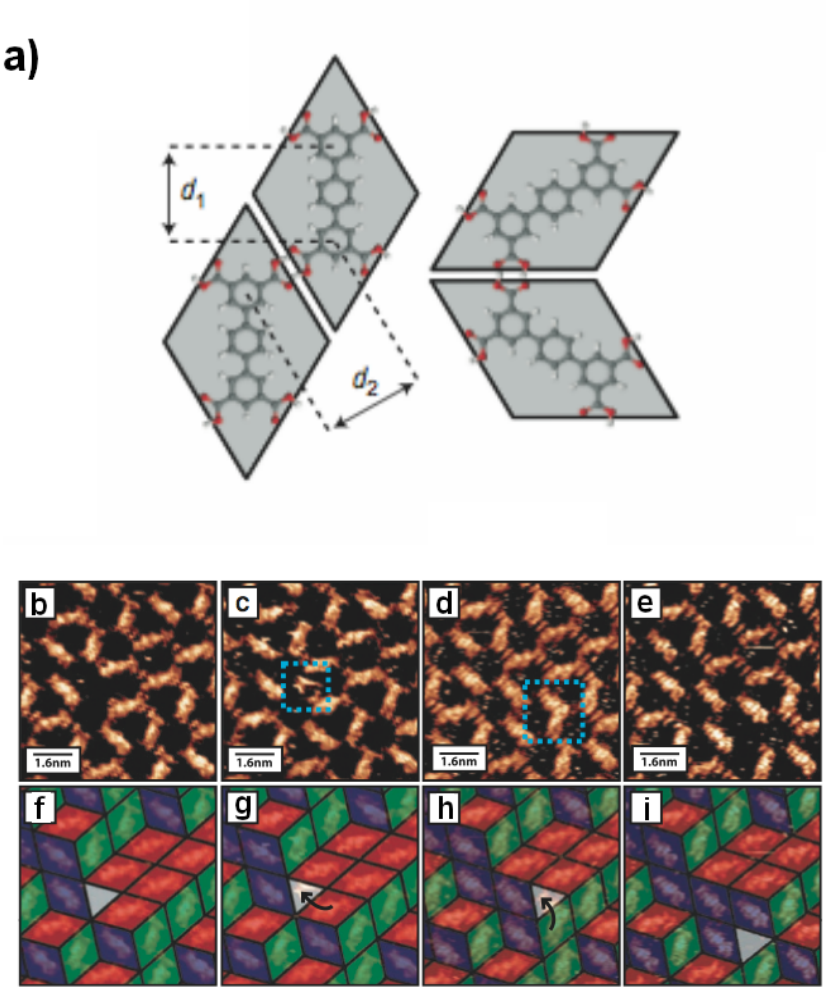


Figure 2.4. a) representation of TPTC molecule in parallel and arrowhead configuration. A rhombus is superimposed over every molecule showing the molecule-tile relationship. b-e) image showing a defect on a site of the network and its gradual propagation to a neighbouring site. f-j) tiling representations of the images shown in figures b-e[58].

It is also possible to observe the existence of tiling defects. (Figure 2.4b) They appear on the surface as triangular voids that are enclosed completely by rhombi. These voids can occur in two states of effective "charge" corresponding to triangles pointing either "up" or "down". Such

defects have been considered theoretically[18-20] but this is the first time that they are observed experimentally. They can also propagate through the network by the movement shown in Figure 2.4(b-e). This leads to a tile rearrangement within the network. It can be also observed that the effective "charge" is preserved as expected. Figures show that the orientation of the triangle remains the same after two consecutive tile rearrangements.

The system is dynamically arrested into a local minimum of a complex energy landscape. This defect motion mediates the only tile rearrangement that has been observed experimentally. It has the lowest activation barrier because only three intermolecular bonds must be broken in order to move a molecule across a defect. The mechanism of defect propagation as a transition to different local energy minima resembles dynamically facilitated models of glass formers[21,22].

2.1.2 1,4-diphenyl-1,3-butadiyne-3,3'-5,5'-tetracarboxylic acid

An examination of the topology of the rhombi in a rhombus tiling, reveals that two adjacent rhombi can have two different orientations in relation to each other. For the realization of a molecular tiling that would resemble an aperiodical rhombus tiling, several things were taken into consideration concerning the choice of the TPTC molecule.

The symmetric placement of carboxylic acid groups was essential because they promote directional hydrogen bonding. This enables the molecules to be held together in a controlled manner and self-assemble into a two-dimensional network[23-30]. Several examples from the

literature can demonstrate the effectiveness of carboxylic acid groups for the formation of stable networks across a surface[31-33].

Figure 2.4a shows the two possible arrangements that can be stabilized through the carboxylic acid groups. They are referred as parallel and arrowhead configurations. In the arrowhead configuration, the two molecules form a 60^{o} angle. A unilateral preference of one of the two configurations would disincline the formation of a random tiling. Furthermore, a simple geometrical consideration of the rhombi shown in Figure 2.4a reveals that in order for a perfect tiling to occur, the distance between the centers of the two phenyl groups carrying the carboxylic acid groups, d_1, and the distance between the centers of the phenyl groups of two adjacent molecules, d_2, must match closely. DFT calculations have shown that for the TPTC molecule d_1 = 8.7 Å and d_2 = 9.6 Å.

Although the energy profiles of the parallel and arrowhead configurations of TPTC have been calculated to be almost identical, the difference between d_1 and d_2 is not optimal. It was hypothesized that if a different spacer could be envisaged that would bring the d_1-d_2 value as close to zero as possible, the resulting degree of tiling randomness would increase. Theoretical calculations performed by Peter Beton's group from the School of Physics and Astronomy of the University of Nottingham have shown that if the phenyl ring of the TPTC molecule is substituted by a diacetylene group (DPBDTC, Figure 2.5), the distance d_1 becomes 9.5 Å[58]. This value is almost identical to d_2. Furthermore, the stabilization energies of non-parallel (e_n) and parallel (e_p) alignments of the DPBDTC molecule have been calculated to be almost identical (-0.80 eV).

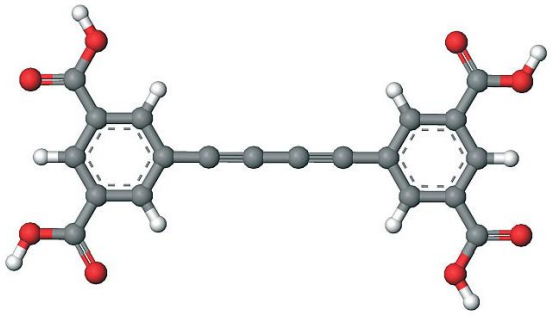


Figure 2.5. Molecular structure of 1,4-diphenyl-1,3-butadiyne-3,3'-5,5'-tetracarboxylic acid (DPBDTC).

Therefore, the objective of this project has been the synthesis of the DPBDTC molecule, its deposition on a HOPG surface and the study of the properties of the network formed. Comparisons with the network formed from depositing TPTC under the same conditions were made. We were also able to fit the data obtained from the network into theoretical models which gave as the opportunity to extract some valuable information.

2.2 Results and discussion

2.2.1 Synthesis of DPBDTC

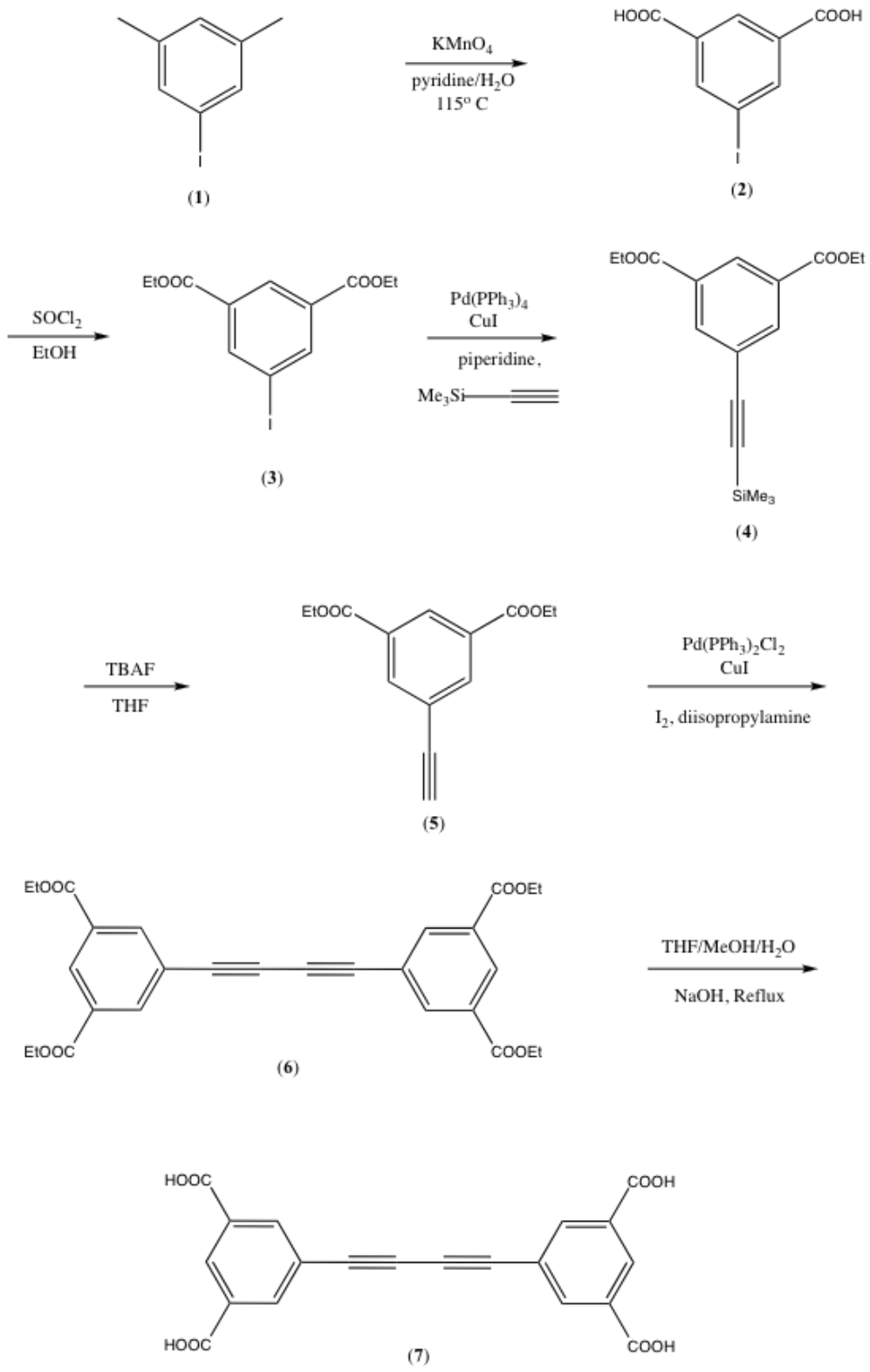
The first step towards the synthesis of 1,4-diphenyl-1,3-butadiyne-3,3'-5,5'-tetracarboxylic acid was to identify the synthetic route. A simple consideration of the symmetry of the molecule

reveals that there is an inversion center in the middle of the diacetylene group. Alkyne homocoupling is a well-known organic reaction[34] allowing us to simplify our problem to the efficient preparation of half of the structure of the final molecule. A detailed schematic of the synthesis is presented in Scheme 2.1.

The synthesis starts with 3,5-dimethyl-iodobenzene (**1**) which is a commercially available cheap starting material. The carboxylic acid groups are introduced through the oxidation of the methyl groups with potassium permanganate[35]. The reactants were left for 24 hours to react under refluxing conditions in water made basic through the addition of pyridine. The product was collected after its precipitation upon acidification of the resulting solution.

In order for the subsequent steps to be carried out without side-reaction problems caused by the carboxylic acid groups and for the intermediates to be soluble in common organic solvents, the carboxylic acid groups had to be protected. The ethyl ester derivatives were chosen as they are easy to insert and easy to remove. Therefore (**2**) was esterified by treatment with thionyl chloride in anhydrous ethanol[36]. This is a 2-step, 1-flask reaction, with thionyl chloride generating the acyl-chloride intermediate and ethanol acting as both a solvent and a reactant. After 5 hours of stirring at room temperature and purification by chromatography on silica gel (**3**) was obtained in 81% yield.

The next step was the insertion of the acetylene group. The Shonogashira coupling reaction conditions were employed[37]. Typically, the reaction serves the purpose of a carbon-carbon bond formation between a halogen-substituted aromatic compound and a mono-substituted acetylene. A Pd(0) catalyst and a CuI co-catalyst are employed in the presence of a mild base. For this reaction a literature procedure was used with slight modifications[38]. The Pd catalyst was tetrakis-



Scheme 2.1. Synthetic route for 1,4-diphenyl-1,3-butadiyne-3,3'-5,5'-tetracarboxylic acid

(triphenylphospine)-palladium and piperidine was used both as a base necessary for the catalytic cycle and as the solvent of the reaction. The mono-substituted acetylene used was trimethylsilylacetylene. The trimethylsilyl-group prevents the product from reacting again with the starting material. Another advantage of this group is that after the reaction and isolation of the product, it can be easily removed through treatment with tetrabutylammonium fluoride[39]. This reaction is almost quantitative, fast and clean. After purification through column chromatography using a silica gel stationary phase, (**5**) was obtained as an off-white solid.

The homo-coupling of (**5**) could be performed under a variety of conditions[40]. Alkyne homo-coupling is a palladium-catalyzed reaction under similar conditions used in the Shonogashira cross-coupling reaction. The difference here is that an oxidant is required. In the past, several successful attempts employing various Pd catalysts [$Pd(PPh_3)_4$, $Pd(dba)_2$ (dba=dibenzylideneacetone), $Pd(PPh_3)_2Cl_2$] and various oxidants (chloroacetone, bromoacetate, iodine) were made[41-44]. In our case, $Pd(PPh_3)_2Cl_2$, CuI were used as catalysts and I_2 was used as the oxidant. Diisopropylethylamine was used as both the solvent and the base and the reaction was carried out under a nitrogen atmosphere and left to react for 6 hours at room temperature. The residue obtained was easily purified by column chromatography giving (**6**) at 82% yield.

The final step for the synthesis of the target molecule was the removal of the ester groups which would lead to the formation of the tetracarboxylic acid. Many different conditions can be found in the literature for ester hydrolysis. Most of them typically involve the reaction of the ester with a base at high temperature in a suitable solvent. The solvent system employed in our case[45] proved to be ideal. A mixture of THF, MeOH and water were used as the solvent system and NaOH was used as the base. The reaction was almost quantitative (98% yield) and it was completed in less than 2 hours. After the reaction was completed, the organic solvents were

removed using a rotary evaporator and the remaining aqueous solution was acidified to pH 1. (**7**) was precipitated and dried thoroughly and crystallization from MeOH/toluene gave a white microcrystalline material. The product was successfully characterized by NMR, elemental analysis and MS spectrometry.

2.2.2 Surface deposition studies

For the preparation and imaging of the network formed on a HOPG surface by depositing the DPBDTC molecule, the same conditions were applied as for TPTC in the previous study[17]. STM images were acquired with an Agilent Technologies 4500 PicoPlus STM using a PicoScan controller and STM tips formed from mechanically cut PtIr (80:20) wire. Saturated solutions of DPBDTC were prepared by placing an excess of solid in the desired solvent (heptanoic or nonanoic acid). All solutions were agitated ultrasonically to ensure complete dissolution. To form the supramolecular networks, a droplet (10 ml) of solution was deposited onto a mechanically cleaved HOPG substrate. Imaging at the alkanoic acid–HOPG interface commenced immediately after the approach of the STM tip.

DPBDTC formed molecular networks in both heptanoic and nonanoic acid. In Figure 2.6 we can see STM images obtained from networks formed in both of the solvents. Here we can see that the backbone of the DPBDTC molecule appears as bright rodlike features. A very nice observation can be made in figure 2.6c which shows an enlarged area of the image of the network obtained in heptanoic acid. It is apparent that the molecules best aligned with the fast scan direction of the STM (movement of the probe from left to right and from right to left) are

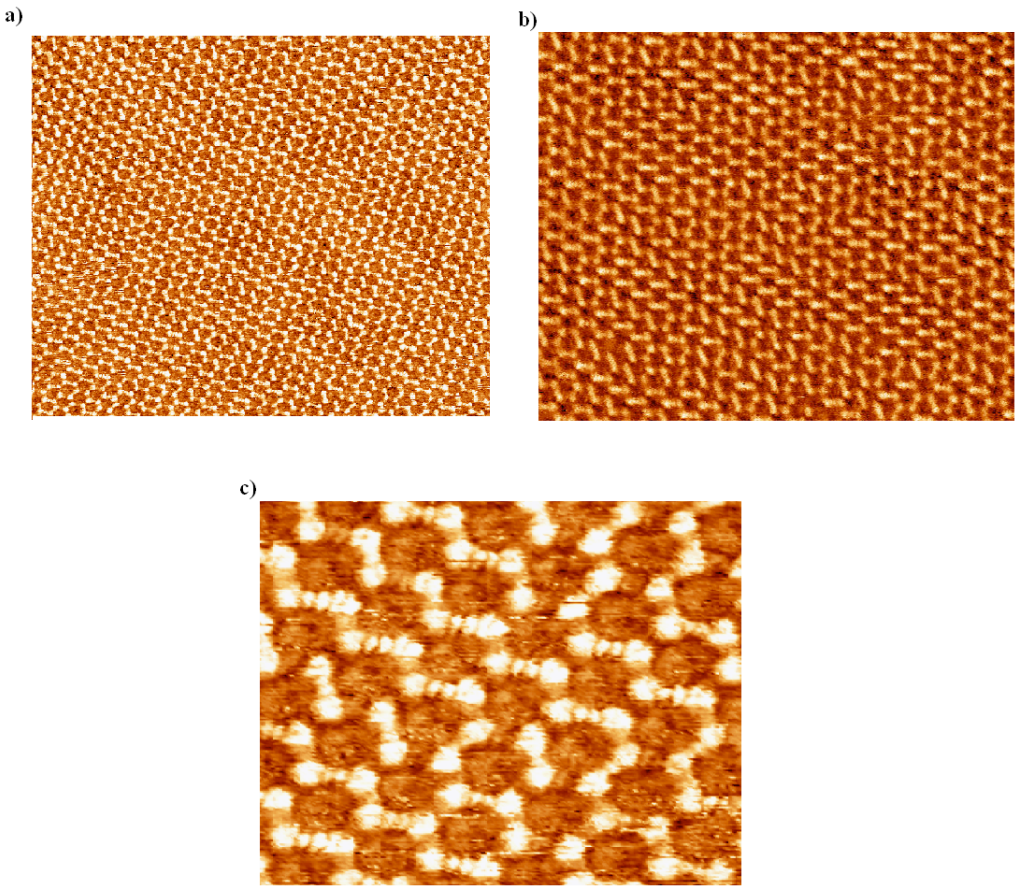


Figure 2.6. STM images of DPBDTC on HOPG surface showing the formation of a porous network with hexagonal orientational order but no translational symmetry. Image in a) heptanoic acid b) nonanoic acid. c) Enlarged area of the networked formed in heptanoic acid showing the appearance of some DPBDTC molecules as four blobs, two of which correspond to the phenyl rings and the other two correspond to the triple bonds.

seen as 4 spots. The two largest spots, located at the edges, correspond to the phenyl rings of DPBDTC while the other two smaller spots, located in the middle correspond to the two triple bonds. Unfortunately many of the molecules that were not orientated with the slow scan axis of

the STM (the axis perpendicular to the fast scan direction) were not fully imaged. For many of these molecules it was just the rings of the molecules that could be seen. As such, we were not able to assign a unique tiling to the assembly as there was more than one way to arrange the tiles that seem to fit with the image. Therefore the network formed in heptanoic acid will not be considered in the analysis that follows.

A tiling representation of the network in nonanoic acid shown in Figure 2.7a has been prepared (Figure 2.7b), every molecule being replaced by a rhombus. Every rhombus has a different colour which signifies one of the three possible directions of the DPBDTC molecule on the surface. In this picture it is apparent that there is complete lack of translational order. The dark regions of the scan in Figure 2.7a can be considered as pores that are enclosed by DPBDTC molecules. On the bottom right corner of the image the pores have been highlighted in order to show that they exhibit hexagonal orientational order. The magnification of certain areas of the network (Figures 2.7c-g) gives further proof of the lack of translational order. In these images we can see five different types of molecular arrangements that can form a hexagonal pore. In Figure 2.7c a hexagon is formed from three molecules with edges alternating between a diacetylenic backbone and a carboxylic acid-carboxylic acid junction. In Figure 2.7d and 2.7e a hexagon is formed by four molecules where two of the edges are constituted by a diacetylenic backbone. Figure 2.7g shows a pore that is formed by 5 molecules. Only one of the edges is formed by a diacetylenic backbone. Finally Figure 2.7f shows a pore that is formed by 6 molecules. All the edges of this type of hexagon are formed by carboxylic acid...carboxylic acid junctions. A molecular ball and stick representation as well as a tiling representation is also shown next to the images of the five different pore types.

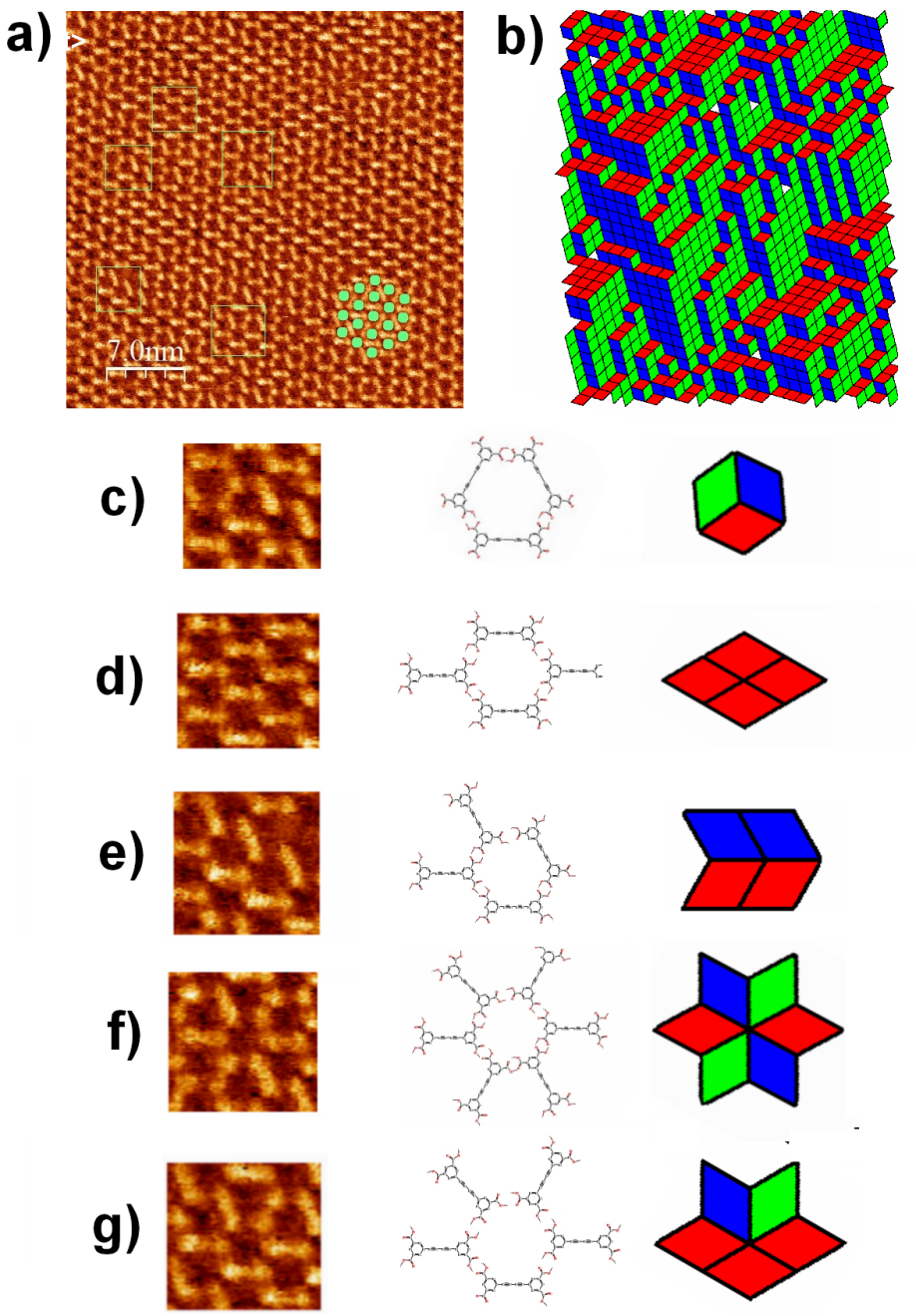


Figure 2.7. a) STM image of DPBDTC network formed in nonanoic acid. b) Tiling representation of the network shown in (a). c-g) Enlarged regions from (a) with molecular ball and stick diagrams and tiling representations of the 5 possible different arrangements of DPBDTC around a network pore.

The intermolecular binding energy for both the parallel and arrowhead arrangements has been calculated to be 0.80 eV. The length of the diacetylenic edge and carboxylic acid…carboxylic acid hydrogen bonds edge has been calculated to be 9.5 Å and 9.6 Å respectively. These distances were mentioned above as d_1 and d_2. With these two values, the hexagons formed are estimated to have a width between 16.4 Å and 16.6 Å. Using calibration scans of the graphite substrate it was found that the hexagonal array had a periodicity of 16.6 ± 0.8 Å oriented at an angle of $\pm 6^{o}$ to the HOPG substrate. This value lies in a good agreement with the theoretical range of the hexagon width.

A quantitative approach was taken to identify the degree of randomness of the tiling. After the successful mapping into a tiling representation, the rhombi consisting of the same colour were measured for two different images of the surface. The first image with dimensions 35 x 35 nm had a total of 975 tiles. 445 were of green colour (45.6%) 227 were of red colour (23.2%) and 303 were of blue colour (31.2%). Also there were measured 954 non-parallel bonds and 1009 parallel bonds. The second image with dimensions 50 x 50 nm had a total of 1213 tiles. 614 were of green colour (50.6%), 310 were of red colour (25.5%) and 289 (23.9%) were of blue colour. The count for non parallel bonds was 1174 and for parallel bonds was 1139. Combining the two sets in regards to the tile colour was not possible because rotation of the image changes the colour of the tiles. However this is not the case in respect to the number of non- parallel and parallel bonds which does not change with rotation. A sum of 2128 (48.6%) of non-parallel and 2248 (51.4%) of parallel bonds were measured. These results show that the split between non-parallel and parallel configuration is almost equal with the parallel configuration being in favor.

In order to get a more meaningful impression of the above numbers, it was necessary to introduce an order parameter Ψ which is defined as:

$$\Psi = (n_0p - p_0n) / (n_0p + p_0n)$$

Where p and n represent the percentage of rhombus tile junctions that are in a parallel and non-parallel orientation respectively and, p_o and n_o are the percentage of rhombus tile junctions of parallel and non-parallel orientation in an ideal, defect free random tiling. Their values are 0.392 and 0.608, respectively. The latter values were attained by numerical calculations. This order parameter can take values between 1 and -1. In a fully parallel phase Ψ will equal to 1 while in a network with zero parallel tile junctions Ψ will equal to -1. Any network with a Ψ value in-between will vary in the degree of randomness. An ideal random tiling will have a Ψ value of 0.

The DPBDTC network formed in nonanoic acid gives a Ψ value of 0.22. This shows that the network characteristics are close to an ideal random tiling but not as close as would have been expected from the careful design of the molecule and from the theoretical calculations of the energy difference between the parallel and non-parallel configurations. However, it is important to mention that the Ψ value of TPTC in nonanoic acid, under the same experimental conditions, equals -0.43. Here we can see that our hypothesis was correct and under the same conditions DPBDTC forms a network that is closer to an ideal random tiling than that of TPTC.

In addition to the tiling representation, a height representation was also used. When analyzing rhombus tilings, it is common that a height map is constructed. In order to construct this map, an "effective height" *h(x,y)* is assigned to every vertex of every rhombus in the area of interest. The in-plane coordinates of the vertices are designated as x and y. During this assignment, a step

along a rhombus edge results in a change in height of ±1 depending on the direction of the step. By assigning the value zero to a random edge, we can build the height map around it in a numerical form as shown in Figure 2.8a. For a visualization of the height map, every number has been assigned a different shadow intensity in the greyscale with zero having an intermediate toning, positive numbers becoming increasingly black and negative numbers becoming increasingly white. An illustration of this principle is shown in Figure 2.8b.

For a tiling consisting solely of tiles in the parallel configuration, one would expect to observe *h(x,y)* increasing monotonically across the surface because all the tiles will be pointing in the same direction. On the other hand, in a perfect non-parallel ordered phase we would expect

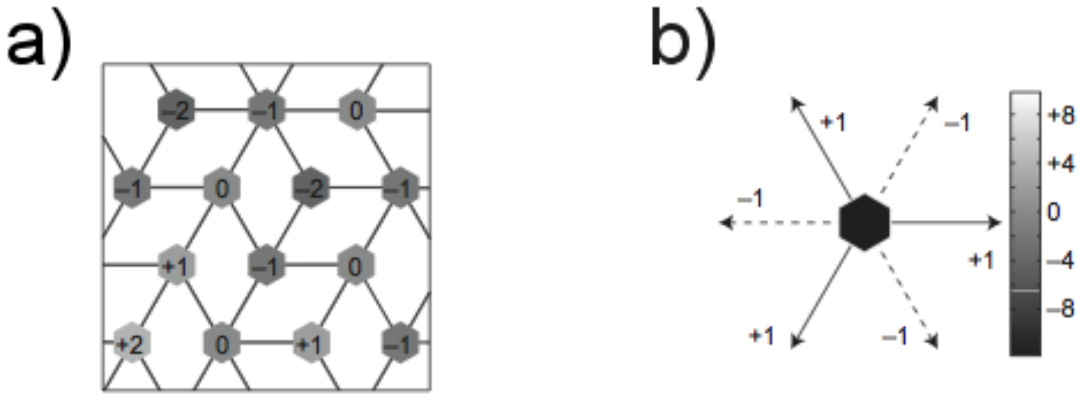


Figure 2.8. Demonstration of the construction of a height representation[58]. a) Rhombus random tiling with edges represented as hexagons. Every hexagon has different x,y coordinates and *h(x,y)* is written inside every hexagon. b) Illustration of change of *h(x,y)* depending on the direction of the step. Relationship of *h(x,y)* with the greyscale colour tone.

h(x,y) to remain constant with fluctuations only limited to ±1. In an ideal random tiling the average *h(x,y)* would be constant but the fluctuations between individual values would be bigger that ±1. Using this approach the height map of the experimentally determined tiling area of DPBDTC shown in Figure 2.9a was constructed. This is shown as a greyscale image in Figure 2.9b. The hexagons appear to be white at the left side of the image and they slowly become progressively darker as we move towards the right direction of the image. This shows that the

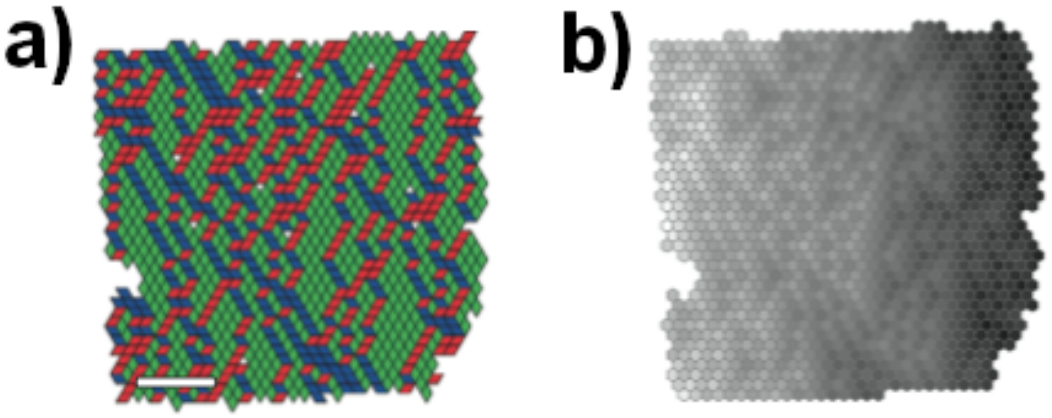


Figure 2.9. Tiling representation of DPBDTC in nonanoic acid (a) and the height representation of the same area (b). The surplus of tiles with parallel orientation is apparent from the gradual shadowing of the hexagons in (b) as we scan the map from left to right[58].

DPBDTC network has more tiles with the parallel configuration than that required for an ideal random tiling. This causes *h(x,y)* to slowly increase. This visual observation was anticipated by the fact that Ψ has a small, but not negligible, positive value.

2.2.3 Experimental exploration of the phase space of interacting random tilings

A random tiling is considered ideal when the configurational energies e_n and e_p of the non-parallel and parallel configurations respectively are identical. If this is the case then the tiling configuration is solely dependent on the maximizing of the configurational entropy. However if there exists a small difference between e_n and e_p then the degeneracy between the exponentially big number of tilings is broken. In this case, there is a small internal energy contribution to the free energy of the system which competes with the entropic term[46-49].

There are many theoretical models describing rhombus tiles with asymmetric interactions[46-49]. Let as consider an energy bias $\Delta = e_n - e_p$.Figure 2.10 shows a schematic of an expected equilibrium phase diagram. Here, the parameters of interest are the temperature T and the energetic bias Δ. Calculations have shown that the random tiling is ideal when $\Delta = 0$. For $\Delta > 0$ non-parallel bonding is favored. When Δ reaches a critical point the system orders into a crystalline phase where non-parallel bonds predominate. Similarly, when $\Delta < 0$, parallel orientation is favoured and a transition to a crystallize phase which is dominated by parallel bonds happens.

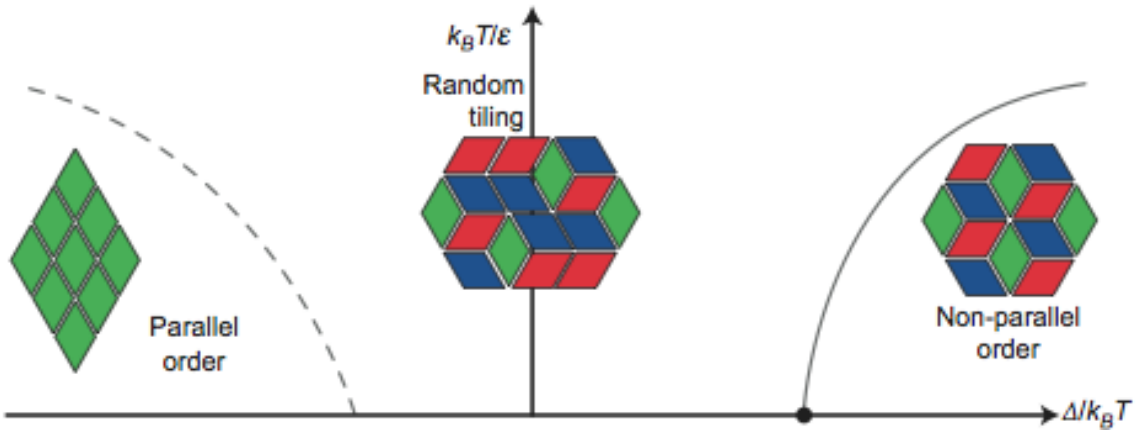


Figure 2.10. Phase diagram of the interacting tiling model. Three phases are expected depending on the value of Δ; a random tiling phase and two crystalline phases dominated by parallel or non-parallel bonds[57]. k_B is the Boltzmann constant, T is the absolute temperature, Δ is the energetic bias between the parallel and non-parallel configuration and ε is the characteristic hydrogen bond energy.

Peter Beton's group from School of Physics and astronomy managed to experimentally explore the phase space of the random tiling model. For this purpose, networks with different degrees of randomness were created by varying the experimental conditions. In this study DPBDTC as well as TPTC and a mixture of TPTC and coronene were dissolved in various solvents and deposited on HOPG surface in various temperatures. In total, 6 networks with a different value of Ψ were created. The data obtained were used in conjunction with numerical results of theoretical models in order to calculate the energetic bias Δ in each case and help reach several interesting conclusions[58].

In summary the study[58] showed that the phase space arising from asymmetrically interacting rhombus tiles may be experimentally explored through the preparation and characterization of the appropriate molecular arrays. It also showed that changes in Δ smaller than 5 meV gave rise to observable changes in the degree of randomness of the networks while changes bigger than 10 meV is sufficient to cause symmetry breaking and a transition to ordered crystalline phases. Finally, it was shown that the solvent molecules play a role on the energy difference between the parallel and non-parallel configuration and Δ cannot be described only by the interactions of the carboxylic acid molecules on the surface. Possible influences of the solvent molecules could arise from their co-adsorption on the graphite surface[52,53] and their weak interactions with the other co-deposited molecules[56].

2.3 Conclusion

The synthesis of 1,4-diphenyl-1,3-butadiyne-3,3'-5,5'-tetracarboxylic acid has been successfully completed. The synthetic route involved the preparation of ester (**5**) and its subsequent homo-coupling to the protected final product. After successful deprotection 1,4-diphenyl-1,3-butadiyne-3,3'-5,5'-tetracarboxylic acid was obtained as a white microcrystalline material.

DPBDTC was deposited on a HOPG surface from a nonanoic acid solution. Comparison with the previously studied TPTC molecule under similar conditions showed that DPBDTC formed a network that was closer to an ideal random tiling, as indicated by the order parameter Ψ. This confirmed our predictions that a closer match between d_1 and d_2 would improve the degree of randomness of the tiling formed. A tiling representation and a height representation was

constructed from an STM image of the network. The images indicated a network with a surplus of tilings with parallel configuration.

DPBDTC and TPTC were deposited on HOPG under various conditions. The experimental data obtained were used for the experimental realization of the phase space of the random tiling model with asymmetric interaction. An estimation of the energetic bias Δ was possible. It was found that differences in energetic bias Δ of less than 5 meV produced measurable variations in the tiling statistics. It was also found that when $\Delta > 10$ meV, the structures are driven into ordered phases. A dependency of Δ on the solvent was also observed. This led to the conclusion that the co-deposition of solvent molecules into the hexagonal nano-pores and other weak interactions between the solvent and the deposited molecules contribute to the already energetically degenerate pores.

2.4 Experimental

All reagents and solvents were purchased from Sigma Aldrich, Alfa Aesar, Fischer Scientific UK, and used without further purification unless otherwise stated. Elemental microanalyses were carried out by Steven Boyer at the Microanalysis Service, London Metropolitan University, UK. ^{1}H and ^{13}C NMR spectra were measured using either a Joel 270 MHz, Bruker 300 MHz, Bruker 400 MHz, DPX 300 MHz, DPX 400 MHz or Bruker 500 MHz spectrometer. MALDI-TOF mass spectra were obtained using Bruker Ultraflex MALDI-TOF mass spectrometer. MALDI-TOF-MS samples were prepared by dissolution of the compounds in CH_2Cl_2 (10 μL) and then mixing this solution with a solution of the matrix DCTB (Trans-2-[3-(4-tertbutylphenyl)-2-methyl-2-

propenylidone]-malonitrile) in MeCN (20 μL). A sample of the resulting solution (5 μL) was loaded onto a plate, the solvent was removed in air, and the sample transferred to the mass spectrometer for analysis. Electrospray ionization mass spectra were collected using a MALDI-TOF mass spectrometer. UV-Vis spectra were obtained using Unicam UV/Vis 2 spectrometer.

STM measurements and tiling calculations were performed by Matthew Blunt and Andrew Stannard from the School of Physics and Astronomy at the University of Nottingham.

Compound Synthesis

Synthesis of 5-iodoisophthalic acid (2)

An aqueous solution of 3,5-dimethyliodobenzene (1.010 mg, 4.358 mmol), potassium permanganate (5 g, 32 mmol) and pyridine (7.5 ml) was brought to reflux at 115 ^{o}C for 15 h. Addition of another portion of potassium permanganate (2.5 g, 16 mmol) was followed by another 5 h reflux. The reaction mixture was brought to room temperature and filtered to remove the precipitated MnO_2. The filtrate was reduced in volume under reduced pressure to approximately 10 ml. The solution was then acidified with concentrated HCl to pH 1. The white solid formed was filtered and recrystallized from boiling water to give 900 mg (71%) of a white powder. ^{1}H NMR (400 MHz, d^{6}-DMSO) : δ ppm = 13.54 (s br, 2H, COOH), 8.40 (s, 3H). ^{13}C NMR (101 MHz, $CDCl_3$): δ ppm 92.72, 129.59, 132.93, 142.06, 165.80. ESI-MS (m/z):

290.9160 $[M-H]^-$. Elemental Analysis (%) Calculated for $C_8H_5IO_4$: C, 32.9; H, 1.73; Found: C, 33.04; H, 1.70.

Synthesis of diethyl-5-iodoisophthaloate (3)

5-Iodosophthalic acid (1000 mg, 3.42 mmol) was dissolved in absolute ethanol (10 ml). Thionyl chloride (800 µl, 7.18 mmol) was added at 0 ^oC and the reaction mixture was brought to reflux under inert atmosphere for a course of 5 h. Ethanol was evaporated in reduced pressure and the residue was dissolved in ethyl acetate. The mixture was washed with a saturated solution of sodium bicarbonate. The organic phase was dried with magnesium sulfate and evaporated under reduced pressure. Column chromatography on silica [CH_2Cl_2/Hexane (70:30)] afforded diethyl 5-iodoisophthalate as a white solid (81%). ^1H NMR (400 MHz, $CDCl_3$) : δ ppm = 8.62 (apparent triplet, J = 1.4 Hz, 1H), 8.53 (d, J = 1.4 Hz, 2H), 4.40 (q, J = 7.1 Hz, 4H), 1.41 (t, J = 7.1 Hz, 6H). ^{13}C NMR (101 MHz, $CDCl_3$): δ ppm 14.30, 61.76, 93.39, 129.83, 132.55, 142.33, 164.41. ESI-MS (m/z): 348.9914 $(M+H)^+$. Elemental Analysis (%) Calculated for $C_{12}H_{13}IO_4$: C, 41.4; H, 3.76; Found C, 41.52; H, 3.78.

Synthesis of diethyl-5-((trimethylsilyl)ethynyl)isophthaloate (4)

The compound was synthesized as described previously using slight modifications. 5-Iodo-isophthaloate (2 g, 6.28 mmol), $Pd(PPh_3)_4$ (166 mg, 0.14 mmol) and CuI (10 mg, 0.05 mmol) where suspended in piperidine (10 ml) in a dry Schlenck flask under nitrogen. Trimethylsilylethylene (1 ml, 6.9 mmol) was added at 0 ^0C and the reaction mixture was stirred

for 3 h at room temperature. The reaction was quenched by the addition of a saturated aqueous solution of NH_4Cl. The aqueous solution was washed twice with dichloromethane and the organic layer was dried with Na_2SO_4. The solvent was removed under reduced pressure and the residue was purified by column chromatography on silica [hexane/dichloromethane (70:30)] to afford diethyl-5-((trimethylsilyl)ethynyl)isophthalate as a pale yellow solid (85%). ^{1}H NMR (400 MHz, $CDCl_3$) : δ ppm = 8.60 (at, J = 1.7 Hz, 1H), 8.28 (d, J = 1.7 Hz, 2H), 4.40 (q, J = 7.1 Hz, 4H), 1.41 (t, J = 7.1 Hz, 6H), 0.27 (s, 9H). ^{13}C NMR (101 MHz, $CDCl_3$): δ ppm 0.18, 14.32, 61.57, 96.56, 102.89, 124.09, 130.27, 131.16, 136.73, 165.16. ESI-MS (m/z): 319.1337 $(M+H)^+$. Elemental Analysis (%) Calculated for $C_{17}H_{22}O_4Si$: C, 64.12; H, 6.96; Found C, 64.14; H, 7.06.

Synthesis of diethyl-5-ethynylisophthalate (5)

Diethyl-5-((trimethylsilyl)ethynyl)isophthalate (70 mg, 0.22 mmol) was dissolved in THF (5 ml). Tetrabutylammonium fluoride (200 µl, 2 M in THF) was added slowly and the reaction mixture was stirred for 30 min. Water was added and the aqueous solution extracted twice with dichloromethane. The organic layer was dried with Na_2SO_4 and the solvent was removed under reduced pressure. The residue was purified by column chromatography on silica [dichloromethane/hexane (70:30)] to afford diethyl-ethynylisophthalate as a pale yellow solid (78%). ^{1}H NMR (400 MHz, $CDCl_3$) : δ ppm = 8.60 (at, J = 1.6 Hz, 1H), 8.28 (d, J = 1.6 Hz, 2H), 4.38 (q, J = 7.1 Hz, 4H), 3.18 (s, 1H), 1.39 (t, J = 7.1 Hz, 6H). ^{13}C NMR (101 MHz, $CDCl_3$): δ ppm 14.30, 61.63, 79.02, 81.71, 123.04, 130.65, 131.32, 136.94, 165.05. ESI-MS (m/z): 247.0975 $(M+H)^+$. Elemental Analysis (%) Calculated for $C_{14}H_{14}O_4$: C, 68.28; H, 5.73; Found C, 68.32; H, 5.61.

Synthesis of tetraethyl-5,5'-(buta-1,3-diyne-1,4-diyl)dibenzene-1,3-dicarboate (6)

Diethyl-ethynylisophthalate (140 mg, 0.568 mmol), dichloro-bis-(triphenylphosphine) palladium (8.5 mg, 0.007 mmol), CuI (5.8 mg, 0.03 mmol) and I_2 (90 mg, 0.354 mmol) were suspended in anhydrous diisopropylamine and stirred for 6 h under nitrogen. After the reaction was completed, diisopropylamine was removed under reduced pressure. The residue was dissolved in dichloromethane and the organic phase was washed thoroughly with a saturated solution of aqueous HS_2O_3 to remove any unreacted I_2. The organic phase was dried with Na_2SO_4 and the solvent was removed under reduced pressure. Column chromatography on silica [dichloromethane/hexane (9:1)] afforded tetraethyl 5,5'-(buta-1,3-diyne-1,4-diyl)dibenzene-1,3-dicarboate as a pale yellow solid (82%). Recrystallization from hot toluene afforded a white crystalline solid. ^{1}H NMR (400 MHz, $CDCl_3$): δ ppm = 8.68 (at, J = 1.7 Hz, 2H), 8.38 (d, J = 1.6 Hz, 4H), 4.43 (q, J = 7.1 Hz, 8H), 1.44 (t, J = 7.16 Hz, 12H). ^{13}C NMR (101 MHz, $CDCl_3$): δ ppm 14.31, 61.75, 75.06, 80.29, 122.45, 131.16, 131.55, 137.25, 164.85. ESI-MS (m/z): 491.1732 $(M+H)^+$. Elemental Analysis (%) Calculated for $C_{28}H_{26}O_8$: C, 68.56; H, 5.34; Found: C, 68.63; H, 5.40.

Synthesis of 5,5'-(buta-1,3-diyne-1,4-diyl)dibenzene-1,3-dicarboic acid (7)

Tetraethyl-5,5'-(buta-1,3-diyne-1,4-diyl)dibenzene-1,3-dicarboate (140 mg, 0.286 mmol) were dissolved in a 2:1 mixture of THF/MeOH (15 ml). The solution was brought to refluxing temperature and another solution containing NaOH (1 g, 25 mmol) in a 5:2 mixture of MeOH/H_2O (7 ml) was added dropwise and left to reflux for 2 h. The solution was allowed to

cool to room temperature and the solvent was removed under reduced pressure. The residue was dissolved in water and acidified to pH 1 with a 2 M aqueous hydrochloric acid solution. The white cloudy suspension was centrifuged and the solid mass was recrystallized from toluene/MeOH to afford a white crystalline solid (98%). ^{1}H NMR (d^{6}-DMSO, 400 MHz): δ ppm = 13.63 (s br, 4H, COOH), 8.51 (s, 2H), 8.31 (s, 4H). ^{13}C NMR (101 MHz, $CDCl_3$): δ ppm 73.95, 79.66, 122.14, 131.10, 132.09, 136.72, 166.23. ESI-MS (m/z): 377.0295 $[M-H]^-$. Elemental Analysis (%) Calculated for $C_{28}H_{26}O_8$: C, 63.50; H, 2.66; Found: C, 63.56; H, 2.60.

2.5 References

1. B. Grunbaum, G.C. Shephard, *Tilings and Patterns,* New York, W.H. Freeman, **1987**.

2. D. Shechtman, I. Blech, D. Gratias, J. Cahn, *Phys. Rev. Lett.,* **1984**, *53*, 1951.

3. D. Levine, P. J. Steinhardt, *Phys. Rev. Lett*., **1984**, *53*, 2477.

4. G. Onoda, P. J. Steinhardt, D. J. DiVincenzo, J. E. S. Socolar, *Phys. Rev. Lett*., **1988**, *60*, 2653.

5. J. Ledieu, J. T. Hoeft, D. E. Reid, J. A. Smerdon, R. D. Diehl, T. A. Lograsso, A. R. Ross, R. McGrath, *Phys. Rev. Lett*., **2004**, *92*, 135507.

6. J. Yuhara, J. Klikovits, M. Schmid, P. Varga, Y. Yokoyama, T. Shishido, K. Soda , *Phys. Rev. B*, **2004**, *70*, 24203.

7. M. E. Fisher, *Phys. Rev.*, **1961**, *124*, 1664.

8. P. Kasteleyn, *J. Math. Phys.,* **1963**, *4*, 287.

9. D. B. Wilson, *Ann. Appl. Probab.*, **2004**, *14*, 274.

10. H. Cohn, R. Kenyon, J. Propp, *J. Am. Math. Soc.*, **2001**, *14*, 297.

11. H. W. J. Blote, H. J. Hilhorst, *J. Phys. A*, **1982**, *15*, L631.

12. R. Moessner, S. L. Sondhi, E. Fradkin, *Phys. Rev. B*, **2002**, *65*, 24504.

13. C. L. Henley, *Quasicrystals, the State of the Art*, D. P. DiVencenzo, P. J. Steinhardt, Eds. (World Scientific, Singapore, **1999**), p. 459.

14. M. Widom, D. P. Deng, C. L. Henley, *Phys. Rev. Lett.*, **1989**, *63*, 310.

15. N. Destainville, *Phys. Rev. Lett.*, **2002**, *88*, 30601.

16. A. S. Keys, S. C. Glotzer, *Phys. Rev. Lett.*, **2007**, *99*, 235503.

17. M. O. Blunt, J. C. Russell, María del Carmen Giménez-López, J. P. Garrahan, Xiang Lin, M. Schröder, N. R. Champness, P. H. Beton, *Science,* **2008**, *322*, 1077.

18. M. E. Fisher, J. Stephenson, *Phys. Rev.*, **1963**, *132*, 1411.

19. J. Linde, C. Moore, M. G. Nordahl, *Discrete Mathematics and Theoretical Computer Science Proceedings* (AA DM-CCG), **2001**, 23.

20. W. Krauth, R. Moessner, *Phys. Rev. B*, **2003**, *67*, 64503.

21. G. H. Fredrickson, H. C. Andersen, *Phys. Rev. Lett.*, **1984**, *53*, 1244.

22. J. P. Garrahan, D. Chandler, *Proc. Natl. Acad. Sci. U.S.A.*, **2003**, *100*, 9710.

23. J. E. Freund, Edelwirth, M., Krobel, P., Heckl, W. M., *Phys. Rev. B*, **1997**, *55*, 5394.

24. M. Bohringer, K. Morgenstern, W. D. Schneider, R. Berndt, F. Mauri, A. De Vita, R. Car, *Phys. Rev. Lett.,* **1999**, *83*, 324.

25. M. M. Reiter, F. Jamitzky, F. Trixler, W. M. Heckl, *Phys. Status Solidi A*, **2001**, *187*, 171.

26. T. Yokoyama, S. Yokoyama, T. Kamikado, *Nature*, **2001**, *413*, 619.

27. L. Scudiero, K. W. Hipps, D. R. J. Barlow, *Phys. Chem. B*, **2003**, *107*, 2903.

28. J. A. Theobald, N. S. Oxtoby, M. A. Phillips, N. R. Champness, P. H. Beton, *Nature,* **2003**, *424*, 1029.

29. S. De Feyter, F. C. De Schryver, *Chem. Soc. Rev*. **2003**, *32*, 139.

30. M. Lackinger, S. Griessl, T. Markert, F. Jamitzky, W. M. J. Heckl, *Phys. Chem. B*, **2004**, *108*, 13652.

31. H. Zhou, H. Dang, Ji-Hyun Yi, A. Nanci, A. Rochefort, J. D. Wuest, *J. Am. Chem. Soc*., **2007**, *129*, 13774.

32. M. Blunt, X. Lin, Maria del Carmen Gimenez-Lopez, M. Schroeder, N. R. Champness, P. H. Beton, *Chem. Commun.*, **2008**, *20*, 2304.

33. M. Li, K. Deng, S. B. Lei, Y. L. Yang, T. S. Wang, Y. T. Shen, C. R. Wang, Q. D. Zeng, C. Wang., *Angew. Chem. Int. Ed.*, **2008**, *47*, 6717.

34. F. Diederich, P. J. Stang, Eds. In *Metal Catalyzed Cross-coupling Reactions,* Wiley-VCH, **1998**.

35. P. Holy, P. Sehnal, T. Milos, J. Zavada, I. Cisarova, *Tetrahedron Asymmetry*, **2004**, *23*, 3805.

36. B. D. Hosangadi, R. H. Dave, *Tetrahedron Lett.,* **1996**, *37*, 6375.

37. R. Chinchilla, C. Najera, *Chem. Rev.*, **2007**, *107*, 874.

38. I. Aujard, J. Baltaze, J. Baudin, E. Cogne, F. Ferrage, L. Jullien, E. Perez, V. Prevost, L. M. Qian, O. Ruel, *J. Am. Chem. Soc,* **2001**, *34*, 8177.

39. G. S. Wilson, H. L. Anderson, *Synlett,* **1996**, *11*, 1039.

40. A. S. Batsanov, J. C. Collings, I. J. S. Fairlamb, J. P. Holland, J. A. K. Howard, Z. Lyn, T. B. Marder, A. C. Parsons, R. M. Ward, J. Zhu, *J. Org. Chem.,* **2005**, *70*, 703.

41. R. Rossi, A. Carpita, C. Bigelli, *Tetrahedron Lett.*, **1985**, *26*, 523.

42. A. Lei, M. Srivastava, X. Zhang, *J. Org. Chem.*, **2002**, *67*, 1969.

43. Q. Liu, D. J. Burton, *Tetrahedron Lett,* **1997**, *38*, 4371.

44. M. Vlassa, I. Ciocan-Tarta, F. Margineanu, I. Oprean,*Tetrahedron,* **1996**, *52*, 1337.

45. C. Muthiah, M. Taniguchi, H. Kim, I. Schmidt, H. L. Kee, D. Holten, D. F. Bocian, J. S. Lindsey, *Photochemistry and Photobiology*, **2007**, *83*, 1513.

46. F. Alet, Y. Ikhlef, J. L. Jacobsen, G. Misguich, V. Pasquier, *Phys. Rev. E*, **2006**, *74*, 41124.

47. S. Papanikolaou, E. Luijten, E. Fradkin, *Phys. Rev. B*, **2007**, *76*, 134514.

48. C. Castelnovo, C. Chamon, C. Mudry, P. Pujol, *Ann. Phys.*, **2007**, *322*, 903.

49. J. L. Jacobsen, F. Alet, *Phys. Rev. Lett.*, **2009**, *102*, 145702.

50. J. P. Garrahan, A. Stannard, M. O. Blunt, P. H. Beton, *Proc. Natl Acad. Sci. USA*, **2009**, *106*, 15209.

51. A. Stannard, M. O. Blunt, P. B. Beton, J. P. Garrahan, *Phys. Rev. E*, **2010**, *82*, 41109.

52. R. Gutzler, T. Sirtl, J. F. Dienstmaier, K. Mahata, W. M. Heckl, M. Schmittel, M. Lackinger, *J. Am. Chem. Soc.*, **2010**, *132*, 5084.

53. Y. Yang, C. Wang, *Curr. Opin. Colloid Interface Sci.*, **2009**, *14*, 135.

54. M. O. Blunt, J. C. Russell, Maria del Carmen Gimenez-Lopez, N. Taleb, X. Lin, M. Schroeder, N. R. Champness P. H. Beton, *Nature Chem.*, **2011**, *3*, 74.

55. J. L. Cook, C. A. Hunter, C. M. R. Low, A. Perez-Velasco, J. G. Vinter, *Angew. Chem. Int. Ed.*, **2007**, *46*, 3706.

56. L. Kampschulte, M. Lackinger, A. K. Maier, R. S. K. Kishore, S. Griessl, M. Schmittel, W. M. Heckl, *J. Phys. Chem. B,* **2006**, *110,* 10829.

57. D. V. Talapin, E. V. Shevchenko, M. I. Bodnarchuk, X. Ye, J. Chen, C. B. Murray, *Nature*, **2009**, *361*, 964.

58. A. Stannard, J. C. Russell, M. O. Blunt, C. Salesiotis, M. Gimenez-Lopez, N. Taleb, M. Schroder, N. R. Champness, J. P. Garrahan, P. H. Beton, *Nat. Chem.,* **2012**, *4*, 112.

Chapter 3:

Design, synthesis and characterization of functionalized porphyrins aiming at applications in molecular memory storage

3.1 Introduction

3.1.1 Molecular electronics

Over recent decades there has been an explosive advance in the science of electronics. This, among many other things, has led to the emergence of computers which in essence are devices that a) can perform billions of mathematical computations per second and b) have the ability to store large amounts of bits of information. The incorporation of computers in our everyday lives has brought many changes in almost every aspect of living and thinking.



Figure 3.1. Modern electronics and the digitalization of our lives.

The rapid development in material science has led to electronic devices that can perform faster, store more information and at the same time become smaller in size. Previously held barriers

have been transcended and the quest for miniaturization seems to have no end. Traditionally, small size transistors needed in order to maximize memory storage and calculation power have been manufactured using the 'top down' approach. For example, one of the techniques belonging in this category is photolithography. Photolithography consists of applying a light sensitive material to a clean surface, covering parts of the surface with a desired pattern (photomask) and exposing the surface to UV light. Chemical treatment is then used in order to enable the deposition of new material upon the pattern formed.[1]

Although the process is technically challenging and wasteful, there are other limitations that hinder its use when smaller sizes are needed. One of them is the limitation imposed by the wavelength of the UV light used which is 193 nm. This allows for sizes of down to 50 nm. More recently, immersion lithography has given promising results in enhanced resolution[2] while Intel has confirmed that it will extend the 193 nm immersion lithography to the 22 nm and 16 nm node and have outlined a path to use it down to 11nm nodes.[3] However this process of miniaturization will find a physical barrier because of the changing properties of silicon when it approaches a certain limit.[4]

Aviram and Ratner in 1974 published a paper suggesting that molecules could perform the functions of semi-conductor electronics.[5] Since then, a lot of progress has been achieved and it has been shown that molecules can act as molecular switches, wires, rectifiers and diodes. It has also been shown that these molecules can be assembled into prototypical memory and logic architectures[6,7]. Examples of such molecular structures are shown in Figure 3.2. For such systems to be functional, the molecules must arrange in a regular fashion. This is mainly achieved through what is known as the 'bottom up' approach. In such a process, molecules are equipped with both functional groups and groups that carry recognition sites in order to guide the

formation of the desired architecture through self-assembly. In some cases, a different molecule is used in order to self-assembly on a surface where it forms a template upon which, the desired functional molecule will arrange itself in the pre-determined positions. In Figure 3.3 we can see a hexagonal network formed by the co-deposition of PTCDI and melamine on an Ag passivated

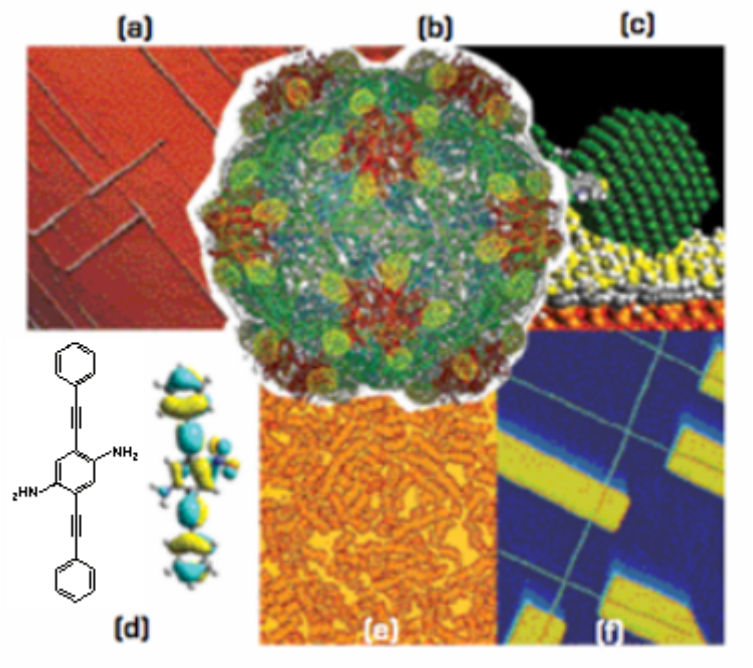


Figure 3.2. Images of molecular structures resembling electronic architectures[6] a) Electron micrograph of self-assembled ErSi2 nanowires b) electron micrograph of cowpea viral particle modified with gold nanoclusters to use as a template for molecular self-assembly c) simulation of gold nanoparticle electrical contacts on a surface in a 'NanoCell' molecular logic structure d) structural diagram of NDR diode switch molecule e) gold nanobars f) electron micrograph of nanowire transistor-based logic circuit.

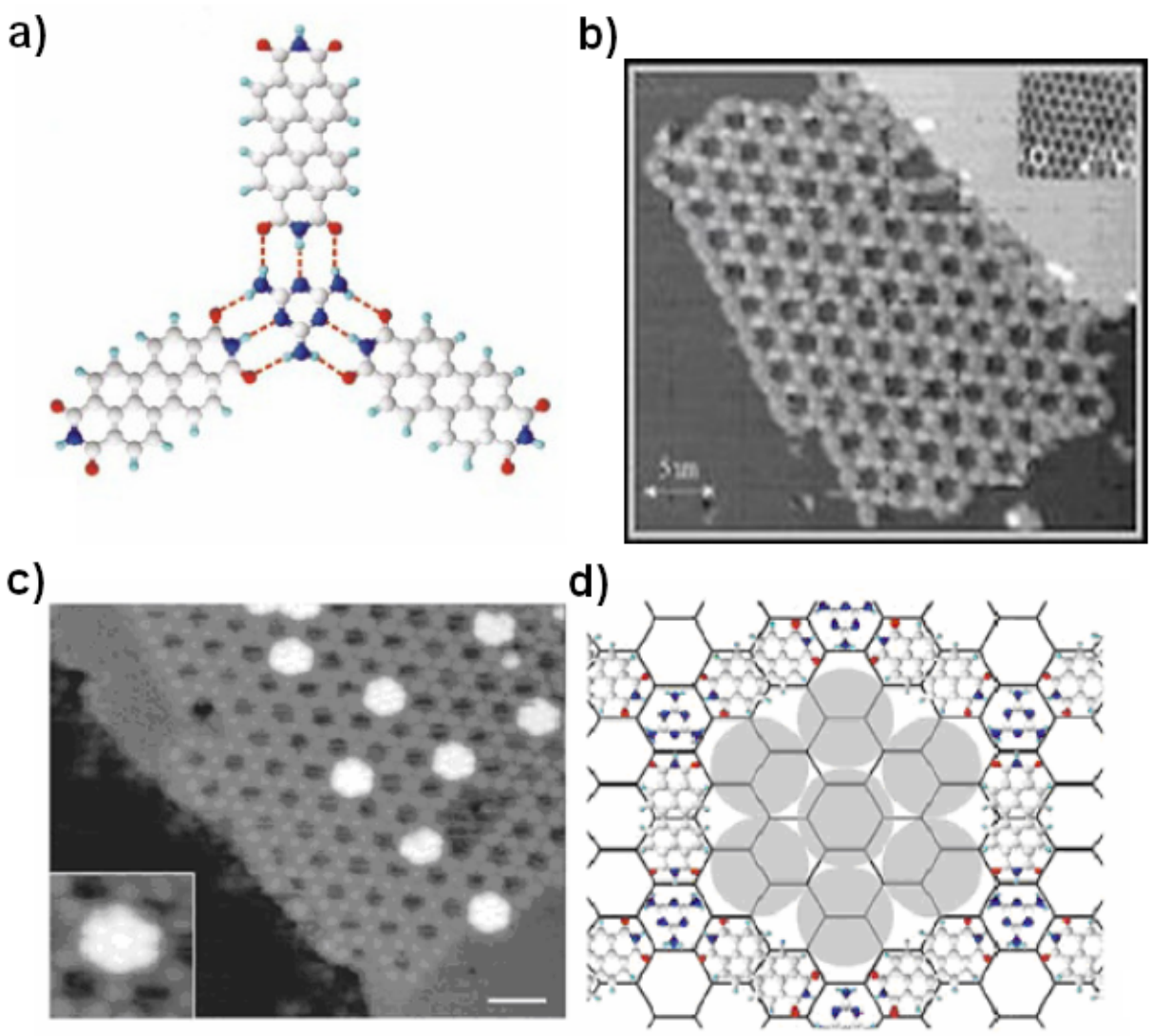


Figure 3.3. a) Triple hydrogen bond between a PTCDI molecule melamine b) STM image of a PTCDI-melamine network formed on Ag passivated Si(111) substrate c) STM image of C_{60} heptamers trapped inside the pores of the PTCDI-melamine network on Ag passivated Si(111) substrate d) schematic representation of a C_{60} heptamer of (d) [8].

Si(111) substrate[8]. This network is formed through the hydrogen bonding interactions between the melamine and the PTCDI molecules. Within the pores, heptamers of fullerene molecules can be trapped.

3.1.2 Molecular memories

The storage of information on a molecular level has attracted much attention[9-18]. A molecule is the smallest unit that can be used for binary information storage. Two different classes of compounds can serve for this purpose. One of those is the single molecule magnet (SMMs). Single molecule magnets can be deposited on a surface and form molecular arrays where the magnetic state of each molecule can be changed[19,20]. One of the limitations of this technique is that, at the present time, very low temperatures are needed in order to prevent the fast relaxation of their magnetization. The second option is to have a collection of redox active molecules attached to an electroactive surface. Information can, in principle, then be stored in the discrete redox states of the molecules.

Such systems, in order to be used in real life applications must be able to maintain each redox state indefinitely. Also, it is desirable that a change of the redox state does not promote a structural change. One of the candidates that comply with these restrictions is ferrocene. Systems incorporating the ferrocene unit[16,17,21-27] have been studied in the past. The ferrocene units are covalently linked to various types of molecules such as carbon nanotubes, phenyl groups and porphyrin molecules. These molecules are used as substrates which are in turn covalently linked to a surface. Figure 3.4 shows two examples of such systems.

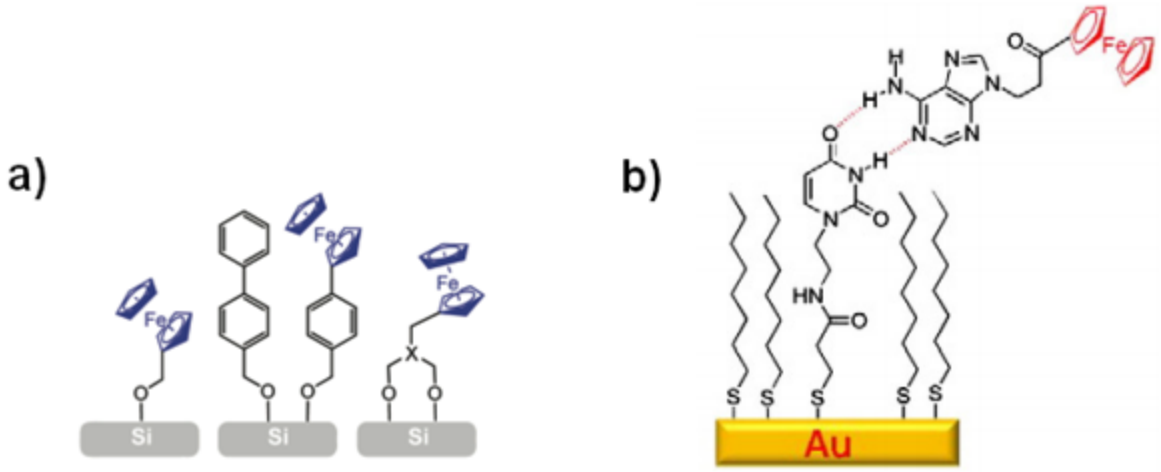


Figure 3.4. a) Si-O Linked ferrocenyl monolayers on Si-H[23] b) Adenine-substituted ferrocene hydrogen bonded on uracil terminated mixed monolayers on gold surfaces[87].

In all previous work that has been done so far, the substrate holding the ferrocene molecule was covalently linked to the surface. The objective of this project has been to create a system where the ferrocene would be covalently linked to a substrate, with the latter being self assembled as a monolayer upon a surface. Thus, we would be able to create molecular arrays of ferrocene units on a surface where we would try to change their redox states with the aid of the STM tip[28,29].

The substrate chosen for carrying the ferrocene units was a porphyrin molecule. There were many reasons for choosing a porphyrin. First of all the porphyrin is a flat, highly conjugated aromatic molecule. π-Conjugated aromatic systems are fruitful compounds for surface depositions as they tend to sit in a flat manner parallel to the surface. They also show high mobility and they can change orientation and position in order to easily follow the dynamics that the peripheral groups impose for the formation of a network. There are several examples in the literature where porphyrins have been successfully deposited on a surface and they have self-

assembled into 2D networks[30-34]. Figure 3.5 shows STM images from selected literature examples.

In our studies we targeted a range of molecules in which two ferrocene units were placed on each porphyrin molecule in opposing meso-positions. Isophthalic acid units were placed in the two remaining meso-positions. The isophthalic acid units were placed in order to drive the network formation. Many examples from the literature show that the carboxylic acid units promote directional hydrogen bonding[35-42]. In addition, three more analogs were designed as candidates

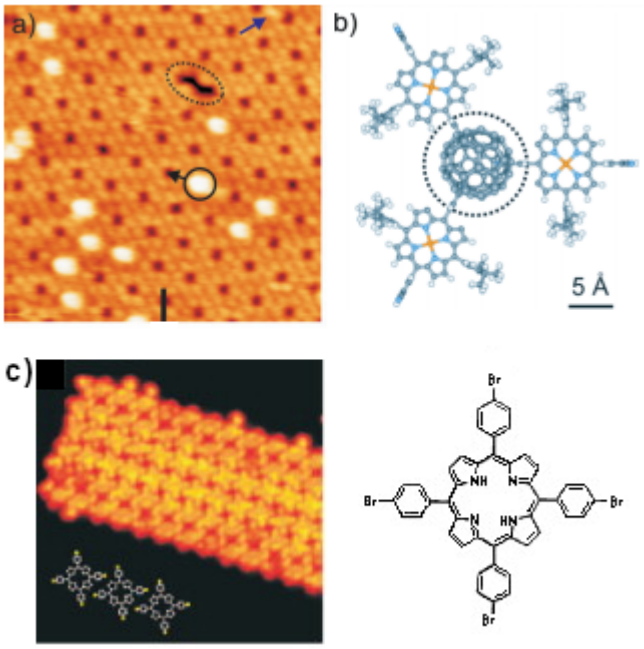


Figure 3.5. a) STM image showing the network formed of the co-deposition of [5,15-Bis(3-cyanophenyl)-10,20-bis[3,5-di(tert-butyl)phenyl]porphyrinato]-zinc(II) and C_{60} on Ag(111) surface[32]. b) Proposed molecular model of a C_{60} molecule hosted inside a supramolecular porphyrin-based pore of the network in Figure 2.5a. c) STM image of a network formed on Au(111) by the porphyrin shown on the right[34].

for surface deposition studies. In tetra-meso-phenyl porphyrins has been shown that steric interactions between the ortho-hydrogens of the phenyl rings and the hydrogens of the pyrole subunits prevent the phenyl rings of being co-planar with the porphyrin ring[43,44]. X-Ray diffraction studies have shown that the dihedral angle can range between 61-63^{o} for H_2TPP and almost 90^{o} in most metal complexes of TPP. Although porphyrin molecules with phenyl rings have been successfully deposited on surfaces with the phenyl rings being tilted, we wanted to maximize the interactions between the surface and the porphyrin molecules. If the phenyl ring was free to rotate and become stabilized in a co-planar orientation with respect to the surface, then this would allow the porphyrin to approach the surface more closely and thus, maximize the surface-network interactions. It would also allow additional forces between the surface and the phenyl rings to stabilize the network. By introducing a spacer between the porphyrin macrocycle and the phenyl rings we anticipated that the longer distance would minimize steric interactions. The chosen spacer was the acetylene group, chosen because it is rigidity and synthetic accessibility.

Porphyrins with the acetylene spacer between the ferrocene and the porphyrin core were also synthesized. This would allow a better communication between the ferrocene and the porphyrin macrocycle making the redox potential of the ferrocene more tunable through the incorporation of metal ions in the porphyrin core. On the other hand, extended communications between the two ferrocenes would be considered an undesirable phenomenon because it might not be possible to address and manipulate each ferrocene group individually, one of the requirements for information storage[45-50]. The molecular structures of the target molecules are depicted in Figure 3.6.

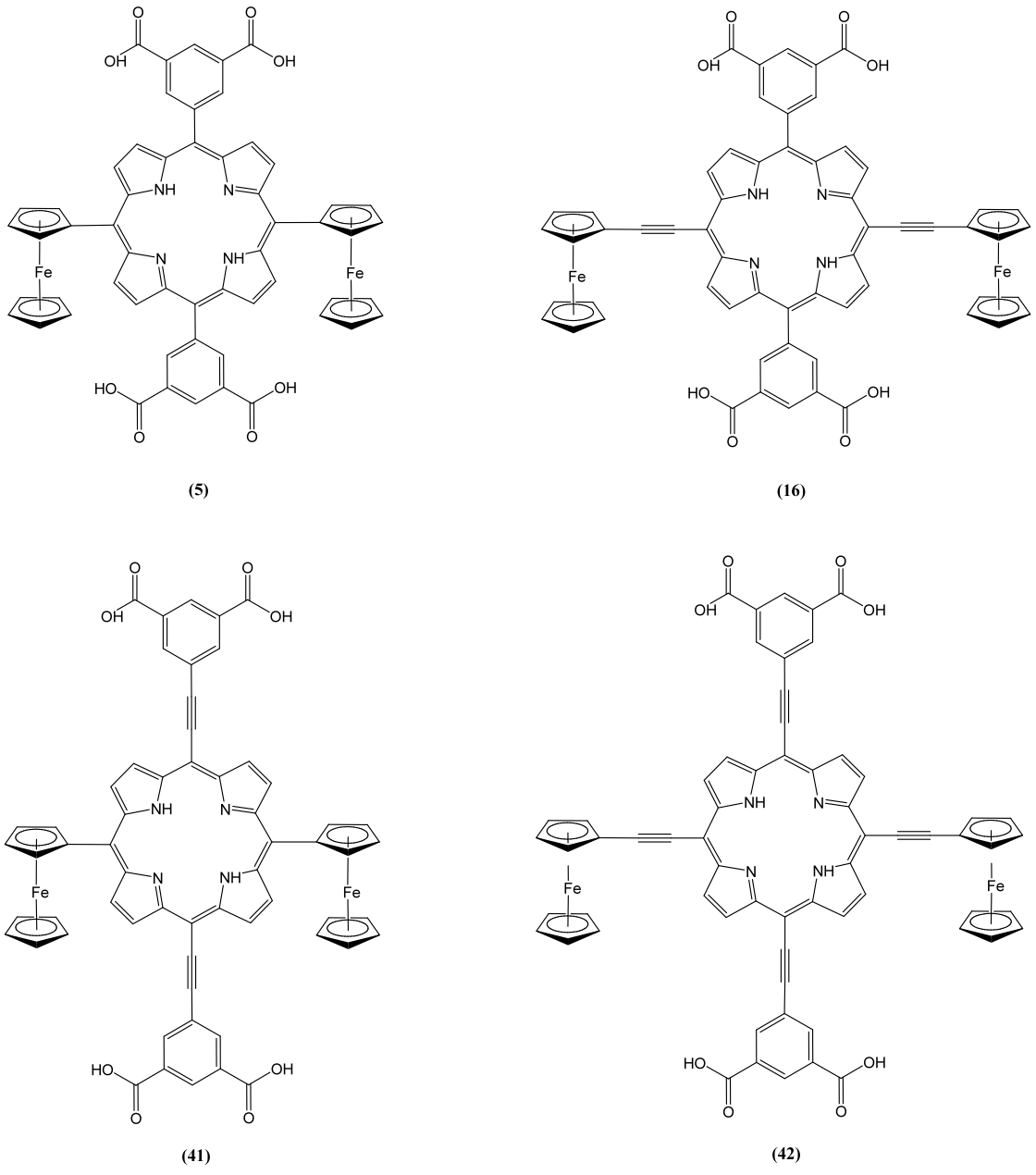


Figure 3.6. Molecular structures of the target molecules.

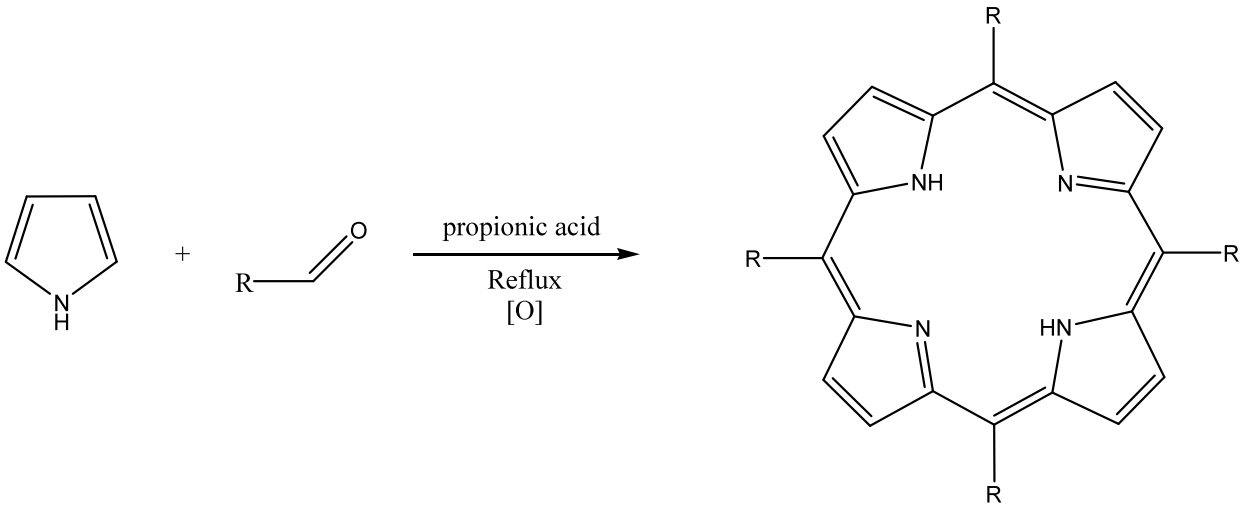
In order to appreciate the electronic redox properties of the compounds they were first studied in solution. The carboxylic acid groups make the situation problematic. Every porphyrin molecule will have four carboxylic acid groups and this, in addition with the tendency of porphyrins to form aggregates due to π-π stacking, reduces the solubility of the compounds. This does not cause a significant problem during the deposition of the molecules because the concentration needed is minimal. However, electrochemical studies require the material to be soluble in the solvent system used. To overcome this problem the electrochemical studies were performed on a diethylester-protected version of the above compounds. No extra synthetic steps needed to be carried out as the diethyl-ester derivatives are intermediates during the synthesis of the target molecules. Although the results of the electrochemistry of these compounds will not be the same as that of the tetracarboxylic acid derivatives these preliminary results give an understanding of the redox processes involved. Magnesium and zinc derivatives of the protected porphyrins were also prepared and studied. By studying these compounds we will get some insight into how changes in the metal center can affect the redox potentials and communication characteristics between the ferrocenes.

3.2 Synthesis

One of the first synthetic methodologies for the preparation of porphyrins that bear substituents only at the meso-positions was proposed by Alder and Longo[51] in 1967. According to this procedure, pyrrole is reacted with the appropriate aldehyde under refluxing conditions in open air for 30 minutes (Scheme 3.1). This method is quick and easy but it has some drawbacks. The

reaction conditions are harsh and a lot of aldehydes carrying a sensitive R-group will not survive. When porphyrins carrying a mixture of different R groups in the meso-positions are desired, this method can still be used by adding multiple aldehydes. In this case, condensation in a statistical manner takes place giving a porphyrin mixture where the desired porphyrin's yield is very low. In addition, the porphyrin mixture is difficult to separate. This method is still used sometimes today especially if multi-gram quantities of the target molecules are needed.

An improved version of the Alder and Logo method was developed by Lindsey[52]. His method avoids the harsh conditions and relies on the formation of the porphyrinogen, a reduced form of the porphyrin macrocycle. The porphyrinogen equilibrates with other forms of open chain polypyrrylmethanes under the presence of an acid catalyst. Oxidation of the porphyrinogen completes the reaction. The drawback of this method is that dilution conditions in the order of

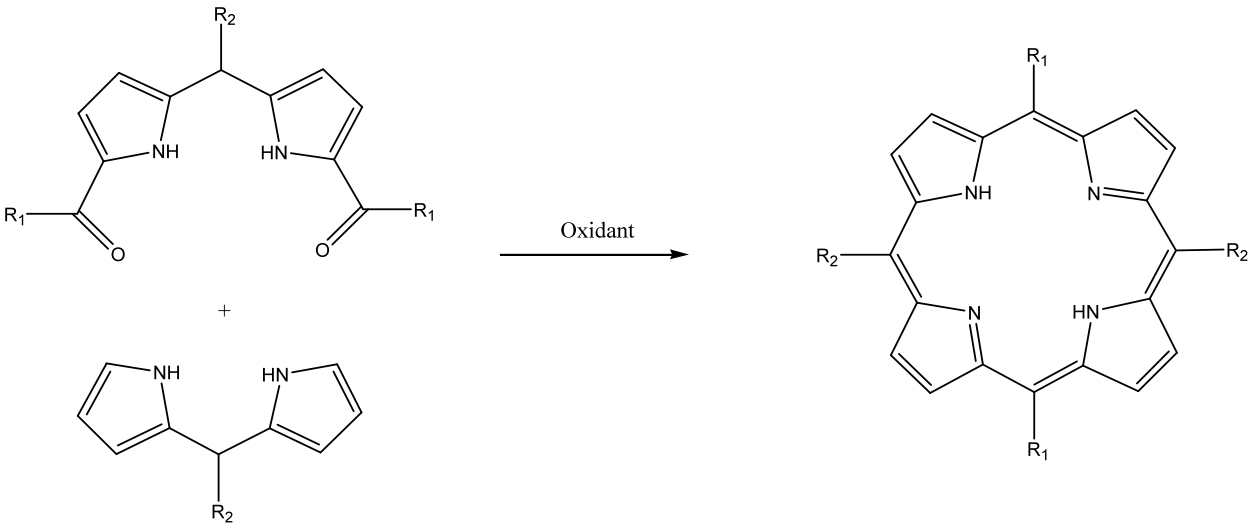


Scheme 3.1. Alder and Logo synthetic route to porphyrins.

10^{-2} M are needed in order to optimize the formation of the porphyrinogen. This inhibits attempts at large-scale synthesis.

All the porphyrins synthesized in this project belong to the trans-A_2B_2 type. This means that there are no substituents at the α- or β- pyrrolic positions and there are two pairs of substituents (A and B) at the meso-positions. The identical substituents have a trans-arrangement in respect to each other. For these types of porphyrins a synthetic route commonly called the "2+2 synthesis" was followed. This method was first pioneered by MacDonald[53] and it involves the formation of porphyrins through the condensation of two dipyrromethanes (Scheme 3.2).

This is an extension of the Lindsey's method and as such, it requires high dilution, an acid catalyst, and a final oxidation step. The reason of its preference is that it provides higher control over the final position of the R-groups at the meso-positions as lacks the statistical character of



Scheme 3.2. 2+2 porphyrin synthesis (McDonald method).

the Lindsey method. The advantage of this is that final yields can exceed 40% which is very high for porphyrin synthesis.

MacDonald's method requires the bis-formylation of a dipyrromethane. Several alternatives to that exist but the one mostly used in this project is the condensation of α-free dipyrromethanes bearing the R_1 group at the 5-position and the formylated form of R_2. The only disadvantage of this method is the probability of the occurrence of 'scrambling'[54,55] which can lead to the formation of mixtures containing all of the products that would be obtained if a statistical method was used. The extension of scrambling and the percentage of side-products in the final mixture is dependent on many factors with the principal one being the nature of the R-groups. Fortunately, in our case, scrambling happened only to a limited extend and the side-products were successfully removed.

All the final porphyrins bear isophthalic acid groups. To avoid solubility and reactivity issues across the synthetic route arising from the carboxylic acid moieties, protection of these groups in the form of their diethyl esters was essential.

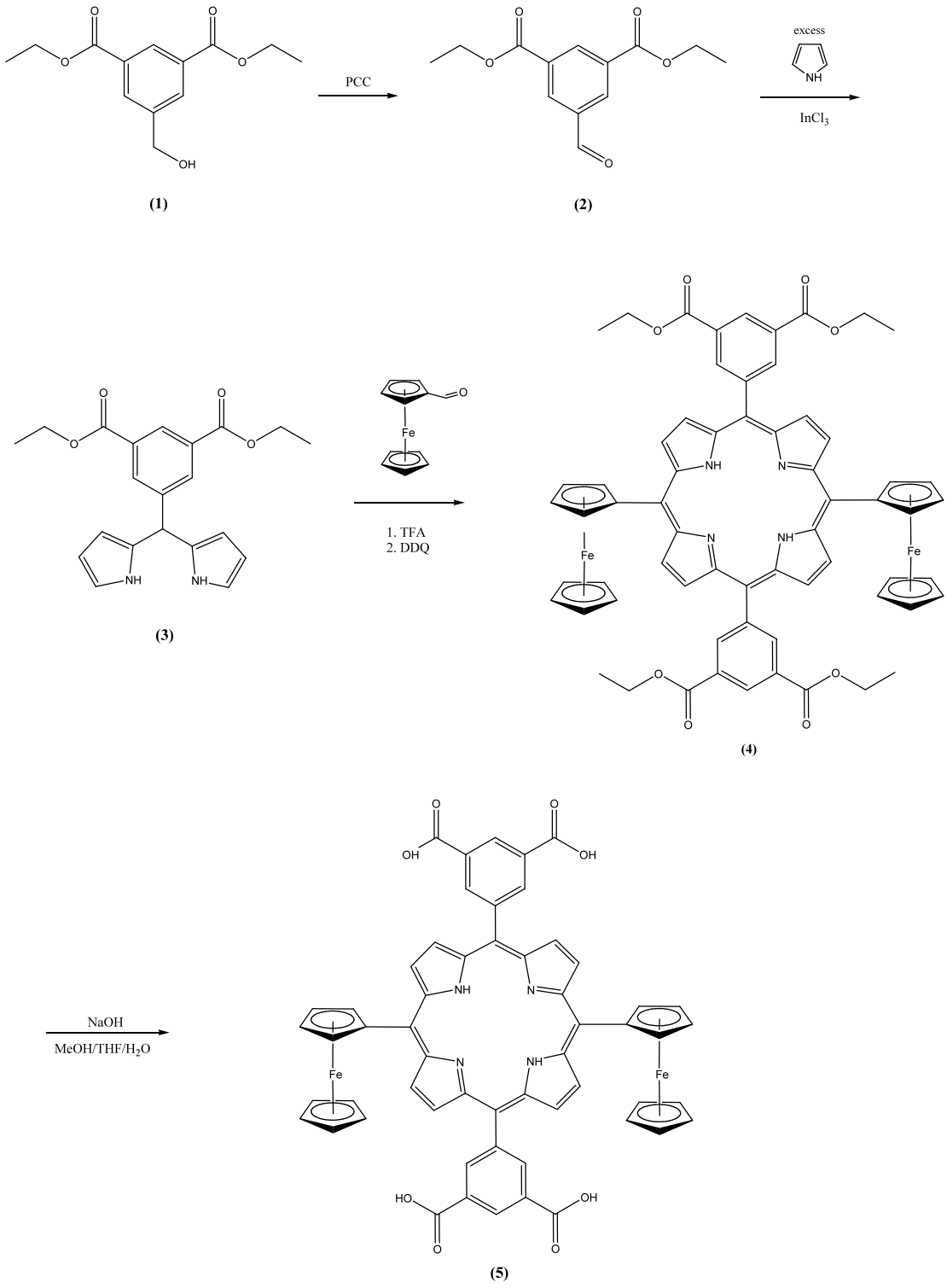
3.2.1 Synthesis of meso-5,15-bis-(isophthalic acid)-10,20-bis(ferrocenyl)-porphyrin

The synthetic route for the simplest molecule of the porphyrin series is shown in Scheme 3.3. The synthesis starts from diethyl-5-hydroxymethyl-isophthalate **(1).** This starting material was chosen because it was commercially available, already protected and one easy step away from the aldehyde **(2)**, the starting material for the dipyrromethane formation. Oxidation with pyridine chlorochromate afforded **(2)** in a very good yield.

Dipyrromethane **(3)** was synthesized using a standard procedure for dipyrromethane synthesis[56]. In this reaction pyrrole is both the reactant and the solvent. 100 equivalents of pyrrole were used and $InCl_3$ served the role of the Lewis acid catalyst. A big excess of pyrrole is used in order to decrease the formation of polypyrrolic species. $InCl_3$ has been proven to be one of the highest yielding acid catalysts in dipyrromethane synthesis. The crude product was easily purified with column chromatography affording **(3)** in a very high yield.

Porphyrin **(4)** was formed through the condensation of dipyrromethane **(3)** and the commercially available ferrocenylcarboxaldehyde. Trifluoroacetic acid was used as the acid catalyst and the reaction was left to react overnight. DDQ was used to oxidize the porphyrinogen. Purification using column chromatography on alumina afforded **(5)** which was purified further with recrystallization from dichloromethane/methanol. The product was characterized with ^{13}C and ^{1}H NMR spectroscopy, elemental analysis MALDI-TOF MS and X-Ray Crystallography.

The final step was the deprotection of **(4)** in order to form the tetracarboxylic acid derivative. Deprotection was achieved through the reaction of **(5)** with NaOH in a solvent system consisting of MeOH/THF/H_2O under refluxing conditions[57]. This solvent system proved to be ideal for the deprotection of porphyrins as well. It provided an ideal polarity for the dissolution of both NaOH and the starting material affording **(5)** in almost quantitative yield in 2 hours. Precipitation through acidification of the reaction mixture and subsequent washings with various solvents afforded a purple solid. The product was characterized with elemental analysis and MALDI-TOF MS. NMR could not be acquired because the solubility of the compound was very poor. Hot DMSO managed to dissolve very little of it but the NMR signal was very weak. MALDI-TOF MS showed only one peak at 1117.92 which is assigned to compound **(5)**. Partially deprotected mono- di- or tri-ester impurities could not be identified in the MALDI spectrum.

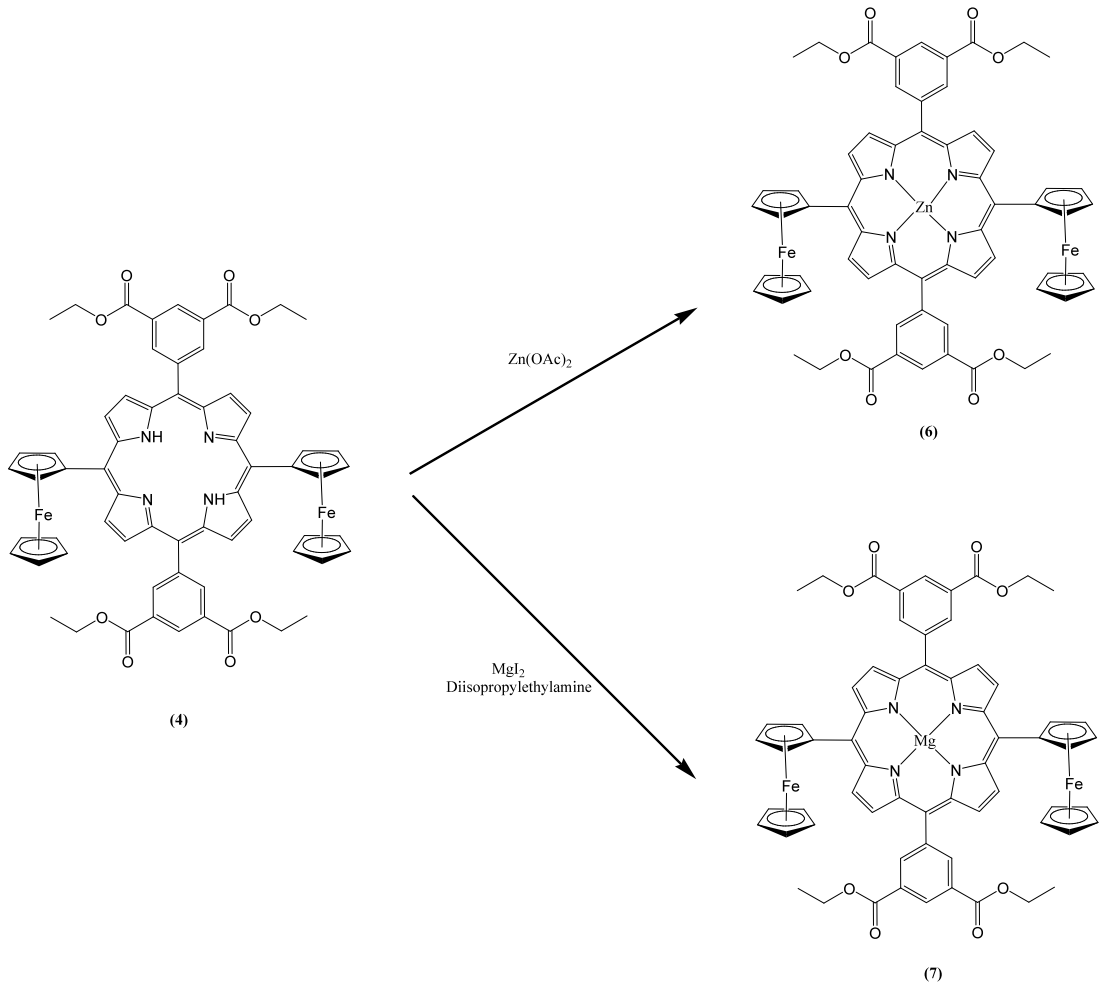


Scheme 3.3. Synthetic route of meso-5,15-bis-(isophthalic acid)-10,20-bis(ferrocenyl)-porphyrin

Zinc(II) and Mg(II) derivatives of **(4)** were successfully prepared. For the insertion of zinc, a standard procedure was followed[58]. Free-base porphyrin was stirred in a mixture of dichloromethane/methanol in the presence of zinc acetate. Application of heat was not needed in our case. Purification was accomplished through column chromatography and subsequent recrystallization from dichloromethane/methanol. The yield was almost quantitative (93%). The product was successfully characterized with elemental analysis, ^{1}H and ^{13}C NMR spectroscopies and MALDI-TOF-MS.

For magnesium(II) insertion, various methods are reported in the literature. Some of them involve the reaction of magnesium salts [$MgCl_2$, $Mg(ClO_4)_2$, $Mg(OAc)_2$] with the porphyrin in a polar solvent such as pyridine, DMF or propanol at high temperatures[59,60]. Polar solvents are typically chosen to increase the solubility of the magnesium salt. A second approach involves the reaction of porphyrins with hindered Grignard reagents acting as metallating agents at room temperature[61-63]. Anaerobic conditions and generation of the Grignard reagent immediately prior to use, are the limiting factors of this method.

More recently a heterogeneous method has been developed which facilitates the magnesium insertion and provides very high yields at room temperature and in short reaction times[59]. **(4)** was dissolved in DCM containing diisopropylethylamine and MgI_2 as the magnesium(II) salt. The suspension was stirred at room temperature and the reaction was completed in less than 30 minutes. Purification using column chromatography on alumina and subsequent recrystallization from dichloromethane/methanol yielded **(7).** The material was characterized with ^{1}H NMR, ^{13}C NMR spectroscopies, X-Ray Crystallography, MALDI-TOF MS and elemental analysis.



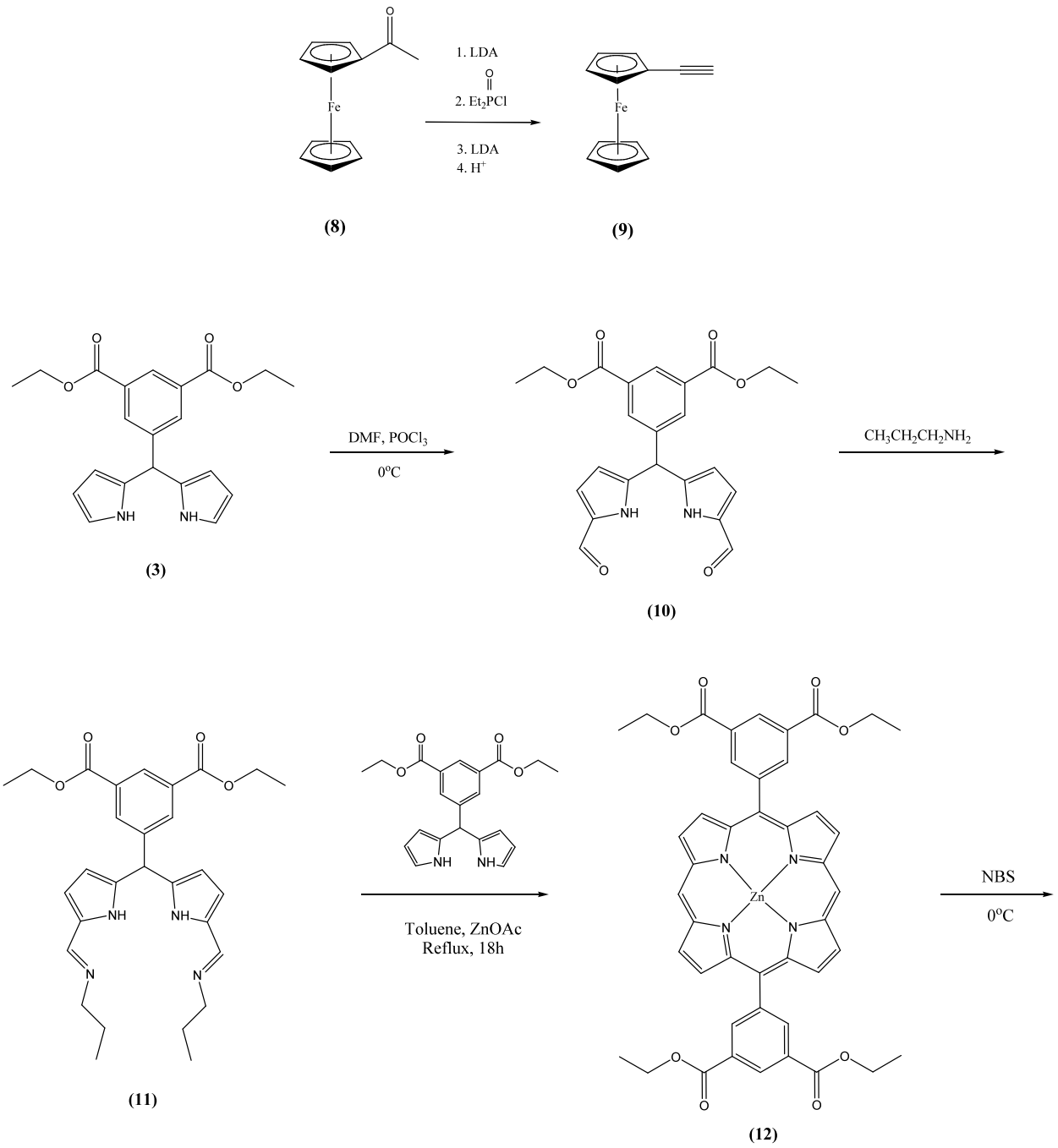
Scheme 3.4. Insertion reactions of Mg(II) and Z(II) inside the porphyrin core of (4).

The synthesis of **(5)** was straightforward and no complications were encoutnered. This was not true for the other members of the porphyrin molecules. A direct route of reacting **(3)** with ferrocenyl(formyl)acetylene to form **(15)**, see below, was unsuccessful. The presence of a triple bond attached to the porphyrin ring and the reactivity of the meso-positions resembling that of a benzene ring, supported the use of a different reaction route. (Scheme 3.5)

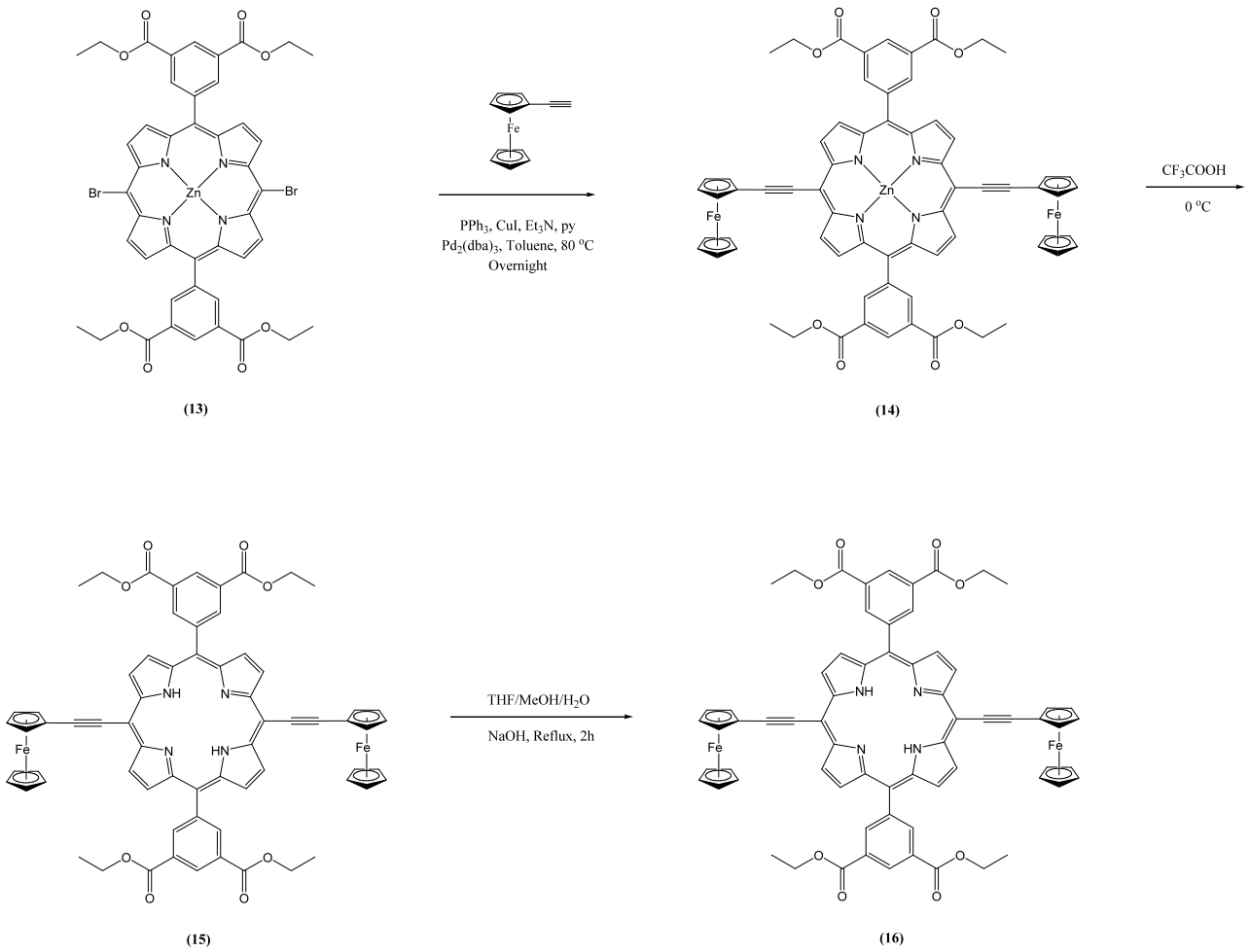
3.2.2 Synthesis of meso-5,15-bis-(isophthalic acid)-10,20-bis(ethynylferrocenyl)-porphyrin

The first step was the formation of the 10,20-unsubstituted porphyrin (**12).** A variation of the 2+2 approach was used. **(3)** was bis-formylated at the 1- and 9- position through treatment with 2 equivalents of the Vilsmeyer reagent[64]. Excess DMF needed to be fully removed by thoroughly drying the crude product for 2 days under high vacuum. DMF interacted strongly with the product during the elution through a silica column, making efficient purification impossible. The bis-formylated dipyrromethane **(10)** was reacted with propylamine in order to form the bis-imino derivative **(11)**[65]. This reaction has been shown to be almost quantitative in the past and after removal of the solvent and the excess propylamine by evaporation, the product obtained was used without any further purification in the next step.

Porphyrin **(12)** was obtained in a good yield (43%) through the reaction of dipyrromethane **(3)** with one equivalent of its bis-imino derivative **(11).** In this case, zinc(II) served as a template in order to assist the formation of the porphyrinogen[65]. The reaction was carried out in refluxing toluene in open air and the extended reaction time assured the oxidation of the porphyrinogen by atmospheric oxygen. Purification using column chromatography was tedious since the harsh reaction conditions produced a lot of byproducts that co-eluted with the desired molecule. The product was further purified through recrystallization from dichloromethane/methanol. Although **(12)** is a zinc(II)-porphyrin, no action was taken to remove the zinc cation because in the end we would have to re-metallate **(15)** in order to get **(14)** which is one of the target molecules of this project.

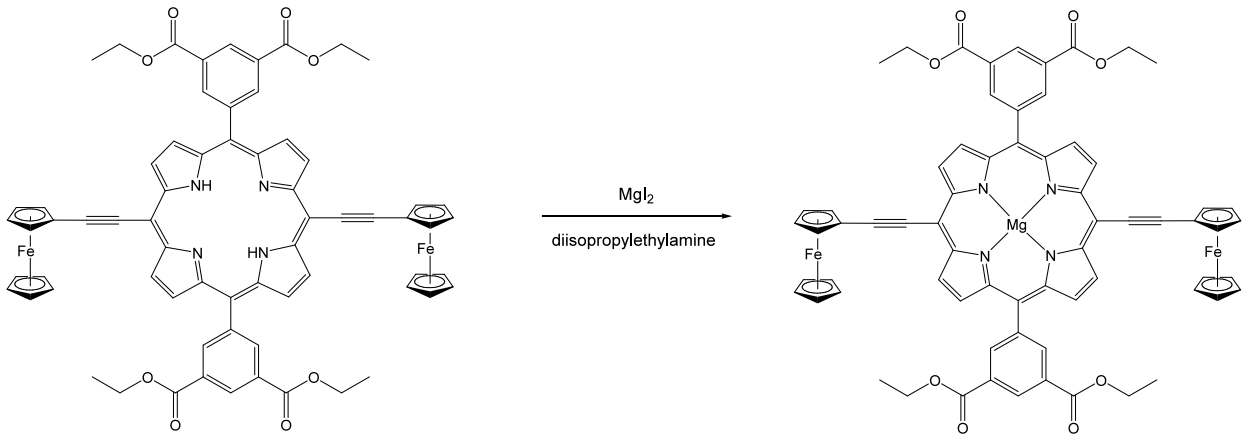


Scheme 3.5. Synthetic route of meso-5,15-bis-(isophthalic acid)-10,20-bis(ferrocenyl-ethynyl)-porphyrin



Scheme 3.5. (Continuation)

The next step was the bromination of positions -10 and -20 in order to form the di-bromo derivative (**13)**. N-bromosuccinimide was used as the brominating agent[66]. Under the conditions used, **(12)** showed a preference in selective bromination of the meso-positions. This is not always the case as will be seen later, where the α- and β- positions of the pyrrolic subunits can be brominated as well.



Scheme 3.6. Insertion reaction of Mg(II) into the porphyrin core of (15)

The porphyrin core shows similar reactivity with benzene thus, bromo-porphyrins can undergo palladium-catalyzed reactions for the formation of C-C bonds. In our case, the Shonogashira cross coupling reaction conditions have been employed. **(13)** was coupled with ethynyl-ferrocene **(9)** which was synthesized using a previously reported route via a two-step one-flask reaction from the readily available acetyl-ferrocene. Triethylamine was used as a base and CuI as the co-catalyst. $Pd_2(dba)_3$ was the chosen form of catalyst employed and PPh_3 was added separately to the reaction mixture in order for the active catalyst to be formed. The product was purified by chromatography and further recrystallization from dichloromethane/methanol. The molecular structure of **(14)** was verified with ^{1}H NMR and ^{13}C NMR spectroscopy, MALDI-TOF MS, elemental analysis and X-Ray crystallography.

Treatment of **(14)** with trifluoroacetic acid[67] afforded the free-base porphyrin **(15).** The product was purified using column chromatography on silica gel with subsequent recrystallization from dichloromethane/methanol. The molecular structure was verified with ^{1}H NMR and ^{13}C NMR spectroscopy, MALDI-TOF MS, elemental analysis and X-Ray crystallography.

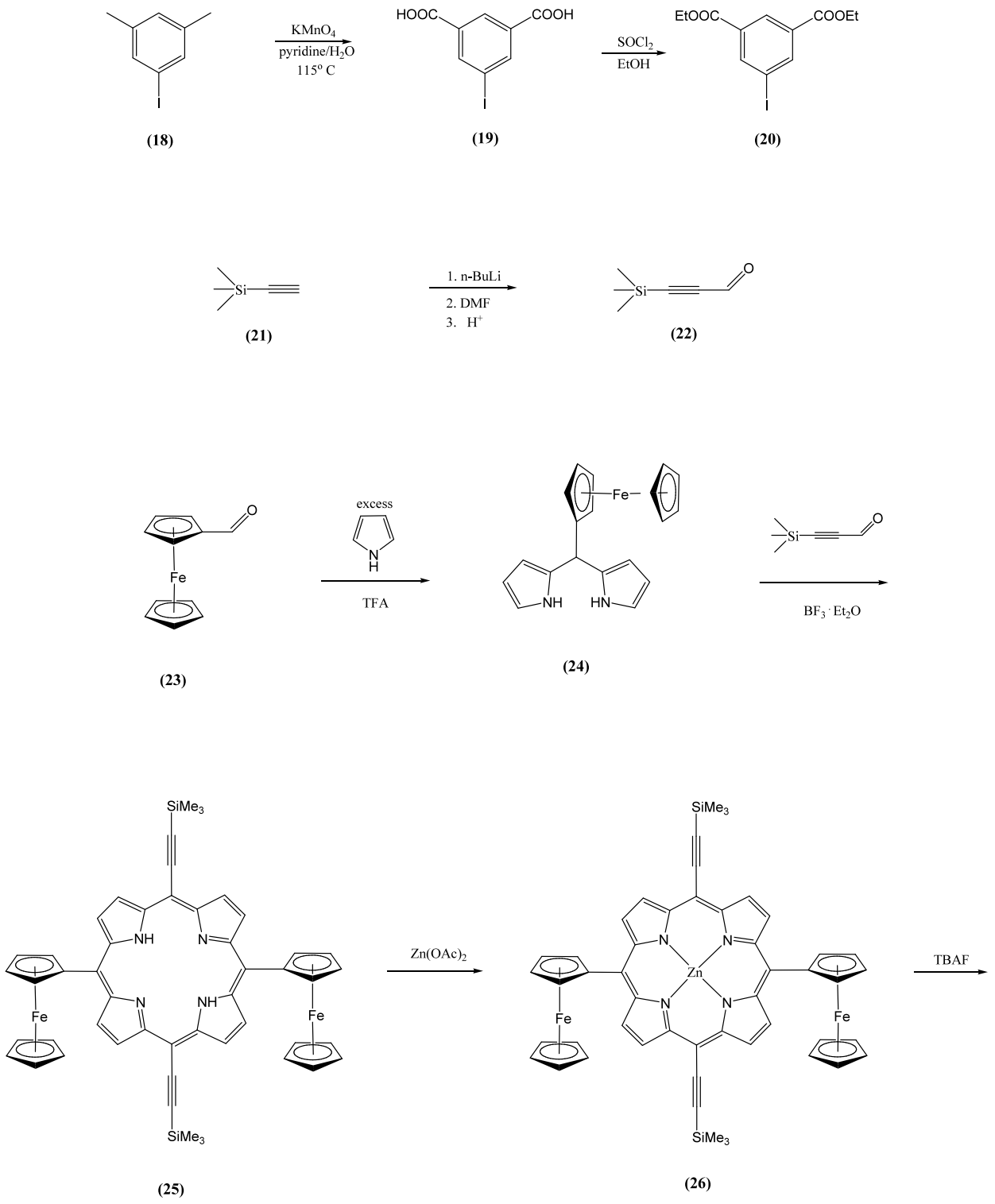
Insertion of magnesium (II) was carried out using the same heterogeneous reaction described above. Chromatographic purification was carried out using an alumina stationary phase followed by recrystallization, using dichloromethane/methanol and afforded **(17)** in an almost quantitative yield. The product was characterized with ^{1}H NMR and ^{13}C NMR spectroscopy, MALDI-TOF MS, elemental analysis and X-Ray crystallography.

A similar procedure used for the deprotection of **(4)** was also applied in this case. Treatment of **(15)** with NaOH in THF/MeOH/H_2O afforded **(16)** in an almost quantitative yield. Characterization by elemental analysis, MALDI-TOF MS and ^{1}H NMR spectroscopy confirmed the nature of the product. In this case, although **(16)** was extremely insoluble as well, by heating it in DMSO we were able to acquire a solution concentrated enough for ^{1}H NMR analysis.

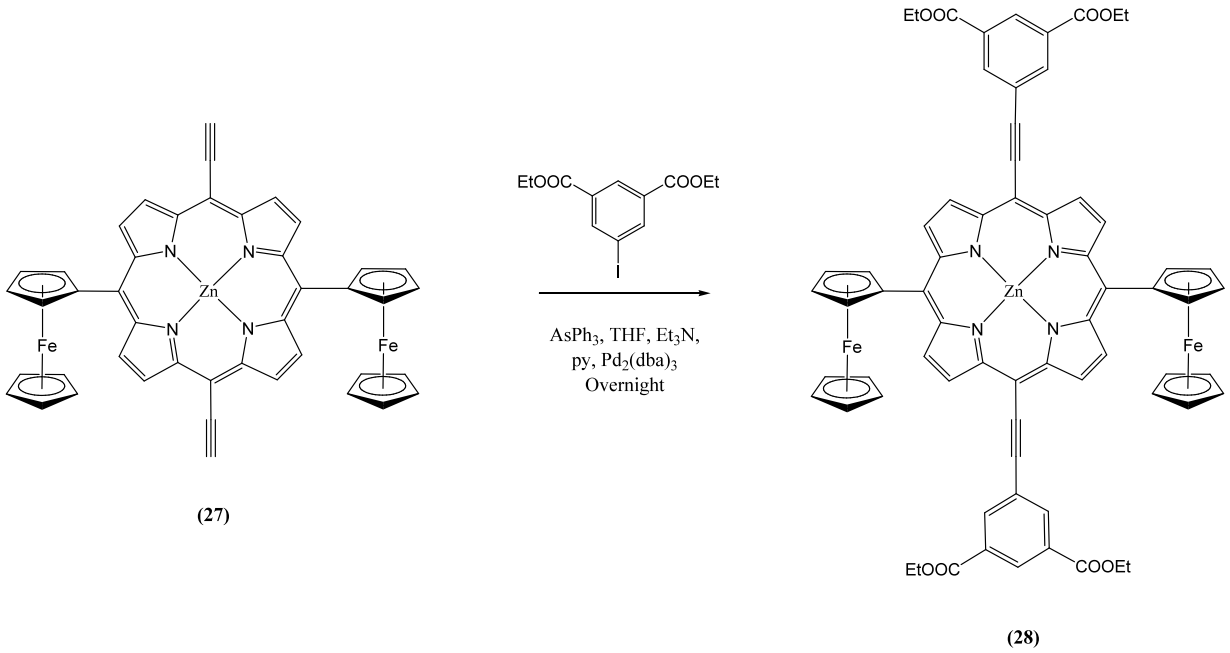
3.2.3 Synthesis of meso-5,15-bis-(5-ethynylisophthalic acid)-10,20-bis(ferrocenyl)-porphyrin

In the case of the synthesis of the series of porphyrins possessing a triple bond spacer between the porphyrin core and the phenyl rings, problems in the stability of the key product **(29)** were encountered. The synthetic route is depicted in Scheme 3.7.

The synthesis starts with the formation of 5-ferrocenyldipyrromethane **(24)**. This compound has been synthesized in the past and the exact literature procedure, involving condensation of pyrrole with ferrocenylcarboxaldehyde, was followed[68]. Porphyrin formation using trimethylsilyl-propynal **(22)** as an aldehyde in the condensation reaction is a well known technique for the introduction of the ethynyl groups in two opposite meso-positions. Trimethylsilylpropynal has

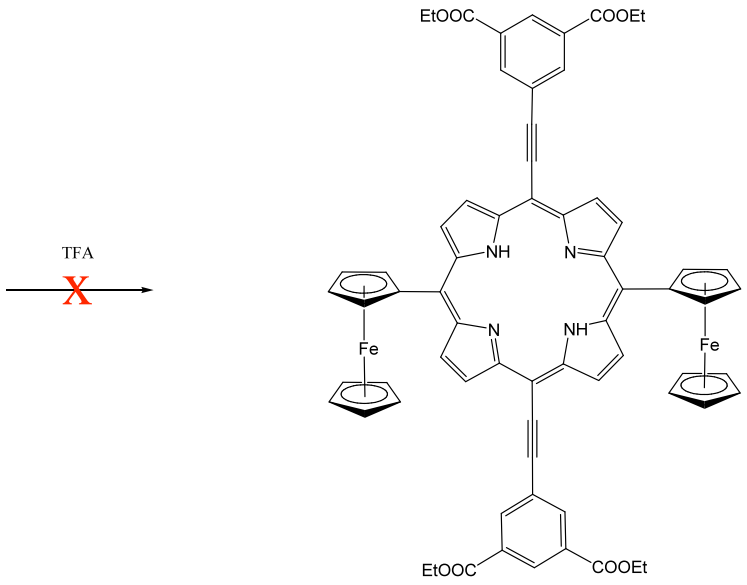


Scheme 3.7. Synthetic route of meso-[5-15-bis-[3,5-bis-(ethoxycarbonyl)-ethynyl]-10,20-bis-ferrocenyl-porpyrin



(27)

(28)



(29)

Scheme 3.7. (Continuation)

been prepared following standard literature methods[69] with slight modifications. Condensation of trimethylsilylpropynal with **(24)** led to the successful formation of porphyrin **(25).**

The removal of the trimethylsilyl-groups in order to form terminal alkynes suitable for Shonogashira cross-coupling reactions is routinely done under treatment with tetrabutylammonium fluoride (TBAF). Reaction of **(25)** with TBAF led to the isolation of the desired product in a very poor yield (6%). To avoid this loss of compound we prepared the zinc(II) analog of **(25)**. Upon treatment of this compound with TBAF **(27)** was isolated in 91% yield.

5-iodo-diethylisophthalate **(20)** was used as the aryl halide in the Sonogashira coupling with **(27).** This compound was prepared from the commercially available 1,3-dimethyliodo benzene. The methyl groups were oxidized with potassium permanganate in a water-pyridine mixture and isophthalic acid **(19)** was isolated in a pure state upon acidification of the reaction medium. **(19)** was transformed into its diethyl-ester derivative following a two-step one-flask reaction with $SOCl_2$ in ethanol. Ethanol in this case was used both as a reagent and as a solvent.

For the Shonogashira reaction between **(27)** and **(20)** different conditions were used. $Pd_2(dba)_3$ was used as the pre-catalyst and $AsPh_3$ was added for the formation of the catalytically active palladium complex. Et_3N was used as the base and the reaction was done in THF. In this case, a copper iodide co-catalyst was not used and the reaction was performed at room temperature due to the higher reactivity of iodine. The product was purified over alumina and subsequently recrystallized from dichloromethane/methanol. The molecular formula of **(28)** was verified with ^1H NMR and ^{13}C NMR spectroscopy, elemental analysis and MALDI TOF MS.

Further reaction of **(28)** with trifluoroacetic acid in order to form the free-base porphyrin **(29)** gave a product that was very unstable and after purification, rapid decomposition took place making definitive identification impossible. No relationship between decomposition and light or temperature was found. The decomposed product was a purple insoluble material. This material was immobile upon elution on a TLC plate. The fact that its colour remained purple indicates that the porphyrin ring is maintained. It is therefore hypothesized that polymerization involving the triple bonds takes place. Unfortunately, the freebase porphyrin was essential for both the formation of the magnesium(II) derivative for spectroelectrochemical studies and the tetracarboxylic acid derivative for surface deposition studies. As a result we were not able to synthesize these two compounds.

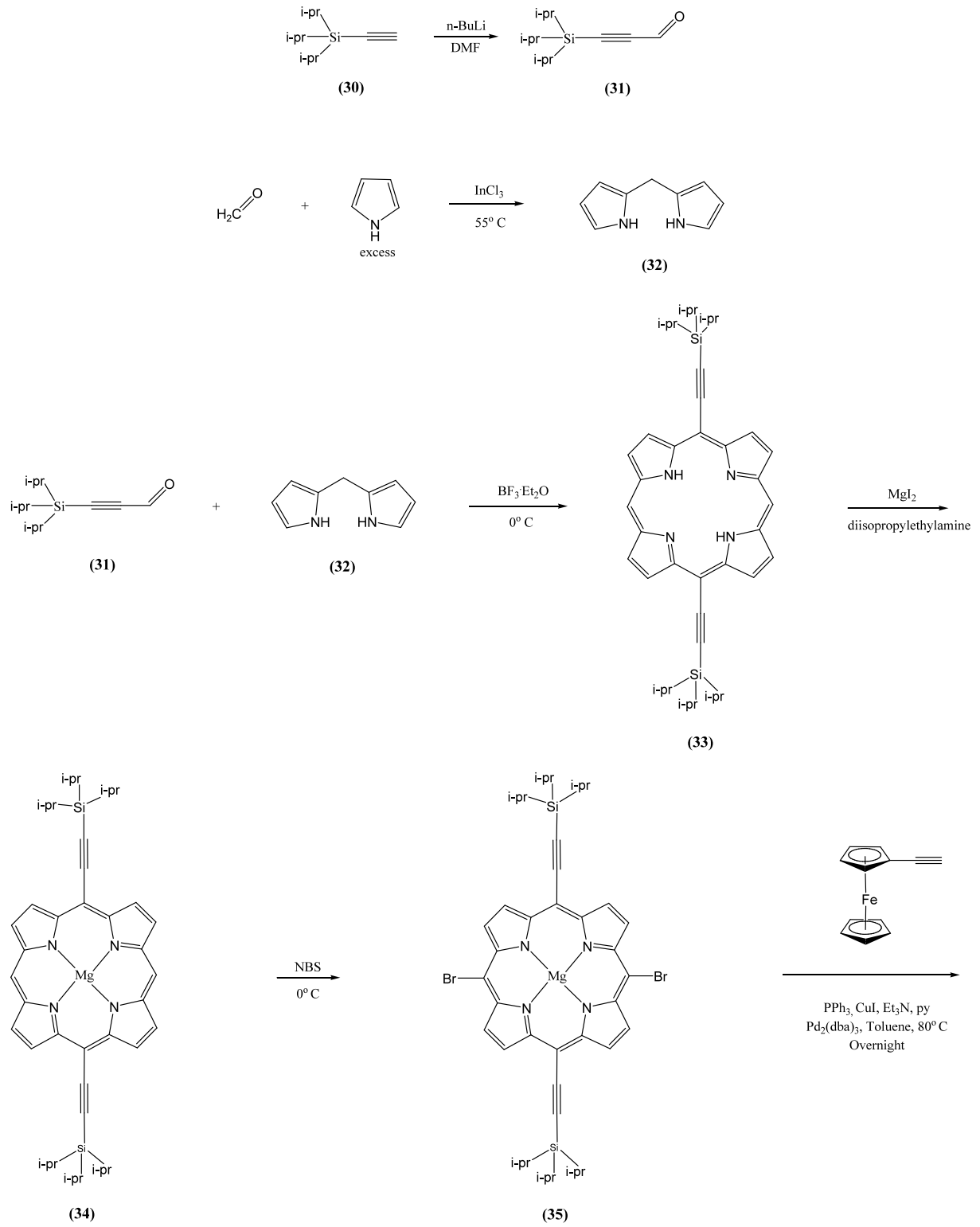
3.2.4 Synthesis of meso-5,15-bis-(5-ethynylisophthalic acid)-10,20-bis-(ethynylferrocenyl)-porphyrin

The final groups of porphyrins are those that have the acetylene spacer in all four meso-positions. For the realization of such a compound, both techniques for the introduction of triple-bonds discussed earlier were applied to the same molecule. The two methods being the introduction of the triple bond during formation of the porphyrin ring and introduction of the triple bond through Sonogashira coupling of the meso-brominated porphyrin. The necessity for this comes from the fact that the groups attached in adjacent triple bonds are different and we needed to differentiate the way they are introduced in the synthetic pathway because a statistical method is likely to give a very low yield and a crude mixture that would be very difficult to

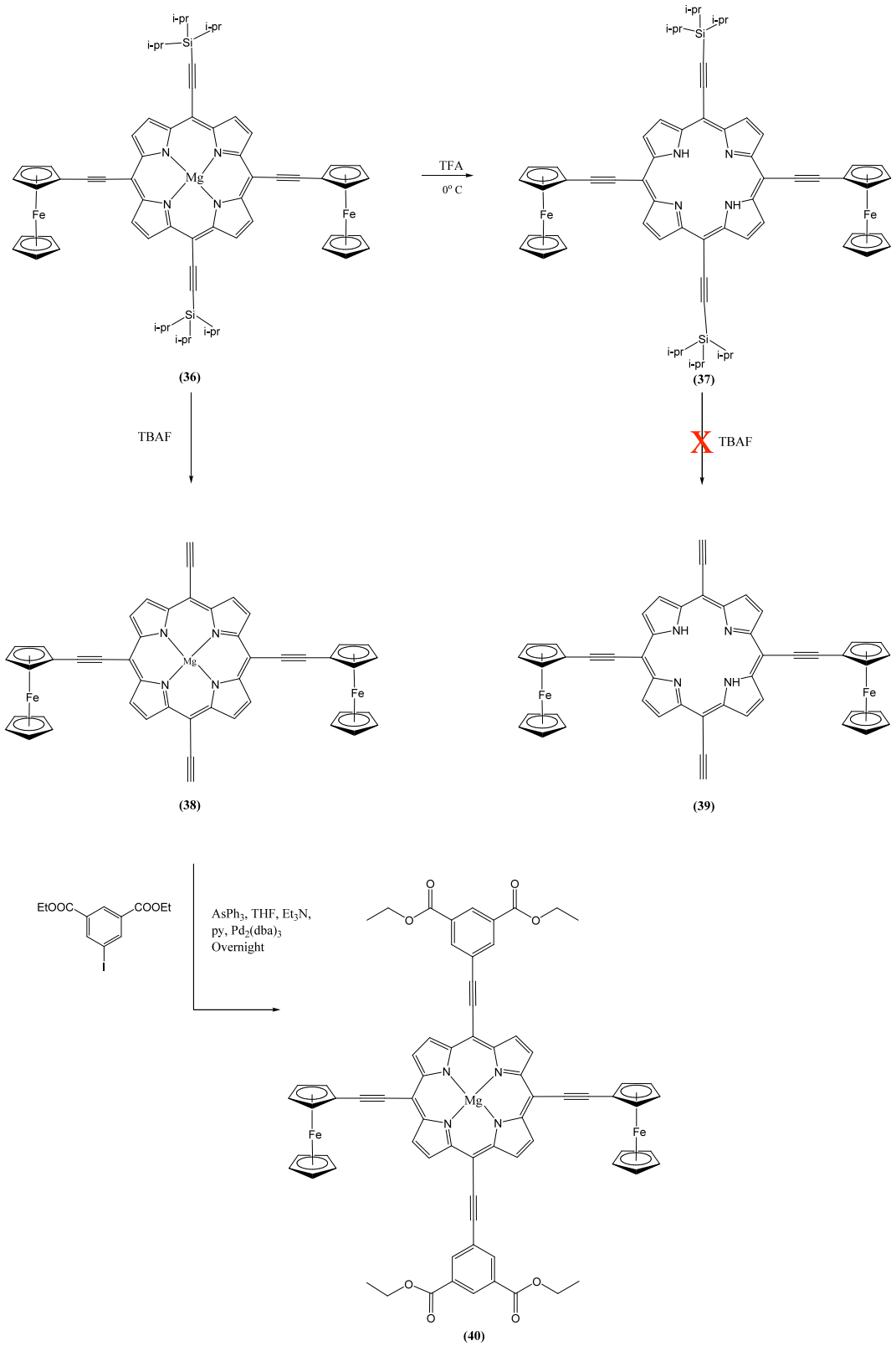
separate. The synthetic route followed is depicted in Scheme 3.8. For the initial porphyrin formation, 5-unsubstituted dipyrromethane **(32)** and triisopropylsilylpropynal **(31)** were used. Dipyrromethane was synthesized by condensation of pyrrole with formaldehyde, which was generated by heating paraformaldehyde. Triisopropylsilylpropynal was synthesized by formylation of commercially available triisopropylsilyl acetylene with n-BuLi and DMF[70].

Porphyrin **(33)** was successfully synthesized upon condensation of **(31)** and **(32)** using $BF_3 \cdot Et_2O$ as the acid catalyst. Oxidation of the porphyrinogen was carried out using DDQ and the crude product was purified on a silica gel column. Bromination of **(33)** would lead to a dibromo-porphyrin suitable for the introduction of the ferrocenyl groups through Sonogashira coupling. The problem with this compound was that unlike **(12)**, bromination of **(33)** was not selective in the meso-positions and α- and β- positions of the pyrrolic sub-units were brominated easily giving a crude material containing inseparable poly-brominated products. Experimentation with the more readily obtainable trimethylsilyl-substituted derivative showed that the poly-brominated products were impossible to separate. Effort was also placed on affecting the selectivity of the bromination sites by incorporating different metal centers in the porphyrin cavity. The results were unsatisfactory.

A literature procedure, employing the magnesium(II) analog of **(33)** for the successful preparation of the dibromo-derivative[71], was followed. Metallation of **(33)** in order to form **(34)** was carried out with the heterogenous procedure described above. The literature method for the preparation of **(35)**, which stated that two equivalents of NBS were needed, proved unsuccessful. The literature report argued that because the α- and β- positions of the pyrrolic sub-units were less reactive than the desired meso-positions they were able to separate the product as, upon



Scheme 3.8. Synthetic route of meso-[5-15-bis-[3,5-bis-(ethoxycarbonyl)-ethynyl]-10,20-bis-ethynylferrocenyl-porpyrin



Scheme 3.8. (Continuation)

purification, polybrominated compounds were eluted at a slower pace. In our hands the mono- and di-brominated products eluted at the same rate and thus were not possible to separate. By very slowly adding 3.2 equivalents of NBS to the reaction mixture this problem was overcome. Our approach ensured that all of the mono-bromo derivative had reacted at the expense of the loss of the desired product as the excess of NBS was reacting with **(35)** to form polybrominated byproducts. The final yield dropped to 58%.

Ethynylferrocene was successfully introduced by employing the same reaction conditions used for **(13)**. In this case though, **(35)** was much more reactive and the reaction was completed in under 2 hours and with temperature held at 60^{o} C instead of the 80^{o} C used for **(13).** Deprotection of **(36)** with TBAF afforded **(38).** Due to the steric hindrance of the triisopropylsilyl group, the deprotection reaction took much longer to complete than the analogous trimethylsilyl species. Coupling of **(38)** with **(20)** was done employing the conditions used previously for the copper-free Sonogashira coupling. Although the TLC indicated that the reaction had gone to completion, a pure product could not be obtained. Although MALDI-TOF MS confirmed the presence of **(40)** the NMR showed peaks from byproducts that we were not able to separate.

Demetallation of **(36)** was tried as an attempt to synthesize the free-base derivative of **(40)** with the anticipation that this would be easier to purify. Unfortunately upon deprotection of the freebase porphyrin **(37)**, the purple solid obtained could not be redissolved in any solvent. Here, again, a decomposition involving triple bond polymerization is suspected to have taken place.

The synthetic efforts for the prepration of the compounds that could not be obtained are not to be considered finished. More routes can be envisaged, applied and have their efficiency tested. Unfortunately this could not happen during the timescale of this project.

3.3 Crystallographic analysis

Crystal structure of (7) · 2MeOH

Single crystals of **(7)** suitable for X-Ray structure analysis were obtained by layering methanol onto a concentrated solution of **(7)** in dichloromethane. A perspective view of the molecular structure of **(7)** and the atom numbering scheme is illustrated in Figure 3.7. The molecule crystallizes with two molecules of methanol in the triclinic space group P-1 (Table 3.1). Because the molecule lies on an inversion center, the asymmetric unit contains only one half of the centrosymmetric molecule. The hydrogen atom of the methanol hydroxyl group was located in the difference map and allowed to refine with its thermal displacement parameter fixed at 1.5 times that of its parent atom. Geometric constraints (DFIX) were applied to the distances between O1A-H1A (0.87 Å) and C2A-H1A (1.91 Å). Surprisngly the hydroxyl group does not donate a hydrogen bond to a traditional acceptor group, instead it is directed towards the cyclopentadienyl ring C45-C49 (H1A-centroid distance 2.52 A). All other hydrogen atoms were geometrically placed and refined using a riding model.

The porphyrin core is slightly deformed and shows a small deviation from planarity with 0.1 Å being the mean deviation of atoms from the porphyrin $C_{20}N_4$ plane and 0.2 Å being the furthest location of an atom away from the porphyrin $C_{20}N_4$ plane. The carbons at the meso-positions (C4, C10) are located on the mean plane of the porphyrin and the core distortion is characteristic of a saddled deformation. Both phenyl rings are planar and tilted at an angle of $70.25(4)^{o}$ (C5-C10-C31-C36) towards the mean plane of the porphyrin core.

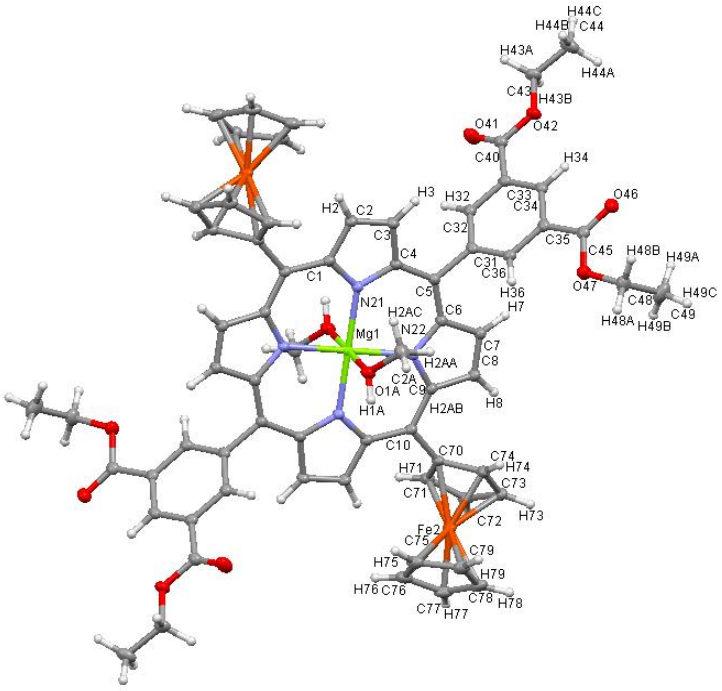


Figure 3.7. A view of molecule (7) · 2MeOH showing the atom labeling scheme. Displacement ellipsoids are drawn at the 50% probability level.

The cyclopentadienyl rings are tilted at an angle of 55.32(5)^{o} with respect to the mean plane of the porphyrin. The Cp rings of each ferrocenyl unit are eclipsed, forming an angle of 8.39(7)^{o} with respect to each other. All the C-C and C-Fe bond lengths are almost identical. The iron cation lies at distances of 1.6594(7) Å and 1.6513(8) Å from the two Cp rings centroids, the longer distance being the Cp ring attached to the porphyrin. The two ferrocenyl units adapt an anti-configuration with respect to each other.

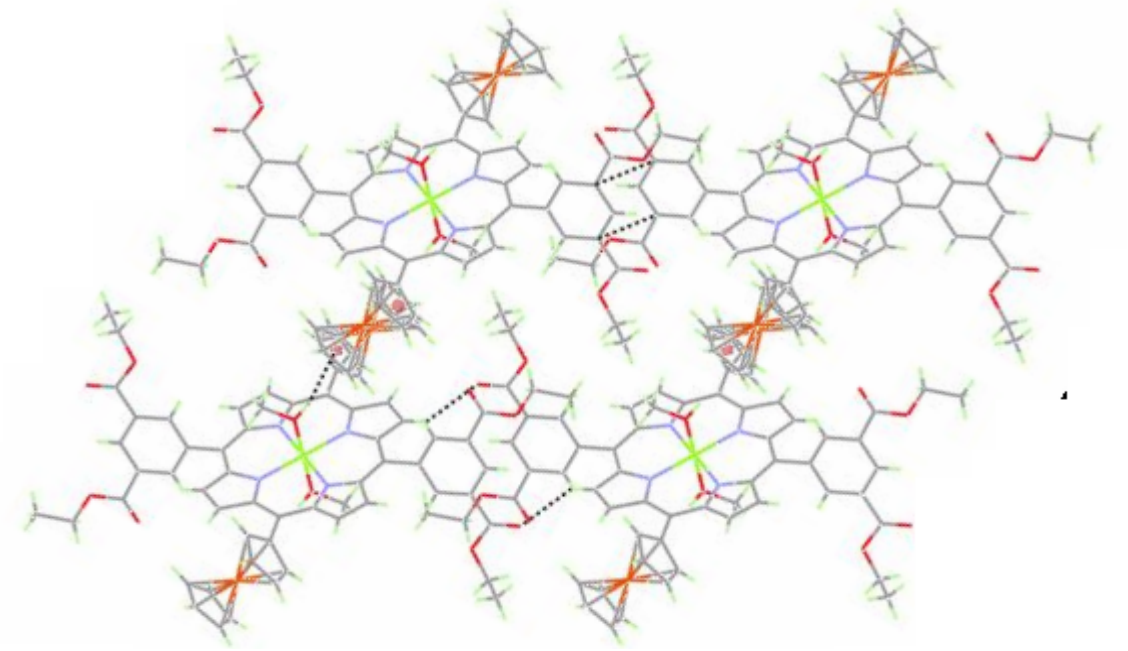


Figure 3.8. Crystal packing of (7) · 2MeOH. π-π stacking, C-H…π interactions and hydrogen bonding are represented as black dashed lines. Hydrogens are coloured green for clarity.

Examination of the crystal packing shows three principle interactions. π-π stacking between the phenyl rings of two adjacent molecules, C-H…π interactions between the hydrogen of the hydroxyl group of the methanol molecule and the Cp ring of the ferrocene and finally, a hydrogen bond between a hydrogen of the porphyrinic core and a carbonylic oxygen of the ester group (Figure 3.8).

Crystal structure of (17) · 6MeOH

Single crystals of **(17)** suitable for X-Ray structure analysis were obtained by layering methanol onto a concentrated solution of **(17)** in dichloromethane. A perspective view of the molecular structure of **(17)** and the atom numbering scheme is illustrated in Figure 3.9. The molecule crystallizes with six molecules of methanol in the monoclinic C2/c space group (Table 3.2). The molecule lies on an inversion center and the asymmetric unit contains only one half of the centrosymmetric molecule. The hydroxyl hydrogen atoms of the methanol molecules were located in the electron difference map and their positions allowed to refine. Their isotropic thermal parameters have been fixed at 1.5 times that of their parent oxygen atoms. The O-H distances of all three methanol molecules have been constrained (DFIX) to 0.84 Å. The C-O distances of methanol molecules B and C have been constrained (DFIX) to 1.40 Å. All other hydrogen atoms in the structure were observed in the electron difference map before being geometrically placed and refined using a riding model. Disorder was observed in the ethoxy group of ester O47-O49. The moiety was modeled in two orientations with the occupancy of residue A being refined to 0.49 and the sum of the two residues constrained to refine to unity. The C-O, O-C and C-C distances along each ethoxy chain were constrained (DFIX) to have values of 1.4 Å, 1.45 Å and 1.50 Å respectively. The thermal displacement parameters of the disordered residues were refined isotropically. Rigid bond and similarity restraints (DELU, SIMU) have been applied to the anisotropic displacement parameters of all atoms in the structure.

The porphyrin core is almost planar with a negligible deviation from planarity compared to the porphyrin $C_{20}N_4$ plane with 0.1 Å being the furthest location of an atom away from the mean porphyrin plane.

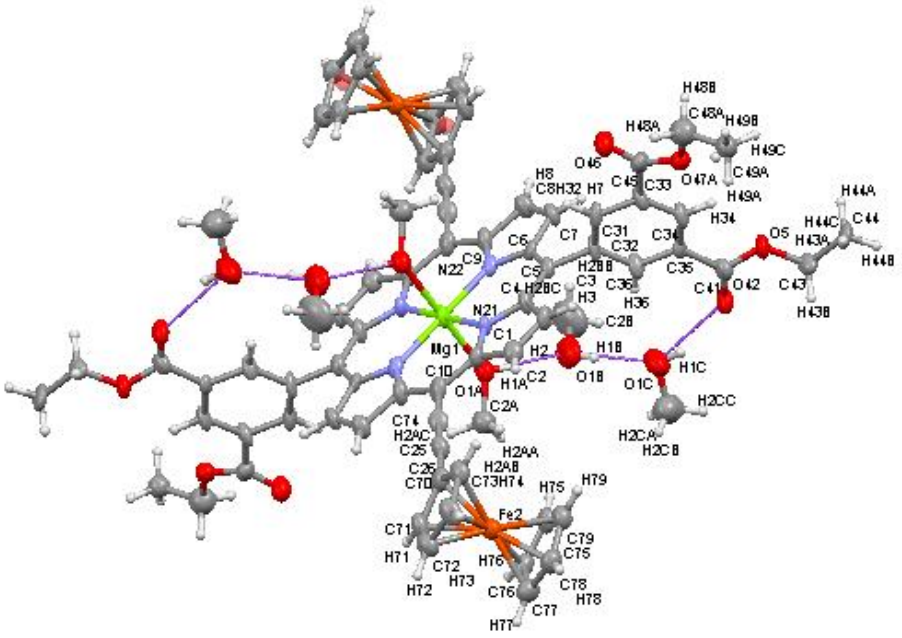


Figure 3.9. A view of molecule (17) · 6MeOH showing the atom labeling scheme. Displacement ellipsoids are drawn at the 50% probability level. The hydrogen bonds between the methanol molecules are highlighted in purple.

Both phenyl rings are planar and tilted at an angle of 78.3(2)^{o} with respect to the mean plane of the porphyrin core.

The cyclopentadienyl rings are tilted at an angle of 30.0(3)^{o} with respect to the mean plane. The Cp rings of each ferrocenyl unit are eclipsed and almost planar forming an angle of 0.4(4)^{o} with respect to each other. All the C-C and C-Fe bond lengths are almost identical within the molecules and the iron cation lies at distances of 1.642(5) Å and 1.659(5) Å from the Cp ring centroids, the longer distance being that to the unsubstituted Cp ring. The two ferrocenyl units adapt an anti-configuration across the porphyrin core.

Three methanol molecules lie on each side of the porphyrin plane. Methanol A is directly coordinated at the axial coordination site of the magnesium metal. The other two molecules are forming hydrogen bonds with the oxygen atom of one methanol molecule acting as the acceptor of the hydrogen of the hydroxyl group of the neighboring methanol. This leads to a small chain which terminates with the hydroxyl hydrogen of methanol C bonding with a carbonyl oxygen of an ester group of the same molecule (Figure 3.9).

Examination of the crystal packing shows a variety of interactions. There is a π-π stacking between the unsubstituted Cp ring of the ferrocene and one of the pyrrolic rings of an adjacent porphyrin. C-H…π interaction is also observed between hydrogens of the methyl groups of the

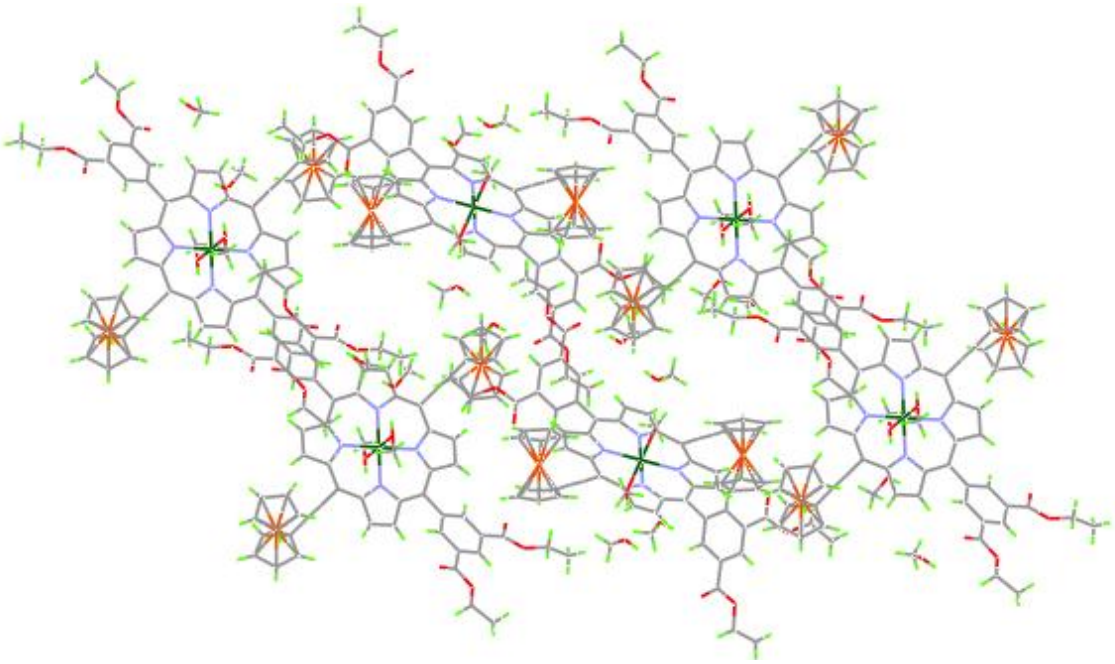


Figure 3.10. Illustration of crystal packing of (17) · 6MeOH. Hydrogens are coloured green for clarity.

methanol molecules and the Cp ring of neighboring porphyrin. There is also a weak hydrogen bond between a hydrogen of a Cp ring and a carbonyl oxygen of an ester group. Figure 3.10 illustrates the crystal packing of **(17)**.

Crystal structure of molecule (14)

Single crystals of **(14)** suitable for X-Ray structure analysis were obtained by layering methanol onto a concentrated solution of **(14)** in dichloromethane. A perspective view of the molecular structure of **(14)** and the atom numbering scheme is illustrated in Figure 3.11. The molecule crystallizes in the triclinic space group P-1 (Table 3.3). Because the molecule lies on an inversion center, the asymmetric unit contains two "half" porphyrin molecules in a parallel arrangement and a third molecule at a 68^{o} angle from the plane of the other two subunits. All non-metal atoms have been refined with isotropic thermal displacement parameters owing to weak data as a result of a weakly diffracting crystal. Rigid bond and similarity restraints (DELU, SIMU) have been applied to the thermal displacement parameters of all atoms in the structure. Hydrogen atoms have been geometrically placed and refined using a riding model.

The porphyrin core is slightly deformed and shows a small deviation from planarity with 0.11 Å being the furthest location of an atom away from the porphyrin $C_{20}N_4$ plane. The carbons at the meso-positions (C5A, C10A, C15A, C20A) are located on the mean plane of the porphyrin and the core distortion shows characteristics of a propeller deformation. The phenyl rings are fairly planar. With the asymmetric unit containing three porphyrin molecules the phenyl rings are tilted at an angle that ranged between 59.71(13)^{o} and 60.69(11)^{o} towards the mean plane of the porphyrin core.

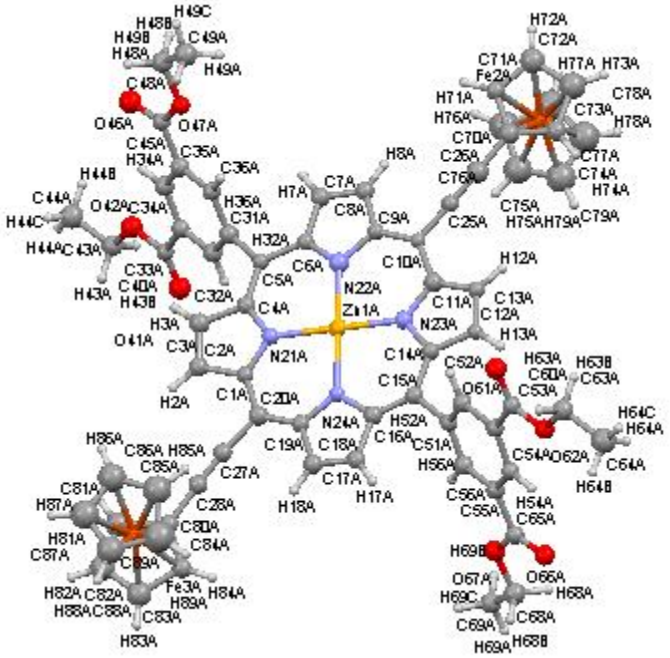


Figure 3.11. A view of the crystal structure of molecule (14) showing the atom labeling scheme. Displacement ellipsoids are drawn at the 50% probability level.

Similarly, the cyclopentadienyl rings are tilted at an angle that ranges between 11.96(19)^{o} and 13.36(17)^{o} in respect to the mean plane of the porphyrin. The Cp rings of each ferrocenyl unit are held in an almost eclipsed conformation and they lie almost parallel with respect to each other. The iron cation lies at 1.627(4) Å and 1.648(3) Å respectively from the Cp rings centroids with the longer distance relating to the Cp ring attached to the porphyrin. The two ferrocenyl units adapt an anti configuration with respect to each other.

Examination of the crystal packing shows a variety of interactions. π-π stacking between the pyrrolic subunits of neighboring porphyrin molecules, π-π stacking between the Cp of the ferrocene groups and the porphyrin core and C-H…π interactions between hydrogens and π-systems of phenyl rings as well as Cp rings are highlighted in Figure 3.12 as selected examples.

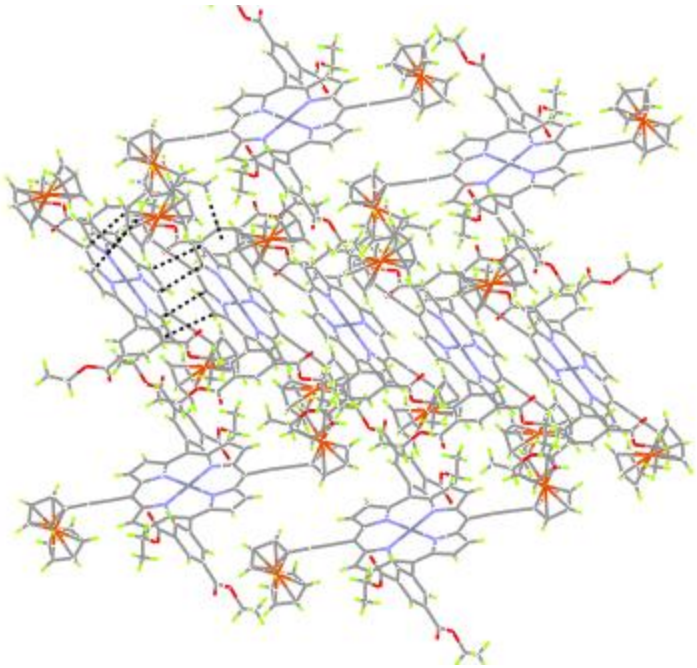


Figure 3.12. Crystal packing of (14). π-π stacking and C-H…π interactions are represented as black dashed lines. Hydrogens are coloured green for clarity.

Crystal structure of (4) – $2H^+$

Single crystals of **(4)** suitable for X-Ray structure analysis were obtained by layering methanol onto a concentrated solution of **(4)** in dichloromethane. A perspective view of the molecular structure of **(4)** and the atom numbering scheme is illustrated in Figure 3.13. The molecule crystallizes in the monoclinic space group $P2_1/n$ (Table 3.4). Because the molecule lies on an inversion center, the asymmetric unit contains only one half of the centrosymmetric molecule. Owing to weak data all non-metal atoms have been refined with isotropic displacement parameters. Rigid bond and similarity restraints (DELU, SIMU) have been applied to the thermal

displacement parameters of all atoms in the structure. Ferrocenyl cyclopentadienyl ring C75-79 is disordered over three positions whose occupancies have been restrained to sum to a value of 1.00 (SUMP) with occupancies of 0.31, 0.28 and 0.24. All cyclopentadienyl rings in the structure have been constrained to be regular pentagons (AFIX 56). Ethyl group C48-C49 is disordered over two positions whose occupancies have been restrained to a sum of 1.0 (occupancy of 0.58 for the major component). Similarity restraints (SADI) have been applied to the bond lengths of these ethyl groups. PLATON SQUEEZE has been applied to the data to remove the scattering contribution from disordered solvent moieties and produce a set of solvent-free diffraction intensities for the final cycles of refinement. A total of 81 electrons were removed from the cell.

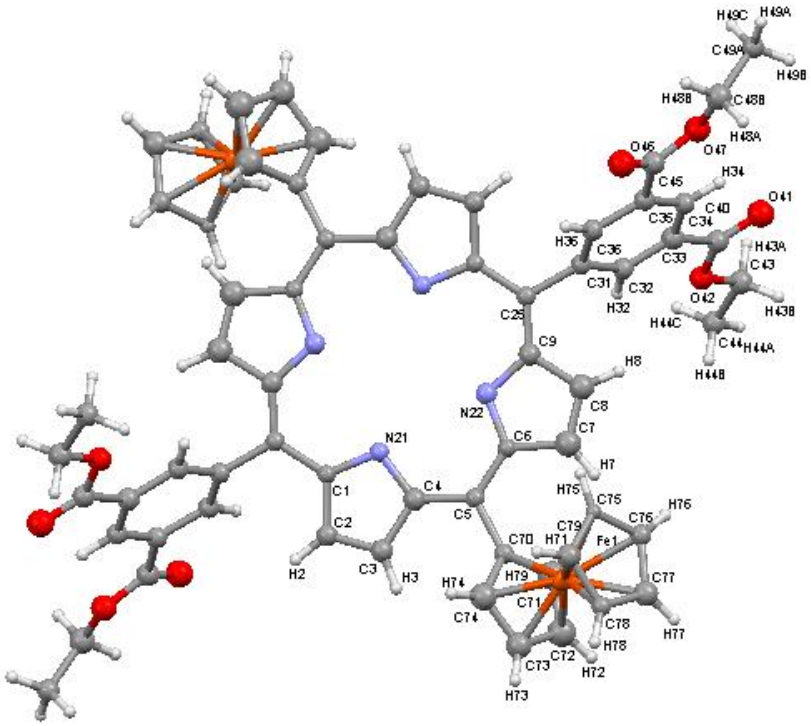


Figure 3.13. A view of the crystal structure of molecule (4) – $2H^+$ showing the atom labeling scheme. Displacement ellipsoids are drawn at the 50% probability level.

The porphyrin core is slightly deformed and shows a small deviation from planarity with 0.1 Å being the mean deviation from the porphyrin $C_{20}N_4$ plane and 0.19 Å being the furthest location of an atom away from the porphyrin $C_{20}N_4$ plane. The carbons at the meso-positions are located on the mean plane of the porphyrin and the core distortion is characteristic of a saddled deformation. Both phenyl rings are planar and tilted at an angle of 65.7(2)^{o} with respect to the mean plane of the porphyrin core.

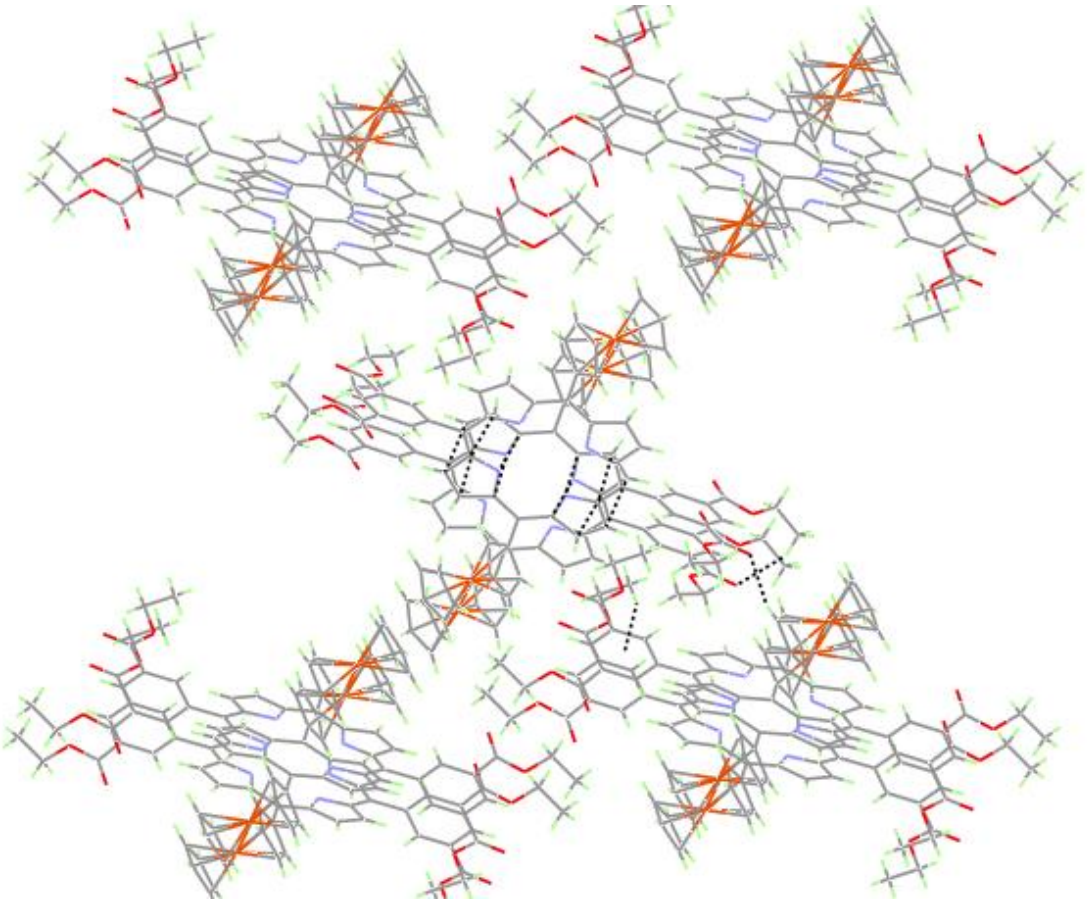


Figure 3.14. Crystal packing of (4) – $2H^+$. π-π stacking, C-H…π interactions and hydrogen bonding are represented as black dashed lines. Hydrogens are coloured green for clarity.

The cyclopentadienyl rings are tilted at an angle of 45.85(3)^{o} with respect to the mean plane of the porphyrin. The Cp rings of each ferrocenyl unit are eclipsed and they form and angle of 4.35(4)^{o} with respect to each other. All the C-C and C-Fe bond lengths are almost identical. The iron atom lies at 1.6343(17) Å and 1.633(2) Å respectively from the Cp rings centroids. The two ferrocenyl units adapt an anti-configuration with respect to the porphyrin core.

Examination of the crystal packing shows three principle interactions. π-π stacking between the pyrrolic rings of the porphyrin core, C-H…π interactions between the hydrogens of the methyl groups and the phenyl rings and weak hydrogen bonding between the carbonylic oxygen of the ester groups and hydrogens of the Cp rings and of adjacent methyl groups. Selected interactions are highlighted in Figure 3.14.

Crystal structure of (15)

Single crystals of **(15)** suitable for X-Ray structure analysis were obtained by layering methanol onto a concentrated solution of **(15)** in dichloromethane. A perspective view of the molecular structure of **(15)** and the atom numbering scheme is illustrated in Figure 3.15. The molecule crystallizes in the monoclinic space group C2/c (Table 3.5). Because the molecule lies on an inversion center, the asymmetric unit contains only one half of the centrosymmetric molecule. Porphyrin hydrogen atoms H21 and H22 were observed in the difference map before being geometrically placed and refined using a riding model at half-occupancy. Rigid bond and similarity restraints (DELU, SIMU) have been applied to the anisotropic displacement

parameters of cyclopentadienyl ring C75-C79. The displacement parameters of these atoms have also been restrained to behave more isotropically (ISOR).

The porphyrin core is almost planar with 0.1 Å being the furthest location of an atom away from the porphyrin $C_{20}N_4$ plane. The carbons at the meso-positions are located on the mean plane of the porphyrin. Both phenyl rings are planar and tilted at an angle of 59.95(7)^{o} with repsect to the mean plane of the porphyrin core.

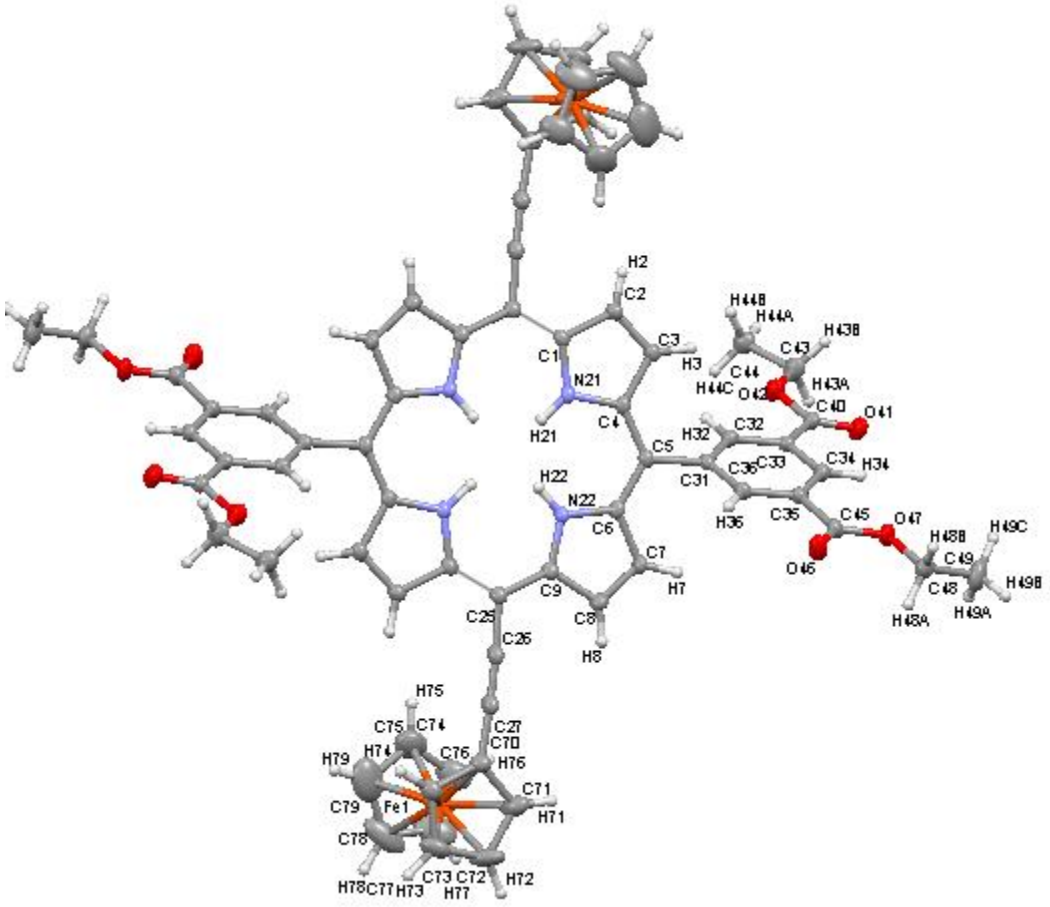


Figure 3.15. A view of the crystal structure of molecule (15) showing the atom labeling scheme. Displacement ellipsoids are drawn at the 50% probability level.

The cyclopentadienyl rings are tilted at an angle of 12.05(10)^{o} with respect to the mean plane. The Cp rings of each ferrocenyl unit are eclipsed and they form and angle of 2.35(17)^{o} with respect to each other. The iron cation lies at 1.6408(16) Å and 1.643(2) Å respectively from the Cp rings' centroids with the longer distance to the unsubstituted Cp ring. The two ferrocenyl units adapt an anti-configuration with respect to the porphyrin.

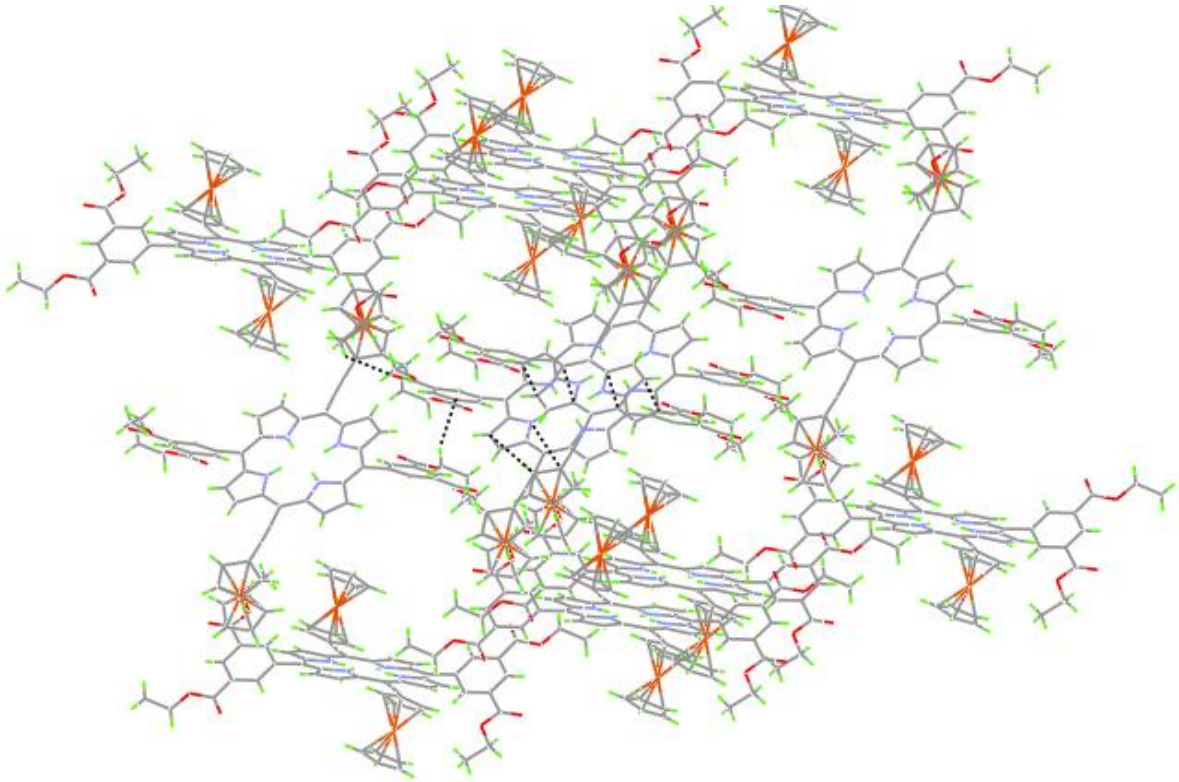


Figure 3.16. Crystal packing of (15). π-π stacking, C-H…π interactions and hydrogen bonding are represented as black dashed lines. Hydrogens are coloured green for clarity.

Examination of the crystal packing shows four principal interactions. π-π stacking between the pyrrolic rings of the porphyrin core, π-π stacking between the pyrrolic rings and the Cp rings, C-H…π interactions between methyl group hydrogens and phenyl rings and weak hydrogen bonding between methyl group hydrogens and the carbonyl oxygen of the ester groups, (Figure 3.16).

The crystal data obtained from the five porphyrins allow as to draw a few conclusions as to the effect of the changes we did at the basic porphyrin molecule (**4**) to the crystal structure of the obtained analogs. The insertion of metal did not cause any measurable change on the planarity of the porphyrin core. The magnesium ion appears to have an affinity with methanol molecules and upon crystallization it causes a weak coordination of a methanol molecule on each side of the porphyrin. Finally the insertion of the triple bond spacer between the ferrocene units showed a marked decrease of more than 40^{o} of the angle formed between the cyclopentadienyl unit and the porphyrin core. This comes into agreement with our hypothesis that the triple bond will decrease the steric interactions between the hydrogens of the pyrrolic units and the groups of the meso-positions allowing for a co-planar configuration and thus an easier deposition on a surface.

Table 3.1. Crystal data and structure refinement parameters for compound (7)

Compound	(7) · 2MeOH
Empirical formula	$C_{66}H_{60}Fe_2MgN_4O_{10}$
Formula weight	1205.19
Temperature	90(2) K
Wavelength	0.71073 Å
Crystal system	Triclinic
Space group	P-1
Unit cell dimensions	a = 9.8012(5) Å α= 68.0390(10)°.
	b = 11.5764(6) Å β= 78.2490(10)°.
	c = 13.5134(8) Å γ = 88.0290(10)°.
Volume	1390.73(13) $Å^3$
Z	1
Density (calculated)	1.439 mg/m^3
Absorption coefficient	0.600 mm^{-1}
F(000)	628
Crystal size	0.06 × 0.06 × 0.02 mm^3
Theta range for data collection	2.00 to 27.52°.
Index ranges	-12<=h<=12, -15<=k<=14, -17<=l<=17
Reflections collected	12177
Independent reflections	6289 [R(int) = 0.0160]
Completeness to theta = 27.50°	98.3 %
Refinement method	Full-matrix least-squares on F^2
Data / restraints / parameters	6289 / 2 / 382
Goodness-of-fit on F2	1.059
Final R indices [I>2sigma(I)]	R1 = 0.0355, wR2 = 0.0923
R indices (all data)	R1 = 0.0411, wR2 = 0.0962
Largest diff. peak and hole	0.620 and -0.345 $e·Å^{-3}$

Table 3.2. Crystal data and structure refinement parameters for compound (17)

Compound	(17) · 6MeOH
Empirical formula	$C_{74}H_{76}Fe_2MgN_4O_{14}$
Formula weight	1381.40
Temperature	100(2) K
Wavelength	0.71073 Å
Crystal system	Monoclinic
Space group	C 2/c
Unit cell dimensions	a = 30.86(3) Å α= 90°.
	b = 9.258(8) Å β= 121.769(13)°.
	c = 27.94(2) Å γ = 90°.
Volume	6787(10) $Å^3$
Z	4
Density (calculated)	1.352 mg/m^3
Absorption coefficient	0.506 mm^{-1}
F(000)	2896
Crystal size	0.20 x 0.06 x 0.02 mm^3
Theta range for data collection	2.33 to 27.52°.
Index ranges	-39<=h<=34, 0<=k<=11, 0<=l<=36
Reflections collected	7220
Independent reflections	7220 [R(int) = 0.0000]
Completeness to theta = 27.50°	92.7 %
Refinement method	Full-matrix least-squares on F^2
Data / restraints / parameters	7220 / 471 / 443
Goodness-of-fit on F2	1.123
Final R indices [I>2sigma(I)]	R1 = 0.1478, wR2 = 0.2861
R indices (all data)	R1 = 0.2380, wR2 = 0.3415
Largest diff. peak and hole	0.732 and -1.039 e·$Å^{-3}$

Table 3.3. Crystal data and structure refinement parameters for compound (14)

Compound	(14)
Empirical formula	$C_{272}H_{208}Fe_8N_{16}O_{32}Zn_4$
Formula weight	4920.82
Temperature	90(2) K
Wavelength	1.54184 Å
Crystal system	Triclinic
Space group	P-1
Unit cell dimensions	a = 13.7490(16) Å α= 89.634(7)°. b = 17.573(2) Å β= 73.709(8)°. c = 24.3864(18) Å γ = 78.940(9)°.
Volume	5543.4(10) $Å^3$
Z	1
Density (calculated)	1.474 mg/m^3
Absorption coefficient	5.164 mm^{-1}
F(000)	2536
Crystal size	0.1690 x 0.0379 x 0.0135 mm^3
Theta range for data collection	3.40 to 71.40°
Index ranges	-16<=h<=15, -21<=k<=20, -29<=l<=26
Reflections collected	32417
Independent reflections	19191 [R(int) = 0.1857]
Completeness to theta = 27.50°	92.3 %
Refinement method	Full-matrix least-squares on F^2
Data / restraints / parameters	19191 / 174 / 706
Goodness-of-fit on F2	1.060
Final R indices [I>2sigma(I)]	R1 = 0.1657, wR2 = 0.4092
R indices (all data)	R1 = 0.3065, wR2 = 0.5082
Largest diff. peak and hole	0.910 and -1.595 $e·Å^{-3}$

Table 3.4. Crystal data and structure refinement parameters for compound (4)

Compound	(4) - $2H^+$
Empirical formula	$C_{64}H_{56}Fe_2N_4O_8$
Formula weight	1120.83
Temperature	90(2) K
Wavelength	1.54184 Å
Crystal system	Monoclinic
Space group	$P2_1/n$
Unit cell dimensions	a = 19.1449(6) Å α = 90°. b = 6.5123(2) Å β = 98.474(3)°. c = 22.9412(9) Å γ = 90°.
Volume	2829.04(18) $Å^3$
Z	2
Density (calculated)	1.316 mg/m^3
Absorption coefficient	4.589 mm^{-1}
F(000)	1168
Crystal size	0.6705 x 0.0620 x 0.0361 mm^3
Theta range for data collection	3.90 to 74.63°
Index ranges	-23<=h<=23, -7<=k<=5, -28<=l<=28
Reflections collected	11758
Independent reflections	5504 [R(int) = 0.4704]
Completeness to theta = 27.50°	97.8 %
Refinement method	Full-matrix least-squares on F^2
Data / restraints / parameters	5504 / 96 / 178
Goodness-of-fit on F2	1.085
Final R indices [I>2sigma(I)]	R1 = 0.1710, wR2 = 0.3962
R indices (all data)	R1 = 0.1952, wR2 = 0.4278
Largest diff. peak and hole	1.427 and -1.086 $e \cdot Å^{-3}$

Table 3.5. Crystal data and structure refinement parameters for compound (15)

Compound	(15)
Empirical formula	$C_{68}H_{54}Fe_2N_4O_8$
Formula weight	1166.85
Temperature	90(2) K
Wavelength	1.54184 Å
Crystal system	Monoclinic
Space group	C2/c
Unit cell dimensions	a = 34.536(3) Å α = 90°.
	b = 6.9048(5) Å β = 92.714(10)°.
	c = 23.351(3) Å γ = 90°.
Volume	5562.1(10) $Å^3$
Z	4
Density (calculated)	1.393 mg/m^3
Absorption coefficient	4.694 mm^{-1}
F(000)	2424
Crystal size	0.08 x 0.02 x 0.005 mm^3
Theta range for data collection	3.79 to 71.31°.
Index ranges	-41<=h<=34, -5<=k<=8, -25<=l<=28
Reflections collected	10343
Independent reflections	5207 [R(int) = 0.0225]
Completeness to theta = 27.50°	98.5 %
Refinement method	Full-matrix least-squares on F^2
Data / restraints / parameters	5207 / 70 / 372
Goodness-of-fit on F2	1.070
Final R indices [I>2sigma(I)]	R1 = 0.0524, wR2 = 0.1375
R indices (all data)	R1 = 0.0603, wR2 = 0.1440
Largest diff. peak and hole	0.968 and -0.733 $e·Å^{-3}$

3.4 Spectroelectrochemistry results

3.4.1 Cyclic voltammetry

Several thousand metalloporphyrins have been studied over the last thirty years. These porphyrins have had a variety of different metal centers, axial ligands and peripheral substitution. Almost all of these have been found to be electroactive showing the existence of one or more oxidation states. The actual number of redox processes and the potential at which they occur is depends on numerous variables such as the central metal ion, other ligands complexed to the central metal ion, number and electronic properties of the porphyrin substituents and experimental conditions such as solvent and electrolyte used[72].

Cyclic voltammetry (CV) measurements were carried out on **(4), (6), (7), (14), (15), (17)** and **(28).** Different scan rates were applied (20, 50 100, 200 and 300 mV/sec) in order to collect information regarding the nature of the electrochemical processes studied. The solvent used in all experiments was dichloromethane containing 0.4M of $[NBu_4][BF_4]$ salt as the supporting electrolyte. In some cases, a trace amount of pyridine was added as some of the porphyrins studied showed a high degree of aggregation. With the addition of pyridine the porphyrins were fully dissolved. No changes were observed in the voltammograms except a marked increase in the current intensity. A three electrode system was used with glassy carbon being the working

electrode, a Pt wire being the secondary electrode and a saturated calomel electrode acting as a reference electrode.

Cited potentials are corrected to be referenced against Fc/Fc^{+} [73] unless otherwise stated. Experimentally, in order to avoid the ferrocene wave overlapping with the oxidation waves due to the ferrocene groups present in the molecules studied, decamethylferrocene (Fc*) was used as an internal standard. Under the conditions of our experiments Fc^{*}/Fc^{*+} couple was found to be at -0.52 mV versus Fc/Fc^{+}. Theoretically, for an electrochemical process to be reversible, the peak potential difference $E_{pa} - E_{pc} = \Delta E_p$ must be 59/n mV at 25^{o} C (where n = the number of electrons involved in the process) and is independent of the scan rate[74]. In our experimental conditions, decamethylferrocene, which is a known one-electron reversible couple, exhibited a mean ΔE_p value of 75 mV. Taken this into account, every couple having a ΔE_p value less than 90 mV was considered to imply an electrochemically reversible behavior while larger ΔE_p values were considered to imply electrochemically quasi-reversible behavior.

All electrochemical couples were subjected to several tests in order to verify their electrochemical reversibility. In some cases we were not able to calculate the I_{pa}/I_{pc} or plot the I_{pa}, I_{pc} versus the square root of the scan rate in order to check for the reversibility by comparing the 2 slopes. This happened because the reverse current could not be accurately measured due to the fact that the second oxidation or reduction was taking effect right after the first. To avoid generating irreversible products from the following processes, we had to set the return point a little bit before the first process was completed (~ 50 mV). As an alternative test we adopted the Nicholson equation[75] :

$$Ipc/Ipa = (Ipc)_o/Ipa + (I_\lambda)_o*0.485/Ipa + 0.086$$

with $(I_\lambda)_o$ being the current at the point of the end potential of the voltammogram and $(Ipc)_o$ being the maximum value of I in the return wave.

The first oxidation of all 7 porphyrins was attributed to the ferrocene groups. The high area included by these waves indicates that this process involves more than one electron. The E_{pa}-E_{pc} values are between 80 mV and 150 mV. These high values indicate that these processes correspond to one electron oxidative processes and that the large area of the waves is due to the presence of two ferrocene groups per molecule. All of the waves appear at potentials between 0.01 V and 0.1 V. These values are a few mV smaller than the ones observed in other compounds containing ferrocene[76-81] and this difference can be attributed to the influence of the rich electron density of the porphyrin ring making the oxidation easier to occur.

A comparison of the $E_{1/2}$ values can give insight into the influence of the metal center and the position of the triple bonds to the electronic properties of the porphyrins and the communication between the ferrocenes. A direct communication between the ferrocenes can be seen from the voltammogram only in the cases of the porphyrins that bear no triple bond spacers, **(4), (6)** and **(7)**. What can be seen in Figure 3.17b which shows the first oxidation of **(7)**, is the initiation of an oxidation process and in the middle of that, there is the initiation of a second oxidation process. This shows that the positive charge generated from the oxidation of the first ferrocene is affecting the electronic density of the second ferrocene making its oxidation occur at a slightly higher potential. In Figure 3.17c we can see the graph obtained from a square wave voltammetry experiment showing two well resolved waves very close to each other in the region of the ferrocene oxidation.

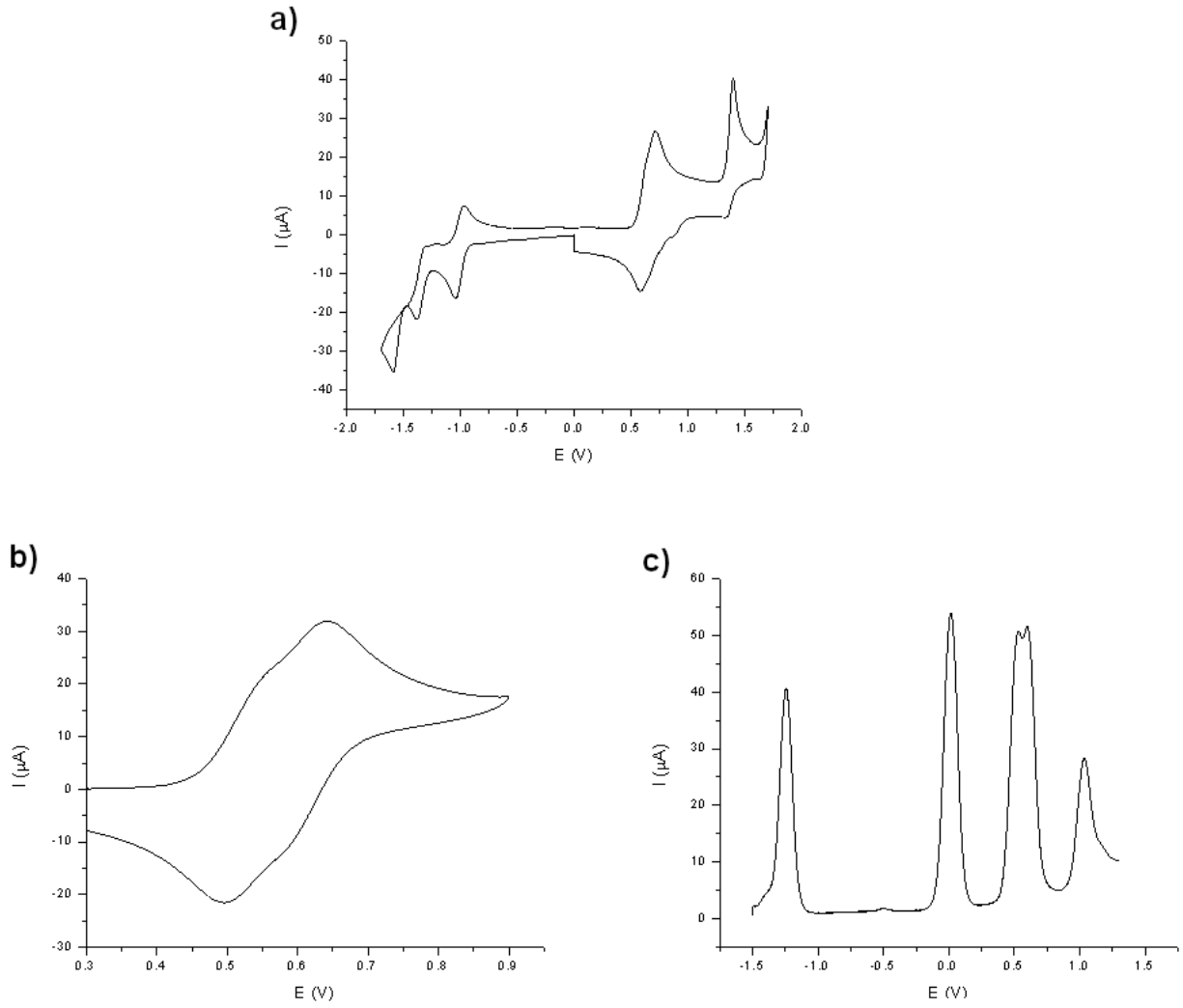


Figure 3.17. a) Cyclic voltammogram of (4) over a wide potential range. b) Cyclic voltammogram of (7) showing the electronic communication of the ferrocene groups. c) Square wave voltammogram of (7) showing two peaks very close to each other at the area of the first oxidation potential. The potentials of the displayed redox processes are versus SCE.

Previous studies have shown that the Gordy electronegativity of Zn^{2+} is 1.1 while the Gordy electronegativity of the two hydrogens inside the porphyrin core is 1.5-1.6 units[68]. Therefore the zinc is anticipated to make the ring electron density richer. On the other hand Mg is more electropositive than Zn and its effect on the ring electron density is anticipated to be even more pronounced. The first oxidation potential of the free-base porphyrin **(4)** has an $E_{1/2}$ value of 0.09V. The Zn-analog has an $E_{1/2}$ value of 0.02 while the Mg-analog has an $E_{1/2}$ value of 0.01V. These values are consistent with the predictions made above. The same trend is not observed for the first oxidations of **(14)**, **(15)** and **(17)** where the $E_{1/2}$ are almost identical with a value of 0.10 V. Although there is a triple bond spacer between the ferrocene and the porphyrin ring and a better communication was anticipated because of the extended π-aromatic system formed, changes in the ring's electron density do not seem to be sensed from the ferrocenes as seen from the lack of variation of the redox potentials. That is also seen in the electronic communication between the ferrocenes which appears quenched. There is only one wave both in the cyclic and the square wave voltammetry.

The first oxidation waves of all the porphyrins studied showed reversible characteristics. I_{pa}/I_{pc} values were very close to 1 either from direct measurement or through the use of Nicholson's equation. The only characteristic that did not seem compatible with reversible processes was the E_{pa}-E_{pc} value. In many cases it was exceeding the set limit of 90 mV and in some cases and scan rates it would go up to 150 mV. Although this behavior might as well signify a quasireversible process, as will be seen later, the first oxidation was fully reversible over longer time-scales as judged from the UV/Vis spectroelectrochemistry. An explanation for the large E_{pa}-E_{pc} values could result from presence of ferrocene communication. As discussed earlier, ferrocene communication was confirmed experimentally for the porphyrins **(4), (6)** and **(7)**. However there

might still be a small communication for the other porphyrins that is not well resolved in the voltammograms. A small widening of the peaks due to an overlap with a second process can lead to a small widening of the E_{pa}-E_{pc} value. It is possible that by applying different experimental conditions, communication, which is not well-resolved under these conditions, could be made visible[68].

The second oxidation is hypothesized to be porphyrin ring centered. The fact that porphyrins show one, two and sometimes three ring-centerd oxidations[72] coupled with the lack of any other oxidation center capable of being oxidized at the potential range of the observed waves led us to this hypothesis. The process is irreversible with the only exception being **(6)** where the process is quasireversible showing a dependence of the reversibility on scan rate. Again, a predictable trend in the decrease of the $E_{1/2}$ value with the central metal ion is apparent. The $E_{1/2}$ values range between 0.53 and 0.83 V.

The first reduction is attributed to a porphyrin ring centered process. The $E_{1/2}$ values range between -1.53 and -1.81 V. This process is fully reversible for all the porphyrins and the reversibility is confirmed through every applied test. The E_{pa}-E_{pc} value is constant for all the porphyrins and its value is ~75 mV. Here we can see that the insertion of Zn^{2+} and Mg^{2+} is decreasing even more the reduction potential as the increased electron density in the ring is making the insertion of an extra electron more difficult. The second reduction is an irreversible process and is attributed to a ring centered reduction. The potential range value is between -1.91 V and -2.24 V. Table 3.6 shows the $E_{1/2}$ values of all the observed waves. For irreversible processes the E_{pa} or E_{pc} value is shown instead. Figure 3.17a shows the cyclic voltamogram of (**4**) from -1.7 V to +1.7 V. The full spectrum voltamograms of the rest of the porphyrins are qualitatively similar.

Table 3.6. Oxidation and reduction potentials (V) obtained from cyclic voltammetry for all the porphyrins studied. The $E_{1/2}$ values are used for the reversible processes (blue) and the Epa,Epc values are used for the non-reversible ones (red).

Compound	1st Ox	2nd Ox	1st Red	2nd Red
(4)	0.09	0.83	-1.57	-1.91
(6)	0.02	0.53	-1.81	-2.24
(7)	0.01	0.53	-1.81	-2.21
(14)	0.09	0.79	-1.33	-1.94
(15)	0.10	0.59	-1.55	-1.95
(17)	0.10	0.56	-1.58	-2.05
(28)	0.05	0.71	-1.53	-2.04

3.4.2 Spectroelectrochemistry

To assess the chemical reversibility of the redox processes observed during the cyclic voltammetry experiments, UV/Vis spectroelectrochemistry was performed on compounds **(4), (6), (7), (14), (15), (17)** and **(28).** The compounds were oxidized in situ at pre-determined appropriate potentials in an optically transparent electrode UV/Vis cell (OTE) in a solution of 0.4 M $[NBu_4][BF_4]$ in dichloromethane. These potentials were selected from careful inspection of the voltamogramms. We used the E values where the diffusion gradient was maximum and the current had been stabilized. In cases where a second redox process was taking place before the first reaching the equilibrium point, the selected potential was chosen before the initiation of the second process. Temperature was kept constant at 0^o C through a steady flow of air passed through a coiled tube immersed in liquid nitrogen.

All porphyrins had a very high extinction coefficient in the order of 200,000-300,000 $M^{-1}cm^{-1}$ at the 400-500 nm region. The UV/Vis spectrum of a porphyrin is characterized by a very sharp high-intensity band in the 400-500 nm region called the Soret peak[82] and a number of smaller intensity bands in the 600-800 nm region called Q-bands. In 1960 Gouterman proposed the 'four orbital' model[83] in order to explain the absorption spectra of porphyrins. According to his theory, the absorption bands arise from transitions between two HOMOs and two LUMOs and the relative energies of these orbitals is affected by the central metal ion and the substituents at the periphery of the porphyrin. Figure 3.18 shows a simplified version of the four orbital model for

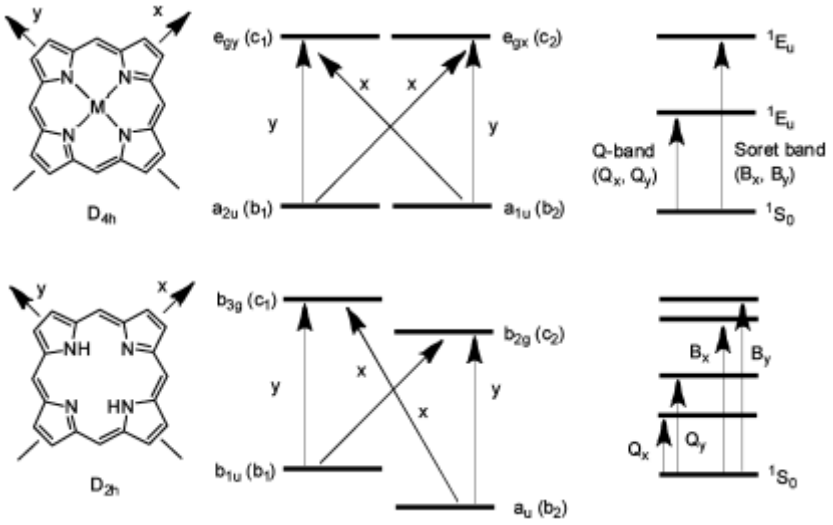


Figure 3.18. Gouterman's four orbital model for metallated porphyrins having a D_{4h} symmetry (top) and for metal-free porphyrins having a D_{2h} symmetry (bottom).

metallated and non-metallated porphyrins and gives the energy levels and the transitions responsible for the Sorret and Q bands.

In Figure 3.19 (a) and (b) the spectrum of **(4)** and **(6)** are shown as representatives of the spectra of a free base and a metallated porphyrin. The first oxidation and the first reduction proved to be completely reversible at the longer timescales of the spectroelectrochemistry experiments. When going to more positive/negative potentials the original spectrum could not be regenerated upon zeroing the applied voltage. Figures 3.19 (c) and (e) shows typical spectra obtained after oxidizing or reducing, respectively, one of the porphyrins **(6)** selected from this project. Figures 3.19 (d) and (f) show the full oxidation and reduction processes as they proceeded through the timescale of the experiments.

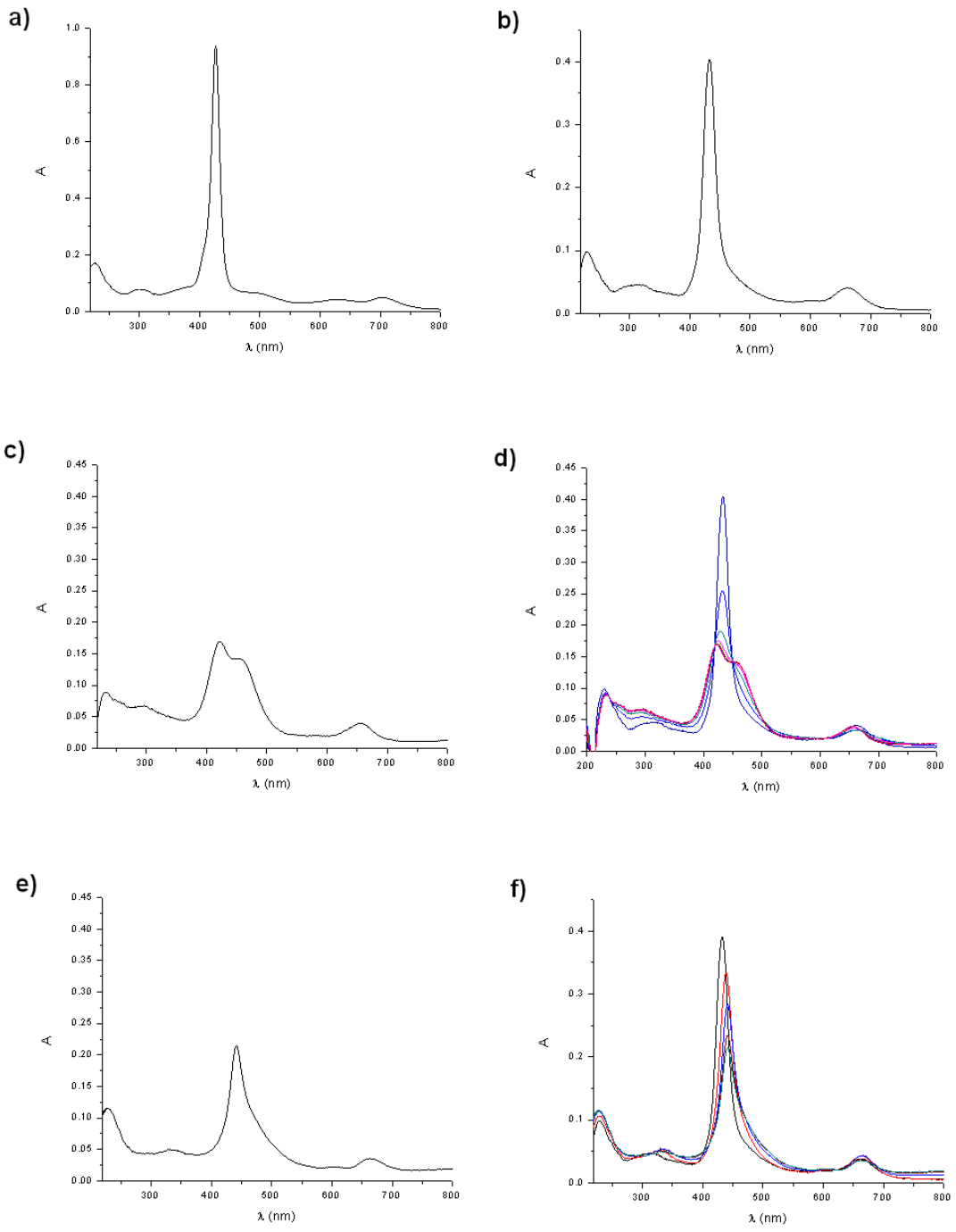


Figure 3.19. UV/Vis Spectrum of a) neutral species of (4) at -0.52 Vb) neutral species of (6) at -0.52 V c) oxidized species of (6) at 0.33 V. e) reduced species of (6) at -1.97 V. Time evolution of the UV/Vis spectrum of (6) during d) the first oxidation process at 0.33 V f) the first reduction process at -1.97 V.

3.5 Surface deposition

STM images were acquired with an Agilent Technologies 4500 PicoPlus STM using a PicoScan controller and STM tips formed from mechanically cut PtIr (80:20) wire. Saturated solutions of **(5)** and **(16)** were prepared by placing an excess of solid in the desired solvent. All solutions were agitated ultrasonically to ensure complete dissolution. Two attempts have been made to deposit the two molecules. In the first attempt, the molecules were dissolved in nonanoic acid and one drop was placed on HOPG. The second attempt involved the dissolution in ethanol which was placed on Au(111) and allowed to evaporate.

The images obtained from the STM did not reveal the formation of an ordered structure in any of the cases. It is not to be concluded though that these molecules cannot form a stable network. As shown from the NMR experiments, the solubility of these compounds was extremely low and only hot DMSO could dissolve enough material (and only in the case of **(16)**) in order to obtain a satisfactory NMR spectra. Although the solubility is very low, it was anticipated that a negligible quality needed for surface deposition would be soluble. It might be the case that no appreciable amount of material managed to enter the solution as it remained colourless after the attempted dissolution of the two porphyrins.

3.6 Conclusion

The aims of this part of the project involved the synthesis, characterization, spectroelectrochemical studies and surface deposition studies of a series of porphyrin molecules. The porphyrins were designed to have two ferrocene units at the 5,15-positions that would act as 'bits' in a molecular memory technology system and two isophthalic acid units at the 10,20-positions that would facilitate network formation on a surface. Various analogs of this general structure were targeted involving the insertion of triple bonds acting as spacers between the porphyrin core and the aforementioned groups as well as the formation of the metallated versions of these porphyrins using Zn^{2+} and Mg^{2+}.

We were not able to synthesize all of the target molecules. Porphyrins with no triple bonds and porphyrins with triple bonds between the ferrocenes and the porphyrin ring as well as the metallated forms of their ester derivatives (**(4), (5), (6), (7), (14), (15), (16)**, and **(17)**) were successfully prepared and characterized. Only the zinc-derivative **(28)** of the ester protected porphyrin bearing triple bonds between the isophthalic groups and the central ring was successfully synthesized. In addition, we were not able to synthesize any of the molecules belonging to the group of porphyrins bearing triple bonds in all four meso- positions.

Surface deposition of porphyrins **(5)** and **(16)** was unsuccessful. It is hypothesized that the reason for this failure was the practically negligible solubility of the molecules in the solvents used. Future work employing much more polar solvents such as DMF might provide better results.

Electrochemical and spectroelectrochemical studies have revealed the existence of one reversible oxidation based at the ferrocene unit and one reversible reduction based on the porphyrin ring. The two ferrocenes were found to communicate in the case of **(4)**, **(6)** and **(7)** but this communication seemed to be quenched when triple bonds are introduced. This is not conclusive though because the E_{pa}-E_{pc} values of some porphyrins suggest that communication might still happen to a lesser degree although not resolved under the experimental conditions used.

3.7 Experimental

All reagents and solvents were purchased from Sigma Aldrich, Alfa Aesar, Fischer Scientific UK, and used without further purification unless otherwise stated. Elemental microanalyses were carried out by Steven Boyer at the Microanalysis Service, London Metropolitan University, UK. ^{1}H and ^{13}C NMR spectra were measured using either a Joel 270 MHz, Bruker 300 MHz, Bruker 400 MHz, DPX 300 MHz, DPX 400 MHz or Bruker 500 MHz spectrometer. MALDI-TOF mass spectra were obtained using Bruker Ultraflex MALDI-TOF mass spectrometer. MALDI-TOF-MS samples were prepared by dissolution of the compounds in CH_2Cl_2 (10 μL) and then mixing this solution with a solution of the matrix DCTB (Trans-2-[3-(4-tertbutylphenyl)-2-methyl-2-propenylidone]-malonitrile) in MeCN (20 μL). A sample of the resulting solution (5 μL) was loaded onto a plate, the solvent was removed in air, and the sample transferred to the mass spectrometer for analysis. Electrospray ionization mass spectra were collected using a MALDI-TOF mass spectrometer. UV-Vis spectra were obtained using Unicam UV/Vis 2 spectrometer.

Cyclic Voltametric studies were carried out using an Autolab PGSTAT20 potentiostat, using a three-electrode arrangement in a single compartment cell. A glassy carbon working electrode, a Pt secondary electrode and a saturated calomel reference electrode (chemically isolated for the test solution *via* a bridge tube containing electrolyte solution and fitted with a porous Vycor frit) were used in the cell. Experiments were performed under an atmosphere of argon. Sample solutions were prepared under an argon atmosphere using Schlenck line techniques. The supporting electrolyte employed was a 0.4M $[NBu_4][BF_4]$ solution. Redox potentials were

referenced vs. the Fc/Fc^+ couple. Decamethylferrocene was used as the internal standard. Compensation for internal resistance was not applied.

UV/Vis spectroelectrochemical experiments were carried out with an optically transparent electrochemical (OTE) cell (modified quartz cuvette, optical path length 0.5mm). A three electrode configuration, consisting of a Pt/Rh gauze working electrode, a Pt wire secondary electrode (in a fritted PTFE sleeve) and a saturated calomel electrode (chemically isolated from the test solution via a bridge tube containing electrolyte solution and terminated in a porous frit) were used in the cell. The potential at the working electrode was controlled by a Sycopel Scientific Ltd. DD10M potentiostat. UV/Vis data were recorded on a Perkin Elmer Lamda 16 spectrophotometer. The cavity was purged with N_2 gas and temperature control at the sample was achieved by flowing cooled N_2 gas across the surface of the cell.

Sample solutions were prepared under an atmosphere of argon using Schlenk line techniques and consisted of a 0.4M $[NBu_4][BF_4]$ solution as the supporting electrolyte and a 10^{-4}M solution of the test compound. The test species in solution was oxidized at constant potential and the redox process was considered complete when consecutive spectra were identical. The reversibility of the process was investigated by applying a potential at the working electrode to re-reduce the electrogenerated product. This process was considered to be reversible, under the conditions of the experiment, if the spectral profile of the starting material was reproduced.

STM measurements were performed by Anna Slater from the School of Chemistry at the University of Nottingham.

Crystallography

All single-crystal X-ray experiments were performed on a Bruker SMART 1000 CCD or a Bruker SMART APEX CCD equipped with an Oxford Cryosystems open flow cryostat, [graphite monochromatic Mo-Ka radiation (λ=0.71073 Å), ω scans]. Absorption corrections, if necessary, were applied by a semiempirical approach. All of the single crystal structures were solved by direct methods using SHELXS-97[84]; all non-H atoms were located using subsequent difference-Fourier methods[85]. Unless otherwise stated, hydrogen atoms were placed in calculated positions and thereafter allow to ride on their parent atoms.

Additional restraints were placed on thermal and geometric parameters as required and appropriate. All graphical representations were generated using Mercury 1.4.1 (Copyright CCDC 2001-2005).

Compound Synthesis

Synthesis of 5-iodoisophthalic acid (19)

An aqueous solution of 3,5-dimethyliodobenzene (1,010 mg, 4.358 mmol), potassium permanganate (5 g, 32 mmol) and pyridine (7.5 ml) was brought to reflux at 115 ^{o}C for 15 h. Addition of another portion of potassium permanganate (2.5 g, 16 mmol) was followed by another 5 h reflux. The reaction mixture was brought to room temperature and filtered to remove the precipitated MnO_2. The volume of solvent in the filtrate was reduced in volume under reduced pressure to approximately 10 ml. The solution was then acidified with concentrated HCl

to pH 1. The white solid formed was filtered and recrystallized from boiling water to give 900 mg (71%) of a white powder. ^{1}H NMR (400MHz, d^{6}-DMSO) : δ ppm = 13.54 (s br, 2H, COOH), 8.40 (s, 3H). ^{13}C NMR (101 MHz, $CDCl_3$): δ ppm 92.72, 129.59, 132.93, 142.06, 165.80. ESI-MS (m/z) : 290.9160 $[M-H]^-$. Elemental Analysis (%) Calculated for $C_8H_5IO_4$: C, 32.9; H, 1.73; Found: C, 33.04; H, 1.70.

Synthesis of diethyl-5-iodoisophthaloate (20)

5-Iodosophthalic acid (1000 mg, 3.42 mmol) was dissolved in absolute ethanol (10 ml). Thionyl chloride (800 µl, 7.18 mmol) was added at 0 ^{o}C and the reaction mixture was brought to reflux under inert atmosphere for a period of 5 h. Ethanol was evaporated in reduced pressure and the residue was dissolved in ethyl acetate. The mixture was washed with a saturated solution of sodium bicarbonate. The organic phase was dried with magnesium sulfate and evaporated under reduced pressure. Chromatography on silica [CH_2Cl_2/Hexane (70:30)] afforded diethyl 5-iodoisophthalate as a white solid (81%). ^{1}H NMR (400 MHz, $CDCl_3$) : δ ppm = 8.62 (at, J = 1.4 Hz, 1H), 8.53 (d, J = 1.4 Hz, 2H), 4.40 (q, J = 7.1 Hz, 4H), 1.41 (t, J = 7.1 Hz, 6H). ^{13}C NMR (101 MHz, $CDCl_3$): δ ppm 14.30, 61.76, 93.39, 129.83, 132.55, 142.33, 164.41. ESI-MS (m/z) : 348.9914 $(M+H)^+$. Elemental Analysis (%) Calculated for $C_{12}H_{13}IO_4$: C, 41.4; H, 3.76; Found C, 41.52; H, 3.78.

Synthesis of ethynyl-ferrocene (9)

The compound was synthesized as described previously[86] using slight modifications. A solution of acetylferrocene (14 g, 61 mmol) in THF (50 ml) was purged with nitrogen for 20 min. The solution was brought to -78^{o}C and a solution of 2.5M LDA in THF (26.8 ml) was added. Stirring was continued for 45 min after which, 1.05 equiv (9.3 ml, 64 mmol) of diethylchlorophosphate was added. The reaction mixture was stirred for an additional 1 hour at -78^{o}C and then allowed to warm to room temperature. An additional 56.1 ml of 2.5M LDA solution in THF were added at -78^{o}C. The solution was allowed to warm to room temperature and poured over 500 ml of an ice-water mixture containing 50 ml of concentrated HCl solution. The organic layer was extracted with CH_2Cl_2 and dried over Mg_2SO_4. Solvent was removed under reduced pressure and the residue was purified by flash chromatography using a 3:1 hexane-ether mixture as the mobile phase. The orange oil obtained was crystallized in the freezer from pentane (11.8 g, 91%). %). ^{1}H NMR (400 MHz, $CDCl_3$) : δ ppm = 4.49 (t, J = 1.9 Hz, 2H), 4.25 (s, 5H), 4.23 (t, J = 1.8 Hz, 2H), 2.75 (s, 1H). ^{13}C NMR (101 MHz, $CDCl_3$): δ ppm 63.87, 68.74, , 70.07, 71.78, 73.52, 82.62. ESI-MS (m/z) : 210.0130 $(M)^{+}$. Elemental Analysis (%) Calculated for $C_{12}H_{10}Fe$: C, 68.62; H, 4.80; Found C, 68.77; H, 4.80.

Synthesis of diethyl-5-(formyl)-isophthalate (2)

Diethyl-5-(hydroxymethyl)-isophthalate (1.5 g, 6 mmol) was dissolved in 30 ml of dichloro-methane and pyridinium chlorochromate (1.94 g, 9.02 mmol) was slowly added to the solution over the course of 10 min. The reaction mixture was left stirring at room temperature for a period

of two hours. After confirmation of completion of the reaction by TLC, the black reaction mixture was diluted with diethyl ether (120 ml). The solvent was decanted and the black remaining tar was washed several times with diethyl ether and scraped continually with a spatula until it became granular. The original filtrate and the ether washings were combined and the solvent was evaporated under reduced pressure. The residue was purified on silica gel with dichloromethane/hexane 2:1 as the elution solvent to give 1.37g (92%) of diethyl-5-(formyl)-isophthalate. ^{1}H NMR (400 MHz, $CDCl_3$) : δ ppm = 10.17 (s, 1H), 8.95 (at, J=1.6 Hz, 1H), 8.74 (d, J=1.8 Hz, 1H), 4.48 (q, J=7.2 Hz, 4H)), 1.47 (t, J = 7.2 Hz, 6H). ^{13}C NMR (101 MHz, $CDCl_3$): δ ppm 14.38, 61.98, 132.24, 134.28, 135.80, 136.86, 164.84, 190.63. ESI-MS (m/z) : 273.0722 $(M+Na)^+$. Elemental Analysis (%) Calculated for $C_{21}H_{18}FeN_2$: C, 62.39; H, 5.64; Found C, 62.50; H, 5.58.

Synthesis of 5-(diethyl-isopthalato)-dipyrromethane (3)

Diethyl-5-(formyl)-isopthalate (1.371 g, 3.74 mmol) was dissolved in of pyrrole (37.5 ml, 2.43 mol). The solution was flushed with nitrogen for 15 min. Indium trichloride (115.3 mg, 0.52 mmol) was added and the reaction was allowed to proceed for three hours. Sodium hydroxide (625.3 mg, 15.5 mmol) was added to quench the reaction and the reaction mixture was stirred for 45 min. The mixture was filtered and the filtrate was concentrated at reduced pressure. The residue was subjected to chromatography on silica with a dichloromethane/ethylacetate 98.5:1.5 solvent mixture as the mobile phase. 1.766 g of a pale yellow solid was recovered in 87.9% yield. ^{1}H NMR (400 MHz, $CDCl_3$) : δ ppm = 8.59 (at, J=1.6Hz, 1H), 8.12 (d, J=1.6 Hz, 2H), 8.02 (br, 2H), 6.75 (m, 2H)), 6.18 (m, 2H), 5.90 (m, 2H), 5.60 (s, 1H), 4.40 (q, J=7.1Hz, 4H),

1.41 (t, J=7.2Hz, 6H). ^{13}C NMR (101 MHz, $CDCl_3$): δ ppm 14.31, 43.87, 61.41, 107.70, 108.69, 117.82, 129.30, 131.32, 131.33, 133.54, 143.28, 165.73. ESI-MS (m/z): 367.1633 $(M+H)^+$. Elemental Analysis (%) Calculated for $C_{21}H_{22}N_2O_4$: C, 68.84; H, 6.05; N, 7.65; Found C, 68.79; H, 6.15; N, 7.57.

Synthesis of meso-5,15-bis-(3,5-(bis-ethoxycarbonyl)-phenyl)-10,20-bis(ferrocenyl)-porphyrin (4)

5-(Diethyl-isopthalato)-dipyrromethane (2.788 g, 7.611 mmol), and ferrocenylcarboxaldehyde (1629 mg, 7.61 mmol) were dissolved in dichloromethane (760 ml). The solution was de-aerated by purging with nitrogen for 15 min. Trifluoroacetic acid (175 μL, 2.28 mmol) was added and the reaction mixture was left stirring at room temperature overnight under a nitrogen atmosphere. DDQ (2.591 g, 11.4 mmol) was added and stirring was continued for a further 30 min. The solution was filtered and evaporated under reduced pressure. The residue was dissolved in dichloromethane and passed through a short pad of silica to remove most of the formed black tar. The material collected was subjected to chromatography on deactivated neutral alumina (Brockmann III) using dichloromethane/hexane (1:1) as a solvent system. The dark green band was collected and the solvent was removed under vacuum. Recrystallization from dichloromethane/methanol afforded 1.786 g (41%) of a purple solid. ^{1}H NMR (400 MHz, $CDCl_3$) : δ ppm = 9.89 (d, J=4.7Hz, 4H), 9.17 (at, J=1.7 Hz, 2H), 9.05 (d, J=1.7Hz, 4H), 8.57 (d, J= 4.9 Hz, 4H), 5.54 (t, J=1.8Hz, 4H), 4.86 (t, J=1.8Hz, 4H), 4.54 (q, J=7.2Hz, 8H), 4.16 (s, 10H), 1.47 (t, J= 7.1Hz, 12H). ^{13}C NMR (101 MHz, $CDCl_3$): δ ppm 14.40, 61.72, 69.43, 70.68, 77.23, 88.73, 117.86, 118.83, 129.56, 130.09, 130.22, 131.38, 138.27, 143.35, 144.52, 148.14,

166.13. MALDI-TOF MS (m/z) 1117.921 $(M)^+$. Elemental Analysis (%) Calculated for $C_{64}H_{54}Fe_2N_4O_8$: C, 68.70; H, 4.86; N, 5.01; Found C, 68.62; H, 4.73; N, 5.00.

Synthesis of meso-[5,15-bis-(3,5-(bis-ethoxycarbonyl)-phenyl)-10,20-bis(ferrocenyl)-porphyrinato]-zinc(II) (6)

Meso-5,15-bis-(3,5-(bis-ethoxycarbonyl)-phenyl)-10,20-bis(ferrocenyl)-porphyrin (200 mg, 0.179 mmol) was dissolved in a mixture of dichloromethane (30 ml) and methanol (10 ml). Zinc acetate hydrate (160 mg, 0.716 mmol) was added and the solution was left stirring at room temperature for 2 h. The solution was washed with water, dried with $MgSO_4$, filtered and the solvent removed under reduced pressure. The residue was subjected to chromatography on silica with dichloromethane containing 1% pyridine as the elution solvent. The collected green fraction was stripped off solvent and the residue was recrystallized from dichloromethane/methanol to afford 196 mg (93%) of a purple microcrystalline material. ^{1}H NMR (400 MHz, $CDCl_3$) : δ ppm = 10.01 (d, J=4.6Hz, 4H), 9.12 (at, J=1.6 Hz, 2H), 9.02 (d, J=1.6Hz, 4H), 8.58 (d, J= 4.6 Hz, 4H), 5.54 (t, J=1.8Hz, 4H), 4.82 (t, J=1.8Hz, 4H), 4.53 (q, J=7.2Hz, 8H), 4.15 (s, 10H), 1.46 (t, J= 7.2Hz, 12H). ^{13}C NMR (101 MHz, $CDCl_3$): δ ppm 14.39, 61.57, 68.80, 70.46, 77.53, 90.67, 118.27, 118.52, 129.11, 129.49, 130.12, 132.50, 138.28, 144.44, 148.46, 151.22, 166.35. MALDI-TOF MS (m/z): 1179.842 $(M)^+$. Elemental Analysis (%) Calculated for $C_{64}H_{52}Fe_2N_4O_8Zn$: C, 65.02; H, 4.43; N, 4.74; Found C, 64.95; H, 4.46; N, 4.68.

Synthesis of meso-[5,15-bis-(3,5-(bis-ethoxycarbonyl)-phenyl)-10,20-bis(ferrocenyl)-porphyrinato]-magnesium(II) (7)

Meso-5,15-bis-(3,5-(bis-ethoxycarbonyl)-phenyl)-10,20-bis(ferrocenyl)-porphyrin (200 mg, 0.179 mmol) was dissolved in a mixture of dichloromethane (20 ml) and N,N-diisopropylethylamine (0.84 ml). MgI_2 (352 mg, 0.63 mmol) was added and the suspension was stirred for 30 min at room temperature. The reaction mixture was diluted with dichloromethane (40 ml), washed with 10% NaOH (2 x 50 ml), dried over $MgSO_4$ and filtered. The solvent was evaporated under reduced pressure and the residue was purified by chromatography on deactivated neutral alumina (Brockmann III grade). The elution solvent used was dichloromethane containing 1% of methanol. Recrystallization from dichloromethane/methanol afforded 196 mg (96%) of a purple solid. ^{1}H NMR (400 MHz, $CDCl_3$) : δ ppm = 10.03 (d, J=4.6Hz, 4H), 9.13 (at, J=1.6 Hz, 2H), 9.04 (d, J=1.6Hz, 4H), 8.59 (d, J= 4.6 Hz, 4H), 5.58 (t, J=1.8Hz, 4H), 4.84 (t, J=1.8Hz, 4H), 4.53 (q, J=7.1Hz, 8H), 4.17 (s, 10H), 1.46 (t, J= 7.1Hz, 12H). ^{13}C NMR (101 MHz, $CDCl_3$): δ ppm 14.41, 61.56, 68.77, 70.48, 77.67, 90.98, 119.47, 119.63, 129.07, 129.43, 130.34, 132.66, 138.41, 144.73, 148.56, 151.33, 166.39. MALDI-TOF MS (m/z): 1139.905 $(M)^+$. Elemental Analysis (%) Calculated for $C_{64}H_{52}Fe_2N_4O_8Mg$: C, 67.36; H, 4.59; N, 4.91; Found C, 67.40; H, 4.50; N, 4.85.

Synthesis of meso-5,15-bis-(isophthalic acid)-10,20-bis(ferrocenyl)-porphyrin (5)

Meso-5,15-bis-(3,5-(bis-ethoxycarbonyl)-phenyl)-10,20-bis(ferrocenyl)-porphyrin (107 mg, 0.096 mmol) was dissolved in a 2:1 mixture of THF/MeOH (30 ml). The solution was brought to

refluxing temperature and another solution containing NaOH (2 g, 50 mmol) in a 5:2 mixture of MeOH/H_2O (14 ml) was added dropwise and left to reflux for 2 h. The solution was left to return to room temperature and the solvent was removed under reduced pressure. The residue was dissolved in water and acidified to pH 1 using a 2 M aqueous hydrochloric acid solution. The greenish-purple cloudy suspension was centrifuged and the solid mass was collected and washed 3 times with water and 2 times with acetone. The residue was redissolved in a small amount of pyridine. Water was added (30 ml) and the suspension was centrifuged again. The residue washed three times with water and once with acetone and dried to yield 89 mg (93%) of a purple solid. MALDI-TOF MS (m/z): 1007.5 $(M)^+$. Elemental Analysis (%) Calculated for $C_{56}H_{38}Fe_2N_4O_8$: C, 66.82; H, 3.81; N, 5.57; Found C, 66.72; H, 3.93; N, 5.50.

Synthesis of 1,9-bis-(formyl)-5-(diethyl-isopthalato)-dipyrromethane (10)

Dimethylformamide (5 ml) was degassed under argon for 10 minutes. Phosphorous oxychloride (0.75 ml, 8.2 mmol) was added to the dimethylformamide at 0 ^oC and the solution was stirred for 10 min (Vilsmeier reagent). A solution of 5-(diethyl-isopthalato)-dipyrromethane (430 mg, 1.18 mmol) in dimethylformamide (4 ml) was degassed under argon for 10 min. 1.8 ml of the Vilsmeier reagent were added to the solution at 0 ^oC and the reaction mixture was left to react for 2.5 h. The reaction was quenched with the addition of saturated aqueous sodium acetate solution. Stirring was continued for an additional hour. The solution was extracted with ethyl acetate and the combined extracts were washed with brine, dried over $MgSO_4$ and then filtered. The filtrate was evaporated under reduced pressure and the residue was left at high vacuum overnight. The brown viscous oil was separated by column chromatography on silica eluting with hexane/ethyl

acetate 3:1. 425.5 mg (85.4%) of 1,9-bis-(formyl)-5-(diethyl-isopthalato)-dipyrromethane were isolated as a white solid. ^{1}H NMR (400 MHz, $CDCl_3$) : δ ppm = 10.19 (s, 2H), 9.32 (s, 2H), 8.63 (at, J=1.4 Hz, 1H), 8.22 (d, J=1.4Hz, 2H), 6.92 (dd, J_1= 2.5 Hz, J_2=3.8Hz, 2H), 6.10 (m, 2H), 5.69 (s, 1H), 4.42 (q, J=7.2Hz, 4H), 1.41 (t, J=7.1Hz, 6H). ^{13}C NMR (101 MHz, $CDCl_3$): δ ppm 14.28, 44.30, 61.63, 111.61, 121.87, 130.03, 131.84, 133.07, 133.65, 139.61, 140.32, 165.37, 179.01. ESI-MS (m/z): 423.1543 $(M+H)^+$. Elemental Analysis (%) Calculated for $C_{23}H_{22}N_2O_6$: C, 65.39; H, 5.25; N, 6.63; Found C, 65.46; H, 5.19; N, 6.49.

Synthesis of 1,9-bis-[(propylimino)methyl]-5-(diethylisopthalato)dipyrromethane (11)

A solution of 1,9-bis-(formyl)-5-(diethyl-isopthalato)-dipyrromethane (500 mg, 1.18 mmol) and n-propylamine (1966 μL, 23.9 mmol) in THF (4 ml) was stirred at room temperature for a period of 1 h. The solvent was evaporated under reduced pressure and was left drying under high vacuum for the removal of the excess n-propylamine. The reaction afforded a dark-brown solid which was used as it is for the next step without further purification.

Synthesis of meso-[5,15-bis-(3,5-(bis-ethoxycarbonyl)-phenyl)-porphyrinato]-zinc(II) (12)

1,9-bis-[(propylimino)methyl]-5-(diethylisopthalato)dipyrromethane (264.2 mg, 0.524 mmol) and 5-(diethyl-isopthalato)-dipyrromethane (191.9 mg, 0.524 mmol) were dissolved in toluene (55 ml). Zinc acetate hydrate (1,15 g, 5.2 mmol) was added and the reaction mixture was refluxed for 18 h. Heating was disconnected and the solution was filtered. The organic phase was extracted with water and the solvent was evaporated under reduced pressure. The residue was

dissolved in dichloromethane containing 10% ethyl acetate and it was passed through a short pad of silica in order to remove a large amount of black tar. After evaporation of solvent the remaining solid was separated by column chromatography on silica. The mobile phase consisted of dichloromethane containing 0.5% of ethyl acetate which was gradually raised to 1.5% until the fluorescent purple band was collected. Evaporation of solvent gave 184.5 mg (43.2%) of a purple solid. ^{1}H NMR (400 MHz, $CDCl_3$) : δ ppm = 10.40 (s, 2H), 9.51 (d, J=4.6Hz, 4H), 9.19 (at, J=1.6 Hz, 2H), 9.12 (d, J=1.6Hz, 4H), 9.05 (d, J= 4.5 Hz, 4H), 4.53 (q, J=7.1Hz, 8H), 1.46 (t, J= 7.1Hz, 12H). ^{13}C NMR (101 MHz, $CDCl_3$): δ ppm 14.40, 61.70, 106.85, 117.74, 129.54, 129.97, 132.23, 132.49, 138.32, 143.31, 149.80, 166.18. MALDI-TOF MS (m/z): 812.472 $(M)^+$. Elemental Analysis (%) Calculated for $C_{44}H_{36}N_4O_8Zn$: C, 64.91; H, 4.46; N, 6.88; Found C, 64.75; H, 4.52; N, 6.97.

Synthesis of meso-[5,15-bis-(3,5-(bis-ethoxycarbonyl)-phenyl)-10,20-dibromoporphyrinato]-zinc(II) (13)

A solution of meso-[5,15-bis-(3,5-(bis-ethoxycarbonyl)-phenyl)-porphyrinato]-zinc(II) (250 mg, 0.308 mmol) in chloroform _(50 ml) containing 1 drop of pyridine, was brought to 0 ^{o}C. N-bromosuccinimide (109.6 mg, 0.62 mmol) was added slowly and the solution was stirred for a period of 20 min. The reaction was quenched with the addition of acetone (5 ml). The solution was washed with water, dried over $MgSO_4$ and filtered. The solvent was evaporated under reduced pressure and the residue was separated by column chromatography on silica. Dichloromethane containing 1% of ethyl acetate and 1% of pyridine was used as the elution solvent. Meso-[5,15-bis-(3,5-(bis-ethoxycarbonyl)-phenyl)-10,20-dibromo-porphyrinato]-

zinc(II) was obtained as a purple solid in 78% yield. ^{1}H NMR (400 MHz, $CDCl_3$) : δ ppm = 9.72 (d, J=4.8Hz, 4H), 9.16 (at, J=1.6 Hz, 2H), 9.01 (d, J=1.6Hz, 4H), 8.77 (d, J= 4.6 Hz, 4H), 4.55 (q, J=7.1Hz, 8H), 1.48 (t, J= 7.1Hz, 12H). ^{13}C NMR (101 MHz, $CDCl_3$): δ ppm 14.41, 61.74, 105.36, 119.42, 129.33, 129.88, 132.92, 133.58, 138.31, 143.41, 145.75, 150.49, 166.17. MALDI-TOF MS (m/z): 970.001 $(M)^+$. Elemental Analysis (%) Calculated for $C_{44}H_{36}Br_2N_4O_8Zn$: C, 54.37; H, 3.53; N, 5.76; Found C, 54.25; H, 3.55; N, 5.67.

Synthesis of meso-[5,15-bis-(3,5-(bis-ethoxycarbonyl)-phenyl)-10,20-bis(ferrocenyl-ethynyl)-porphyrinato]-zinc(II) (14)

Meso-[5,15-bis-(3,5-(bis-ethoxycarbonyl)-phenyl)-10,20-dibromo-porphyrinato]-zinc-(II) (325 mg, 0.334 mmol), ethynylferrocene (210.6 mg, 1.002 mmol), triphenyl-phosphine (45.5 mg, 0.173 mmol), copper iodide (16.2 mg, 0.085 mmol), triethylamine (20.8 ml) and pyridine (1,2 ml) were disolved in toluene (97.5 ml). The solution was purged with nitrogen for 15 min. Tris-(dibenzylidene-acetone)-dipalladium (18.7 mg, 0.032 mmol) were added to the solution which was left stirring overnight at 80 ^{o}C. The reaction mixture was left to warm to room temperature and then extracted with water. The organic phase was dried over $MgSO_4$, filtered, and the filtrate was evaporated under reduced pressure. The residue was separated by column chromatography on silica eluting with a solvent mixture of dichloromethane/ethyl acetate/pyridine (98:1:1). The purple solid obtained was recrystallized from dichloromethane/methanol to afford 275 mg (67%) of a microcrystalline material. ^{1}H NMR (400 MHz, $CDCl_3$) : δ ppm = 9.71 (d, J=4.6Hz, 4H), 9.16 (at, J=1.6 Hz, 2H), 9.04 (d, J=1.6Hz, 4H), 8.75 (d, J= 4.6 Hz, 4H), 4.96 (t, J=1.8Hz, 4H), 4.54 (q, J=7.2Hz, 8H), 4.50 (s, 10H), 4.49 (t, J=1.8Hz, 4H), 1.47 (t, J= 7.1Hz, 12H). ^{13}C NMR

(101 MHz, $CDCl_3$): δ ppm 14.40, 61.64, 66.27, 69.30, 70.07, 71.71, 89.10, 95.83, 102.51, 119.83, 129.37, 129.76, 131.27, 131.95, 138.28, 143.63, 149.40, 152.38, 166.22. MALDI-TOF MS (m/z): 1227.826 $(M)^+$. Elemental Analysis (%) Calculated for $C_{68}H_{52}Fe_2N_4O_8Zn$: C, 66.39; H, 4.26; N, 4.55; Found C, 66.46; H, 4.20; N, 4.57.

Synthesis of meso-5,15-bis-[3,5-(bis-ethoxycarbonyl)-phenyl]-10,20-bis(ferrocenyl-ethynyl)-porphyrin (15)

Meso-[5,15-bis-(3,5-(bis-ethoxycarbonyl)-phenyl)-10,20-bis(ferroce-nyl-ethynyl)-porphyrinato]-zinc(II) (200 mg, 0.163 mmol) were dissolved in dichloromethane (12 ml) and the solution was treated with trifluoroacetic acid (60 μL, 0.815 mmol) at 0 ^oC. The reaction mixture was washed with a 10 mM aqueous NaOH solution. The organic phase was dried over $MgSO_4$, filtered and evaporated under reduced pressure. The residue was separated by column chromatography on silica with dichloromethane/ethyl acetate/pyridine (98:1:1) as the elution solvent. Evaporation of the solvent and recrystallization from dichloromethane/methanol afforded 180 mg (95%) of a purple solid. ^1H NMR (400 MHz, $CDCl_3$) : δ ppm = 9.67 (d, J=4.7Hz, 4H), 9.19 (at, J=1.6 Hz, 2H), 9.06 (d, J=1.7Hz, 4H), 8.73 (d, J= 4.7 Hz, 4H), 4.97 (t, J=2.4Hz, 4H), 4.55 (q, J=7.2Hz, 8H), 4.52 (t, J=1.6Hz, 4H), 4.50 (s, 10H),1.47 (t, J= 7.2Hz, 12H) -1.81 (s, 2H). ^{13}C NMR (101 MHz, $CDCl_3$): δ ppm 1.03, 14.38, 29.71, 61.73, 65.54, 69.90, 70.15, 71.87, 87.92, 97.77, 102.78, 119.23, 128.40, 128.98, 129.90, 130.30, 138.20, 142.19, 165.98. MALDI-TOF MS (m/z): 1165.911 $(M)^+$. Elemental Analysis (%) Calculated for $C_{68}H_{54}Fe_2N_4O_8$: C, 69.99; H, 4.66; N, 4.80; Found C, 70.05; H, 4.61; N, 4.78.

Synthesis of meso-[5,15-bis-(3,5-(bis-ethoxycarbonyl)-phenyl)-10,20-bis(ferrocenyl-ethynyl)-porphyrinato]-magnesium(II) (17)

Meso-5,15-bis-(3,5-(bis-ethoxycarbonyl)-phenyl)-10,20-bis(ferroce-nyl-ethynyl)-porphyrin (100 mg, 0.086 mmol) was dissolved in a mixture of dichloromethane (10 ml) and N,N-diisopropylethylamine (0.42 ml). MgI_2 (176 mg, 0.63 mmol) was added and the suspension was stirred for 30 min in room temperature. The reaction mixture was diluted with dichloromethane (20 ml), washed with 10% NaOH (2 x 20 ml), dried over $MgSO_4$ and filtered. The solvent was evaporated under reduced pressure and the residue was chromatographed under deactivated neutral alumina (Brockmann III grade). The elution solvent was dichloromethane containing 1% of methanol. Recrystallization from dichloromethane/methanol afforded 95 mg (93%) of a purple solid. ^{1}H NMR (400 MHz, $CDCl_3$) : δ ppm = 9.71 (d, J=4.5Hz, 4H), 9.16 (at, J=1.6 Hz, 2H), 9.05 (d, J=1.6Hz, 4H), 8.75 (d, J= 4.4 Hz, 4H), 4.96 (t, J=1.9Hz, 4H), 4.54 (q, J=7.2Hz, 8H), 4.51 (s, 10H), 4.49 (t, J=1.9Hz, 4H), 1.47 (t, J= 7.1Hz, 12H). ^{13}C NMR (101 MHz, $CDCl_3$): δ ppm 14.41, 61.63, 66.39, 69.28, 70.07, 71.70, 89.45, 95.74, 103.44, 120.91, 129.33, 129.69, 131.45, 132.18, 138.37, 143.88, 149.30, 152.37, 166.25. MALDI-TOF MS (m/z): 1187.887 $(M)^+$. Elemental Analysis (%) Calculated for $C_{68}H_{52}Fe_2N_4O_8Mg$: C, 68.68; H, 4.41; N, 4.71; Found C, 68.60; H, 4.40; N, 4.74.

Synthesis of meso-5,15-bis-(isophthalic acid)-10,20-bis(ferrocenyl-ethynyl)-porphyrin (16)

Meso-5,15-bis-(3,5-(bis-ethoxycarbonyl)-phenyl)-10,20-bis(ferrocenylethynyl)-porphyrin (101 mg, 0.086 mmol) was dissolved in a 2:1 mixture of THF/MeOH (30 ml). The solution was

brought to refluxing temperature and another solution containing NaOH (2 g, 50 mmol) in a 5:2 mixture of MeOH/H_2O (14 ml) was added dropwise. The mixture was left to reflux for 2 h. The solution was left to return to room temperature and the solvent was removed under reduced pressure. The residue was dissolved in water and acidified to pH 1 using a 2 M aqueous hydrochloric acid solution. The greenish-purple cloudy suspension was centrifuged and the solid mass was collected and washed 3 times with water and 2 times with acetone. The residue was redissolved in a small amount of pyridine. Water was added (30 ml) and the suspension was centrifuged again. The residue washed 3 times with water and one time with acetone and dried to yield 85 mg (94%) of a purple solid. ^{1}H NMR (400 MHz, DMSO-d^6) : δ ppm = 9.64 (s, 4H), 8.91 (m, 6H), 6.57 (s, 4H), 6.49 (d, 4H), 5.11 (s, 4H), 4.62 (s, 4H), 4.52 (s, 10H), -2.17 (s, 2H). MALDI-TOF MS (m/z): 1055.5 $(M)^+$. Elemental Analysis (%) Calculated for $C_{60}H_{38}Fe_2N_4O_8$: C, 68.33; H, 3.63; N, 5.31; Found C, 68.22; H, 3.72; N, 5.25.

Synthesis of 3-(trimethylsilyl)-1-propynal (22)

Trimethylsilylacetylene (2.337 g, 23.8 mmol) was dissolved in anhydrous THF (150 ml) and the solution was bubbled with nitrogen for 15 min. A solution of 2.5 M n-BuLi in hexanes (10 ml, 25 mmol) were added dropwise at -78^o C and the reaction mixture was left to react at this temperature for 1 h. Dimethylformamide (2 ml) was added, the ice bath was removed and the solution was allowed to slowly reach room temperature. After stirring for 30 min, the solution was poured in 150 ml of an ice-water mixture containing 5% of HCl. The solution was neutralized with $NaHCO_3$ and extracted with dichloromethane (2x100 ml). The organic phases were combined, dried over $MgSO_4$, filtered and the solvent was evaporated under reduced

pressure. The yellow residue was separated by column chromatography on silica eluting with a mixture of hexane/dichloromethane (1:1) to yield 2.399 g (80%) of a pale yellow oil. ^{1}H NMR (400 MHz, $CDCl_3$) : δ ppm = 9.15 (s, 1H), 0.25 (s, 9H). ^{13}C NMR (101 MHz, $CDCl_3$): δ ppm 0.88, 102.3, 103.0, 176.7. ESI-MS (m/z) 127.0578 $(M+H)^+$. Elemental Analysis (%) Calculated for $C_{12}H_{22}OSi$: C, 57.09; H, 7.99; Found C, 57.16; H, 7.85.

Synthesis of 5-ferrocenyldipyromethane (24)

Ferrocenylcarboxaldehyde (4.00 g, 18.7 mmol) was dissolved in pyrrole (52 ml, 750 mmol) and the solution was degassed with nitrogen for 15 min. Trifluoroacetic acid (213 mg, 1.87 mmol) were added and the solution was stirred for 15 min at room temperature in the dark. The reaction mixture was diluted by the addition of 500 ml dichloromethane and washed with 0.1 M NaOH (200 ml). The organic phase was collected, dried with $MgSO_4$, filtered and evaporated under reduced pressure. The residue was thoroughly dried under high vacuum to remove all the remaining pyrrole. Chromatography on silica gel eluting with dichloromethane, afforded 4.56 g (74%) of a yellow solid. ^{1}H NMR (400 MHz, $CDCl_3$) : δ ppm = 7.98 (s, 2H), 6.69 (m, 2H), 6.18 (m, 2H), 6.05 (br s, 2H), 5.25 (s, 1H), 4.18 (t, J=1.9Hz, 2H). 4.13 (s, 5H), 4.12 (t, J=1.8Hz, 2H). ^{13}C NMR (101 MHz, $CDCl_3$): δ ppm 38.17, 67.61, 68.02, 68.93, 90.25, 106.49, 108.09, 116.76, 133.14. ESI-MS (m/z) 330.0803 $(M)^+$. Elemental Analysis (%) Calculated for $C_{19}H_{18}FeN_2$: C, 69.11; H, 5.49; N, 8.48; Found C, 68.99; H, 5.35 ; N, 8.39.

Synthesis of meso-5-15-bis(trimethylsilyl-ethynyl)-10,20-bis-ferrocenyl-porphyrin (25)

5-Ferrocenyldipyromethane (3126 mg, 9.48 mmol) and 3-(trimethylsilyl)-1-propynal (1404 µl, 9.58 mmol) were added in dichloromethane (560 ml). The solution was purged with nitrogen for 15 min. $BF_3 \cdot Et_2O$ (390 µl, 3.10 mmol) was added and the reaction was left stirring at room temperature for 30 min. p-Chloranil (3470 mg, 14.11 mmol) was added and the reaction mixture was stirred for 10 more min. The solution was passed through a column packed with silica in order to remove most of the black tar. The dark green residue left after evaporation of the solvent was separated by column chromatography on silica gel. The mobile phase consisted of a mixture of hexane/dichloromethane 50:50. The third dark-green tailing band was collected and removal of solvent left a purple solid which after recrystallization with dichloromethane/methanol afforded 1.133 g (27.4%) of a purple microcrystalline material. ^{1}H NMR (400 MHz, $CDCl_3$) : δ ppm = 9.87 (d, J=4.8Hz, 4H), 9.55 (d, J=4.8 Hz, 4H), 5.51 (t, J=1.8Hz, 4H), 4.87 (t, J= 1.8 Hz, 4H), 4.22 (s, 10H), 0.67 (s, 18H), -1.1 (s, 2H). ^{13}C NMR (101 MHz, $CDCl_3$): δ ppm 0.37, 69.37, 70.75, 88.34, 100.78, 102.03, 107.38, 119.89, 130.20, 131.38, 146.59, 148.03. MALDI-TOF MS (m/z): 870.964 $(M)^+$. Elemental Analysis (%) Calculated for $C_{50}H_{46}Fe_2N_4Si_2$: C, 68.96; H, 5.32; N, 6.43; Found C, 69.01; H, 5.40; N, 6.40.

Synthesis of meso-[5-15-bis(trimethylsilyl-ethynyl)-10,20-bis-ferrocenyl-porpyrinato]-zinc(II) (26)

Meso-5-15-bis(trimethylsilyl-ethynyl)-10,20-bis-ferrocenyl-porphyrin (300 mg, 0.344 mmol) was dissolved in a mixture of dichloromethane (60 ml) and methanol (20 ml). Zinc acetate

hydrate (307.2 mg, 1.374 mmol) was added and the solution was left stirring at room temperature for 45 min. The solution was washed with water, dried with $MgSO_4$, filtered and the solvent removed under reduced pressure. The residue was separated by column chromatography on silica gel eluting with a mixture of dichloromethane/hexane/ethyl acetate (50:50:1). The collected green fraction was stripped off solvent and the residue was recrystallized from dichloromethane/methanol to afford 289 mg (90%) of a purple microcrystalline material. ^{1}H NMR (400 MHz, $CDCl_3$) : δ ppm = 9.98 (d, J=4.6Hz, 4H), 9.53 (d, J=4.6 Hz, 4H), 5.51 (t, J=1.8Hz, 4H), 4.84 (t, J= 1.8 Hz, 4H), 4.18 (s, 10H), 0.64 (s, 18H). ^{13}C NMR (101 MHz, $CDCl_3$): δ ppm 0.47, 68.91, 70.53, 90.22, 100.28, 100.76, 108.69, 119.63, 129.76, 132.70, 150.88, 151.06. MALDI-TOF MS (m/z): 931.891 $(M)^+$. Elemental Analysis (%) Calculated for $C_{50}H_{44}Fe_2N_4Si_2Zn$: C, 64.28; H, 4.75; N, 6.00; Found C, 64.16; H, 4.73; N, 5.90.

Synthesis of meso-[5-15-bis(ethynyl)-10,20-bis-ferrocenyl-porpyrinato]-zinc(II) (27)

A solution of meso-[5-15-bis(trimethylsilyl-ethynyl)-10,20-bis-ferrocenyl-porpyrinato]-zinc(II) (200 mg, 0.214 mmol) in dichloromethane (30 ml) was cooled to 0 ^{o}C. A solution of 1.0 M tetrabutylammonium fluoride in THF (454 µl, 0.227 mmol) was added dropwise and the reaction was left stirring at 0 ^{o}C for 15 min. The reaction mixture was washed with water (2 x 30 ml), the organic phase dried with $MgSO_4$, filtered and the solvent evaporated under reduced pressure. The residue was separated by column chromatography on alumina eluting with dichloromethane containing 1% of pyridine. Recrystallization from dichloromethane/methanol afforded 153 mg (91%) of a purple solid. ^{1}H NMR (400 MHz, $CDCl_3$) : δ ppm = 10.01 (d, J=4.6Hz, 4H), 9.57 (d, J=4.6 Hz, 4H), 5.52 (t, J=1.8Hz, 4H), 4.84 (t, J= 1.8 Hz, 4H), 4.17 (s, 10H), 4.15 (s, 2H). ^{13}C

NMR (101 MHz, $CDCl_3$): δ ppm 68.89, 70.55, 70.60, 82.86, 86.98, 90.14, 99.45, 119.63, 129.81, 132.96, 150.92, 151.17. MALDI-TOF MS (m/z): 787.817 $(M)^+$. Elemental Analysis (%) Calculated for $C_{44}H_{28}Fe_2N_4Zn$: C, 66.91; H, 3.57; N, 7.09; Found C, 66.82; H, 3.63 ; N, 6.97.

Synthesis of meso-[5-15-bis-[3,5-bis-(ethoxycarbonyl)-ethynyl]-10,20-bis-ferrocenyl-porpyrinato]-zinc(II) (28)

Meso-[5-15-bis(ethynyl)-10,20-bis-ferrocenyl-porpyrinato]-zinc(II) (210 mg, 0.267 mmol), triphenylarsine (90 mg, 0.294 mmol), 3,5-diethyl-iodoisophthalate (420 mg, 1.206 mmol) and pyridine (1 ml) were dissolved in a mixture of anhydrous triethylamine (43 ml) and anhydrous THF(90 ml). The reaction mixture was purged with nitrogen for 15 min after which, bis-(dibenzylidene-acetone)-dipalladium (23 mg, 0.025 mmol) was added. The solution was left stirring overnight at room temperature. Completion of reaction was confirmed by TLC and the solvent was evaporated under reduced pressure. The residue was left to dry thoroughly under high vacuum and the solid obtained was purified by chromatography on alumina. Dichloromethane/hexane 2:1 containing 1% of pyridine was used as the mobile phase. The dark green band was collected, evaporated and the residue recrystallized from dichloromethane/methanol to afford 249 mg (76%) of a purple solid. ^1H NMR (400 MHz, $CDCl_3$): δ ppm = 10.04 (d, J=4.6Hz, 4H), 9.63 (d, J=4.6 Hz, 4H), 8.86 (d, J=1.5Hz, 4H), 8.78 (at, J=1.6Hz, 2H), 5.54 (t, J=1.8Hz, 4H), 4.86 (t, J= 1.8 Hz, 4H), 4.56 (q, J=7.2Hz, 8H), 4.19 (s, 10H), 1.55 (t, J=7.2Hz, 12H). ^{13}C NMR (101 MHz, $CDCl_3$): δ ppm14.45, 61.72, 68.97, 70.59, 70.63, 90.07, 93.80, 95.47, 100.23, 120.44, 125.40, 129.59, 129.82, 131.61, 133.03, 136.22,

150.63, 151.16, 165.50. MALDI-TOF MS (m/z): 1227.808 $(M)^+$. Elemental Analysis (%) Calculated for $C_{68}H_{52}Fe_2N_4O_8Zn$: C, 66.39; H, 4.26; N, 4.55; Found C, 66.45; H, 4.22; N, 4.54.

Synthesis of 3-(triisopropylsilyl)-1-propynal (31)

Triisopropylsilylacetylene (4.11 g, 22.5 mmol) was dissolved in anhydrous diethyl ether (20 ml) and the solution was bubbled with nitrogen for 15 min. A solution of 2.5M n-BuLi in hexanes (20 ml, 25 mmol) were added dropwise at 0 ^oC and the reaction mixture was left to react at this temperature for 1 h. Dimethylformamide (5.22 ml) was added at -78 ^oC and the mixture was left to react at this temperature for 1 h. The ice bath was removed and the solution was allowed to slowly reach room temperature over the course of 1 h. The solution was poured in 150 ml of an ice-water mixture containing 5% of HCl. Neutralization with $NaHCO_3$ was followed by extraction with dichloromethane (2x100 ml). The organic phases were combined, dried over $MgSO_4$, filtered and the solvent was evaporated under reduced pressure. The yellow residue was separated by column chromatography on silica eluting with a mixture of hexane/dichloromethane (9:1) to yield 4.536 g (96%) of a pale yellow oil. ^1H NMR (400 MHz, $CDCl_3$) : δ ppm = 9.22 (s, 1H), 1.11-1.17 (m, 21H). ^{13}C NMR (101 MHz, $CDCl_3$): δ ppm 10.96, 18.42, 100.82, 104.49, 176.58. ESI-MS (m/z): 211.1514 $(M+H)^+$. Elemental Analysis (%) Calculated for $C_{12}H_{22}OSi$: C, 68.51; H, 10.54; Found C, 68.41; H, 10.65.

Synthesis of dipyrromethane (32)

Paraformaldehyde (3.00 g, 100.0 mmol) were added into a 1 L round bottom flask containing pyrrole (700 ml, 10 mol). The mixture was purged with nitrogen for 15 min and the temperature raised to 55 ^{o}C until a clear solution was obtained. Indium trichloride (2.22 g, 10 mmol) was added and the reaction was left stirring at 55 ^{o}C for 2.5 h under an inert atmosphere. Heating was removed and NaOH (12 g, 0.30 mol) was added to quench the reaction. The mixture was stirred for 1 h after which it was filtered to remove any solids present. Pyrrole was removed by evaporation under reduced pressure and the residue was separated by column chromatography on silica with hexane/ethyl acetate/triethylamine (10:1:0.1) as the elution solvent. Dipyrromethane was obtained as a white solid in 40% yield. ^{1}H NMR (400 MHz, $CDCl_3$): δ ppm = 7.87 (br s, 2H), 6.69 (ddd, J_1=2.6Hz, J_2=2.6Hz, J_3=2.6Hz, 2H), 6.19 (m, 2H), 6.07 (m, 2H), 4.01 (s, 2H). ^{13}C NMR (101 MHz, $CDCl_3$): δ ppm 26.41, 106.40, 108.43, 117.27, 129.06. ESI-MS (m/z): 147.0917 $(M+H)^{+}$. Elemental Analysis (%) Calculated for $C_9H_{10}N_2$: C, 73.94; H, 6.89; N, 19.16; Found C, 73.81; H, 6.82 ; N, 19.07 .

Synthesis of meso-5,15-bis[(triisopropylsilyl)ethynyl]porphyrin (33)

3-(triisopropylsilyl)-1-propynal (5,59 g, 26.6 mmol) and dipyrromethane (1,944 g, 13.3 mmol) were dissolved in dichloromethane (800 ml). The solution was degassed by purging with nitrogen for 20 min. $BF_3{\cdot}Et_2O$ (556 µl, 4.42 mmol) were added slowly at 0 ^{o}C and the reaction was stirred at this temperature for 45 min. DDQ (4600 mg, 20.26 mmol) was added and the stirring was continued for a further 10 min. The solvent volume was reduced to approximately 100 ml and the solution was passed through a packed column of silica gel in order to remove

most of the black tar. The material obtained was separated by column chromatography on silica gel using dichloromethane as the elution solvent. The collected purple fraction was evaporated and the solid obtained was recrystallized from dichloromethane/methanol to afford 5,15-bis[(triisopropylsilyl)ethynyl]porphyrin in 29% yield. ^{1}H NMR (400 MHz, $CDCl_3$) : δ ppm = 10.05 (s, 2H), 9.69 (d, J=4.5Hz, 4H), 9.27 (d, 4.6Hz, 4H), 1.51-1.57 (m, 42H). ^{13}C NMR (101 MHz, $CDCl_3$): δ ppm 11.93, 19.16, 99.46, 99.93, 106.66, 107.96, 130.24, 131.90, 145.18, 149.12. MALDI-TOF MS (m/z): 670.199 $(M)^+$. Elemental Analysis (%) Calculated for $C_{42}H_{54}N_4Si_2$: C, 75.17; H, 8.11; N, 8.35; Found C, 75.07; H, 8.11; N, 8.27.

Synthesis of meso-[5,15-bis[(triisopropylsilyl)ethynyl]porphyrinato]magnesium(II) (34)

Meso-5,15-bis[(triisopropylsilyl)ethynyl]porphyrin (200 mg, 0.398 mmol) was dissolved in a mixture of dichloromethane (50 ml) and N,N-diisopropylethylamine (1.87 ml). MgI_2 (387.2 mg, 1.393 mmol) was added and the suspension was stirred for 30 min at room temperature. The reaction mixture was diluted with dichloromethane (100 ml), washed with 10% NaOH (2 x 100 ml), dried over $MgSO_4$ and filtered. The solvent was evaporated under reduced pressure and the residue was separated by column chromatography on deactivated neutral alumina (Brockmann III grade). The elution solvent was dichloromethane containing 1% of methanol. Recrystallization from dichloromethane/methanol afforded 202 mg (97%) of a purple solid. ^{1}H NMR (400 MHz, $CDCl_3$) : δ ppm = 10.16 (s, 2H), 9.84 (d, J=4.3Hz, 4H), 9.35 (d, 4.4Hz, 4H), 1.50-1.55 (m, 42H). ^{13}C NMR (101 MHz, $CDCl_3$): δ ppm. 12.03, 19.20, 97.11, 100.90, 108.48, 110.42, 131.58, 132.36, 149.39, 152.40. MALDI-TOF MS (m/z): 692.131 $(M)^+$. Elemental

Analysis (%) Calculated for $C_{42}H_{52}N_4Si_2Mg$: C, 72.75; H, 7.56; N, 8.08; Found C, 72.20; H, 7.61; N, 8.02.

Synthesis of meso-[5,15-bis[(triisopropylsilyl)ethynyl-10,20-dibromo]porphyrin-ato]-magnesium(II) (35)

Meso-[5,15-bis[(triisopropylsilyl)ethynyl]porphyrinato]magnesium(II) (950 mg, 1.81 mmol) was dissolved in dichloromethane containing 1% pyridine. The reaction mixture was cooled to 0 ^{o}C. N-bromosuccinimide (322.18 mg, 5.79 mmol) was dissolved in dichloromethane and the solution was transferred to an addition funnel. The NBS solution was allowed to drip into the porphyrin solution very slowly over the course of one hour at 0 ^{o}C. When the addition was complete, the cold bath was removed and the reaction was left to reach room temperature. The solution was washed twice with water, dried over $MgSO_4$ and filtered. Evaporation of the solvent under reduced pressure gave a dark green solid. Further purification was performed with column chromatography on silica gel eluting with a mixture of hexane/ethyl acetate/pyridine (10:1:0.1). Recrystallization of the material obtained from dichloromethane/methanol afforded 715 mg (58%) of a purple solid. ^{1}H NMR (400 MHz, $CDCl_3$): δ ppm = 9.67 (d, J=4.5Hz, 4H), 9.63 (d, 4.6Hz, 4H), 1.47-1.55 (m, 42H). ^{13}C NMR (101 MHz, $CDCl_3$): δ ppm.11.96, 19.15, 98.63, 103.30, 107.64, 109.66, 132.64, 133.84, 148.86, 153.00. MALDI-TOF MS (m/z): 849.941 $(M)^{+}$. Elemental Analysis (%) Calculated for $C_{42}H_{50}Br_2N_4Si_2Mg$: C, 59.27; H, 5.92; N, 6.58; Found C, 59.13; H, 6.02 ; N, 6.41.

Synthesis of meso-[5,15-bis[(triisopropylsilyl)ethynyl-10,20-bis(ferrocenylethynyl)]porphyrinato]magnesium(II) (36)

Meso-[5,15-bis[(triisopropylsilyl)ethynyl-10,20-dibromo]porphyrinato]magnesium(II) (486 mg, 0.715 mmol), triphenylphosphine (112 mg, 0.42 mmol), ferrocenylacetylene (500 mg, 2.38 mmol), copper iodide (41 mg, 0.215 mmol) and pyridine (3 ml) were dissolved in a mixture of toluene (242 ml) and anhydrous triethylamine (52 ml). The solution was degassed by purging nitrogen for 15 min. Bis-(dibenzylidene-acetone)-dipalladium (46.6 mg, 0.08 mmol) were added and the reaction was left to proceed at 60 ^{o}C for 2 h. Heating was removed and the reaction mixture was washed with water (2x100 ml), dried over $MgSO_4$, filtered and the solvent evaporated under reduced pressure. The residue was left for several hours under high vacuum in order to remove any traces of solvent. The product was purified by chromatography on silica gel. The mobile phase consisted initially of dichloromethane/hexane (1:1) in order to remove some unwanted byproducts. After that the mobile phase was changed to dichloromethane/hexane (2:1) and the dark green band was collected and the solvent evaporated. The material obtained was purified further by recrystallization from dichloromethane/methanol affording 416 mg (62%) a purple microcrystalline material. ^{1}H NMR (400 MHz, $CDCl_3$) : δ ppm = 9.66 (d, J=4.4Hz, 4H), 9.63 (d, 4.4Hz, 4H), 4.98 (t, J=1.8Hz, 4H), 4.54 (s, 10H), 4.52 (t, J=1.9Hz, 4H), 1.46-1.54 (m, 42H). ^{13}C NMR (101 MHz, $CDCl_3$): δ ppm. 11.98, 19.18, 66.30, 69.31, 70.13, 71.71, 103.50, 125.42, 128.41, 128.98, 130.52, 131.54, 131.67, 143.37, 151.94, 151.96 . MALDI-TOF MS (m/z): 1108.056 $(M)^{+}$. Elemental Analysis (%) Calculated for $C_{66}H_{68}Fe_2N_4Si_2Mg$: C, 71.45; H, 6.18; N, 5.05; Found C, 71.57; H, 6.15; N, 4.94.

Synthesis of meso-5,15-bis[(triisopropylsilyl)ethynyl-10,20-bis(ferrocenylethynyl)-porphyrin (37)

Meso-[5,15-bis[(triisopropylsilyl)ethynyl-10,20-bis(ferrocenylethynyl)]porphyrinato]-magnesium(II) (200 mg, 0.180 mmol) was disolved in dichloromethane (12 ml) and the solution treated with trifluoroacetic acid (60 μL, 0.815 mmol) at 0 ^{o}C. The reaction mixture was washed with a 10 mM aqueous NaOH solution. The organic phase was dried over $MgSO_4$, filtered and evaporated under reduced pressure. The residue was separated by column chromatography on silica with dichloromethane/ethyl acetate/pyridine (98:1:1) as the elution solvent. Evaporation of the solvent and recrystallization from dichloromethane/methanol afforded 180 mg (95%) of a purple solid. ^{1}H NMR (400 MHz, $CDCl_3$) : δ ppm = 9.70 (d, J=4.7Hz, 4H), 9.68 (d, J=4.7Hz, 4H), 5.00 (t, J=1.8Hz, 4H), 4.54 (s, 10H), 4.52 (t, J=1.8Hz, 4H), 1.46-1.58 (m, 42H). ^{13}C NMR (101 MHz, $CDCl_3$): δ ppm 11.96, 19.20, 69.33, 70.14, 71.71, 103.46, 104.42, 125.38, 128.43, 129.00, 130.56, 131.53, 131.66, 134.77, 143.11, 151.92. MALDI-TOF MS (m/z): 1086.115 $(M)^{+}$. Elemental Analysis (%) Calculated for $C_{66}H_{70}Fe_2N_4Si_2$: C, 72.92; H, 6.49; N, 5.15; Found C, 72.93; H, 6.42; N, 5.12.

Synthesis of meso-[5,15-bis(ethynyl)-10,20-bis(ferrocenylethynyl)]porphyrina-to]magnesium(II) (38)

Meso-[5,15-bis[(triisopropylsilyl)ethynyl-10,20-bis(ferrocenylethynyl)]porphyrinato]magnesium(II) (142 mg, 0.151 mmol) was dissolved in dichloromethane (20 ml). A solution of 1.0M TBAF (0.37 mmol, 2.1 equiv.) was added slowly and the reaction was left stirring at room temperature for 2 h. The solution was washed with water (2x10 ml), dried over $MgSO_4$, filtered

and the solvent was evaporated under reduced pressure. The residue was purified by chromatography on deactivated alumina (Brockman III). Dichloromethane was initially used as the mobile phase to remove a small amount of impurities. A dark-brown band came off after elution with dichloromethane containing 2% of methanol. Recrystallization from dichloromethane/methanol afforded 108 mg (90%) of a purple solid. ^{1}H NMR (400 MHz, $CDCl_3$): δ ppm = 9.63 (s, 8H), 4.99 (t, J=1.9Hz, 4H), 4.53 (s, 10H), 4.52 (t, J=1.9Hz, 4H), 4.20 (s, 2H). ^{13}C NMR (101 MHz, $CDCl_3$): δ ppm 12.17, 17.60, 19.18, 30.55, 69.38, 70.12, 71.79, 127.78, 127.90, 129.95, 131.68, 151.72, 152.06. MALDI-TOF MS (m/z): 795.92 $(M)^+$. Elemental Analysis (%) Calculated for $C_{48}H_{28}Fe_2N_4Mg$: C, 72.36; H, 3.54; N, 7.03; Found C, 72.25; H, 3.51; N, 7.00.

Attempted synthesis of meso-[5-15-bis-[3,5-bis-(ethynyl)]-10,20-bis-(ferrocenylethynyl)-porphyrin (39)

Meso-5,15-bis[(triisopropylsilyl)ethynyl-10,20-bis(ferrocenylethynyl)-porphyrin (100 mg, 0.092 mmol) was dissolved in dichloromethane (15 ml) and the solution was cooled to 0 ^{o}C. A solution of 1.0M TBAF (193 μl, 0.193mmol) was added slowly and the reaction was left stirring at 0 ^{o}C for 4 h. The solution was washed with water (2x10 ml), dried over $MgSO_4$, filtered and the solvent was passed through a deactivated alumina (Brockman III) column eluting with dichloromethane containing 1% methanol. After evaporation of the solvent, the purple solid obtained could not be redissolved in any solvent.

Attempted synthesis of meso-[5-15-bis-[3,5-bis-(ethoxycarbonyl)-ethynyl]-10,20-bis-(ferrocenylethynyl)-porpyrinato]-magnesium(II) (40)

Meso-[5,15-bis(ethynyl)-10,20-bis(ferrocenylethynyl)]porphyrinato]magnesium(II) (269 mg, 0.338 mmol), triphenylarsine (113.4 mg, 0.370 mmol), 3,5-diethyl-iodoisophthalate (529 mg, 1.52 mmol) and pyridine (1 ml) were dissolved in a mixture of anhydrous triethylamine (54 ml) and anhydrous THF(113 ml). The reaction mixture was purged with nitrogen for 15 min after which, bis-(dibenzylidene-acetone)-dipalladium (29 mg, 0.0315 mmol) was added. The solution was left stirring overnight at room temperature. The solvent was evaporated under reduced pressure. The residue was left to dry thoroughly under high vacuum in order to remove every trace of solvent. Several attempts to purify the residue did not lead to a sufficiently pure material.

3.8 References

1. F. Cerrina, *J. Phys. D: Appl. Phys*., **2000**, *33*, R103.

2. H. Sewell and J. Mulkens, *J. Annu. Rev. Mater. Res.*, **2009**, *29*, 127.

3. Institute of Microelectronics of Chinese Academy of Sciences, http://english.ime.cas.cn/ns/es/201002/t20100223_50959.html

4. R. W. Keyes, *Proc. IEEE*, **2001**, *3*, 227.

5. A. Aviram, M. A. Ratner, *Chem. Phys. Lett*., **1974**, *29*, 277.

6. K. S. Kwok, J. C. Ellenbogen, *Mater. Today*, **2002**, *2*, 28.

7. R. L. Carroll, C. B. Gorman, *Angew. Chem. Int. Ed.*, **2002**, *41*, 4378.

8. J. A. Theobald, N. S. Oxtoby, M. A. Phillips, N. R. Champness, P. H. Beton, *Nature*, **2003**, *424*, 1029.

9. M. A. Reed, J. Chen, A. M. Rawlett, D. W. Price, J. M. Tour, *Appl. Phys. Lett.* **2001**, *23*, 3735.

10. M. Diehl, S. N. Yaliraki, R. A. Beckman, M. Barahona, J. R. Heath, *Angew. Chem. Int. Ed.*, **2002**, *2*, 353.

11. M. Lieberman, C. S Lent, B. Isaksen, *J. Am. Chem. Soc.*, **2003**, *4*, 1056.

12. P. J. Kuekes, R. S. Williams, *U. S. Patent No. 6,256,767*, 3 July **2001**.

13. K. M. Roth, N. Dontha, R. B. Dabke, D. T. Gryko, C. Clausen, J. S. Lindsey, D. F. Bocian, W. G. Kuhr, *J. Vac. Sci. Technol. B*, **2000**, *5*, 2359.

14. D. Gryko, J. Li, J. R. Diers, K. M. Roth, D. F. Bocian, D. G. Kuhr, J. S. Lindsey, *J. Mater. Chem.*, **2001**, *11*, 1162.

15. K. M. Roth, J. S. Lindsey, D. F. Bocian, D. G. Kuhr, *Langmuir*, **2002**, *18*, 4030.

16. K. M. Roth, A. A. Yasseri, Z. Liu, R. B. Dabke, V. Malinovskii, K. Schweikart, L. Yu, H. Tiznado, F. Zaera, J. S. Lindsey, W. G. Kuhr, D. F. Bocian, *J. Am. Chem. Soc*., **2003**, *125*, 505.

17. T. D. Gryko, F. Zhao, A. A. Yasseri, K. M. Roth, D. F. Bocian, W. G. Kuhr, J. S. Lindsey, *J. Org. Chem.*, **2000**, *65*, 7356.

18. Z. Liu, A. A. Yasseri, J. S. Lindsey, D. F. Bocian, *Science,* **2003,** *302*, 1543.

19. M. Mannini, F. Pineider, P. Sainctavit, C. Danieli, E. Otero, C. Sciancalepore, A. M. Talarico, M. A. Arrio, A. Cornia, D. Gatteschi, R. Sessoli, *Nature Materials,* **2009**, *8*, 194.

20. D. Gatteschi , R. Sessoli, A. Cornia, *Chem. Commun.*, **2000**, *9*, 725.

21 J. Yu, S. Mathew, B. S. Flavel, J. S. Quinton, M. R. Johnston, J. G. Shapter , *Nanoscience and Nanotechnology*, **2008**. ICONN, 176.

22. Q. Li, G. Mathur, S. Gowda, S. Surthi, Q. Zhao, L. Yu, J. S. Lindsey, D. F. Bocian, V. Misra, *Adv. Mater.*, **2004**, *16*, 133.

23. B. Fabre, *Acc. Chem. Res.,* **2010**, *43*, 1509.

24. K. M. Roth, J. S. Lindsey, D. F. Bocian, W. G. Kuhr, *Langmuir*, **2002**, *18*, 4030.

25. D. Kalita, M. Morisue, Y. Kobuke, *New J. Chem.*, **2006**, *30*, 77.

26. L. Wei, K. Padmaja, W.J. Youngblood, A.B. Lysenko, J.S. Lindsey, D.F. Bocian, *J. Org. Chem.*, **2004**, *69*, 1461.

27. K. M. Roth, D. T. Gryko, C. Clausen, J. Li, J. S. Lindsey, W. G. Kuhr, D. F. Bocian, *J. Phys. Chem. B,* **2002,** *106,* 8639.

28. J. R. Hahn, W. Ho, *Phys. Rev. Lett.*, 2001, *87*, 166102.

29. M. Lastapis, D. Riedel, L. Hellner, G. Comtet and G. Dujardin, *Science*, **2005**, *308*, 1000.

30. D. Heim, K. Seufert, W. Auwa rter, C. Aurisicchio, C. Fabbro, D. Bonifazi, J. V. Barth

31**.** S. Mohnania, D. Bonifazia, *Coord. Chem. Rev.,* **2010**, *254*, 2342.

32. H. Spillmann, A. Kiebele, M. Stöhr, T. A. Jung, D. Bonifazi, F. Cheng, F. Diederich, *Adv. Mater.*, **2006**, *18*, 275.

33. S. Yoshimoto, K. Itaya, *J. Porphyrins Phthalocyanines,* **2007**, *11*, 313.

34. L.Grill, M. Dyer, L. Lafferentz, M. Persson, M.V. Peters, S. Hecht, *Nat. Nanotechnol*., **2007**, *2*, 687.

35. J. E. Freund, M. Edelwirth, P. Krobel, W. M. Heckl, *Phys. Rev. B*, **1997**, i, 5394.

36. M. Bohringer, K. Morgenstern, W. D. Schneider, R. Berndt, F. Mauri, A. De Vita, R. Car, *Phys. Rev. Lett.,* **1999**, *83*, 324.

37. M. M. Reiter, F. Jamitzky, F. Trixler, W. M. Heckl, *Phys. Status Solidi A*, **2001**, *187*, 171.

38. T. Yokoyama, S. Yokoyama, T. Kamikado, *Nature*, **2001**, *413*, 619.

39. L. Scudiero, K. W. Hipps, D. R. J. Barlow, *Phys. Chem. B*, **2003**, *107*, 2903.

40. J. A. Theobald, N. S. Oxtoby, M. A. Phillips, N. R. Champness, P. H. Beton, *Nature,* **2003**, *424*, 1029.

41. S. De Feyter, F. C. De Schryver, *Chem. Soc. Rev*. **2003**, *32*, 139.

42. M. Lackinger, S. Griessl, T. Markert, F. Jamitzky, W. M. J. Heckl, *Phys. Chem. B*, **2004**, *108*, 13652.

43. E. B. Fleischer, *Acc. Chem. Res*., **1070**, *3*, 105.

44. S. S. Eaton, G. R. Eaton, *J. Am. Chem. Soc.*, **1975**, *97*, 3660.

45. D. T. Win, *AU. Journal of. Tech.*, **2010**, *13*, 151.

46. A. Cornia, A. C. Fabretti, M. Pacchioni, L. Zobbi, D. Bonacchi, A. Caneschi, D. Gatteschi, R. Biagi, U. Del Pennino, V. De Renzi, L. Gurevisch, H. S. J. Van der Zant, *Angew. Chem. Int. Ed.*, **2003**, *42*, 1645.

47. L. Bogani, W. Wernsdorfer, *Nature Materials*, **2008**, *7*, 179.

48. E. Coronado, C. Marti-Gastaldo, S. Tatay, *Appl. Surf. Science*, **2007**, *254*, 225.

49. D. A. Thomson, J. S. Best, *J. Res. Dev*., **2000**, *3*, 311.

50. M. Affronte, F. Troiani, A. Ghirri, A. Candini, M. Evangelisti, V. Corradini, S. Carretta, P. Santini, G. Amoretti, F. Tuna, G. Timco, R. E. P. Winpenny, *J. Phys D : Appl. Phys.*, **2007**, i, 2999.

51. A. D. Adler, F. R. Longo, J. D. Finarelli, J. Goldmacher, J. Assour, L. Korsakoff, *J. Org. Chem.,* **1967**, *32*, 476.

52. J. S. Lindsey, I. C. Schreiman, H. C. Hsu, P. C. Kearney, A. M. Marguerettaz, *J. Org. Chem.* **1987**, 52, 827.

53. G. P. Arsenault, E. Bullock, S. F. MacDonald, *J. Am. Chem. Soc.,* **1960**, *82*, 4384.

54. B. J. Littler, Y. Ciringh, J. S. Lindsey, *J. Org. Chem.*, **1999**, *64*, 2864.

55. D. M. Wallace, S. H. Leung, M. 0. Senge, K. M. Smith, *J. Org. Chem.***, 1993**, *58*, 1245.

56. J. K. Laha, S. Dhanalekshmi, M. Taniguchi, A. Ambroise, J. S. Lindsey, *Org. Proc. Res. & Devel.*, **2003**, *7*, 799.

57. C. Muthiah, M. Taniguchi, H. Kim, I. Schmidt, H. L. Kee, D. Holten, D. F. Bocian, J. S. Lindsey, *Photochemistry and Photobiology*, **2007**, *83*, 1513.

58. F. C. Grozema, C. Houarner-Rassin, P. Prins, Laurens, D. A. Siebbeles, H. L. Anderson, *J. Am. Chem. Soc.*, **2007**, *129,* 13370.

59. J. S. Lindsey, J. N. Woodford, *Inorg. Chem.,* **1995**, *34*, 1063.

60. M. Strell, T. Urumow, *Liebigs Ann. Chem.,* **1977**, *6*, 970.

61. H. P. Isenring, E. Zass, K. Smith, H. Falk, H. J. L. Luisier, A. Eschenmoser, *Helv. Chim. Acta,* **1975**, *1*,58.

62. E. Zass, H. P. Isenring, R. Etter, A. Eschenmoser, *Helv. Chim. Acta,* **1980**, *63*, 1048.

63. M. R. Wasielewski, *Tetrahedron Lett.,* **1977**, *16*, 1373.

64. M. Ptaszek, B. E. McDowell, J. S. Lindsey, *J. Org. Chem.,* **2006**, *71*, 4328.

65. M. Taniguchi, A. Balakumar, D. Fan, Brian E. McDowell, Jonathan S. Lindsey, *J. of Porph. And Phthal.,* **2005**, *9*, 554.

66. L. R. Nudy, H. G. Hutchinson, C. Schieber, F. R. Longo, *Tetrahedron*, **1984**, *40*, 2359.

67. T. E. O. Screen, K. B. Lawton, G. S. Wilson, N. Dolney, R. Ispasoiu, T. Goodson, S. J. Martin, D. D. C. Bradley, H. L. Anderson, *J. Mater. Chem.,* **2001**, *11*, 312.

68. A. Auger, J. C. Swarts, *Organometallics,* **2007**, *26*, 102.

69. R. Chauvin, *Tetrahedron Lett.*, **1995**, *36*, 401.

70. O. Robles, F. E. McDonald, *Org Lett.*, **2008**, *10*, 1811.

71. E. O. Thomas, K. B. Screen, L. G. Scott, W. N. Dolney, R. I. T. Goodson, S. J. M. Donal, D. C. Bradley, H. L. Anderson, *J. Mater. Chem.*, **2001**, *11*, 312.

72. K. M. Kadish, K. M. Smith, R. Guilard, The Porphyrin Handbook, Vol 8, **1999**, Elsevier.

73. G. Gritzner, J. Kuta, *Pure Appl. Chem.*, **1984**, *56*, 461.

74. (a) D. H. Evans, K. M. O'Connell, R. A. Peterson, M. J. Kelly, *J. Chem. Educ.*, **1983**, *60*, 291. (b) P. T. Kissinger, W. R. J. Heineman, *Chem. Educ.* **1983**, *60*, 702. (c) J. J. Van Benshoten, J. Y. Lewis, W. R. J. Heineman, *Chem. Educ.*, **1983**, *60*, 772.

75. R. S. Nicholson, *Anal. Chem.*, **1966**, *38*, 1406.

76. L. Cuffe, R. D. A. Hudson, J. F. Gallagher, S. Jennings, C. J. McAdam, R. B. T. Connelly, A. R. Manning, B. H. Robinson, J. Simpson, *Organomettalics*, **2005**, *24*, 2051.

77. J. Tiburcio, V. M. Ugalde-Salvidar, S. J. Loeb, H. Torrens, *Inorg. Chim. Acta*, **2009**, *362*, 4241.

78. H. Fink, N. J. Long, A. J. Martin, G. Opromolla, A. J. P. White, D. J. Williams, P.

Zanello, *Organomettalics*, **1997**, *16*, 2646.

79. a) E. McGale, B. H. Robinson, J. Simpson, *Organomettalics*, **2003**, *22*, 931. b) A. Klein, O. Lavastre, J. Fiedler, *Organometallics*, **2006**, *25*, 635.

80. N. Chawdhury, N. J. Long, M. F. Mahon, L-L. Ooi, P. R. Raithby, S. Rooke, A. J. P. White, D. J. Williams, M. Younus, *J. Org. Chem*., **2004**, *689*, 840.

81. O. Lavastre, J. Plass, P. Bachmann, S. Guesmi, C. Moinet, P. H. Dixneuf, *Organomettalics*, **1997**, *16*, 184.

82. J. L. Soret, *Comptesrendus de l'Académie des sciences,* **1883**, *97*, 1269.

83. M. Gouterman, *J. Mol. Spec.,* **1961**, *6*, 138.

84. G. Ulrich, R. Ziessel, *J. Org. Chem.,* **2004**, *69*, 2070.

85. Á. Díez, E. Lalinde, M. T. Moreno, S. Sánchez, *Dalton Trans.*, **2009**, 3434.

86. G. Doisneau, G. Balavoine, T. Fillebeen-Khan, *J. Organomet. Chem.*, **1992**, *425*, 113.

87. B. Fabre, S. Ababou-Girard, P. Singh, J. Kumar, S. Verma, A. Bianco, *Electrochem. Comm.*, **2010,** *12*, 831.

Chapter 4:

Design, synthesis, characterisation and spectroelectrochemical studies of homoleptic and heteroleptic dipyrrin metal complexes.

4.1 Introduction

4.1.1 Dye-Sensitized Solar Cells

Global warming is a major problem that humanity faces. As years pass by and energy consumption rises along with population growth, an efficient solution to this problem needs to be found. In addition, fossil fuel exhaustion will have enormous political and social implications on a global scale. A new energy source needs to be found that will be renewable, abundant and friendly to the environment.

The sun has been the primal source of most energy forms that have been utilized by man. It supplies the Earth with 3×10^{24} J per year. This equals with 10^4 times more energy than that of global human consumption[1]. A direct harnessing and utilization of this energy form would solve the aforementioned problems. Solar cells are devices that directly convert light into electricity. A lot of interest and an increased amount of research is directed towards this technology. It has been calculated that from a device that has an energy conversion efficiency of 10%, a 0.1% coverage of the earth's surface would yield enough renewable energy to cover all our energy needs. In addition, this technology can offer great decentralization opportunities causing the minimization of energy losses through electric power transmission as well as big political changes.

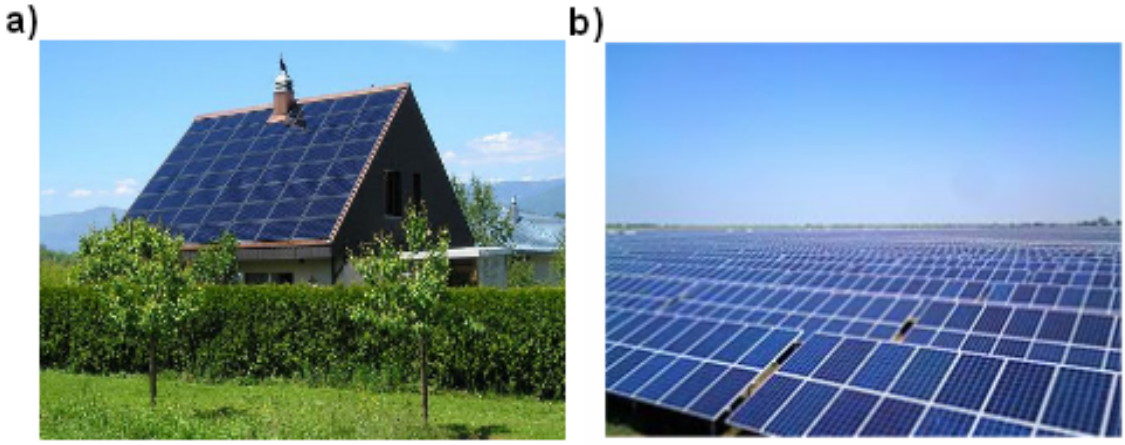


Figure 4.1. Solar cell applications a) Futuristic house comprising a roof dressed with solar cells b) Photovoltaic plant in Okhotnykovo, Ukraine, capable of producing ~80 MW.

Today, the most popular solar cell technology destined for light harvesting on the Earth's surface consists of cells based on crystalline silicon. The crystalline silicon acts as a semiconductor diode which absorbs the incoming photons and transforms them into electron-hole pairs. During this photogeneration step, all photons whose energy is smaller than the semiconductor's bandgap ($E_{gap)}$ do not contribute to the produced energy while all photons whose energy is larger than E_{gap}, loose this extra energy in the form of heat[2]. Under this principle of operation, the sun's energy cannot be effectively harnessed. Another disadvantage of silicon-based solar cells is their manufacturing cost. While it is still one of the most cost efficient solar cells (comparing to their energy conversion efficiency), grid parity cannot be achieved.

Michael Grätzel invented the dye-sensitized solar cell (DSSC) in 1991 which is a promising technology for the conversion of solar radiation into electrical energy on a large scale[3]. DSSCs offer many advantages. Fabrication without the use of expensive materials and energy demanding processes are attractive qualities which lower the manufacturing cost. Furthermore,

the ability to tune their absorption characteristics, as will be described later, allow for greater exploitation of the sun's energy. Flexibility concerning the choice of substrate and the variety of their presentation and appearance make them attractive for domestic, architectural or decorative applications.

A DSSC consists of several components. A sensitizer (dye), an electrolyte, a nanocrystalline, mesoscopic wide-bandgap semiconductor and a counter electrode need to be assembled into one unit with each component collaborating harmoniously with the others in order to perform the desired function. The dye forms a monolayer on the surface of the semiconductor material which is in contact with one of the electrodes. A solution containing the electrolyte is in direct contact

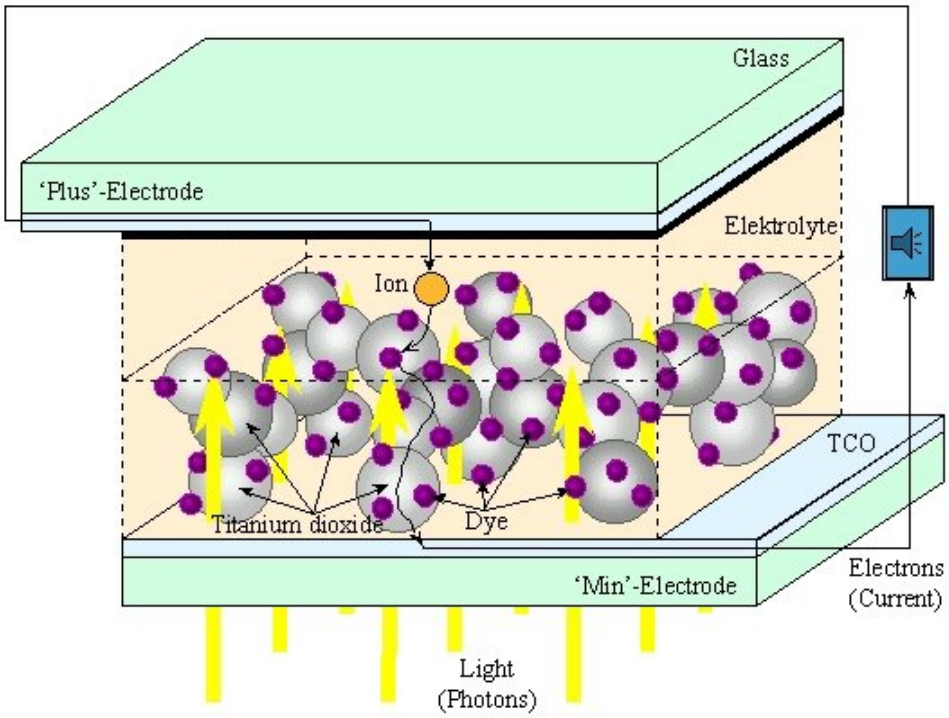


Figure 4.2. Schematic of a DSSC cell showing all the different materials assembled into a functional cell.

with both the semiconductor-sensitizer complex and with the second electrode. A schematic of the DSSC is shown in Figure 4.2.

The principle of operation is as follows: Light hits the cell and is absorbed by the sensitizer. The absorption of light causes the excitation of an electron from the HOMO to the LUMO of the dye molecule. The electron is then injected into the conduction band of the semiconductor. Such an injection is possible as the dye molecules are anchored on the semiconductor's surface mainly by interactions with a carboxylic acid group located on the dye-molecule. The electron reaches the first electrode where the semiconductor is bound. After that, the electrode is ingested into the circuit where it performs its function as a flow of electric charge. When the electron reaches the second electrode, it reduces a molecule of the oxidized form of the electrolyte which is in contact with that electrode. The now-reduced electrolyte migrates through a diffusion controlled process towards the semiconductor-dye complex. Upon contact of the electrolyte with a dye molecule that has previously lost its electron, dye-regeneration occurs. The now oxidized electrolyte can migrate again towards the second electron, acting as a hole transport material and, the dye is ready for a new cycle of light absorbance. The electricity that is generated, does not cause any overall chemical change thus, theoretically, can continue indefinitely without any chemical or environmental consequences. The principle of operation is illustrated in Figure 4.3.

During the last 20 years since its first appearance, and with increased understanding of the chemistry and device physics[1,4-8] scientists are trying to improve the efficiency and working characteristics of DSSCs. The Shockley Queisser limit[9], which is the maximum theoretical power conversion efficiency, is around 32%. The current maximum efficiency of DSSCs are a little above 12%[10]. Many investigations in search of the most appropriate combination of semiconductors, electrolytes and sensitizers have been undertaken. Many semiconductor

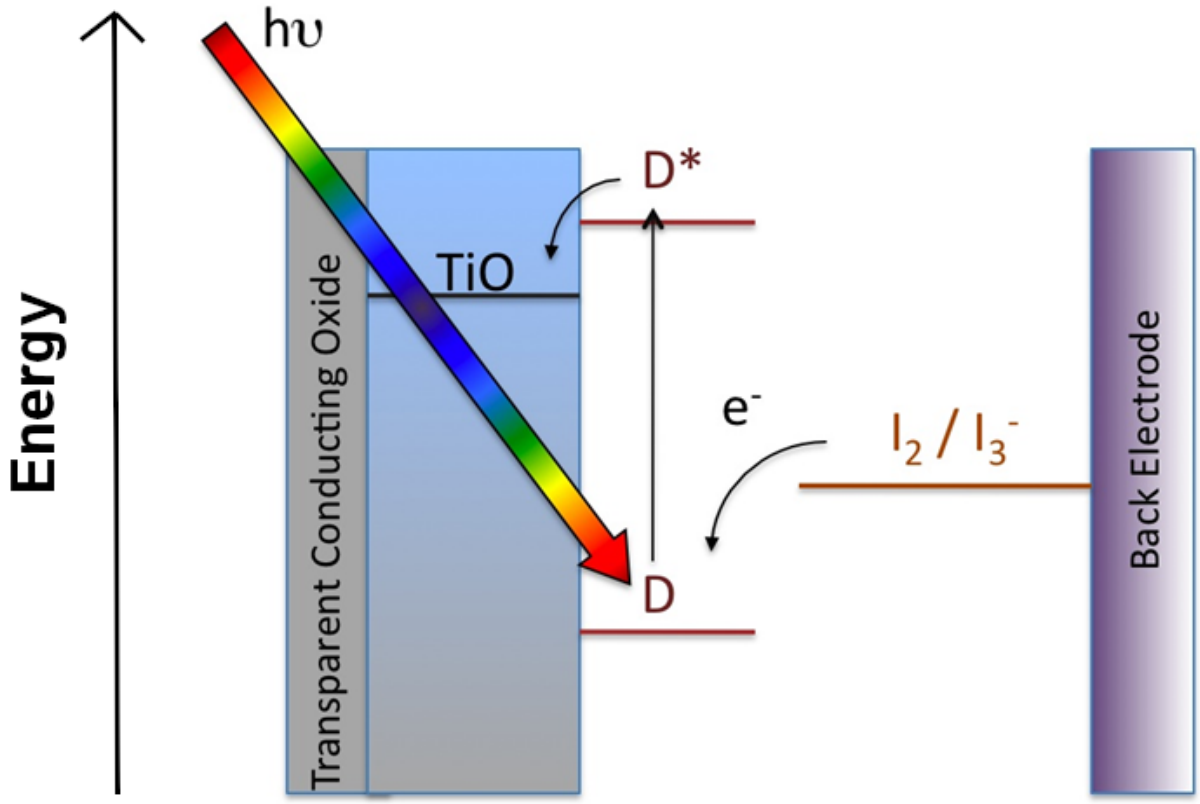


Figure 4.3. Energetic diagram showing electron generation and dye regeneration of a DSSC

materials have been tested including ZnO, TiO_2, Nb_2O_5 and NiO. DSSCs made of porous nanocrystalline TiO_2 has been shown to achieve the highest efficiencies. The nanoparticles are multiplying the surface area by a fraction of 1000 thus, allowing a much higher amount of the sensitizer to be absorbed[11-15]. As a result, light is absorbed more efficiently. The porous structure of the TiO_2 nanocrystals also permits the more efficient diffusion of the electrolyte. In addition to its high efficiency, TiO_2 is very inexpensive, non toxic and chemically stable under light irradiation. All these factors contribute to its monopoly as the semiconductor of choice.

The optimization of the sensitizer is an area of on-going investigation. Usually, the sensitizer is a coordination compound but purely organic dyes have been employed as well[16,17]. But despite their chemical classification, for any dye to be considered suitable for DSSCs must possess certain characteristics. These characteristics are: a) the ability to bind strongly at the TiO_2 semiconductor interface. The most common way is the utilization of carboxylic acid groups which form strong bonds with the TiO_2. Carboxylic acids also provide strong electronic coupling. b) the ability to absorb radiation strongly and in the widest range possible c) the possession of a high redox potential. The dye must have a high enough LUMO for efficient electron injection but a low enough HOMO for efficient regeneration by the electrolyte. d) Electron injection to the TiO_2 should happen considerably faster than the decay of the excited state back to the ground state. e) the ability to remain stable and chemically inert over many years of exposure to sunlight.

An optimum combination of all the characteristics described above is very difficult. Ruthenium complexes coordinated with polypyridyl derivatives have shown excellent results in all of the above criteria giving efficiencies greater that 10%. N719 (commonly known as “the black dye”), N3 and the unnamed thiocyanate dye shown in Figure 4.4 are commercially manufactured and used by scientists as standards to which spectroscopic properties and efficiencies of newly synthesized dyes are compared.

The iodide/triiodide system has been the most efficient electrolyte for DSSCs. The slow kinetics of the transference of the injected electron from the TiO_2 to the oxidized electrolyte (recombination rate) and the fast regeneration of the oxidized species from the second electrode are key factors for its success[18-20]. Another important aspect is its small size which makes it diffuse quickly from the semiconductor’s surface to the second electrode and vice versa. The

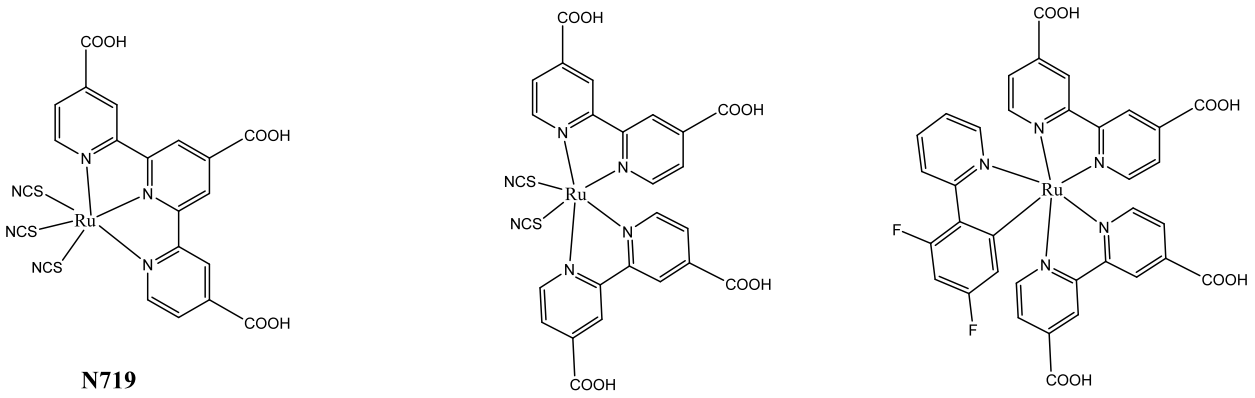


Figure 4.4. Ruthenium-polypyridyl based dyes that are being manufactured commercially.

iodide/triiodide system has disadvantages as well. One of them is that it is very corrosive and causes dissolution of commonly used sealants and metal interconnections such as silver, copper, aluminium and gold. Another disadvantage is that it regenerates itself via a two-step process which results in a loss in potential in the order of 300 mV[19,21]. This makes the efficiency of the cell drop.

Although scientists have discovered redox couples which are less corrosive than the iodide/triiodide system, their extremely fast recombination rates gave poor efficiencies (<5%). More recently though there have been advances in using molecules which utilize redox systems such as the Co(III)/Co(II) couple[22-25], Fc(III) /Fc(II) couple[26,27] and the Cu(II)/Cu(I) couple[28,29] with promising results. These systems offer space for experimentation and fine tuning of properties. For example, in the Co(III) /Co(II) system various ligands can be incorporated with effects that vary from tuning the redox potential to providing effective protection from the fast recombination process between the electrolyte and the TiO_2.

4.1.2 Dipyrrins

Dipyrrins are a group of molecules that consist of two pyrrolic units fused together through a methine group (-CH=) at the 2,2' positions. Dipyrrins in the literature have been named in many different ways such as 4,6-dipyrrin, dipyrromethene, 4,6-dipyrromethene, dipyrrylmethene, pyrrylmethene, pyrromethene, 2,2′dipyrrolylmethene, dipyrrolemethene, diaza-*s*-indacene, 2-pyrrol-2-ylmethylene-*2H*-pyrrolenine and 2-(*2H*-pyrrol-2-ylidenemethyl)-pyrrole. Figure 4.5 shows the general structure of a dipyrrin along with the numbering system used for their systematic naming[30]. Freebase dipyrrins exist as tautomers and are essentially planar with the nitrogen atoms adopting a *syn*-conformation with respect to each other. They are considered to be relatively strong bases[31]. However, they can be deprotonated under the appropriate conditions in order to form the monoanionic species which can act as a bidentate ligand in metal-complex formation.

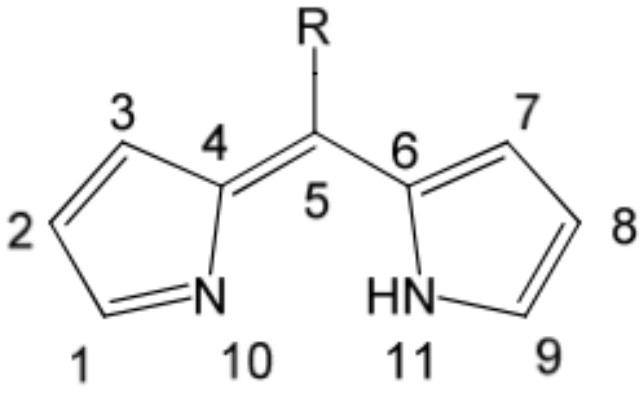


Figure 4.5. General molecular structure of a dipyrrin along with the numbering scheme used in its nomenclature.

A dipyrrin can be considered as a "half porphyrin" and historically their synthesis was intended to help in porphyrin synthesis. The stability of the dipyrrins depends on their substitution. Substituents can be placed both at the meso-position and at the α,β pyrrolic positions with the most common being the meso-substitution due to the ease of synthesis. The totally unsubstituted dipyrrin is the least stable because the ring is susceptible to electrophilic and nucleophilic attack[32]. The stability of the dipyrrins is greatly increased upon complexation with a metal center.

Dipyyrins have an extended π-system which gives them interesting optical properties. Boron dipyrrinato complexes for example, have been extensively studied due to their intense fluorescence with tunable emission maxima allowing for their use in a variety of applications such as biological staining and dye laser applications[33]. A number of homoleptic and heteroleptic dipyrinnato transition metal complexes have been prepared in the past and they show very strong light absorption in the visual region of the electromagnetic radiation[36]. In addition, it has been demonstrated that bis-(5-phenyl-dippyrinato)zinc(II) chromophore when covalently linked to a porphyrin can transfer energy to the porphyrin from a photoexcited electronic state[34]. The same was found to be true in another study where electron transfer was observed when the same dipyrrin chromophore was linked to a fullerene[35]. Owing to these properties, dipyrrins can find potential use in the design of chromophores that would act as dyes in DSSCs. However, there has only been one study[36] so far which considers this possibility and has shown promising results.

The aim of this project was to develop and prepare a series of dipyrrin complexes and study their properties with the prospect of using them, or modified versions of them, either as dyes or as electrolytes in DSSCs.

Since the best dyes contain an electron rich (donor) and an electron poor (acceptor) section[37], we incorporated the ferrocene group in the 5-position of the dipyrrin. Ferrocene acts as a strong electron donor[38] and by placing an acetylene spacer between the ferrocene and the dipyrrin we anticipated that electronic communication will be more pronounced and the whole dipyrrin ligand would possess better electron donor properties. Figure 4.6 shows the molecular formula 5-ethynylferrocenyldipyrrin.

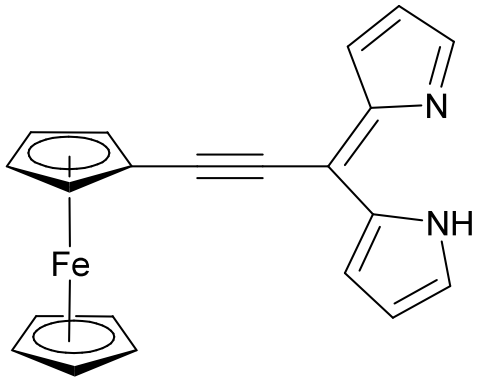
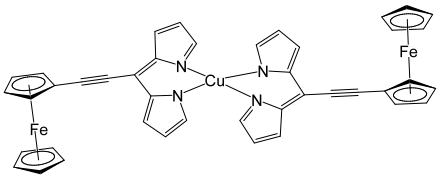
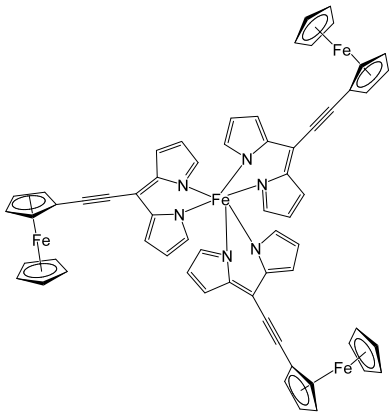
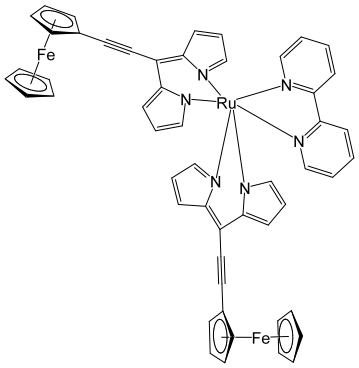


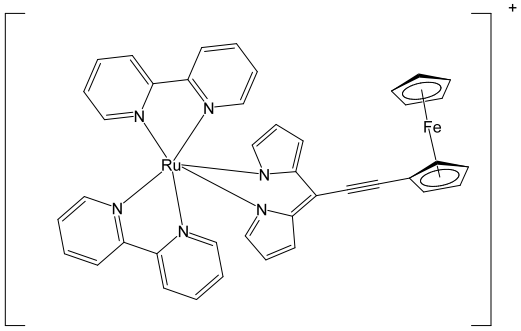
Figure 4.6. Molecular structure of 5-ethynylferrocenyl-dipyrrin.

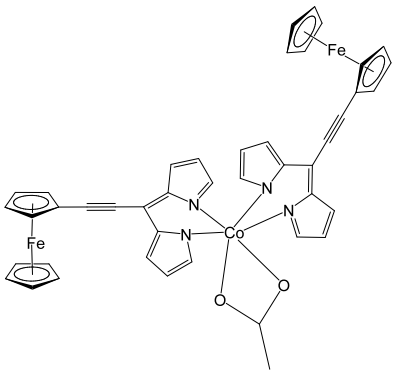
Through preparation of ruthenium(II) complexes of the 5-ethynylferrocenyldipyrrin ligand with varying degrees of substitution (with the other co-ligand being the unsubstituted bipyridine ligand), we would anticipate an increase in the absorption coefficient of the dye due to the very high absorption coefficients that metallated dipyrrins show[36,40]. This would be of great advantage since smaller quantities of dye would be needed for complete light absorption (within the λ_{max} region of the dye). This corresponds to smaller manufacturing costs of the solar cell. It also











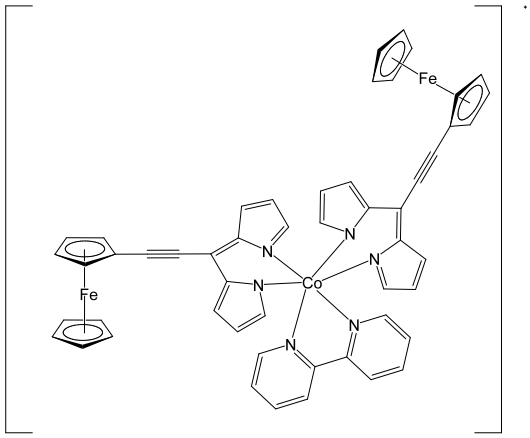


Figure 4.7. Structure of molecules synthesized or discussed in this project.

translates to thinner semiconductor films which decreases the required electrolyte diffusion distance thus indirectly increasing the efficiency[10].

Another feature of the dipyrrin ligand complexes is the red-shift of the characteristic MLCT absorption maxima in comparison to the Ru(II)/bipyridine complexes, the transition that is responsible for the charge transfer qualities of these complexes. The shift of this transition to longer wavelengths[39,40] is beneficial as it provides an increase in the overall efficiency of the DSSCs. Also, by creating a set of compounds that absorb at different wavelengths, a larger part of the visible radiation is exploited and the possibility of the manufacturing of a mixed dye DSSC is clear.

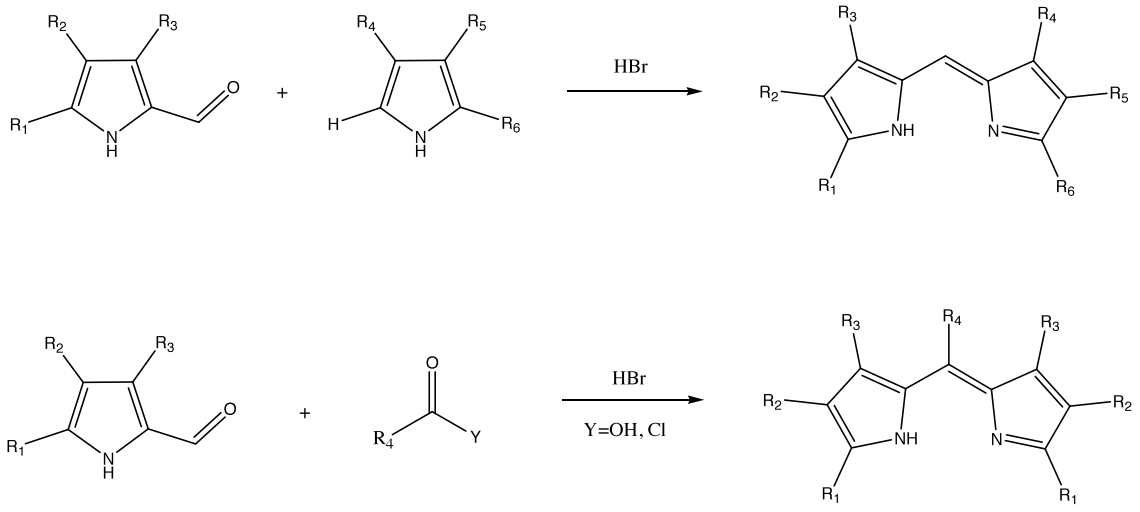
Complexes of the above ligands with various other metals such as Fe(III), Cu(II) and Co(III) were prepared. Their preparation allowed greater insight into the optical and electrochemical properties of the dipyrrin ligand. In addition, Cu(II) and Co(III) complexes could be used as electrolyte couples in DSSCs. The structures synthesized or discussed in this Chapter are depicted in Figure 4.7.

Unfortunately the Ru(II) complexes could not be obtained for reasons explained below. For the rest of the compounds, electrochemical and spectroelectrochemical studies have been performed.

4.2 Synthesis

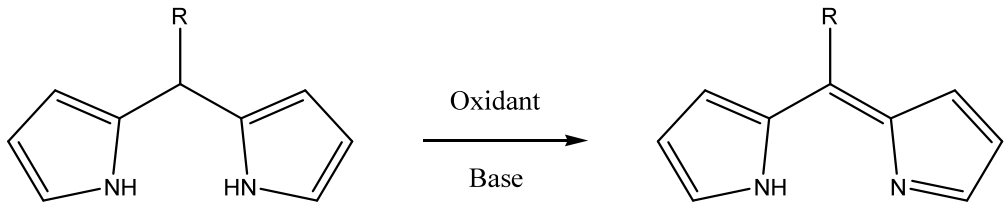
Traditionally dipyrrins have been synthesized through the acid catalyzed condensation of 2-formyl pyrrole with a pyrrole that is unsubstituted in the 2-position[31]. This reaction is usually

referred as the McDonald coupling[41]. The limitation of this procedure is that it is mainly used for the preparation of dipyrrins that have no functionality in the 5-position. It is also more suitable for the preparation of asymmetric dypyrrins. If a symmetric 5-substituted dipyrrin is required then an alternative synthetic route can be employed which allows the condensation of two equivalents of a 2-unsubstituted pyrrole with a carboxylic acid or acid halide that carries the group that is desired to be placed in the 5-position of the final product. Scheme 4.1 offers a better understanding of the capabilities and limitations of each method.



Scheme 4.1. Traditional routes for the synthesis of asymmetric 5-unsubstituted and symmetric 5-substituted dipyrrins. The scheme illustrates a general case where R_1-R_6 could be all different R-groups.

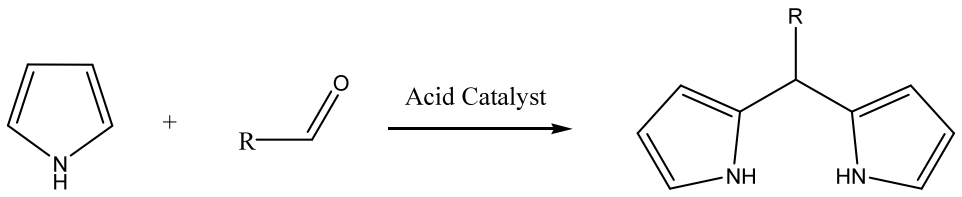
Although the previous methods are high yielding and offer great flexibility for the desired outcome, they are less suitable as a synthetic route when a simple dipyrrin substituted only in the 5-position is desired. In this case, the oxidation of the corresponding dipyrromethane has been proven an efficient and simple method. (Scheme 4.2).



Scheme 4.2. Dypyrrin synthesis by oxidation of dipyrromethane.

The use of base is essential and serves as a trap for the hydrogen cations formed after the oxidation of dipyrromethane. An oxidant that was commonly used in the past is elemental bromine, the reaction taking place in CCl_4[42]. Recently, more sophisticated oxidants belonging to the quinone family have been successfully employed. The most commonly used oxidant is 2,3-dichloro-5,6-dicyano-1,4-benzoquinone (DDQ) because of its selectivity, ease of handling and very short reaction times[43].

5-substituted dipyrromethanes are routinely prepared through the treatment of an appropriate aldehyde with 100 equivalents of pyrrole with the aid of an acid catalyst, (Scheme 4.3). This reaction is well studied[44] and is often used during the synthesis of porphyrins.

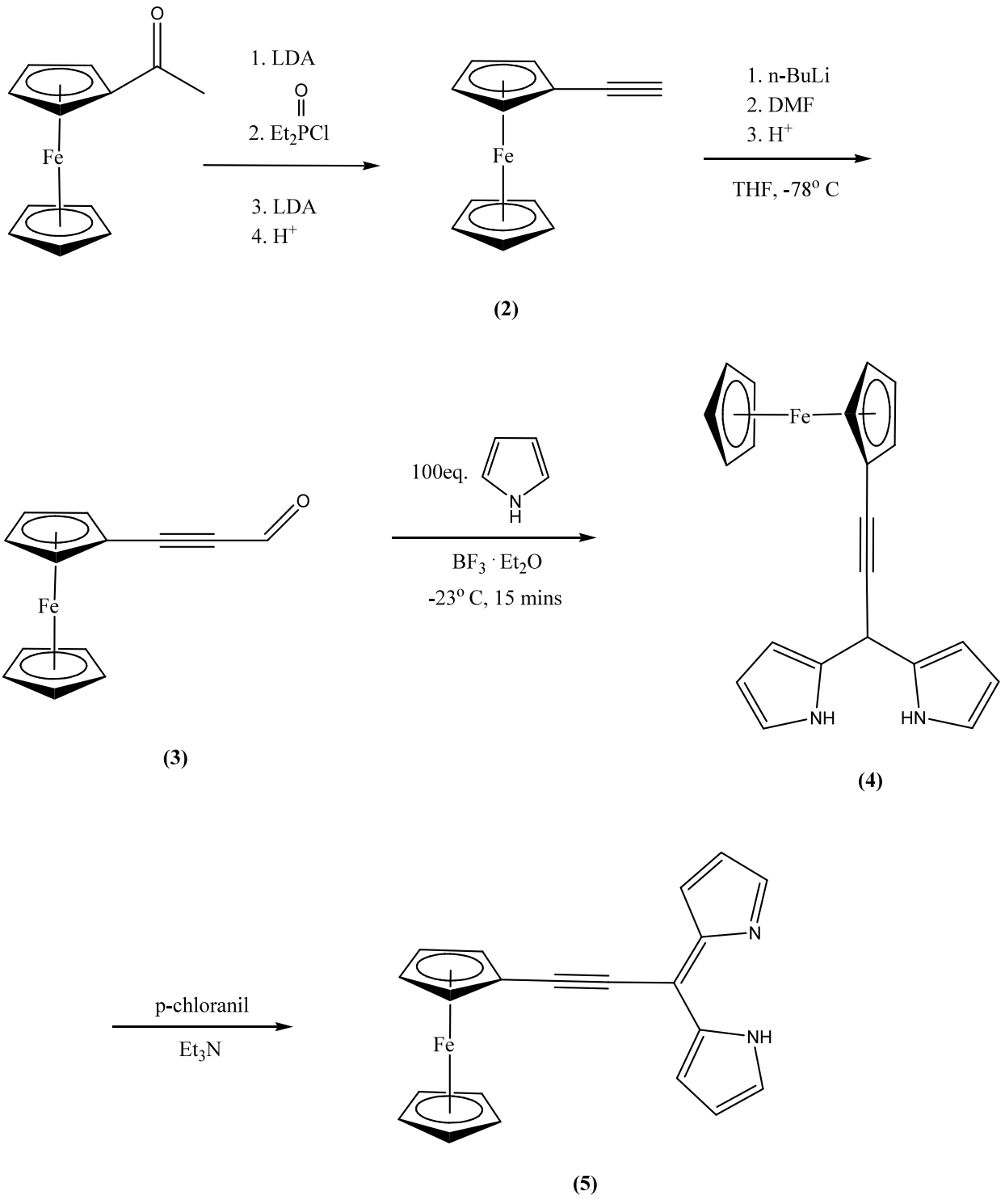


Scheme 4.3. Synthesis of 5-substituted dipyrromethanes.

For the synthesis of 5-ethynylferrocenyl-dipyrrin, the route with the dipyrromethane intermediate was chosen. A full illustration of the synthetic route used is shown in Scheme 4.4. For the formation of 5-ethynylferrocenyl-dipyromethane **(4)**, ferrocenyl(formyl)acetylene **(3)** needed to be synthesized first. This molecule has been prepared in the past and literature procedures[45] with modifications in reaction times and purification technique were effectively used.

The synthesis of **(3)** starts from acetyl-ferrocene **(1)**, a commercially available starting material. The formation of ethynyl-ferrocene is a two-step one-flask reaction type. The first step is the formation of the enol-phosphate intermediate. LDA is used in order to remove one of the α-hydrogens of the methyl ketone and thus, aid in the formation of the ketone-enol tautomer. The later, reacts with the chlorophosphate reagent in order to give the enol-phosphate intermediate. LDA is again introduced as the second step of the reaction, and acts as a base in the β-elimination reaction taking place. The reaction mixture is poured into acidified water in order to eliminate the excess of base and complete the reaction. Purification is achieved with chromatography and subsequent crystallization of the oil obtained from hexanes.

The next step is the formation of ferrocenyl(formyl)acetylene **(3).** Ethynylferrocene is a terminal alkyne and the acidic proton is easily removed with n-butyl-lithium in order to form a lithium-



Scheme 4.4. Synthetic route of 5-ethynylferrocenyl-dipyrrin.

acetylidide intermediate. Hydrolysis in acidic water and purification with chromatography affords **(3)** in a very good yield.

The formation of dipyrromethane **(4)** is accomplished through the reaction of **(3)** with an excess of pyrrole (100 eq). The reaction takes place in an inert atmosphere and care is taken in order to exclude light. Boron trifluoride is used as the acid catalyst. The intermediates formed are very reactive and the temperature was kept at -23^{o} C with a reaction time of 15 minutes. Addition of base was used in order to quench the reaction. Purification by column chromatography on silica was very difficult as this reaction had a lot of side products having similar elution times. A solvent system consisting of hexane/ethyl acetate/triethylamine was employed and a product of sufficient purity was obtained. The product was obtained as thick brown oil with some minor impurities believed to inhibiting its solidification. 5-Ethynyl-dipyrromethane had to be stored in the fridge because it degraded slowly with time.

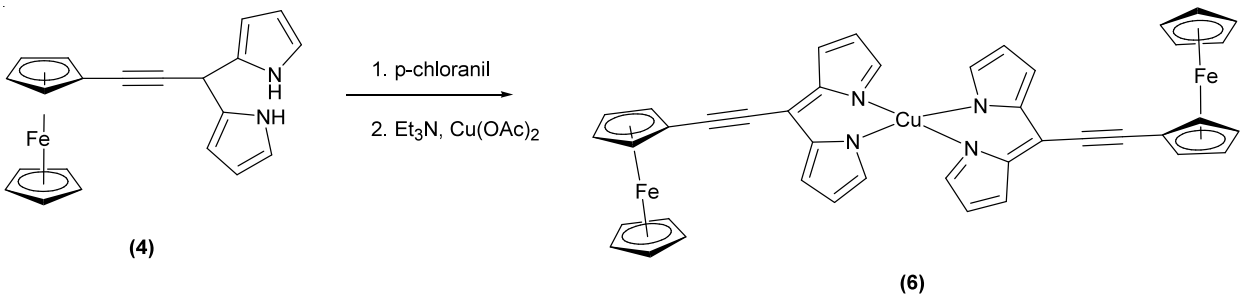
The final step is the oxidation of **(4)** to the dipyrrin derivative. During the first trials of this reaction, DDQ was used as the oxidant as described earlier. After addition of DDQ, a deep blue coloration was observed but TLC experiments showed that this blue compound was very polar. It was hypothesized then that DDQ was a very strong oxidant that was causing the oxidation of ferrocene into ferrocenium. Previous experiments of oxidizing 5-ferrocenyl-dipyromethane with DDQ were successful so it was deduced that the triple bond must have facilitated better communication between the ferrocene and the dipyrrin unit causing an increase of its reduction potential. This hypothesis was verified through the use of p-chloranil (2,3,5,6-tetrachlorocyclohexa-2,5-diene-1,4-dione) as a milder oxidant. The starting material was consumed within 2 minutes and a deep red-brown solution was formed.

The problems with this synthesis continued through to purification stage, with the compound showing unusual behavior on silica substrates. TLC experiments using dichloromethane as the mobile phase showed good separation; however, using the same conditions on a preparative scale resulted in an almost complete decomposition of the product. If the reaction was performed in THF and the product was loaded and eluted in a THF-containing solvent system, no decomposition was observed. The drawback was that any solvent combination with THF was too polar for the effective separation of **(5)** and the chloro-substituted hydroquinone formed as a sideproduct. In addition when solutions containing **(5)** were evaporated to dryness the product fully decomposed leading to a material that was insoluble in all solvents tried. Changes in evaporation temperature and light conditions did not improve results. The only occasion that the product survived solvent evaporation was when solutions contained a very low concentration of the product. The possibility of the product reacting with the hydroquinone, formed in the reaction, upon concentration of the solution was excluded as hydroquinone-free solutions were re-tested with no success in isolating a product. It is hypothesized that when **(5)** starts packing during the transition to the solid state, some form of polymerization involving the triple bond spacer is favoured. Identification of **(5)** was achieved only by MALTI-TOF spectrometry where a valid mass was observed. Further indirect identification was achieved as, upon metal complexation, stability was restored. Successful identification of its metal complexes provides proof for the existence of **(5)**. In order to proceed further in the synthesis of homoleptic and heteroleptic metal complexes of **(5)**, two approaches were followed. Firstly, **(5)** was obtained directly from the column chromatography and evaporated partially until a solution of known volume was formed. A quantitative conversion was assumed and a final yield was calculated after metallation. The second approach was to add the oxidant in the presence of the metal and

allow both oxidation and metallation to happen in the same flask. The drawback of this method was that metals such as iron(II) could compete with the dipyrromethane in the redox process.

Synthesis of metallated dipyrrinato complexes

Bis-(5-ethynylferrocenyl-dipyrromethene) copper(II) was synthesized in two steps. 5-ethynyl-ferrocenyl-dipyrromethane was oxidized with p-chloranil in dichloromethane at 0^{o} C followed by the addition of $Cu(OAc)_2$ and triethylamine. The solution was purified by column chromatography on silica affording a pure product. Slow evaporation of a concentrated solution of **(6)** in dichloromethane afforded crystals of an appropriate quality sufficient for X-Ray crystallography. The structure of **(6)** was also confirmed through MALDI-TOF MS and elemental analysis. A schematic of the synthesis of **(6)** is shown in Scheme 4.5. The NMR spectrum could not provide any structural identification because the complex is paramagnetic and the peaks were broadened and shifted in a way that peak overlaps were not uncommon.



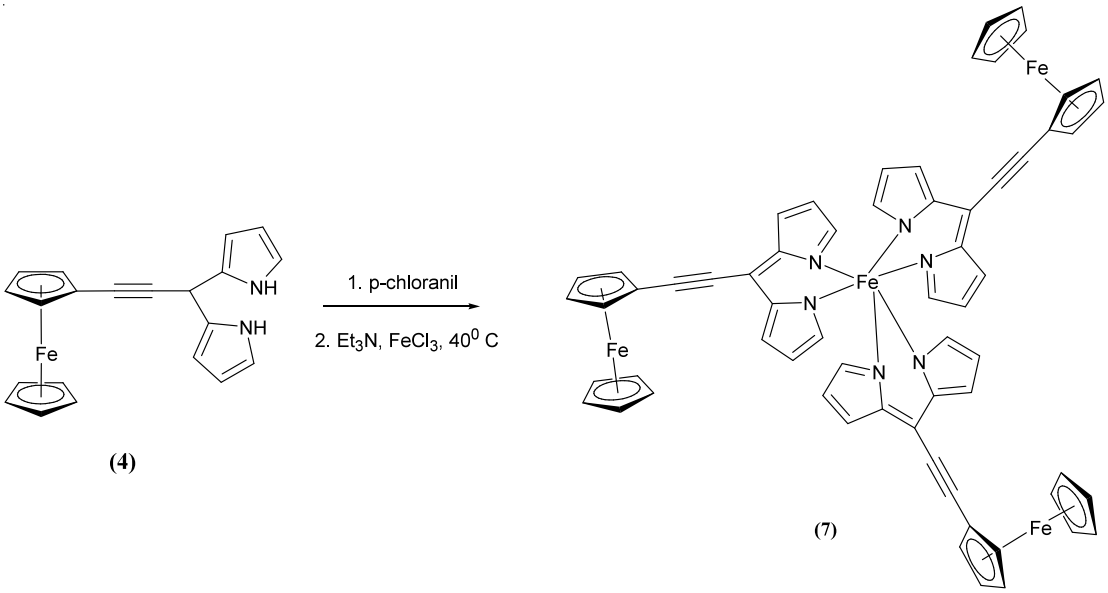
(4) (6)

Scheme 4.5. Synthesis of bis-(5-ethynylferrocenyl-dipyrromethene) copper(II)

We were unable to synthesize the Fe(II) complex with any of the methods used. Various solvents and methods were tried but the outcome was always a green insoluble tar precipitating immediately after the addition of the iron(II) salt. A variety of iron(II) salts were tried and variables such as reaction temperature and the type of base used were explored, however, the iron(II) complex was never detected. It has been suggested that iron(II) complexes of dipyrrins form only oxidatively unstable products and in the presence of excess ligand iron(III) complexes are formed. These observations agree with our experimental results, indeed, a small amount of the iron(III) complex was been isolated from the above reactions.

Tris-(5-ethynylferrocenyl-dipyrromethene) iron(III) **(7)** was successfully synthesized. Very polar solvents such as ethanol, methanol and THF were unsuitable for this reaction. Even addition of small amounts of polar solvent to make the iron(III) starting material more soluble had a great impact on the course of the reaction and no product could be isolated. Dichloromethane was found to be the most appropriate solvent and after the addition of iron(III) chloride it was necessary to raise the temperature to 40^{o} C for efficient conversion. This is probably due to the insolubility of iron(III) chloride in dichloromethane rather than any difficulty of the iron(III) cation reacting with the dipyrrin ligand. An octahedral complex was obtained (Scheme 4.6) and the molecular structure was successfully characterized with X-Ray crystallography, MALDI-TOF MS, elemental analysis and NMR spectroscopy. Although the complex is paramagnetic, the peaks in the NMR spectrum were only slightly broadened. Big negative shifts were observed, especially for the dipyrrin-based protons, but it was not possible to unambiguously assign all the peaks.

We were not able to synthesize any of the ruthenium(II) complexes. Scheme 4.7 shows the attempted synthetic routes. Although the intermediate species were successfully synthesized according to literature procedures, any attempt of coordinating the dipyrrin ligand **(5)** was not successful despite the variety of conditions used. A review of the literature will reveal that ruthenium chemistry needs elevated temperatures and prolonged reaction times. All reactions involving molecule **(5),** independent of conditions and starting materials, when performed at



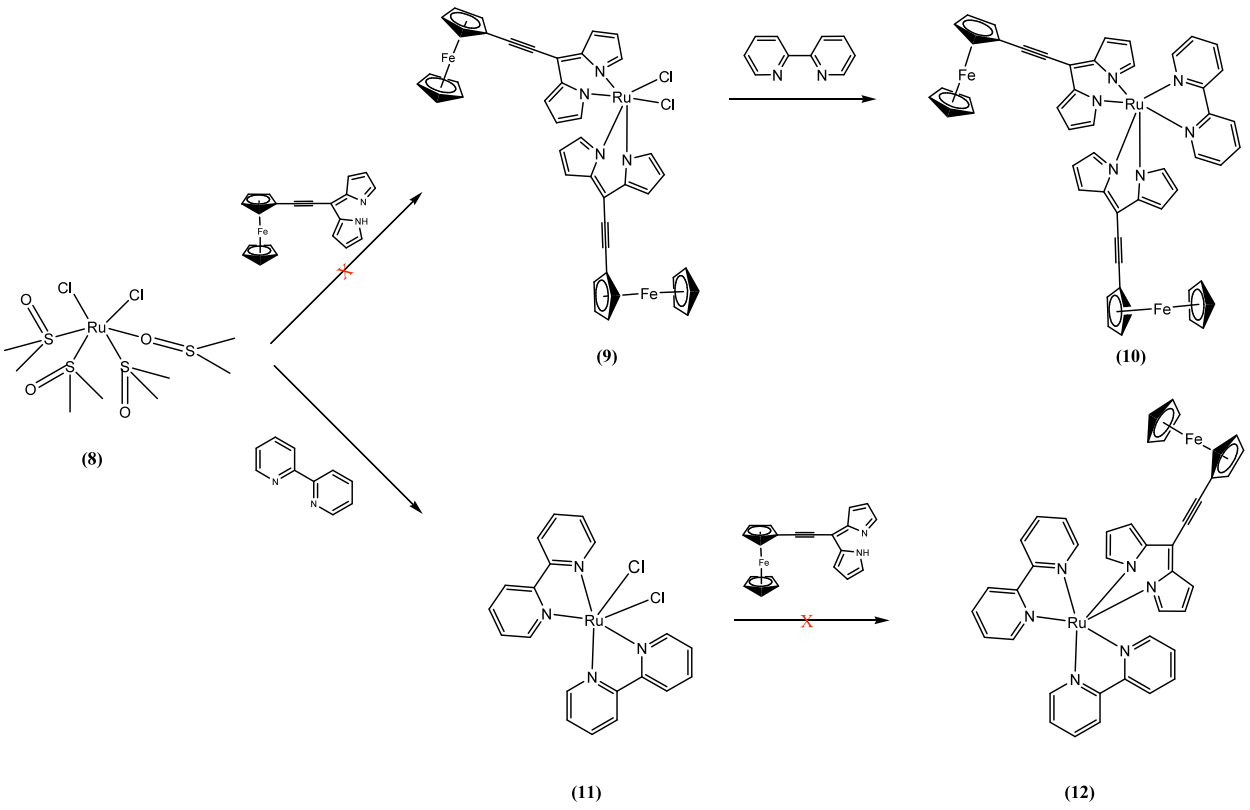
(4) (7)

Scheme 4.6. Synthetic route to tris-(5-ethynylferrocenyl-dipyrromethene) iron(III)

elevated temperatures gave a consistent reaction mixture consisting of decomposition products. It was found that **(5)** was unstable at high temperatures and the highest approximate temperature that it could survive was 40^{o} C. This temperature was not high enough to promote the reaction between the dipyrrin ligand and the Ru(II) metal center and even after prolonged stirring, starting material was found to be intact and no detectable product could be obtained.

One of the most challenging tasks of this project was the synthesis and identification of homoleptic and heteroleptic dipyrrin complexes of cobalt. One reason for this was that the data were inconclusive for the exact molecular structure and the products decomposed upon contact with silica or alumina.

Preliminary reactions involved the addition of cobalt(II) acetate to a solution containing a crude mixture of previously oxidized 5-ethynylferrocenyl-dipyrromethane. The solution was turning



Scheme 4.7. Synthetic route of Ru(II) heteroleptic dipyrrin complexes.

into a deep violet colour but the main product could not be isolated because of its sensitivity to silica/alumina as mentioned above. We were able to obtain a sufficiently pure product forcing a quick elution through silica with a mobile phase consisting of a mixture of dichloromethane and 5% triethylamine. The product's MALDI-TOF MS spectrum showed a major peak at 761.1 which corresponds to the mass of two dipyrrins and a cobalt atom. While this shows the possible existence of a tetrahedral Co(II) homoleptic complex, the NMR spectrum had two rather unconvincing characteristics. First of all the spectrum showed no broadened or shifted peaks expected for a paramagnetic Co(II) complex, suggesting that the Co(II) had been oxidized to Co(III). The second observation was that six peaks corresponding to the hydrogens of the dipyrrin rings were observed instead of three expected from the assumed molecular structure. The possibilities that either all six hydrogens of each dipyrrin unit had a different chemical environment or the two ligands adopted distinct environments, influenced differently by the metal center were disregarded as literature NMR data[69] indicated that each dipyrrin unit would be expected to be symmetric and no configuration that would allow the two ligands to be in different environment could be envisaged.

All the synthesized complexes of Co(III) appeared to have this same NMR pattern. In one of the by-products, we were able to perform X-Ray crystallography but the data obtained were still not supporting this NMR spectrum. A possible explanation arises if we assume that there is an extended π-system formed between the cyclopentadienyl ring, the triple bond and the dipyrrin unit which prevents the rotation of the ferrocene in respect to the dipyrrin. With such a fixed stereochemistry, upon formation of the complex, the ferrocenes could adopt a syn- or anti-configuration towards each other as shown in Figure 4.8. These two complexes would provide a

slightly different NMR spectrum and because our samples would contain both of them, a combined spectrum explains our observations.

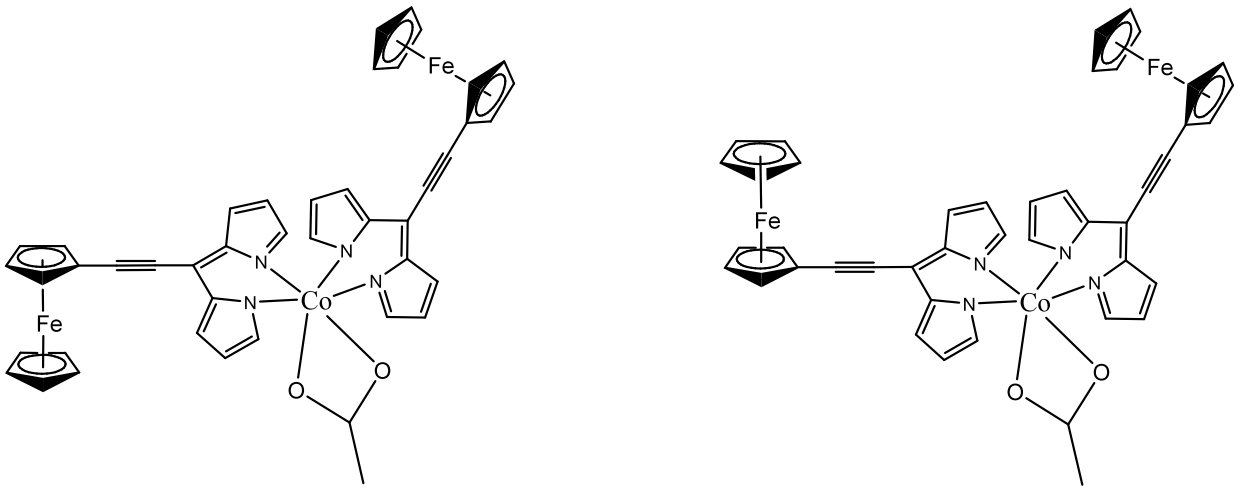


Figure 4.8. Compound (13) having the ferrocene groups in two different orientations.

A second explanation arises if we examine the stereogenic centers of the proposed structure. The complex belongs to the general formula cis-M(A-A)$_2$(B-B) which has two optical isomers as shown in Figure 4.9a. In addition, if we maintain the assumption that the ferrocene unit connot rotate around the triple bond, then two more optically active compounds can be generated. This is illustrated in Figure 4.9b where the molecule on the left is reflected at a mirror plane that is parallel to the page and so the molecule on the right is produced. These two drawings are simplified versions of **(13)** that help visualize the chirality produced due to the ferrocene units. What we have is a molecule with two optically active sites. One of the prerequisites for a

diastereoisomer formation is the simultaneous formation of both chiral centers with a configurational preference. In our case we can see that the ligand field stabilization energy is very high ($2.4\Delta_o - 3P$). This makes the ligands very strongly attached to the metal centers. As a consequence, upon formation, the ligands are not labile enough to de-complex and re-complex thus creating a complex with a different stereochemistry. So if the reaction is selective, we would expect the Δ- and Λ- configurations to be diastereoisomers. The two compounds will have different physical properties and consequently a different NMR spectrum.

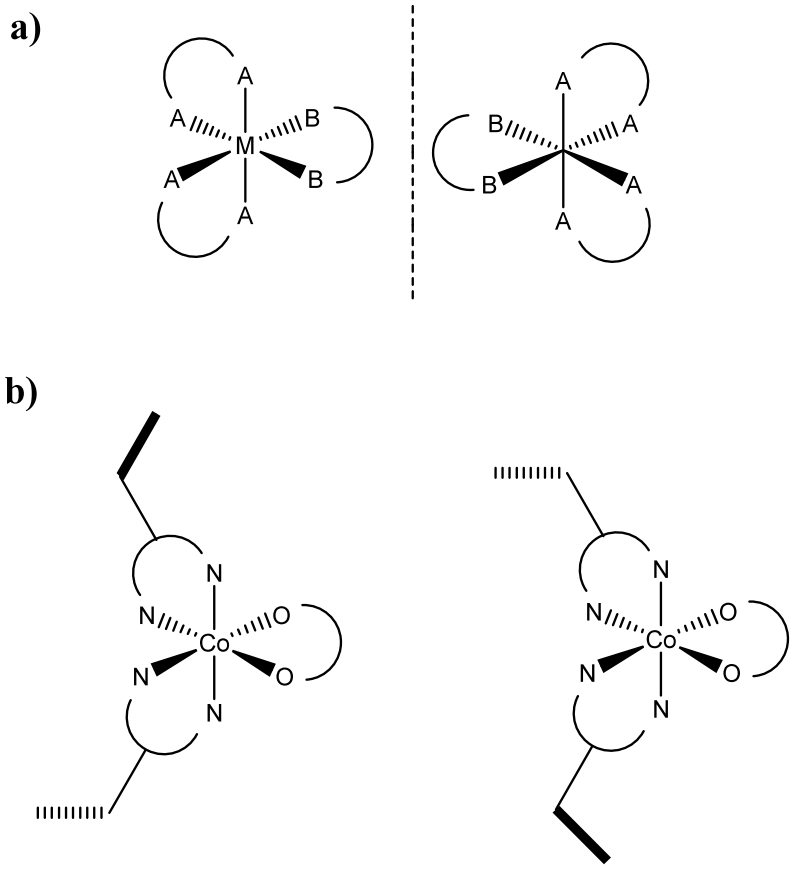
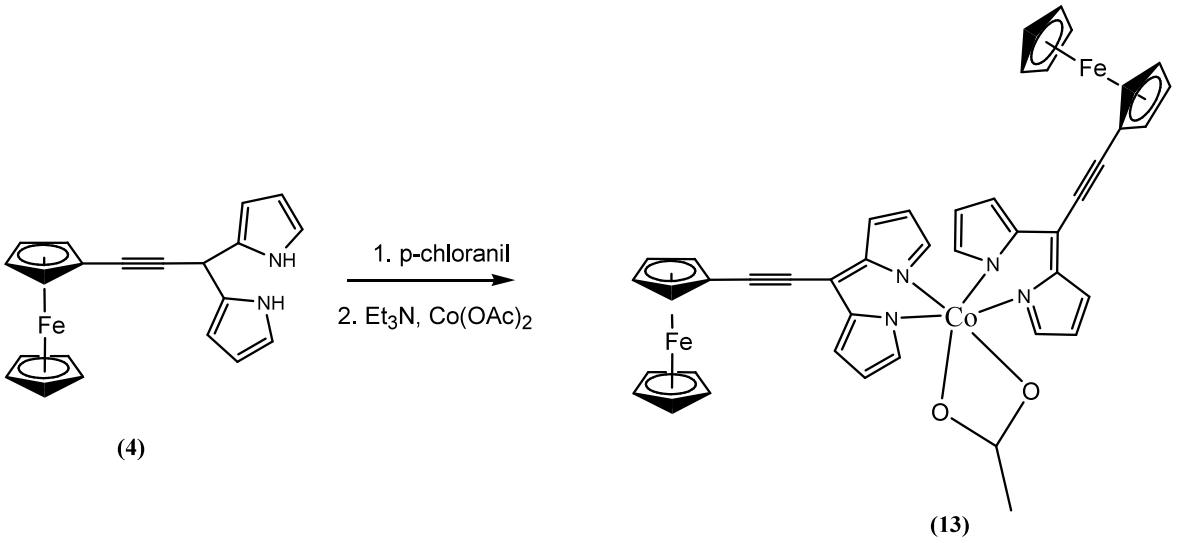


Figure 4.9. a) Δ- and Λ configurations of a cis-M(A-A)$_2$(B-B) type complex. b) simplified drawing of (13) showing the enantiomeric relationship of the two configurations.

Subsequent reactions also involved the removal of the reduced form of p-chloranil by the extraction of the reaction mixture with 0.1 M aqueous NaOH solution. Applying this technique before the addition of the Co(II) species lead to reaction mixtures with less side products and increased yields.

Cobalt acetate was added to a dichloromethane solution containing **(5)** and the mixture turned to a deep violet colour. The primary product was very unstable in contact with silica or alumina and



(4) **(13)**

Scheme 4.8. Synthetic route of bis-(5-ethynyl-ferrocenyl)-acetato-cobalt(III).

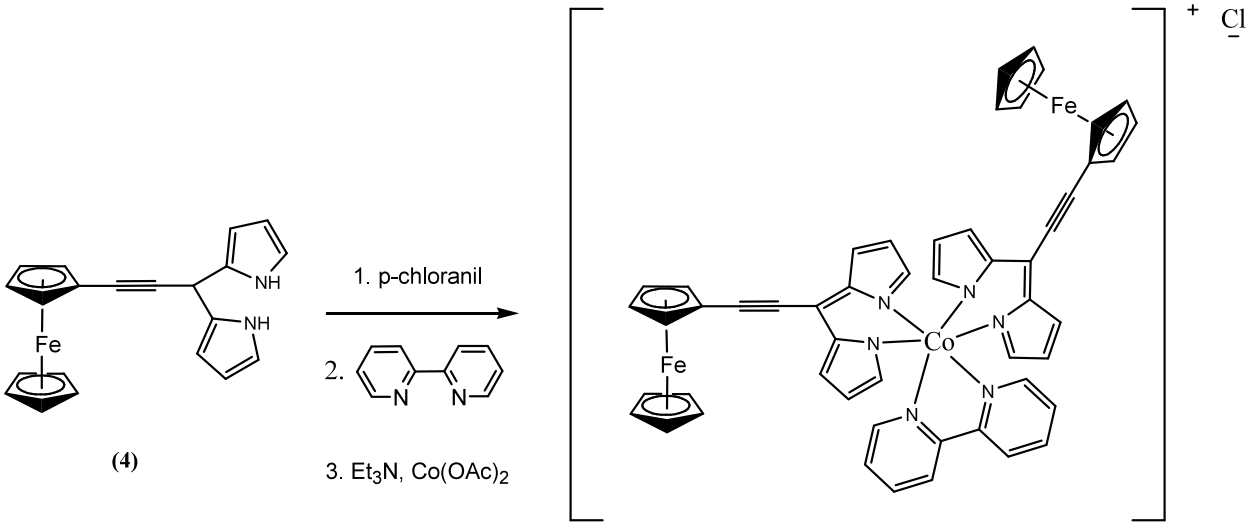
is hypothesized that it is the same product formed as before even with the presence of 2,3,5,6-tetrachloro-benzene-1,4-diol. Separation was achieved by eluting with dichloromethane containing 5% of Et_3N. The synthetic route is shown in Scheme 4.8.

Characterization of the exact structure of this compound proved difficult and only assumptions derived from the available data can be made. MALDI-TOF MS gave two peaks. The major peak at 761.1 corresponds to an ion consisting of a cobalt atom and two deprotonated molecules of **(5).** Another peak with a much smaller intensity at 820 is attributed to a species consisting of one cobalt atom, two deprotonated molecules of **(5)** and an acetate ion. The formal charge of a complexed dipyrrin unit is -1 and in our case cobalt has a +3 charge. One more negatively charged ion is needed to provide a neutral complex and acetate seems to serve this purpose. As encountered above, the major peak at 761.1 arises from the (5-ethynylferrocenyl)$_2$Co(III)$^+$ ion. The ^{1}H-NMR spectrum of this product also shows a peak related to the acetate ion at 1.67 ppm with integration corresponding to 3 hydrogens. It is unclear whether the acetate ion is coordinated or not, however the rarity of tetrahedral Co(III) complexes supports a neutral octahedral configuration, while electrochemical data discussed later supports a tetrahedral cationic configuration. Elemental analysis gave unsatisfactory results which may be accounted for by additional coordinated or guest solvent molecules.

A heteroleptic complex of cobalt(III) with bipyridine as a co-ligand has been successfully synthesized. The same procedure as that followed for complex **(13)** was used, but using $CoCl_2$ instead of $Co(OAc)_2$. Addition of half an equivalent of 2,2'-bipyridine preceded the addition of the metal. The crude product could only be purified using preparative TLC.

Column chromatography proved inadequate due to the co-elution of many byproducts. A mobile phase consisting of a mixture of dichloromethane/methanol 85:15 had to be used due to the high polarity of the complex. Elemental analysis of the purple solid obtained was unsatisfactory. Again, minor impurities or trapped solvent molecules could have accounted for this. The ^{1}H NMR spectrum showed the characteristic pattern of the two complexed molecules of **(5)** to a

cobalt(III) ion, as well as signals corresponding to the bipyridine hydrogens. Further characterization was performed with ^{13}C NMR and MALDI-TOF MS. The MALDI spectrum showed a mass of 916.98 which corresponds to the bis-[(5-ethynyl-ferrocenyl)-bipyridine-cobalt(III)]$^{+}$ cation. In negative ion detection mode, a small peak at 951.98 was detected which corresponds to a negative ion of molecule **(14)**. The chloride counterion was also detected indirectly upon addition of a methanolic solution of $AgNO_3$ to a methanolic solution of **(15)**. A white suspension formed immediately. The synthetic route is shown in Scheme 4.9.



(4)

(14)

Scheme 4.9. Synthetic route to bis-[(5-ethynyl-ferrocenyl)-bipyridine-cobalt(III)] chloride.

4.3 Crystallographic analysis

Crystal structure of (7).

Single crystals suitable for X-Ray structure analysis of **(7)** were obtained by slow evaporation of a chloroform/hexane (50:50) saturated solution of the complex. A perspective view of the molecular structure of **(7)** and the atom numbering scheme is illustrated in Figure 4.10. The molecule crystallizes with three molecules of chloroform in the monoclinic space group $P2_1/c$ (Table 4.1). Owing to weak data all non-metal atoms were refined with isotropic displacement parameters. The four Fe atoms were modelled with anisotropic displacement parameters which have all be restrained to isotropic character (ISOR). Geometric similarity restraints (SAME) were applied to the 1,2 and1,3 bond lengths of the dipyrromethene and alkyne units of the three ligands. The cyclopentadienyl rings of all the ferrocene moieties were constrained to have regular pentagonal geometry (AFIX 56) and geometric similarity restraints (SAME) were applied to the 1,2 and 1,3 bond lengths of the three dichloromethane solvent molecules. Three of the chlorine atoms had their isotropic displacement parameters fixed at values of 0.15. PLATON SQUEEZE was applied to the data to remove the scattering contribution from disordered solvent moieties and produce a set of solvent-free diffraction intensities for the final cycles of refinement. A total of 379 electrons were removed from the unit cell equating to 1.5 chloroform molecules per asymmetric unit which have been included in the unit cell contents.

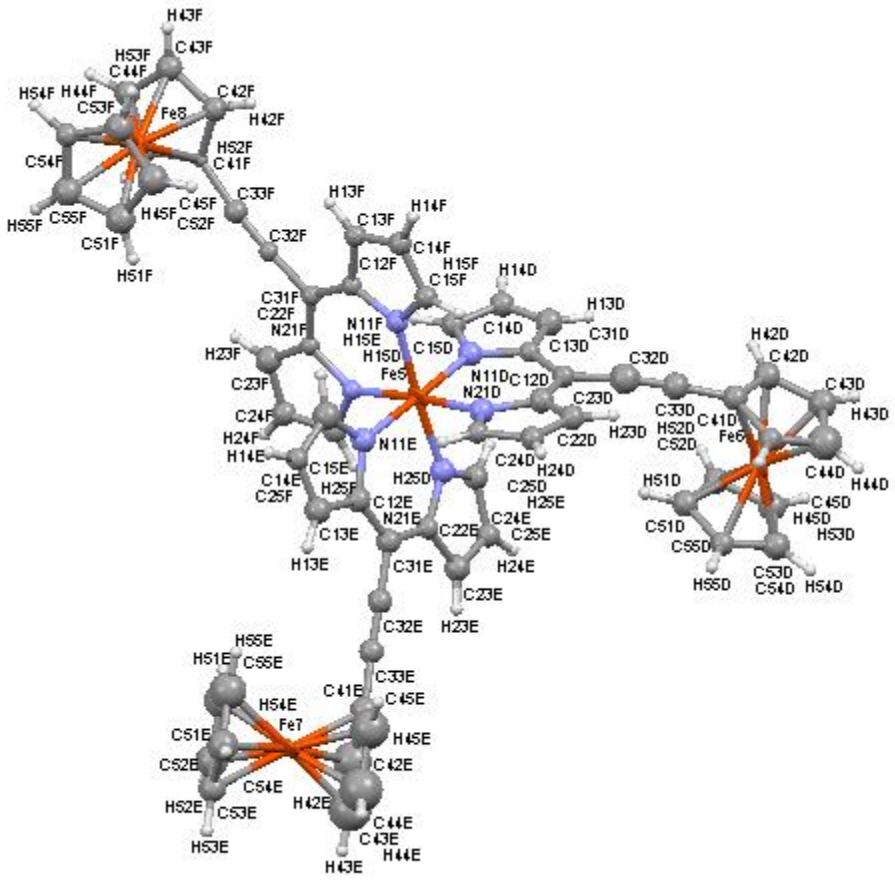


Figure 4.10. Crystal structure of (7) showing the atom labeling scheme. Displacement ellipsoids are drawn at the 50% probability level.

The aromatic region of the dipyrrin backbone is planar. The angle formed between the mean plane of the dipyrrin unit and the cyclopentadienyl ring is different in every ligand and it varies between 8.9(4)^{o} and 49.6(2)^{o} The Cp rings of each ferrocenyl unit are eclipsed, forming an angle that ranges between 1.2(3)^{o} and 3.01(13)^{o} with respect to each other. The ethynyl linkages are essentially linear. The ligands adopt an almost perfect octahedral arrangement around the central iron(III) center.

Table 4.1. Crystal data and structure refinement parameters for compound (7).

Compound	(7)
Empirical formula	$C_{130.50}H_{94.50}Cl_{13.50}Fe_8N_{12}$
Formula weight	2756.06
Temperature	150(2) K
Wavelength	0.71073 Å
Crystal system	Monoclinic
Space group	P2(1)/c
Unit cell dimensions	a = 25.25(10) Å α= 90°.
	b = 30.41(11) Å β= 97.56(9)°.
	c = 15.22(5) Å γ = 90°.
Volume	11583(73) $Å^3$
Z	4
Density (calculated)	1.580 mg/m^3
Absorption coefficient	1.342 mm^{-1}
F(000)	5596
Crystal size	0.49 x 0.08 x 0.01 mm^3
Theta range for data collection	1.05 to 20.00°
Index ranges	-24<=h<=24, -29<=k<=29, -14<=l<=14
Reflections collected	41125
Independent reflections	10816 [R(int) = 0.2847]
Completeness to theta = 20.00°	0.999
Refinement method	Full-matrix least-squares on F^2
Data / restraints / parameters	10816 / 645 / 562
Goodness-of-fit on F2	1.028
Final R indices [I>2sigma(I)]	R1 = 0.1314, wR2 = 0.3076
R indices (all data)	R1 = 0.2137, wR2 = 0.3596
Largest diff. peak and hole	1.867 and -1.554 e·$Å^{-3}$

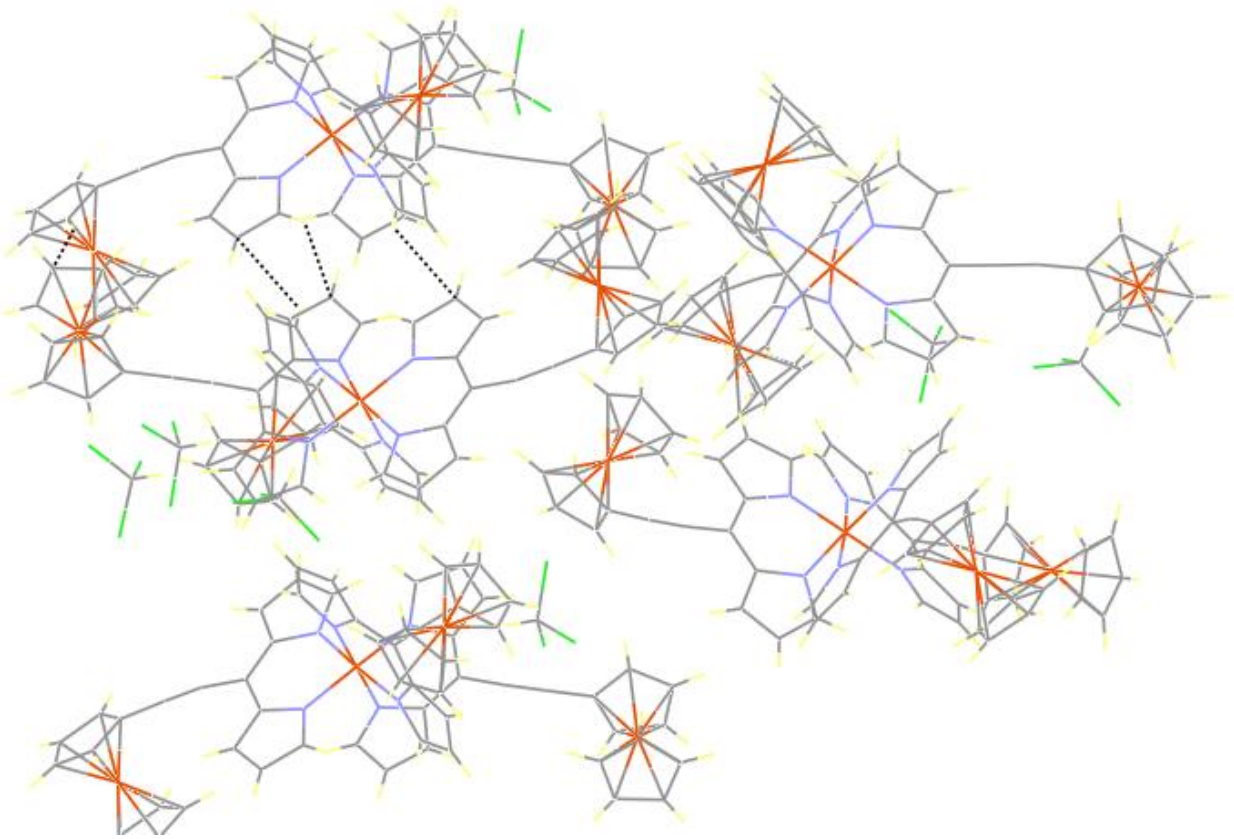


Figure 4.11. Crystal packing of (7). C-H…π interactions are represented as black dashed lines. Hydrogens are coloured yellow for clarity.

The molecules are packed into a crystal mainly through C-H…π interactions between a) the hydrogens of a dipyrrin ring and the π system of an adjacent molecule's dipyrrin ring and b) between the Cp ring's hydrogens and a neighboring Cp ring's π system. Selected interactions are highlighted in Figure 4.11 with dashed black lines.

Crystal structure of (6).

Single crystals of **(6)** suitable for X-ray structure analysis were obtained by slow evaporation of a saturated dichloromethane/methanol (50:50) solution of **(6).** A perspective view of the molecular structure of **(6)** and the atom numbering scheme is illustrated in Figure 4.12. The molecule crystallizes in the orthorhombic $Pca2_1$ spacegroup (Table 4.2). Rigid bond and similarity restraints (DELU, SIMU) were applied to the anisotropic displacement parameters of all the cyclopentadienyl rings. The highest peak of 1.51 e/A^3 in the difference Fourier synthesis lies 0.92 A from Cu1 and is of no chemical significance.

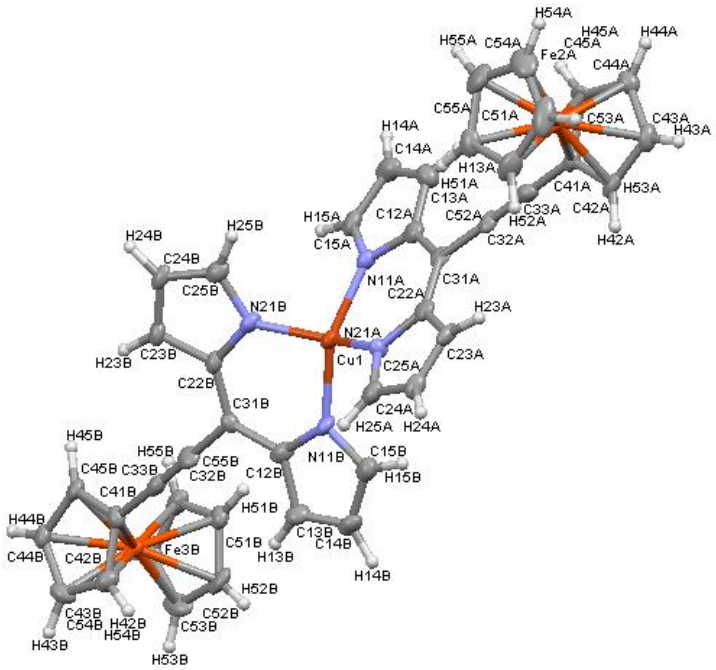


Figure 4.12. Crystal structure of (6) showing the atom labeling scheme. Displacement ellipsoids are drawn at the 50% probability level.

Table 4.2. Crystal data and structure refinement parameters for compound

Compound	(6)
Empirical formula	$C_{42}H_{30}CuFe_2N_4$
Formula weight	765.94
Temperature	150(2) K
Wavelength	0.71073 Å
Crystal system	Orthorhombic
Space group	P c a 21
Unit cell dimensions	a = 20.0347(8) Å α= 90°.
	b = 21.5255(8) Å β= 90°.
	c = 7.6334(3) Å γ = 90°.
Volume	3292.0(2) $Å^3$
Z	4
Density (calculated)	1.545 mg/m^3
Absorption coefficient	1.548 mm^{-1}
F(000)	1564
Crystal size	0.59 x 0.19 x 0.05 mm^3
Theta range for data collection	2.15 to 27.37°
Index ranges	-25<=h<=25, -27<=k<=26, -9<=l<=9
Reflections collected	38566
Independent reflections	7406 [R(int) = 0.0642]
Completeness to theta = 20.00°	0.999
Refinement method	Full-matrix least-squares on F^2
Data / restraints / parameters	7406 / 161 / 442
Goodness-of-fit on F2	1.283
Final R indices [I>2sigma(I)]	R1 = 0.0763, wR2 = 0.1701
R indices (all data)	R1 = 0.0824, wR2 = 0.1728
Largest diff. peak and hole	1.512 and -0.984 $e \cdot Å^{-3}$

The aromatic region of the dipyrrin backbone is planar. The angle formed between the cyclopentadienyl rings and the mean dipyrrin plane is different in the two ligands with the one being 25.5(2)^{o} and the other 22.8(2)^{o} .. The Cp rings of each ferrocenyl unit are eclipsed and they form an angle of 1.2(3)^{o} with respect to each other. The iron atom on one ligand lies at 1.639(3) Å from both the Cp rings centroids while on the other ligand the iron-Cp centroid distance is 1.654(4) Å. The ethynyl linkages are essentially linear with angles being 177.7 Å and 178.1(8) Å at C32A and C33A respectively. The coordination geometry lies between that of a tetrahedral and a square planar complex. The angle formed between the mean planes of the two dipyrrin subunits being 50.85(9)^{o}.

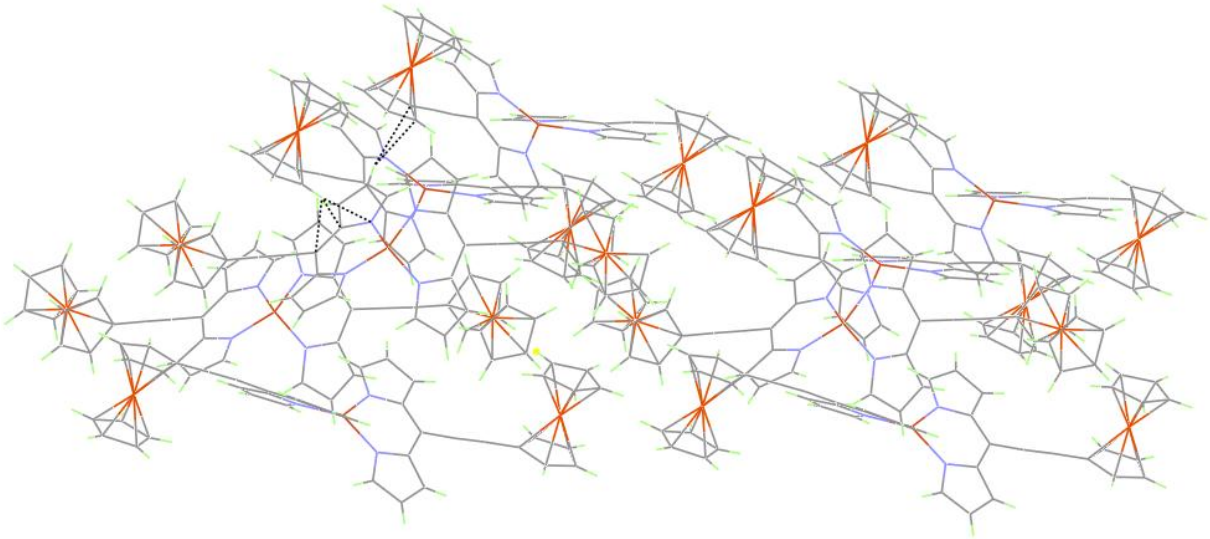


Figure 4.13. Crystal packing of (6). C-H…π interactions are represented as black dashed lines. Hydrogens are coloured yellow for clarity.

4.4 Cyclic voltammetry measurements

Borondifluoride dipyrrins are the only class of dipyrrin derivatives for which the electrochemistry has been extensively studied[46] and has provided information regarding their electrochemical HOMO-LUMO levels of these compounds[47,48]. Generally, these compounds show a reversible one-electron oxidation and a reversible one-electron reduction[49]. The electrochemistry of free-base dipyrrins show the same behavior as that of their protonated analogs although the latter are harder to oxidize and easier to reduce due to the extra positive charge[50]. Substitution of the 5-position of the dipyrrin effects the electrochemistry of the species and indicating a direct correlation between the Hammet constants and the redox potentials[48]. However, later studies have shown that the site of substitution does not affect the redox potentials[51]. On the other hand, reports of electrochemical characterization of metallated dipyrrins have been rare. Ni(II)[48], Cu(II)[52,53], Pd(II),[53] Fe(III)[54] and Zn(II)[55] complexes show one or two redox waves with various degrees of reversibility depending on the substitution of the dipyrrin as well as the metal center.

Cyclic voltammetry (CV) measurements were carried out on **(6), (7), (13)** and **(14).** Different scan rates were applied (20, 50 100, 200 and 300 mV/sec) in order to probe the nature of the electrochemical processes studied. The solvent used in all experiments was dichloromethane containing 0.4M of $[NBu_4][BF_4]$ salt as the supporting electrolyte. A three electrode system was used with glassy carbon being the working electrode, a Pt wire being the secondary electrode and a saturated calomel electrode acting as a reference electrode.

Cited potentials are corrected to be referenced against Fc/Fc^{+} [56] unless otherwise stated. Experimentally, in order to avoid the ferrocene wave overlapping with the oxidation waves due to the ferrocene groups present in the molecules studied, decamethylferrocene (Fc*) was used as an internal standard. Under the conditions of our experiments the Fc^{*}/Fc^{*+} couple was found to be at -0.52 mV versus Fc/Fc^{+}. Theoretically, for an electrochemical process to be reversible, the peak potential difference $E_{pa} - E_{pc} = \Delta E_p$ must be 59/n mV at 25° C (where n = the number of electrons involved in the process) and is independent of the scan rate[57]. In our experimental conditions, decamethylferrocene, which is a known one-electron reversible couple, exhibited a mean ΔE_p value of 72 mV. Taken this into account, every couple having a ΔE_p value less than 90 mV was considered to imply an electrochemically reversible behavior while larger ΔE_p values were considered to imply electrochemically quasi-reversible behavior.

All electrochemical couples were subjected to several tests in order to verify their electrochemical reversibility. In some cases we were not able to calculate the I_{pa}/I_{pc} or plot the I_{pa}, I_{pc} versus the square root of the scan rate in order to check for reversibility by comparing the two slopes. This was because the reverse current could not be accurately measured due to overlap of the second and second oxidation or reduction waves. To avoid generating irreversible products from the following processes, we had to set the return point just before the first process was completed. As an alternative test we adopted the Nicholson equation[58] :

$$Ipc/Ipa = (Ipc)_o/Ipa + (I_\lambda)_o*0.485/Ipa + 0.086$$

with $(I_\lambda)_o$ being the current at the point of the end potential of the voltammorgam and $(Ipc)_o$ being the maximum value of I in the return wave.

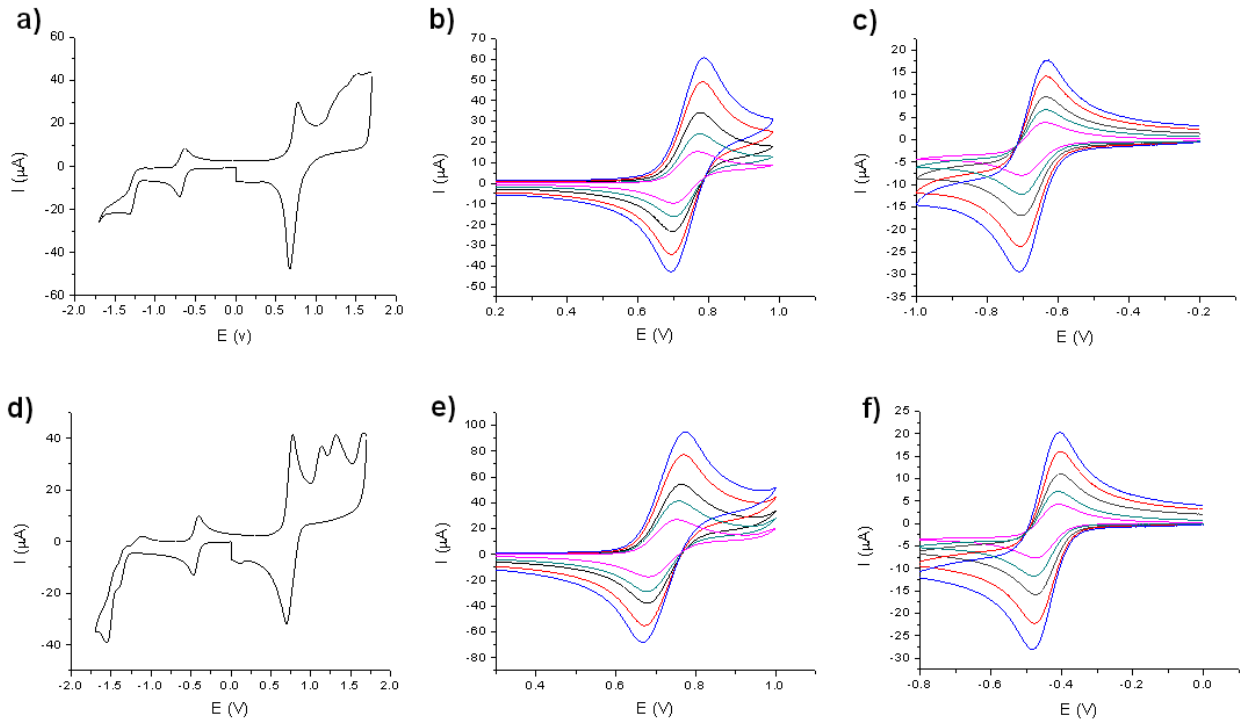


Figure 4.14. Cyclic voltammograms of a) (7) over a wide potential range. b) first oxidation of (7) at various scan rates c) first reduction of (7) at various scan rates d) (6) over a wide potential range e) first oxidation of (6) at various scan rates f) first reduction of (6) at various scan rates. The displayed potentials are versus SCE. Correlation of colour and scan rate is as follows: 20 mV/sec-Magenta, 50 mV/sec-Green, 100 mV/sec-Dark grey, 200 mV/sec-Red, 300 mV/sec-Blue.

Cyclic voltammograms of complexes **(6)** and **(7)** revealed similar behavior for the two complexes. Both complexes show three reduction and three oxidation waves (Figure 4.14a,d). The first oxidation seems to be a reversible process for both complexes. At the scan rate of 100mV/s we can see that for the Cu(II) complex ΔE_p = 79 mV and for the Fe(III) complex ΔE_p = 86 mV. Both values are below 90 mV which signifies a reversible behavior. I_{pa}/I_{pc} calculated

from the Nicholson equation gave a value very close to 1 for both complexes and for all the scan rates. The values of $E_{1/2}$ are 0.23 and 0.20 V for **(6)** and **(7)** respectively. This wave is assigned to the oxidation of the ferrocene units. These potentials are very similar to values reported in the literature[59-64] and are more anodic due to the electron withdrawing effect of the ethylene and dipyrrin groups. Every complex has more than one ferrocene unit. The value of ΔEp shows that the process is a 1-electron 2-step oxidation for **(6)** and an 1-electron 3-step oxidation for **(7).** This is evident from the excessively large size of these peaks compared to the reduction waves. The fact that we can only see one peak is an indication that the oxidations of the ferrocene units are independent and, upon the oxidation of one ferrocene unit, the change in the electronic properties of one ligand do not affect the others.

The second and third oxidations are irreversible and they are believed to be dipyrrin-centered oxidation processes. In the literature, the irreversibility of these oxidations is attributed to the demetallation of the complex upon formation of the mono- or dications[55]. For the Cu(II) complex the E_{pa} values of the oxidations are 0.70 and 0.83 V and for the Fe(III) complex the E_{pa} values are 0.62 and 0.80 V. Although the presence of ferrocene is expected to act as an electron donor, stabilizing the oxidized species, the order of the oxidative processes means that the ferrocene groups have already been oxidized into ferrocenium cations, prior to dipyrrin oxidation. Ferrocenium has a group electronegativity $\chi_{Fc+} = 2.82$ which makes it electron withdrawing[65,66], comparable to the CF_3 group ($\chi_{CF3} = 3.01$)[65,67], explaining the relatively high oxidation potentials for the two complexes.

The first reduction has an $E_{1/2}$ value of -1.18 for the Cu(II) complex and -0.96 for the Fe(III) complex. The ΔEp is 70mV for both complexes and the I_{pa}, I_{pc} versus the square root of the scan rate plot gives two straight lines with almost equal gradients (Figure 4.15). These processes are

one electron reversible reductions and are attributed to the reduction of the central metal cation; Cu(II) is reduced to Cu(I) and Fe(III) is reduced to Fe(II).

The Cu(II) complex shows a second irreversible reduction at -1.83 V while the Fe(III) complex shows two very close irreversible waves at -1.98 and -2.12 V. These reductions are believed to be dipyrrin centered. This assumption comes on the basis of previous studies[46] indicating that metallated dipyrrins can exhibit up to two reductions. Cyclic voltammograms of compounds **(6)** and **(7)** as well as the first oxidation and first reduction wave of each compound are shown in Figure 4.14.

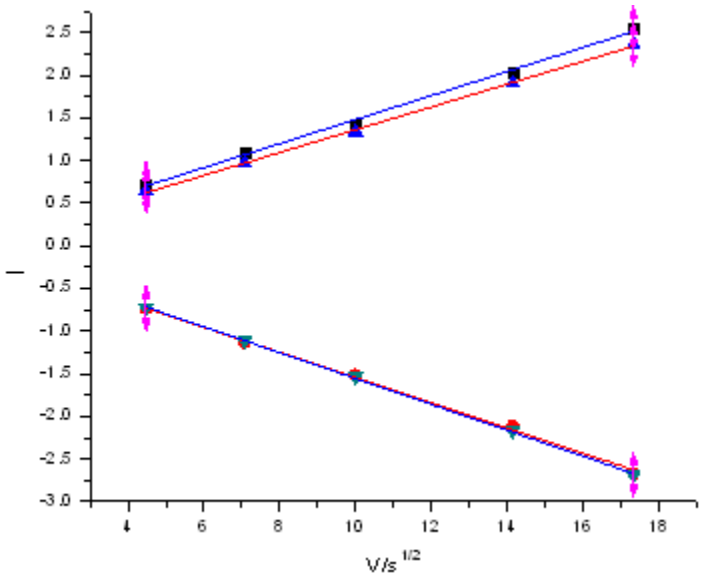


Figure 4.15. Plot of I_{pa},I_{pc} versus the square root of scan rate for the first reduction wave of Cu(II) (blue) and Fe(III) (red) complexes. The R factors are almost 1 and the slopes are almost equal indicating a reversible process.

The cobalt(III) complexes **(13)** and **(14)** show an oxidation wave at 0.21 and 0.22 V respectively, attributed, as above, to the ferrocene moieties. While the waves seem reversible upon first visual inspection, the Nicholson equation for **(14)** gives a value of 0.74 at a scan rate of 20 mV/s while it progressively increases until it reaches the value of 0.999 at 300 mV/s. This does not necessarily imply that the process is quasi-reversible because as will be seen later, during spectroelectrochemistry experiments where the timescales are much longer, full chemical reversibility is observed. A possible explanation of the above observation is the deposition of the oxidized species upon the electrode. Thus, at slow scan rates, upon reduction there is not enough time for the deposited compound to be reduced and enter the solution again, a feature that has been observed previously for ferrocene containing compounds[68].

A second oxidation is observed at 0.74 V for **(13)** and at 0.75 V for **(14)** which is attributed to a dipyrrin centered oxidation. As in the cases of the other metal complexes, these oxidations are irreversible.

The reduction waves differ from the Cu(II) and Fe(III) complexes. **(13)** shows two waves very close to each other at $E_{1/2}$ values of -1.45 and -1.60 V. The ΔEp values are 100 mV for the first reduction and 84 mV for the second. These values are consistent across the spectrum of the scan rates used but the value of 100 mV signifies a quasi-reversible process. On the other hand, **(14)** shows a reduction wave at -0.97 V with quasi-reversible characteristics and two more reduction waves at -1.44 and -1.59 V which have a similar appearance to the two reduction waves of **(13)** both in appearance and properties (Figures 4.16 and 4.17). The reduction at -0.97 mV is attributed to the reduction of Co(III) to Co(II). The peculiarity lies upon the fact that such a wave was absent for in the case of **(13)**. The two waves shown in Figures 4.16c and 4.17d are attributed to dipyrrin centered reductions. It is not clear if the second reduction is found at a more

negative potential due to the electronic influence of the first reduction to the rest of the molecule or if the two complexed dipyrrins differ as discussed above.

Table 4.3 shows a summary of the redox potentials of all four synthesized complexes. From the table we can see that the dipyrrin centered reductions of the cobalt(III) complexes take place at a less negative potential than those of the Fe(III) and Cu(II) complexes. This indicates a decreased electron density of the neutral species. In the case of **(14)** the active species that is being reduced is the $[(dpr)_2bipyCo(III)]^+$ cation, the positive charge possibly affecting the reduction potential of the dipyrrin ring. The fact that the reductions of **(13)** and **(14)** come at the same potentials is an indication that the acetate in **(13)** may be a counterion and not directly linked to the metal.

Table 4.3. Summary of redox potentials ($E_{1/2}$) of compounds (6), (7), (13) and (14)

Compound	Ox1	Ox2	Ox3	Red1	Red2	Red3
$Cu(II)(dpr)_2$ **(6)**	0.23	0.7	0.83	-1.18	-1.83	-
$Fe(III)(dpr)_3$ **(7)**	0.2	0.62	0.8	-0.96	-1.98	-2.12
$Co(III)(OAc)(dpr)_2$ **(13)**	0.21	0.74	-	-	-1.45	-1.6
$[Co(III)(dpr)_2bipy]Cl$ **(14)**	0.22	0.75	-	-0.97	-1.44	-1.59

dpr = 5-ethynylferrocenyldipyrrin, bipy = bipyridine

Potentials reported in blue represent either the Epa or Epc due to irreversibility

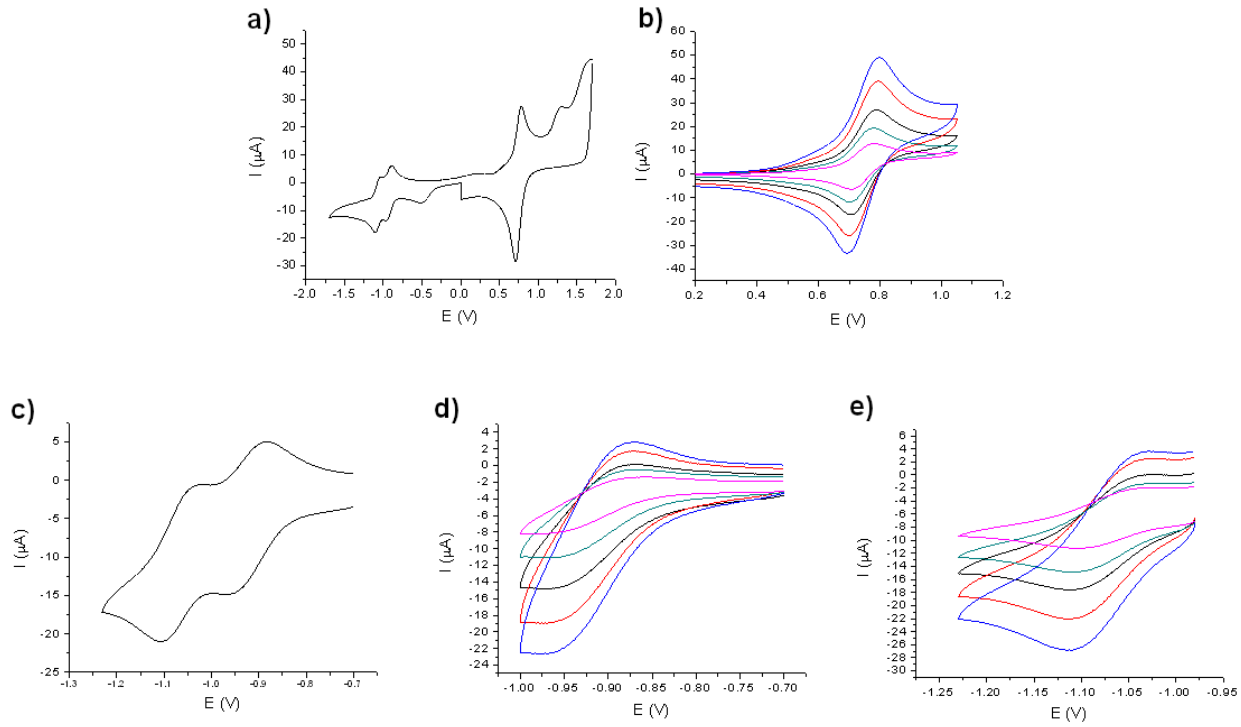


Figure 4.16. Cyclic voltammograms of a) (13) over a wide potential range. b) first oxidation of (13) at various scan rates c) first and second reduction of (13) d) first reduction of (13) at various scan rates e) second reduction of (13) at various scan rates. The displayed potentials are versus SCE. The quasi-reversible characteristics of the reductions are apparent from the dependence of current on the scan rate as shown in the coloured graphs. Correlation of colour and scan rate is as follows: 20 mV/sec-Magenta, 50 mV/sec-Green, 100 mV/sec-Dark grey, 200 mV/sec-Red, 300 mV/sec-Blue.

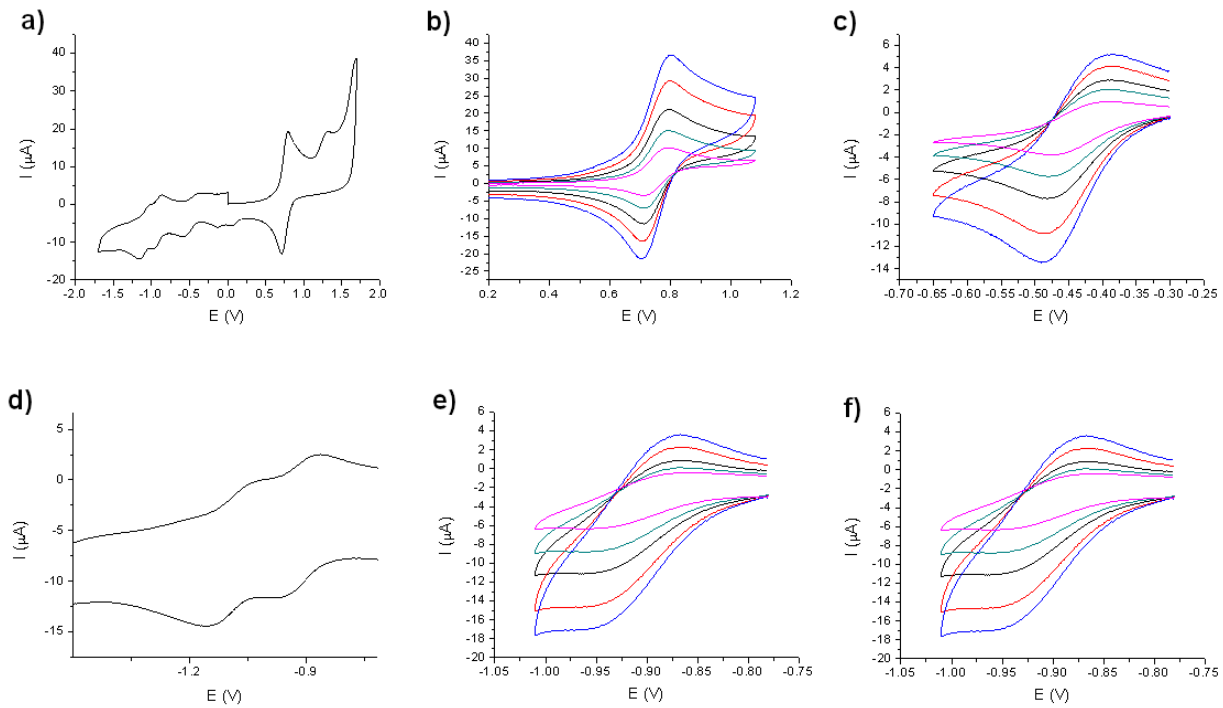


Figure 4.17. Cyclic voltammograms of a) (14) over a wide potential range. b) first oxidation of (14) at various scan rates c) first reduction of (14) at various scan rates d) second and third reduction of (14) e) second reduction of (14) at various scan rates e) third reduction of (14) at various scan rates. The displayed potentials are versus SCE. The quasi-reversible characteristics of the reductions are apparent from the dependence of current on the scan rate as shown in the coloured graphs. Correlation of colour and scan rate is as follows: 20 mV/sec-Magenta, 50 mV/sec-Green, 100 mV/sec-Dark grey, 200 mV/sec-Red, 300 mV/sec-Blue.

4.5 UV-Vis Spectroelectrochemistry

To ensure the chemical reversibility of the redox processes observed during the cyclic voltammetry experiments, UV/Vis spectroelectrochemistry was performed on compounds **(6), (7), (13)** and **(14)**. The compounds were oxidized in situ at the pre-determined appropriate potentials in an optically transparent electrode UV/Vis cell (OTE) in CH_2Cl_2. The temperature was kept constant at 0^o C through a steady flow of air passed through a coiled tube immersed in liquid nitrogen. Figure 4.18 shows the recorded UV/Vis spectra of the neutral species.

The spectra in Figure 4.18 are typical of other metallated dipyrrin compounds. In the literature there have been different opinions as to the correct assignment of the peaks. Some authors[69,70] conclude that the peak between 300 and 400 nm is a π-π* transition localized on the ligand while the peak between 400-600 nm is a metal to ligand charge transfer (MLCT). More recently though the opinion that both peaks arise from π-π* transitions occurring within orbitals located on the dipyrrin site is more accepted[71,72]. Dipyrrins have very high absorption coefficients (20,000-80,000 $M^{-1}cm^{-1}$ at the 400-600 nm region) which is attributed to the extended π-system and the planarity of the molecule. Sometimes (as is the case in all the complexes studied in this project) the lower energy peak is split in two or a shoulder is evident on the left or the right side of the main peak. This splitting is attributed to the exciton effect[73]. The highest energy transition located below 270 nm has been attributed to transitions occurring at the group attached at the 5-position[54,74].

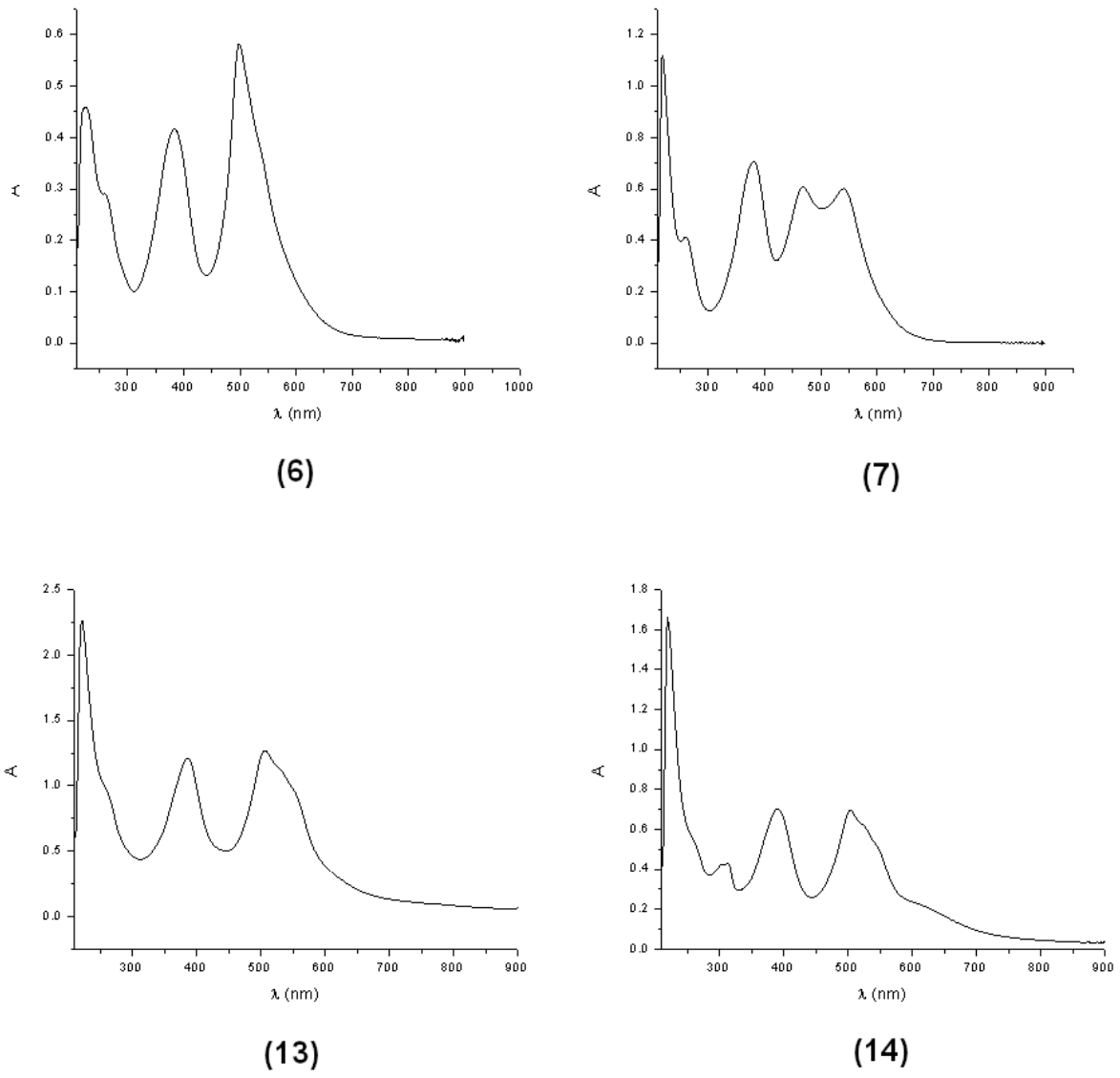


Figure 4.18. UV/Vis absorption spectra of the neutral species of (6), (7), (13) and (14).

The UV/Vis spectrum of ethynylferrocene shows a transition at 236 nm[75] which leads us to assume that the transition at 219 nm which is evident in all our complexes is based on the ethynylferrocene group. **(14)** shows an extra peak at 309 nm which is assigned to the bipyridine ligand.

The first oxidative process gives mixed results. For the Cu(II) and Fe(III) based complexes **(6)** and **(7)** the process is irreversible while for the cobalt(III) based complexes **(13)** and **(14)** the process is fully reversible. All the spectra from the oxidized species show a marked decrease of the intensity of the peak attributed to the transition based on the ethynylferrocene unit (Figure 4.19a), further establishing that this oxidation is ferrocene centered. On the other hand, all the reductions of the cobalt complex are irreversible processes while for the reductions of **(6)** and **(7)**, which were attributed to metal centered reductions, the processes are completely reversible. Figure 4.19b shows the spectra of the neutral and the reduced form of **(6).** There are no significant changes regarding the positions and intensities of the peaks of the redox couples, an indication that the reduction is taking place at the metal center. Figure 4.20 shows the time evolution of the UV/Vis spectrum of all the reverible processes of complexes **(6)**, **(7)**, **(13)**, **(14)**.

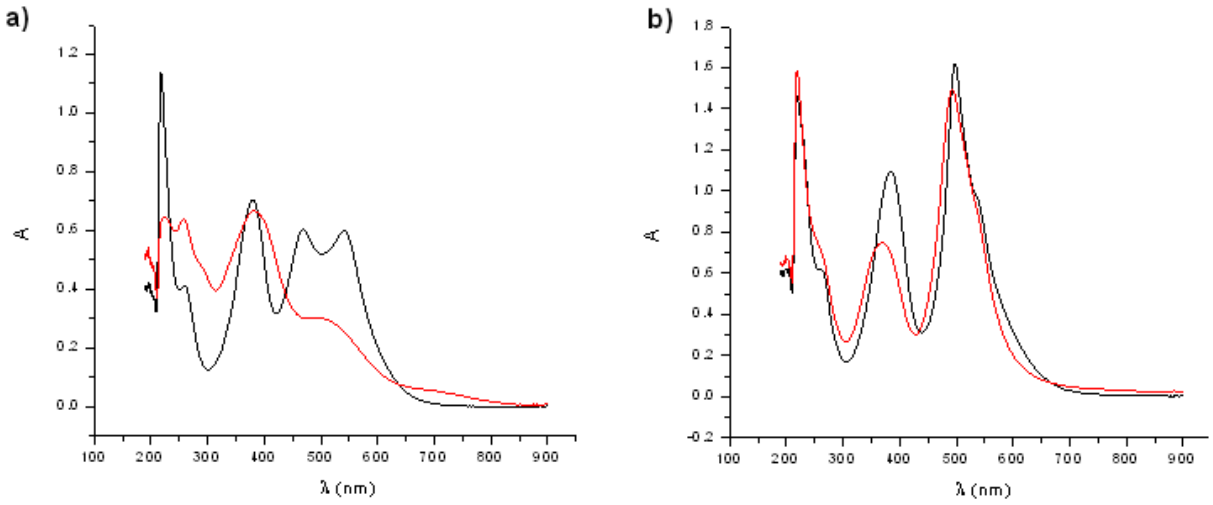


Figure 4.19. UV/Vis spectrum of a) the neutral species of (7) (black line) and the species produced after the first oxidation (red line) b) the neutral species of (6) (black line) and the species produced after the first reduction (red line).

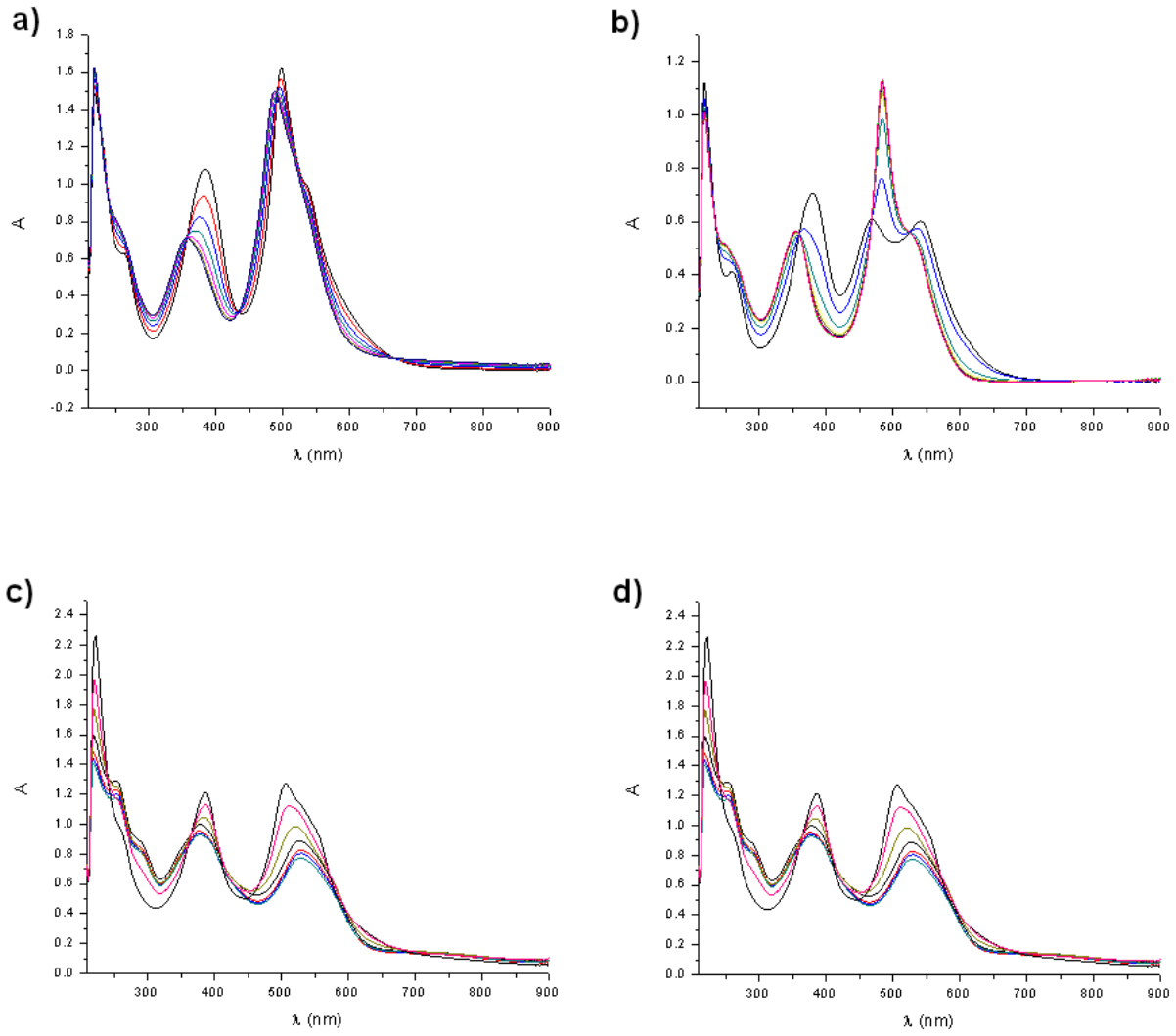


Figure 4.20. Time evolution of the UV/Vis spectrum of a) (6) during the first reduction process at -1.50 V b) (7) during the first reduction process at 1.29 V c) (13) during the first oxidation process at 0.50 V d) (14) during the first oxidation process at 0.56 V.

4.6 Conclusion

The aims of the present project involved the synthesis and characterization of 5-ethynylferrocenyl-dipyrrin and a series of homoleptic and heteroleptic dipyrrinato complexes of Ru(II), Co(II), Co(III), Fe(II), Fe(III) and Cu(II) followed by spectroelectrochemical studies. Not all of these aims were achieved. 5-ethynylferrocenyl-dipyrrin was effectively synthesized although full characterization has not been possible due to decomposition.

Homoleptic 5-ethynylferrocenyl-dipyrrinato complexes of Fe(III) and Cu(II) have been successfully prepared and characterized. We were unable to prepare the corresponding Fe(II) complex. The series of Ru(II) heteroleptic complexes with dipyrrin and bipyridine ligands was not successful either, probably due to the thermal instability of the dipyrrin ligand at the elevated temperatures needed for the ruthenium chemistry. As a result we were not able to study these compounds and make direct comparisons on the effect of the dipyrrin ligands on the light absorption characteristics and on the characteristic MLCT band of these complexes.

The synthesis of the Co(II) complexes were unsuccessful, but a molecule with properties resembling those of Co(III) complexes was isolated. The available data supported the presence of two dipyrrin and one acetate ligands, but it was not possible to confirm that the acetate molecule was directly bound to the cobalt(III) center or if it was acting as a counterion. The rarity of tetrahedral Co(III) complexes supported the former possibility while electrochemical data showing the electron density around the cobalt(III) center of (13) being roughly the same as that

of (14) supported the latter possibility. Addition of bipyridine to the reaction mixture afforded the octahedral [(bis-5-ferrocenylethynyldipyrrin)-bipyridine-Co(III)] chloride complex.

Cyclic voltammetry revealed rich electrochemistry with all compounds showing reversible one electron oxidative processes assigned to the ferrocene units and further non reversible oxidation waves assigned to the dipyrrin rings. Demetallation was assumed during the ring-centered oxidations. For the Fe(III), Cu(II) and the heteroleptic Co(III) complexes reversible reduction waves were recorded and assigned to metal-centered reductions. For the Cu(II) and Fe(III) complexes further non-reversible reductions were observed that were attributed to ring-centered processes, but the Co(III) reductions were found to be quasi-reversible. Spectroelectrochemical data showed that for the Cu(II) and Fe(III) complexes the ferrocene based oxidations were not chemically reversible.

All complexes had very high extinction coefficients (90,000-150,000 $M^{-1}cm^{-1}$ at the 480-570 nm range) indicating that the dipyrrin ligand used has the potential to be a very efficient light absorbing unit. The electrochemistry has shown that all the complexes were able to be oxidized and reduced, indicating that they would all be able to be regenerated by the I^-/I_3^- redox couple. The Co(III) complexes could also, in principle, be used as electrolytes to replace the I^-/I_3^- couple however, further research is needed. The presence of high redox potentials is a desirable property for a compound to be used as a dye in DSSCs and the ability to tune the redox potentials and the stability of the generated species gives more flexibility for the fine tuning of desired properties. Future work including the synthesis and study of more metal complexes of this kind and the incorporation of carboxylic acid groups for TiO_2 binding capabilities could provide efficient dyes for further research in solar energy conversion.

4.7 Experimental

All reagents and solvents were purchased from Sigma Aldrich, Alfa Aesar, Fischer Scientific UK, and used without further purification unless otherwise stated. Elemental microanalyses were carried out by Steven Boyer at the Microanalysis Service, London Metropolitan University, UK. ^{1}H and ^{13}C NMR spectra were measured using either a Joel 270 MHz, Bruker 300 MHz, Bruker 400 MHz, DPX 300 MHz, DPX 400 MHz or Bruker 500 MHz spectrometer. MALDI-TOF mass spectra were obtained using Bruker Ultraflex MALDI-TOF mass spectrometer. MALDI-TOF-MS samples were prepared by dissolution of the compounds in CH_2Cl_2 (10 μL) and then mixing this solution with a solution of the matrix DCTB (trans-2-[3-(4-tertbutylphenyl)-2-methyl-2-propenylidone]-malonitrile) in MeCN (20 μL). A sample of the resulting solution (5 μL) was loaded onto a plate, the solvent was removed in air, and the sample transferred to the mass spectrometer for analysis. Electrospray ionization mass spectra were collected using a MALDI-TOF mass spectrometer. UV-Vis spectra were obtained using Unicam UV/Vis 2 spectrometer.

Cyclic Voltametric studies were carried out using an Autolab PGSTAT20 potentiostat, using a three-electrode arrangement in a single compartment cell. A glassy carbon working electrode, a Pt secondary electrode and a saturated calomel reference electrode (chemically isolated for the test solution *via* a bridge tube containing electrolyte solution and fitted with a porous vycor frit) were used in the cell. Experiments were performed under an atmosphere of argon. Sample solutions were prepared under an argon atmosphere using Schlenck line techniques. The supporting electrolyte employed was a 0.4M $[NBu_4][BF_4]$ solution. Redox potentials were

referenced vs. the Fc/Fc^+ couple. Decamethylferrocene was used as the internal standard. Compensation for internal resistance was not applied.

UV/Vis spectroelectrochemical experiments were carried out with an optically transparent electrochemical (OTE) cell (modified quartz cuvette, optical path length 0.5mm). A three electrode configuration, consisting of a Pt/Rh gauze working electrode, a Pt wire secondary electrode (in a fritted PTFE sleeve) and a saturated calomel electrode (chemically isolated from the test solution via a bridge tube containing electrolyte solution and terminated in a porous frit) were used in the cell. The potential at the working electrode was controlled by a Sycopel Scientific Ltd. DD10M potentiostat. UV/Vis data were recorded on a Perkin Elmer Lamda 16 spectrophotometer. The cavity was purged with N_2 gas and temperature control at the sample was achieved by flowing cooled N_2 gas across the surface of the cell.

Sample solutions were prepared under an atmosphere of argon using Schlenk line techniques and consisted of a 0.4M $[NBu_4][BF_4]$ solution as the supporting electrolyte and a 10^{-4}M solution of the test compound. The test species in solution was oxidized at constant potential and the redox process was considered complete when consecutive spectra were identical. The reversibility of the process was investigated by applying a potential at the working electrode to re-reduce the electrogenerated product. This process was considered to be reversible, under the conditions of the experiment, if the spectral profile of the starting material was reproduced.

Crystallography

All single-crystal X-ray experiments were performed on a Bruker SMART 1000 CCD or a Bruker SMART APEX CCD equipped with an Oxford Cryosystems open flow cryostat,

[graphite monochromatic Mo-Ka radiation (λ=0.71073 Å), ω scans]. Absorption corrections, if necessary, were applied by a semi-empirical approach. All of the single crystal structures were solved by direct methods using SHELXS-97[74]; all non-hydrogen atoms were located using subsequent difference-Fourier methods[75]. Unless otherwise stated, hydrogen atoms were placed in calculated positions and thereafter allowed to ride on their parent atoms.

Additional restraints were placed on thermal and geometric parameters as required and appropriate. All graphical representations were generated using Mercury 1.4.1 (Copyright CCDC 2001-2005).

Compound synthesis

Synthesis of ethynyl-ferrocene (2)

The compound was synthesized as described previously[45] using slight modifications. A solution of acetylferrocene (14 g, 61 mmol) in THF (50 ml) was purged with nitrogen for 20 min. The solution was brought to -78 ^{o}C and a solution of 2.5M LDA in THF (26.8 ml) was added. Stirring was continued for 45 min after which, 1.05 equiv (9.3 ml, 64 mmol) of diethylchlorophosphate was added. The reaction mixture was stirred for an additional 1 h at -78 ^{o}C and then brought to room temperature. An additional 56.1 ml of 2.5M LDA solution in THF were added at -78 ^{o}C. The solution was allowed to warm to room temperature and poured over 500 ml of an ice-water mixture containing concentrated HCl solution (50 ml). The organic layer was extracted with CH_2Cl_2 and dried over Mg_2SO_4. Solvent was removed under reduced pressure

and the residue was purified by flash chromatography on silica using a 3:1 hexane-ether mixture as the mobile phase. The orange oil obtained was crystallized in the freezer from pentane (11.8 g, 91%). %). ^{1}H NMR (400 MHz, $CDCl_3$) : δ ppm = 4.49 (t, J = 1.9 Hz, 2H), 4.25 (s, 5H), 4.23 (t, J = 1.8 Hz, 2H), 2.75 (s, 1H). ^{13}C NMR (101 MHz, $CDCl_3$): δ ppm 63.87, 68.74, , 70.07, 71.78, 73.52, 82.62. ESI-MS (m/z): 210.0130 $(M)^+$. Elemental Analysis (%) Calculated for $C_{12}H_{10}Fe$: C, 68.62; H, 4.80; Found C, 68.77; H, 4.80.

Synthesis of ferrocenyl(formyl)acetylene (3)

The compound was synthesized as described previously[45] using slight modifications. A solution of 2.5 M ^{n}BuLi in hexanes (9.6 ml, 25 mmol) was added to a solution of ethynylferrocene (5 g, 24 mmol) in THF (50 ml) at -78 ^{o}C. The solution was stirred for 30 min after which anhydrous DMF (5 ml) was added. Stirring was continued for 1 h at -78 ^{o}C. The reaction mixture was brought to room temperature and then poured over 250 ml of an ice-water mixture containing concentrated HCl solution (25 ml). The solution was neutralized with $NHCO_3$ after which its colour turned from deep violet to red. The organic phase was extracted with dichloromethane and dried over $MgSO_4$. Solvent was removed under reduced pressure and the residue was purified by flash chromatography using a 2:1 dichloromethane/hexane mixture as the mobile phase. A red solid was obtained at 91% yield. ^{1}H NMR (400 MHz, $CDCl_3$): δ ppm = 9.32 (s, 1H), 4.65 (t, J = 1.9 Hz, 2H), 4.46 (t, J = 1.9 Hz, 2H), 4.30 (s, 5H). ^{13}C NMR (101 MHz, $CDCl_3$): δ ppm 59.31, 70.62, 71.25, 73.35, 76.72, 87.70, 99.48, 176.25. ESI-MS (m/z): 239.0151 $(M+H)^+$. Elemental Analysis (%) Calculated for $C_{13}H_{10}FeO$: C, 65.59; H, 4.23; Found C, 65.61; H, 4.20.

Synthesis of 5-ethynylferrocenyl-dipyrromethane (4)

A solution of ferrocenyl(formyl)acetylene (4 g, 17 mmol) in pyrrole (60 ml) was cooled to -23 ^{o}C and nitrogen was bubbled through the solution for 15 min to remove oxygen. Boron trifluoride diethyl etherate (616 μL) was added and the reaction mixture was stirred at -23 ^{o}C for 15 min. The solution was removed from the ice bath, diluted with DCM (200) ml and extracted immediately with 100 ml of 0.1 M NaOH. The organic phase was collected, dried over $MgSO_4$ and the solvent was removed under reduced pressure. The residue was purified by column chromatography on silica. An 86:13:1 mixture of hexane/ethyl acetate/triethylamine was used as the mobile phase. 5-ethynylferrocenyl-dipyrromethane was obtained as a dark-brown viscous oil in 84% yield. ^{1}H NMR (400 MHz, $CDCl_3$): δ ppm = 8.21 (s, 2H), 6.76 (m, 2H), 6.21 (m, 4H), 5.32 (s, 1H)), 4.46 (t, J = 1.8 Hz, 2H), 4.24 (s, 5H), 4.23 (t, J = 1.8 Hz, 2H). ^{13}C NMR (101 MHz, $CDCl_3$): δ ppm 30.95, 64.99, 68.61, 69.85, 71.44, 81.84, 83.02, 106.18, 108.68, 117.49, 129.29. ESI-MS (m/z): 377.0705 $(M+Na)^{+}$. Elemental Analysis (%) Calculated for $C_{21}H_{18}FeN_2$: C, 71.20; H, 5.12; N, 7.91; Found C, 71.23; H, 5.13; N, 7.82.

Synthesis of bis-(5-ethynylferrocenyl-dipyrromethene) copper(II) (6)

p-Chloranil (35 mg, 0.141 mmol) was added to a solution of 5-ethynylferrocenyl-dipyrromethane (50 mg, 0.141 mmol) in dichloromethane (10 ml) at 0 ^{o}C. The reaction mixture was stirred for 5 min at room temperature followed by the addition of one drop of triethylamine and copper acetate monohydrate (28 mg, 0.141 mmol). The colour of the solution changed to a deep violet. The solvent was removed under vacuum and the residue was purified by column chromatography on silica with a mixture of dichloromethane/hexane (50/50) as the elution

solvent. The purple solid obtained was recrystallized from dichloromethane/hexane affording 30 mg (55.8%) of a golden coloured crystalline material. ^{1}H NMR (400 MHz, $CDCl_3$) : δ ppm = 4.46 (br s, 4H), 4.34 (br s, 4H), 4.23 (br s, 10H), 1.58 (br s, 12H). ^{13}C NMR (101 MHz, $CDCl_3$): δ ppm 29.73, 53.47, 62.14, 70.04, 70.21, 72.22, 97.93, 140.82, 169.59, 171.77, 172.71. MALDI-TOF MS (m/z): 764.988 $(M)^+$. Elemental Analysis (%) Calculated for $C_{42}H_{30}CuFe_2N_4$: C, 65.86; H, 3.95; N, 7.31; Found C, 65.92; H, 3.89; N, 7.29.

Synthesis of bis-(5-ethynylferrocenyl-dipyrromethene) iron(III) (7)

p-Chloranil (35 mg, 0.141 mmol) was added to a solution of 5-ethynylferrocenyl-dipyrromethane (50 mg, 0.141 mmol) in dichloromethane (10 ml) at 0 ^{o}C. The reaction mixture was stirred for 5 min at room temperature followed by extraction with aqueous 0.1M NaOH solution (10 ml). One drop of triethylamine and anhydrous iron(III) chloride (7.6 mg, 0.047 mmol) was added to the organic layer and the mixture was left stirring for an additional one hour at 40 ^{o}C. The solvent was evaporated under reduced pressure and the residue was purified by column chromatography on silica eluting with a mixture of dichloromethane/hexane (1:1). The purple solid obtained was recrystallized with dichloromethane/hexane to afford 7 mg (13%) of a golden-coloured crystalline material. ^{1}H NMR (400 MHz, $CDCl_3$) : δ ppm = 5.86 (d, J=9.9 Hz, 6H), 5.10 (s, 15H), 4.98 (s, 6H), -5.33 (s, 6H), -6.30 (s, J = 6H), -29.27 (s, 6H). ^{13}C NMR (101 MHz, $CDCl_3$): δ ppm 29.73, 46.93, 67.73, 70.67, 70.95, 72.24, 94.22, 100.07, 119.92, 124.92, 141.59. MALDI-TOF (m/z): 1109.011 $(M)^+$. Elemental Analysis (%) Calculated for $C_{21}H_{18}FeN_2$: C, 71.20; H, 5.12; N, 7.91; Found C, 71.23; H, 5.13; N, 7.82.

Synthesis of [bis-(5-ethynylferrocenyl-dipyrromethene)-cobalt(III)] acetate (13)

p-Chloranil (210 mg, 0.846 mmol) was added to a solution of solution of 5-ethynylferrocenyl-dipyrromethane (300 mg, 0.846 mmol) in dichloromethane (60 ml) at 0 ^{o}C. The reaction mixture was stirred for 5 min at room temperature followed by extraction with aqueous 0.1M NaOH solution (60 ml). Six drops of triethylamine, ethanol (60 ml) and cobalt acetate tetrahydrate (210 mg, 0.846 mmol) were added and the reaction mixture was left stirring for 10 min. The solution was extracted with water, dried with $MgSO_4$, filtered and the solvent removed under reduced pressure. The residue was dissolved in a small amount of dichloromethane containing 5% triethylamine and passed through silica gel column with the same solvent system being used as the mobile phase. The collected violet solution was evaporated to dryness. The residue was redisolved in dichloromethane (5 ml) and a purple solid was precipitated by the addition of hexane. Filtration and drying afforded 207 mg (64%) of [bis-(5-ethynylferrocenyl-dipyrromethene)-cobalt(III)] acetate. ^{1}H NMR (400 MHz, $CDCl_3$): δ ppm = 7.95 (t, J=1.5Hz, 2H), 7.86 (dd, J_1=4.2 Hz, J_2=1.4Hz, 2H), 7.47 (dd, J_1=4.3 Hz, J_2=1.5Hz, 2H), 6.85 (dd, J_1=4.3 Hz, J_2=1.6Hz, 2H), 6.44 (t, J=1.6Hz, 2H), 6.27 (dd, J_1=4.3 Hz, J_2=1.7Hz, 2H), 4.7 (t, J=1.9Hz, 4H), 4.44 (t, 1.9Hz, 4H). 4.36 (s, 10H), 1.67 (s, 3H). ^{13}C NMR (101 MHz, $CDCl_3$): δ ppm = 23.94, 63.45, 70.17, 70.27, 70.26, 84.11, 101.71, 119.06, 119.45, 127.51, 130.94, 133.21, 137.10, 137.76, 149.76, 154.85, 192.24. MALDI-TOF MS (m/z): 820 $(M)^{+}$.

Synthesis of [bis-(5-ethynylferrocenyl-dipyrromethene)-bipyridine-cobalt(III)]chloride (14)

p-Chloranil (210 mg, 0.846 mmol) was added to a solution of solution of 5-ethynylferrocenyl-dipyrromethane (300 mg, 0.846 mmol) in dichloromethane (60 ml) at 0 ^{o}C. The reaction mixture

was stirred for 5 min at room temperature followed by extraction with aqueous 0.1M NaOH solution (60 ml). Six drops of triethylamine, ethanol (60 ml), bipyridine (60 mg, 0.423 mmol) and cobalt(II) chloride (109.8 mg, 0.823 mmol) were added and the reaction mixture was left stirring for 10 min. The solution was extracted with water, the organic phase was dried with $MgSO_4$, filtered and the solvent was evaporated under reduced pressure. The residue was purified by preparative TLC on silica. The mobile phase consisted of a mixture of dichloromethane/methanol (85:15). The intensely purple band was scraped off the plate and placed in a column. Passing a mixture of dichloromethane/methanol through the material and evaporating the resulting solution afforded 156 mg (40.2%) of a purple solid. ^{1}H NMR (400 MHz, $CDCl_3$) : δ ppm = 10.05 (s, 2H), 8.44 (s, 2H), 7.67 (dd, J_1=4.3Hz, J_2=1.4Hz, 2H), 7.59, (d, J=4.3Hz, 2H), 7.53 (m, 2H), 7.4 (d, J=5.5Hz, 2H), 6.52 (dd, J_1=4.4Hz, J_2=1.6Hz, 2H), 6.41 (m, 2H), 6.16 (s, 2H), 5.86 (s, 2H), 4.69 (m, 4H), 4.49 (m, 4H), 4.36 (s, 10H). ^{13}C NMR (101 MHz, $CDCl_3$): δ ppm = 62.52, 70.37, 70.71, 72.38, 72.42, 83.88, 104.40, 120.24, 120.71, 128.06, 128.37, 132.37, 133.34, 136.15, 136.29, 142.33, 147.45, 149.63, 152.21, 156.63. MALDI-TOF MS (m/z): 951.98 $(M)^-$.

4.8 References

1. M. Gratzel, *Inorg. Chem.*, **2005**, *44*, 6841.

2. A. Shah, P. Torres, R. Tscharner, N. Wyrsch, H. Keppner, *Science* , **1999**, *285*, 692.

3. B. O'Regan, M. Grätzel, *Nature,* **1991**, *353***,** 737.

4. T. W. Hamann, R. A. Jensen, A. B. F. Martinson, H. V. Ryswyk, J. T. Hupp, *Energ. Environ. Sci.,* **2008**, *1***,** 66.

5. L. M. Peter, *Phys. Chem. Chem. Phys.,* **2007**, *9***,** 2630.

6 H. J. Snaith, L. Schmidt-Mende, *Adv. Mater.,* **2007** *19***,** 3187.

7 M. Grätzel, *J. Photochem. Photobiol. A,* **2004**, *164***,** 3.

8 A. Listorti, B. O'Regan, J. R. Durrant, *Chem. Mater.,***2011**, *23*, 3381.

9. W. Shockley, H. J. Queisser, *J. Appl. Phys.,* **1961,** *32*, 510.

10. A. Yella, H. Lee, H. N. Tsao, C. Yi, A. K. Chandiran, M. K. Nazeeruddin, E. W. Diau, C. Yeh, S. M. Zakeeruddin, M. Grätzel, *Science,* **2011**, *334*, 629.

11. M. Grätzel, *Nature,* **2001**, *414*, 338.

12. K. Kalyanasundaram, M. Grätzel, *Coord. Chem. Rev*., **1998**, *177*, 347.

13. A, Hagfeldt, M. Grätzel, *Chem. Rev*., **1995**, *95*, 49.

14. C. A. Kelly, G. J. Meyer, *Coord. Chem. Rev*., **2001**, *211*, 295.

15. M. Grätzel, *Curr. Opin. Colloid Interface Sci.,* **1999**, *4*, 314.

16. K. Hara, T. Sato, R. Katoh, A. Furube, Y. Ohga, A. Shinpo, S. Suga, K. Sayama, H. Sugihara, H. Arakawa, *J. Phys. Chem. B,* **2003**, *107,* 597.

17. K. Hara, Y. Tachibana, Y. Ohga, A. Shinpo, S. Suga, K. Sayama, H. Sugihara, H. Arakawa, *Sol. Energy Mater. Sol. Cells,* **2003**, *77*, 89.

18. S. Huang, G. Schlichthorl, A. Nozik, M. Grätzel, A. Frank, *J. Phys. Chem. B,* **1997**,*101*, 2576.

19. G. Boschloo, A. Hagfeldt, A., *Acc. Chem. Rec.,* **2009**, *42*, 1819.

20. J. Bisquert, F. Fabregat-Santiago, I. N. Mora-Seró, G. Garcia-Belmonte, S. Giménez, *J. Phys. Chem. C,* **2009,** *113*, 17278.

21. S. Ardo, G. J. Meyer, *Chem. Soc. Rev.,* **2009**, *38*, 115.

22. H. Nusbaumer, J. E. Moser, S. M. Zakeeruddin, M. K. Nazeeruddin, M. Grätzel, *J. Phys. Chem. B,* **2001***, 105*, 10461.

23. A. Yella, H. Lee, H. N. Tsao, C. Yi, A. K. Chandiran, M. K. Nazeeruddin, E. W. Diau, C. Yeh, S. M. Zakeeruddin, M. Grätzel, *Science*, **2011**, *334*, 629.

24. S. M. Feldt, E. A. Gibson, E. Gabrielsson, L. Sun, G. Boschloo, A. Hagfeldt, *J. Am. Chem. Soc.,* **2010,** *132*, 16714.

25. S. A. Sapp, C. M. Elliott, C. Contado, S. Caramori, C. A. Bignozzi, *J. Am. Chem. Soc.,* **2002**, *124*, 11215.

26. B.A. Gregg, F. Pichot, S. Ferrere, C. L. Fields, *J. Phys. Chem. B,* **2001**, *105*, 1422.

27. T. Daeneke, T. Kwon, A. B. Holmes, N. W. Duffy, U. Bach, L. Spiccia, *Nature Chem.,* **2011**, *3*, 211.

28. S. Hattori, Y. Wada, S. Yanagida, S. Fukuzumi, *Jpn. J. Appl. Phys.,* **2005**, *127*, 9648.

29. Y. Bai, Q. Yu, N. Cai, Y. Wang, M. Zhang, P. Wang, *Chem. Commun.,* **2011,** *47*, 4376.

30. H. B. F. Dixon, A. Cornish-Bowden, C. Liebecq, K. L. Loening, G. P. Moss, J. Reedijk, S. F. Velick, P. Venetianer, J. F. G. Vliegenthart, *Pure Appl. Chem,.* **1987**, *59*, 779.

31. J. B. Paine, In *The Porphyrins*; D. Dolphin, Ed.; Academic Press: New York, **1978**; Vol. 1.

32. J. A. Van Koeveringe, J. Lugtenburg, *Recl. Tra. Chim. Pays-Bas,* **1977**, *96*, 55.

33. F. Lopez Arbeloa, J. Banuelos, V. Martinez, T. Arbeloa, I. Lopez Arbeloa, *Int. Re. Phys. Chem.,* **2005**, *24*, 339.

34. L. Yu, K. Muthukumaran, I. V. Sazanovich, C. Kirmaier, E. Hindin, J. R. Diers, P. D. Boyle, D. F. Bocian, D. Holten and J. S. Lindsey, *Inorg. Chem*., **2003**, *42*, 6629.

35. Y. Rio, D. Sanchez-Garcia, W. Seitz, T. Torres, J. L. Sessler and D. M. Guldi, *Chem. Eur. J*, **2009**, *15*, 3956.

36. D. J. Hall, T. M. McLean, S. J. Smalley, M. R. Waterland. S. G. Telfer, *Dalton Trans*., **2010**, *39*, 437.

37. B. E. Hardin, H. J. Snaith, M. D. McGehee, *Nature photonics*, **2012**, *6*, 162.

38. D. M. Guldi, M. Maggini, G. Scorrano, M. Prato, *J. Am. Chem. Soc*., **1997**, *119*, 974.

39. D. M. Klassen, G. A. Crosby, *J. Chem. Phys.,* **1968**, *48*, 1853.

40. S. J. Smalley, M. R. Waterland, S. G. Telfer, *Inorg. Chem.* **2009**, *48*, 13.

41. G. P. Arsenault,, E. Bullock, S. F. MacDonald, *J. Am. Chem. Soc.,* **1960**, *82*, 4384.

42. B. R. J. Hoteksitis, X. E. Mertell, *Inorganic Chemistry,* **1970**, *9,* 1832.

43. R. W. Wagner, J. S. Lindsey, *J. Am. Chem. Soc.,* **1994**, *116*, 9759.

44. K. Joydev, Laha, S. Dhanalekshmi, M. Taniguchi, A. Ambroise, J. S. Lindsey, *Org. Proc. Res. Dev.*, **2003**, *7*, 799.

45. G. Doisneau, G. Balavoine, T. Fillebeen-Khan, *J. Organomet. Chem.*, **1992**, *425*, 113.

46. E. T. Wood, A. Thompson, *Chem. Rev*., **2007**, *107*, 1831.

47. M. Galletta, F. Puntoriero, S. Campagna, C. Chiorboli, M. Quesada, S. Goeb, R. Ziessel, *J. Phys. Chem. A,* **2006**, *110*, 4348.

48. M. Broering, C. D. Brandt, J. Lex, H. U. Humpf, J. Bley-Escrich, J. P. Gisselbrecht, *Eur. J. Inorg. Chem.* **2001**, *11*, 2549.

49. C. Goze, G. Ulrich, R. Ziessel, *J. Org. Chem.,* **2007**, *72*, 313.

50. H. D. Tabba, J. A. S. Cavaleiro, D. Jeyakumar, M. Graca, P. M. S. Neves, K. M. Smith, *J. Org. Chem.,* **1989**, *54*, 1943.

51. C. W. Wan, A. Burghart, J. Chen, F. Bergstroem,,L. B. A. Johansson, M. F. Wolford, T. G. Kim, M. R. Topp, R. M. Hochstrasser, K. Burgess, *Chem. Eur. J.,* **2003**, *9*, 4430.

52. H. S. Gill, I. Finger, I. Bozidarevic, F. Szydlo, M. J. Scott, M. J., *New J. Chem.,* **2005**, *29*, 68.

53. M. Broering, C. D. Brandt, J. Bley-Escrich, J. P. Gisselbrecht, *Eur. J. Org. Chem.,* **2002**, *3*, 910.

54. S. R. Halper, S. M. Cohen, *Chem. Eur. J.,* **2003**, *9*, 4661.

55. L. Yu, K. Muthukumaran, I. V. Sazanovich, C. Kirmaier, E. Hindin, J. R. Diers, P. D. Boyle, D. F. Bocian, D. Holten, J. S. Lindsey, *Inorg. Chem.* **2003**, *42*, 6629.

56. G. Gritzner, J. Kuta, *Pure Appl. Chem.*, **1984**, *56*, 461.

57. (a) D. H. Evans, K. M. O'Connell, R. A. Peterson, M. J. Kelly, *J. Chem. Educ.*, **1983**, *60*, 291. (b) P. T. Kissinger, W. R. J. Heineman, *Chem. Educ.* **1983**, *60*, 702. (c) J. J. Van Benshoten, J. Y. Lewis, W. R. J. Heineman, *Chem. Educ.*, **1983**, *60*, 772.

58. R. S. Nicholson, *Anal. Chem.*, **1966**, *38*, 1406.

59. L. Cuffe, R. D. A. Hudson, J. F. Gallagher, S. Jennings, C. J. McAdam, R. B. T. Connelly, A. R. Manning, B. H. Robinson, J. Simpson, *Organomettalics*, **2005**, *24*, 2051.

60. J. Tiburcio, V. M. Ugalde-Salvidar, S. J. Loeb, H. Torrens, *Inorg. Chemi. Acta*, **2009**, *362*, 4241.

61. H. Fink, N. J. Long, A. J. Martin, G. Opromolla, A. J. P. White, D. J. Williams, P. Zanello, *Organomettalics*, **1997**, *16*, 2646.

62. a) E. McGale, B. H. Robinson, J. Simpson, *Organomettalics*, **2003**, *22*, 931. b) A. Klein, O. Lavastre, J. Fiedler, *Organometallics*, **2006**, *25*, 635.

63. N. Chawdhury, N. J. Long, M. F. Mahon, L-L. Ooi, P. R. Raithby, S. Rooke, A. J. P. White, D. J. Williams, M. Younus, *J. Org. Chem*., **2004**, *689*, 840.

64. O. Lavastre, J. Plass, P. Bachmann, S. Guesmi, C. Moinet, P. H. Dixneuf, *Organomettalics*, **1997**, *16*, 184.

65. W. C. Du Plessis, J. J. C. Erasmus, G. J. Lamprecht, J. Conradie, T. S. Cameron, M. A. S. Aquino, J. C. Swarts, *Can. J. Chem.* **1999**, *77*, 378.

66. W. L. Davis, R. F. Shago, E. H. G Langner, J. C. Swarts, *Polyhedron*, **2005**, *24*, 1611.

67. W. C. Du Plessis, T. G. Vosloo, J. C. J. Swarts, Chem. Soc., *Dalton Trans.*, **1998**, *15*, 2507.

68. G. Goretzki, E. S. Davies, S. P. Argent, J. E. Warren, A. J. Blake, N. R. Champness, *Inorg. Chem.*, **2009**, *48*, 10264.

69. C. Brückner, Y. Zhang, S. J. Rettig, D. Dolphin, *Inorganica Chimica Acta*, **1997**, *263*, 279.

70. S. R. Halper, S. M. Cohen, *Chem. Eur. J.* **2003**, *9*, 4661.

71. V. S. Thoi, J. R. Stork, D. Magde, S. M. Cohen, *Inorg. Chem.*, **2006,** 45, 10688.

72. C. Bruckner, V. Karunaratne, S. J. Rettig, D. Dolphin, *Can. J. Chem*. **1996**, *74*, 2182.

73. B. Bosnich, *Acc. Chem. Res.*, **1969**, *2*, 266.

74. G. Ulrich, R. Ziessel, *J. Org. Chem.* **2004**, *69*, 2070.

75. Á. Díez, E. Lalinde, M. T. Moreno, S. Sánchez, *Dalton Trans.*, **2009**, *18*, 3434.

Appendix 1. Crystallographic data of structures discussed in Chapter 3

A1.1. Table of selected bond lengths [Å] and angles [^{o}] for (7) · 2MeOH

Mg(1)-N(21)#1	2.0675(13)	C(3)-H(3)	0.9500
Mg(1)-N(21)	2.0675(13)	C(4)-N(21)	1.3683(19)
Mg(1)-N(22)	2.0829(13)	C(4)-C(5)	1.411(2)
Mg(1)-N(22)#1	2.0829(13)	C(5)-C(6)	1.410(2)
Mg(1)-O(1A)#1	2.1876(12)	C(5)-C(31)	1.494(2)
Mg(1)-O(1A)	2.1876(12)	C(6)-N(22)	1.3698(19)
Fe(2)-C(78)	2.0323(17)	C(6)-C(7)	1.448(2)
Fe(2)-C(73)	2.0364(17)	C(7)-C(8)	1.354(2)
Fe(2)-C(72)	2.0375(16)	C(7)-H(7)	0.9500
Fe(2)-C(77)	2.0402(17)	C(8)-C(9)	1.454(2)
Fe(2)-C(74)	2.0441(16)	C(8)-H(8)	0.9500
Fe(2)-C(79)	2.0460(17)	C(9)-N(22)	1.3726(19)
Fe(2)-C(76)	2.0579(17)	C(9)-C(10)	1.419(2)
Fe(2)-C(71)	2.0636(16)	C(10)-C(1)#1	1.421(2)
Fe(2)-C(75)	2.0645(17)	C(10)-C(70)	1.489(2)
Fe(2)-C(70)	2.1023(15)	C(31)-C(36)	1.392(2)
O(1A)-C(2A)	1.430(2)	C(31)-C(32)	1.392(2)
O(1A)-H(1A)	0.855(9)	C(32)-C(33)	1.398(2)
C(2A)-H(2AA)	0.9800	C(32)-H(32)	0.9500
C(2A)-H(2AB)	0.9800	C(33)-C(34)	1.391(2)
C(2A)-H(2AC)	0.9800	C(33)-C(40)	1.494(2)
C(1)-N(21)	1.3726(19)	C(34)-C(35)	1.391(2)
C(1)-C(10)#1	1.421(2)	C(34)-H(34)	0.9500
C(1)-C(2)	1.442(2)	C(35)-C(36)	1.393(2)
C(2)-C(3)	1.356(2)	C(35)-C(45)	1.490(2)
C(2)-H(2)	0.9500	C(36)-H(36)	0.9500
C(3)-C(4)	1.446(2)	C(40)-O(41)	1.205(2)

C(40)-O(42)	1.3415(19)		
O(42)-C(43)	1.4540(19)	N(21)#1-Mg(1)-N(21)	180.000(1)
C(43)-C(44)	1.503(2)	N(21)#1-Mg(1)-N(22)	88.61(5)
C(43)-H(43A)	0.9900	N(21)-Mg(1)-N(22)	91.39(5)
C(43)-H(43B)	0.9900	N(21)#1-Mg(1)-N(22)#1	91.39(5)
C(44)-H(44A)	0.9800	N(21)-Mg(1)-N(22)#1	88.61(5)
C(44)-H(44B)	0.9800	N(22)-Mg(1)-N(22)#1	180.000(1)
C(44)-H(44C)	0.9800	N(21)#1-Mg(1)-O(1A)#1	90.10(5)
C(45)-O(46)	1.210(2)	N(21)-Mg(1)-O(1A)#1	89.90(5)
C(45)-O(47)	1.3412(19)	N(22)-Mg(1)-O(1A)#1	88.69(5)
O(47)-C(48)	1.456(2)	N(22)#1-Mg(1)-O(1A)#1	91.31(5)
C(48)-C(49)	1.512(3)	N(21)#1-Mg(1)-O(1A)	89.90(5)
C(48)-H(48A)	0.9900	N(21)-Mg(1)-O(1A)	90.10(5)
C(48)-H(48B)	0.9900	N(22)-Mg(1)-O(1A)	91.31(5)
C(49)-H(49A)	0.9800	N(22)#1-Mg(1)-O(1A)	88.69(5)
C(49)-H(49B)	0.9800	O(1A)#1-Mg(1)-O(1A)	180.00(7)
C(49)-H(49C)	0.9800	C(78)-Fe(2)-C(73)	101.10(7)
C(70)-C(71)	1.435(2)	C(78)-Fe(2)-C(72)	117.11(7)
C(70)-C(74)	1.436(2)	C(73)-Fe(2)-C(72)	40.85(7)
C(71)-C(72)	1.423(2)	C(78)-Fe(2)-C(77)	40.86(7)
C(71)-H(71)	0.9500	C(73)-Fe(2)-C(77)	117.73(7)
C(72)-C(73)	1.422(2)	C(72)-Fe(2)-C(77)	103.98(7)
C(72)-H(72)	0.9500	C(78)-Fe(2)-C(74)	119.30(7)
C(73)-C(74)	1.429(2)	C(73)-Fe(2)-C(74)	41.00(6)
C(73)-H(73)	0.9500	C(72)-Fe(2)-C(74)	68.65(7)
C(74)-H(74)	0.9500	C(77)-Fe(2)-C(74)	154.69(7)
C(75)-C(76)	1.423(2)	C(78)-Fe(2)-C(79)	40.97(7)
C(75)-C(79)	1.425(3)	C(73)-Fe(2)-C(79)	118.61(7)
C(75)-H(75)	0.9500	C(72)-Fe(2)-C(79)	153.73(7)
C(76)-C(77)	1.426(3)	C(77)-Fe(2)-C(79)	68.68(7)
C(76)-H(76)	0.9500	C(74)-Fe(2)-C(79)	106.70(7)
C(77)-C(78)	1.422(3)	C(78)-Fe(2)-C(76)	68.56(7)
C(77)-H(77)	0.9500	C(73)-Fe(2)-C(76)	156.18(7)
C(78)-C(79)	1.427(2)	C(72)-Fe(2)-C(76)	123.35(7)
C(78)-H(78)	0.9500	C(77)-Fe(2)-C(76)	40.71(7)
C(79)-H(79)	0.9500	C(74)-Fe(2)-C(76)	162.71(7)

C(79)-Fe(2)-C(76)	68.32(7)	C(10)#1-C(1)-C(2)	125.42(14)
C(78)-Fe(2)-C(71)	155.26(7)	C(3)-C(2)-C(1)	107.46(13)
C(73)-Fe(2)-C(71)	68.43(7)	C(3)-C(2)-H(2)	126.3
C(72)-Fe(2)-C(71)	40.60(6)	C(1)-C(2)-H(2)	126.3
C(77)-Fe(2)-C(71)	122.77(7)	C(2)-C(3)-C(4)	106.63(14)
C(74)-Fe(2)-C(71)	68.18(7)	C(2)-C(3)-H(3)	126.7
C(79)-Fe(2)-C(71)	163.68(7)	C(4)-C(3)-H(3)	126.7
C(76)-Fe(2)-C(71)	111.70(7)	N(21)-C(4)-C(5)	125.64(14)
C(78)-Fe(2)-C(75)	68.51(7)	N(21)-C(4)-C(3)	109.70(13)
C(73)-Fe(2)-C(75)	157.24(7)	C(5)-C(4)-C(3)	124.66(14)
C(72)-Fe(2)-C(75)	161.91(7)	C(6)-C(5)-C(4)	127.26(14)
C(77)-Fe(2)-C(75)	68.33(7)	C(6)-C(5)-C(31)	116.72(13)
C(74)-Fe(2)-C(75)	125.26(7)	C(4)-C(5)-C(31)	115.98(13)
C(79)-Fe(2)-C(75)	40.56(7)	N(22)-C(6)-C(5)	125.31(14)
C(76)-Fe(2)-C(75)	40.40(7)	N(22)-C(6)-C(7)	109.81(13)
C(71)-Fe(2)-C(75)	128.84(7)	C(5)-C(6)-C(7)	124.88(14)
C(78)-Fe(2)-C(70)	158.13(7)	C(8)-C(7)-C(6)	106.78(14)
C(73)-Fe(2)-C(70)	68.44(6)	C(8)-C(7)-H(7)	126.6
C(72)-Fe(2)-C(70)	68.20(6)	C(6)-C(7)-H(7)	126.6
C(77)-Fe(2)-C(70)	160.99(7)	C(7)-C(8)-C(9)	107.30(13)
C(74)-Fe(2)-C(70)	40.49(6)	C(7)-C(8)-H(8)	126.3
C(79)-Fe(2)-C(70)	125.97(7)	C(9)-C(8)-H(8)	126.3
C(76)-Fe(2)-C(70)	128.16(7)	N(22)-C(9)-C(10)	125.24(14)
C(71)-Fe(2)-C(70)	40.28(6)	N(22)-C(9)-C(8)	109.12(13)
C(75)-Fe(2)-C(70)	113.58(6)	C(10)-C(9)-C(8)	125.50(14)
C(2A)-O(1A)-Mg(1)	123.64(10)	C(9)-C(10)-C(1)#1	125.11(14)
C(2A)-O(1A)-H(1A)	109.7(12)	C(9)-C(10)-C(70)	115.07(13)
Mg(1)-O(1A)-H(1A)	112.8(13)	C(1)#1-C(10)-C(70)	119.57(13)
O(1A)-C(2A)-H(2AA)	109.5	C(4)-N(21)-C(1)	106.95(12)
O(1A)-C(2A)-H(2AB)	109.5	C(4)-N(21)-Mg(1)	124.96(10)
H(2AA)-C(2A)-H(2AB)	109.5	C(1)-N(21)-Mg(1)	127.64(10)
O(1A)-C(2A)-H(2AC)	109.5	C(6)-N(22)-C(9)	106.99(12)
H(2AA)-C(2A)-H(2AC)	109.5	C(6)-N(22)-Mg(1)	124.66(10)
H(2AB)-C(2A)-H(2AC)	109.5	C(9)-N(22)-Mg(1)	127.40(10)
N(21)-C(1)-C(10)#1	125.33(14)	C(36)-C(31)-C(32)	118.99(14)
N(21)-C(1)-C(2)	109.25(13)	C(36)-C(31)-C(5)	119.34(14)

C(32)-C(31)-C(5)	121.64(14)	O(47)-C(48)-C(49)	111.03(14)
C(31)-C(32)-C(33)	120.38(14)	O(47)-C(48)-H(48A)	109.4
C(31)-C(32)-H(32)	119.8	C(49)-C(48)-H(48A)	109.4
C(33)-C(32)-H(32)	119.8	O(47)-C(48)-H(48B)	109.4
C(34)-C(33)-C(32)	120.29(14)	C(49)-C(48)-H(48B)	109.4
C(34)-C(33)-C(40)	121.77(14)	H(48A)-C(48)-H(48B)	108.0
C(32)-C(33)-C(40)	117.94(14)	C(48)-C(49)-H(49A)	109.5
C(33)-C(34)-C(35)	119.37(14)	C(48)-C(49)-H(49B)	109.5
C(33)-C(34)-H(34)	120.3	H(49A)-C(49)-H(49B)	109.5
C(35)-C(34)-H(34)	120.3	C(48)-C(49)-H(49C)	109.5
C(34)-C(35)-C(36)	120.24(14)	H(49A)-C(49)-H(49C)	109.5
C(34)-C(35)-C(45)	118.67(14)	H(49B)-C(49)-H(49C)	109.5
C(36)-C(35)-C(45)	121.09(14)	C(71)-C(70)-C(74)	106.64(13)
C(31)-C(36)-C(35)	120.67(14)	C(71)-C(70)-C(10)	126.39(14)
C(31)-C(36)-H(36)	119.7	C(74)-C(70)-C(10)	125.78(14)
C(35)-C(36)-H(36)	119.7	C(71)-C(70)-Fe(2)	68.40(9)
O(41)-C(40)-O(42)	124.11(15)	C(74)-C(70)-Fe(2)	67.57(9)
O(41)-C(40)-C(33)	124.37(15)	C(10)-C(70)-Fe(2)	138.47(11)
O(42)-C(40)-C(33)	111.51(14)	C(72)-C(71)-C(70)	108.64(14)
C(40)-O(42)-C(43)	115.70(13)	C(72)-C(71)-Fe(2)	68.71(9)
O(42)-C(43)-C(44)	107.21(14)	C(70)-C(71)-Fe(2)	71.31(9)
O(42)-C(43)-H(43A)	110.3	C(72)-C(71)-H(71)	125.7
C(44)-C(43)-H(43A)	110.3	C(70)-C(71)-H(71)	125.7
O(42)-C(43)-H(43B)	110.3	Fe(2)-C(71)-H(71)	125.9
C(44)-C(43)-H(43B)	110.3	C(73)-C(72)-C(71)	108.29(14)
H(43A)-C(43)-H(43B)	108.5	C(73)-C(72)-Fe(2)	69.53(9)
C(43)-C(44)-H(44A)	109.5	C(71)-C(72)-Fe(2)	70.69(9)
C(43)-C(44)-H(44B)	109.5	C(73)-C(72)-H(72)	125.9
H(44A)-C(44)-H(44B)	109.5	C(71)-C(72)-H(72)	125.9
C(43)-C(44)-H(44C)	109.5	Fe(2)-C(72)-H(72)	125.5
H(44A)-C(44)-H(44C)	109.5	C(72)-C(73)-C(74)	107.68(14)
H(44B)-C(44)-H(44C)	109.5	C(72)-C(73)-Fe(2)	69.62(9)
O(46)-C(45)-O(47)	124.03(15)	C(74)-C(73)-Fe(2)	69.79(9)
O(46)-C(45)-C(35)	124.09(15)	C(72)-C(73)-H(73)	126.2
O(47)-C(45)-C(35)	111.87(13)	C(74)-C(73)-H(73)	126.2
C(45)-O(47)-C(48)	115.93(13)	Fe(2)-C(73)-H(73)	126.0

C(73)-C(74)-C(70)	108.70(14)	C(78)-C(77)-C(76)	108.04(16)
C(73)-C(74)-Fe(2)	69.21(9)	C(78)-C(77)-Fe(2)	69.27(10)
C(70)-C(74)-Fe(2)	71.94(9)	C(76)-C(77)-Fe(2)	70.31(10)
C(73)-C(74)-H(74)	125.7	C(78)-C(77)-H(77)	126.0
C(70)-C(74)-H(74)	125.7	C(76)-C(77)-H(77)	126.0
Fe(2)-C(74)-H(74)	124.8	Fe(2)-C(77)-H(77)	126.0
C(76)-C(75)-C(79)	108.01(15)	C(77)-C(78)-C(79)	108.01(16)
C(76)-C(75)-Fe(2)	69.55(10)	C(77)-C(78)-Fe(2)	69.87(10)
C(79)-C(75)-Fe(2)	69.02(10)	C(79)-C(78)-Fe(2)	70.03(10)
C(76)-C(75)-H(75)	126.0	C(77)-C(78)-H(78)	126.0
C(79)-C(75)-H(75)	126.0	C(79)-C(78)-H(78)	126.0
Fe(2)-C(75)-H(75)	127.0	Fe(2)-C(78)-H(78)	125.7
C(75)-C(76)-C(77)	108.02(16)	C(75)-C(79)-C(78)	107.91(16)
C(75)-C(76)-Fe(2)	70.05(10)	C(75)-C(79)-Fe(2)	70.42(10)
C(77)-C(76)-Fe(2)	68.98(10)	C(78)-C(79)-Fe(2)	69.00(10)
C(75)-C(76)-H(76)	126.0	C(75)-C(79)-H(79)	126.0
C(77)-C(76)-H(76)	126.0	C(78)-C(79)-H(79)	126.0
Fe(2)-C(76)-H(76)	126.5	Fe(2)-C(79)-H(79)	126.1

Symmetry transformations used to generate equivalent atoms:
#1 -x,-y+1,-z+1

A1.2. Table of selected bond lengths [Å] and angles [°] for (17) · 6MeOH

Mg(1)-N(22)#1	2.075(7)	C(2C)-H(2CC)	0.9800
Mg(1)-N(22)	2.075(7)	C(1)-N(21)	1.376(10)
Mg(1)-N(21)#1	2.084(7)	C(1)-C(10)#1	1.414(12)
Mg(1)-N(21)	2.084(7)	C(1)-C(2)	1.442(12)
Mg(1)-O(1A)	2.204(7)	C(2)-C(3)	1.374(13)
Mg(1)-O(1A)#1	2.204(7)	C(2)-H(2)	0.9500
Fe(2)-C(74)	2.021(10)	C(3)-C(4)	1.448(12)
Fe(2)-C(72)	2.022(9)	C(3)-H(3)	0.9500
Fe(2)-C(71)	2.030(10)	C(4)-N(21)	1.382(10)
Fe(2)-C(76)	2.035(10)	C(4)-C(5)	1.416(12)
Fe(2)-C(79)	2.043(10)	C(5)-C(6)	1.414(11)
Fe(2)-C(70)	2.049(10)	C(5)-C(31)	1.523(11)
Fe(2)-C(77)	2.061(12)	O(5)-C(41)	1.335(11)
Fe(2)-C(78)	2.065(11)	O(5)-C(43)	1.464(10)
Fe(2)-C(75)	2.065(8)	C(6)-N(22)	1.382(10)
Fe(2)-C(73)	2.066(9)	C(6)-C(7)	1.421(12)
O(1A)-C(2A)	1.459(12)	C(7)-C(8)	1.343(12)
O(1A)-H(1A)	0.85(2)	C(7)-H(7)	0.9500
C(2A)-H(2AA)	0.9800	C(8)-C(9)	1.477(12)
C(2A)-H(2AB)	0.9800	C(8)-H(8)	0.9500
C(2A)-H(2AC)	0.9800	C(9)-N(22)	1.351(11)
O(1B)-C(2B)	1.378(13)	C(9)-C(10)	1.420(12)
O(1B)-H(1B)	0.84(2)	C(10)-C(1)#1	1.414(12)
C(2B)-H(2BA)	0.9800	C(10)-C(25)	1.463(13)
C(2B)-H(2BB)	0.9800	C(25)-C(26)	1.183(13)
C(2B)-H(2BC)	0.9800	C(26)-C(70)	1.439(13)
O(1C)-C(2C)	1.426(13)	C(31)-C(32)	1.378(13)
O(1C)-H(1C)	0.85(2)	C(31)-C(36)	1.379(11)
C(2C)-H(2CA)	0.9800	C(32)-C(33)	1.425(12)
C(2C)-H(2CB)	0.9800	C(32)-H(32)	0.9500

C(33)-C(34)	1.383(12)	C(72)-H(72)	0.9500
C(33)-C(45)	1.481(13)	C(73)-C(74)	1.403(14)
C(34)-C(35)	1.371(12)	C(73)-H(73)	0.9500
C(34)-H(34)	0.9500	C(74)-H(74)	0.9500
C(35)-C(36)	1.403(11)	C(75)-C(79)	1.399(13)
C(35)-C(41)	1.501(12)	C(75)-C(76)	1.423(14)
C(36)-H(36)	0.9500	C(75)-H(75)	0.9500
C(41)-O(42)	1.206(11)	C(76)-C(77)	1.442(14)
C(43)-C(44)	1.505(13)	C(76)-H(76)	0.9500
C(43)-H(43A)	0.9900	C(77)-C(78)	1.397(14)
C(43)-H(43B)	0.9900	C(77)-H(77)	0.9500
C(44)-H(44A)	0.9800	C(78)-C(79)	1.454(15)
C(44)-H(44B)	0.9800	C(78)-H(78)	0.9500
C(44)-H(44C)	0.9800	C(79)-H(79)	0.9500
C(45)-O(46)	1.226(11)		
C(45)-O(47B)	1.352(14)	N(22)#1-Mg(1)-N(22)	180.0(5)
C(45)-O(47A)	1.354(14)	N(22)#1-Mg(1)-N(21)#1	90.0(3)
O(47A)-C(48A)	1.464(17)	N(22)-Mg(1)-N(21)#1	90.0(3)
C(48A)-C(49A)	1.504(17)	N(22)#1-Mg(1)-N(21)	90.0(3)
C(48A)-H(48A)	0.9900	N(22)-Mg(1)-N(21)	90.0(3)
C(48A)-H(48B)	0.9900	N(21)#1-Mg(1)-N(21)	180.0(5)
C(49A)-H(49A)	0.9800	N(22)#1-Mg(1)-O(1A)	91.4(3)
C(49A)-H(49B)	0.9800	N(22)-Mg(1)-O(1A)	88.6(3)
C(49A)-H(49C)	0.9800	N(21)#1-Mg(1)-O(1A)	90.4(3)
O(47B)-C(48B)	1.428(16)	N(21)-Mg(1)-O(1A)	89.6(3)
C(48B)-C(49B)	1.498(17)	N(22)#1-Mg(1)-O(1A)#1	88.6(3)
C(48B)-H(48C)	0.9900	N(22)-Mg(1)-O(1A)#1	91.4(3)
C(48B)-H(48D)	0.9900	N(21)#1-Mg(1)-O(1A)#1	89.6(3)
C(49B)-H(49D)	0.9800	N(21)-Mg(1)-O(1A)#1	90.4(3)
C(49B)-H(49E)	0.9800	O(1A)-Mg(1)-O(1A)#1	180.0(3)
C(49B)-H(49F)	0.9800	C(74)-Fe(2)-C(72)	67.4(4)
C(70)-C(71)	1.439(14)	C(74)-Fe(2)-C(71)	69.3(4)
C(70)-C(74)	1.440(12)	C(72)-Fe(2)-C(71)	40.3(4)
C(71)-C(72)	1.396(13)	C(74)-Fe(2)-C(76)	156.2(4)
C(71)-H(71)	0.9500	C(72)-Fe(2)-C(76)	126.1(4)
C(72)-C(73)	1.416(13)	C(71)-Fe(2)-C(76)	107.3(4)

C(74)-Fe(2)-C(79)	107.9(4)	C(77)-Fe(2)-C(73)	124.6(4)
C(72)-Fe(2)-C(79)	155.5(4)	C(78)-Fe(2)-C(73)	107.2(4)
C(71)-Fe(2)-C(79)	162.9(4)	C(75)-Fe(2)-C(73)	154.9(4)
C(76)-Fe(2)-C(79)	68.1(4)	C(2A)-O(1A)-Mg(1)	127.7(5)
C(74)-Fe(2)-C(70)	41.4(4)	C(2A)-O(1A)-H(1A)	102(8)
C(72)-Fe(2)-C(70)	67.9(4)	Mg(1)-O(1A)-H(1A)	124(8)
C(71)-Fe(2)-C(70)	41.3(4)	O(1A)-C(2A)-H(2AA)	109.5
C(76)-Fe(2)-C(70)	120.5(4)	O(1A)-C(2A)-H(2AB)	109.5
C(79)-Fe(2)-C(70)	125.6(4)	H(2AA)-C(2A)-H(2AB)	109.5
C(74)-Fe(2)-C(77)	161.2(4)	O(1A)-C(2A)-H(2AC)	109.5
C(72)-Fe(2)-C(77)	108.0(5)	H(2AA)-C(2A)-H(2AC)	109.5
C(71)-Fe(2)-C(77)	119.9(5)	H(2AB)-C(2A)-H(2AC)	109.5
C(76)-Fe(2)-C(77)	41.2(4)	C(2B)-O(1B)-H(1B)	120(10)
C(79)-Fe(2)-C(77)	68.3(5)	O(1B)-C(2B)-H(2BA)	109.5
C(70)-Fe(2)-C(77)	155.7(4)	O(1B)-C(2B)-H(2BB)	109.5
C(74)-Fe(2)-C(78)	125.5(4)	H(2BA)-C(2B)-H(2BB)	109.5
C(72)-Fe(2)-C(78)	120.2(4)	O(1B)-C(2B)-H(2BC)	109.5
C(71)-Fe(2)-C(78)	153.8(5)	H(2BA)-C(2B)-H(2BC)	109.5
C(76)-Fe(2)-C(78)	68.0(4)	H(2BB)-C(2B)-H(2BC)	109.5
C(79)-Fe(2)-C(78)	41.5(4)	C(2C)-O(1C)-H(1C)	108(10)
C(70)-Fe(2)-C(78)	163.5(4)	O(1C)-C(2C)-H(2CA)	109.5
C(77)-Fe(2)-C(78)	39.6(4)	O(1C)-C(2C)-H(2CB)	109.5
C(74)-Fe(2)-C(75)	121.2(4)	H(2CA)-C(2C)-H(2CB)	109.5
C(72)-Fe(2)-C(75)	163.4(4)	O(1C)-C(2C)-H(2CC)	109.5
C(71)-Fe(2)-C(75)	126.2(4)	H(2CA)-C(2C)-H(2CC)	109.5
C(76)-Fe(2)-C(75)	40.6(4)	H(2CB)-C(2C)-H(2CC)	109.5
C(79)-Fe(2)-C(75)	39.8(4)	N(21)-C(1)-C(10)#1	124.4(8)
C(70)-Fe(2)-C(75)	108.3(4)	N(21)-C(1)-C(2)	109.6(8)
C(77)-Fe(2)-C(75)	68.4(4)	C(10)#1-C(1)-C(2)	126.0(8)
C(78)-Fe(2)-C(75)	68.1(4)	C(3)-C(2)-C(1)	107.7(8)
C(74)-Fe(2)-C(73)	40.1(4)	C(3)-C(2)-H(2)	126.1
C(72)-Fe(2)-C(73)	40.5(4)	C(1)-C(2)-H(2)	126.1
C(71)-Fe(2)-C(73)	69.2(4)	C(2)-C(3)-C(4)	106.0(8)
C(76)-Fe(2)-C(73)	162.6(4)	C(2)-C(3)-H(3)	127.0
C(79)-Fe(2)-C(73)	120.2(4)	C(4)-C(3)-H(3)	127.0
C(70)-Fe(2)-C(73)	68.9(4)	N(21)-C(4)-C(5)	123.7(8)

N(21)-C(4)-C(3)	110.2(8)	C(34)-C(33)-C(45)	123.0(8)
C(5)-C(4)-C(3)	126.1(8)	C(32)-C(33)-C(45)	117.9(8)
C(4)-C(5)-C(6)	128.6(8)	C(35)-C(34)-C(33)	120.6(8)
C(4)-C(5)-C(31)	115.3(8)	C(35)-C(34)-H(34)	119.7
C(6)-C(5)-C(31)	116.1(8)	C(33)-C(34)-H(34)	119.7
C(41)-O(5)-C(43)	116.2(7)	C(34)-C(35)-C(36)	120.1(8)
N(22)-C(6)-C(5)	124.0(8)	C(34)-C(35)-C(41)	122.1(8)
N(22)-C(6)-C(7)	109.6(7)	C(36)-C(35)-C(41)	117.8(8)
C(5)-C(6)-C(7)	126.4(8)	C(31)-C(36)-C(35)	120.2(8)
C(8)-C(7)-C(6)	108.1(8)	C(31)-C(36)-H(36)	119.9
C(8)-C(7)-H(7)	125.9	C(35)-C(36)-H(36)	119.9
C(6)-C(7)-H(7)	125.9	O(42)-C(41)-O(5)	123.1(8)
C(7)-C(8)-C(9)	106.1(8)	O(42)-C(41)-C(35)	125.5(8)
C(7)-C(8)-H(8)	126.9	O(5)-C(41)-C(35)	111.3(8)
C(9)-C(8)-H(8)	126.9	O(5)-C(43)-C(44)	105.9(7)
N(22)-C(9)-C(10)	126.3(8)	O(5)-C(43)-H(43A)	110.6
N(22)-C(9)-C(8)	109.0(7)	C(44)-C(43)-H(43A)	110.6
C(10)-C(9)-C(8)	124.6(8)	O(5)-C(43)-H(43B)	110.6
C(1)#1-C(10)-C(9)	126.5(9)	C(44)-C(43)-H(43B)	110.6
C(1)#1-C(10)-C(25)	115.1(8)	H(43A)-C(43)-H(43B)	108.7
C(9)-C(10)-C(25)	118.4(8)	C(43)-C(44)-H(44A)	109.5
C(1)-N(21)-C(4)	106.6(7)	C(43)-C(44)-H(44B)	109.5
C(1)-N(21)-Mg(1)	126.6(6)	H(44A)-C(44)-H(44B)	109.5
C(4)-N(21)-Mg(1)	126.8(6)	C(43)-C(44)-H(44C)	109.5
C(9)-N(22)-C(6)	107.0(7)	H(44A)-C(44)-H(44C)	109.5
C(9)-N(22)-Mg(1)	126.1(6)	H(44B)-C(44)-H(44C)	109.5
C(6)-N(22)-Mg(1)	126.8(6)	O(46)-C(45)-O(47B)	125.1(11)
C(26)-C(25)-C(10)	177.6(10)	O(46)-C(45)-O(47A)	117.8(10)
C(25)-C(26)-C(70)	177.3(10)	O(47B)-C(45)-O(47A)	30.8(7)
C(32)-C(31)-C(36)	120.1(8)	O(46)-C(45)-C(33)	125.3(9)
C(32)-C(31)-C(5)	120.5(7)	O(47B)-C(45)-C(33)	107.9(9)
C(36)-C(31)-C(5)	119.3(8)	O(47A)-C(45)-C(33)	114.5(10)
C(31)-C(32)-C(33)	119.9(8)	C(45)-O(47A)-C(48A)	121.2(13)
C(31)-C(32)-H(32)	120.0	O(47A)-C(48A)-C(49A)	109.2(17)
C(33)-C(32)-H(32)	120.0	O(47A)-C(48A)-H(48A)	109.8
C(34)-C(33)-C(32)	119.1(8)	C(49A)-C(48A)-H(48A)	109.8

O(47A)-C(48A)-H(48B)	109.8	C(72)-C(73)-Fe(2)	68.1(5)
C(49A)-C(48A)-H(48B)	109.8	C(74)-C(73)-H(73)	127.2
H(48A)-C(48A)-H(48B)	108.3	C(72)-C(73)-H(73)	127.2
C(45)-O(47B)-C(48B)	117.9(14)	Fe(2)-C(73)-H(73)	128.0
O(47B)-C(48B)-C(49B)	108.5(19)	C(73)-C(74)-C(70)	110.0(9)
O(47B)-C(48B)-H(48C)	110.0	C(73)-C(74)-Fe(2)	71.7(6)
C(49B)-C(48B)-H(48C)	110.0	C(70)-C(74)-Fe(2)	70.3(6)
O(47B)-C(48B)-H(48D)	110.0	C(73)-C(74)-H(74)	125.0
C(49B)-C(48B)-H(48D)	110.0	C(70)-C(74)-H(74)	125.0
H(48C)-C(48B)-H(48D)	108.4	Fe(2)-C(74)-H(74)	124.5
C(48B)-C(49B)-H(49D)	109.5	C(79)-C(75)-C(76)	107.9(9)
C(48B)-C(49B)-H(49E)	109.5	C(79)-C(75)-Fe(2)	69.2(5)
H(49D)-C(49B)-H(49E)	109.5	C(76)-C(75)-Fe(2)	68.6(5)
C(48B)-C(49B)-H(49F)	109.5	C(79)-C(75)-H(75)	126.0
H(49D)-C(49B)-H(49F)	109.5	C(76)-C(75)-H(75)	126.0
H(49E)-C(49B)-H(49F)	109.5	Fe(2)-C(75)-H(75)	127.7
C(71)-C(70)-C(74)	106.3(8)	C(75)-C(76)-C(77)	108.1(9)
C(71)-C(70)-C(26)	125.6(9)	C(75)-C(76)-Fe(2)	70.8(6)
C(74)-C(70)-C(26)	128.0(10)	C(77)-C(76)-Fe(2)	70.4(6)
C(71)-C(70)-Fe(2)	68.6(6)	C(75)-C(76)-H(76)	125.9
C(74)-C(70)-Fe(2)	68.2(6)	C(77)-C(76)-H(76)	125.9
C(26)-C(70)-Fe(2)	126.9(6)	Fe(2)-C(76)-H(76)	124.5
C(72)-C(71)-C(70)	106.6(9)	C(78)-C(77)-C(76)	107.8(10)
C(72)-C(71)-Fe(2)	69.5(6)	C(78)-C(77)-Fe(2)	70.3(7)
C(70)-C(71)-Fe(2)	70.1(5)	C(76)-C(77)-Fe(2)	68.4(6)
C(72)-C(71)-H(71)	126.7	C(78)-C(77)-H(77)	126.1
C(70)-C(71)-H(71)	126.7	C(76)-C(77)-H(77)	126.1
Fe(2)-C(71)-H(71)	125.3	Fe(2)-C(77)-H(77)	126.7
C(71)-C(72)-C(73)	111.5(10)	C(77)-C(78)-C(79)	107.8(9)
C(71)-C(72)-Fe(2)	70.2(5)	C(77)-C(78)-Fe(2)	70.1(6)
C(73)-C(72)-Fe(2)	71.4(5)	C(79)-C(78)-Fe(2)	68.5(6)
C(71)-C(72)-H(72)	124.2	C(77)-C(78)-H(78)	126.1
C(73)-C(72)-H(72)	124.2	C(79)-C(78)-H(78)	126.1
Fe(2)-C(72)-H(72)	125.8	Fe(2)-C(78)-H(78)	126.9
C(74)-C(73)-C(72)	105.5(9)	C(75)-C(79)-C(78)	108.3(10)
C(74)-C(73)-Fe(2)	68.2(5)	C(75)-C(79)-Fe(2)	70.9(5)

C(78)-C(79)-Fe(2)	70.1(6)	C(78)-C(79)-H(79)	125.9
C(75)-C(79)-H(79)	125.9	Fe(2)-C(79)-H(79)	124.7

Symmetry transformations used to generate equivalent atoms:

#1 -x+1/2,-y+1/2,-z

A1.3. Table of selected bond lengths [Å] and angles [°] for (14).

Zn(1A)-N(23A)	2.034(3)	C(4A)-C(5A)	1.401(6)
Zn(1A)-N(22A)	2.039(4)	C(5A)-C(6A)	1.445(5)
Zn(1A)-N(24A)	2.062(4)	C(5A)-C(31A)	1.474(6)
Zn(1A)-N(21A)	2.065(3)	C(6A)-N(22A)	1.372(6)
Fe(2A)-C(73A)	2.013(7)	C(6A)-C(7A)	1.423(7)
Fe(2A)-C(71A)	2.015(5)	C(7A)-C(8A)	1.383(6)
Fe(2A)-C(74A)	2.017(5)	C(7A)-H(7A)	0.9500
Fe(2A)-C(78A)	2.027(9)	C(8A)-C(9A)	1.408(6)
Fe(2A)-C(79A)	2.033(10)	C(8A)-H(8A)	0.9500
Fe(2A)-C(75A)	2.037(8)	C(9A)-C(10A)	1.390(5)
Fe(2A)-C(70A)	2.041(6)	C(9A)-N(22A)	1.402(5)
Fe(2A)-C(77A)	2.048(9)	C(10A)-C(25A)	1.422(6)
Fe(2A)-C(72A)	2.052(8)	C(10A)-C(11A)	1.439(7)
Fe(2A)-C(76A)	2.114(8)	C(11A)-C(12A)	1.392(6)
Fe(3A)-C(89A)	1.990(9)	C(11A)-N(23A)	1.395(6)
Fe(3A)-C(85A)	1.998(8)	C(12A)-C(13A)	1.331(6)
Fe(3A)-C(88A)	2.001(8)	C(12A)-H(12A)	0.9500
Fe(3A)-C(84A)	2.030(6)	C(13A)-C(14A)	1.438(5)
Fe(3A)-C(83A)	2.033(8)	C(13A)-H(13A)	0.9500
Fe(3A)-C(86A)	2.048(9)	C(14A)-N(23A)	1.390(6)
Fe(3A)-C(82A)	2.049(7)	C(14A)-C(15A)	1.421(7)
Fe(3A)-C(81A)	2.054(6)	C(15A)-C(16A)	1.359(6)
Fe(3A)-C(87A)	2.056(8)	C(15A)-C(51A)	1.511(6)
Fe(3A)-C(80A)	2.059(5)	C(16A)-N(24A)	1.384(5)
C(1A)-N(21A)	1.337(5)	C(16A)-C(17A)	1.455(7)
C(1A)-C(20A)	1.404(7)	C(17A)-C(18A)	1.348(6)
C(1A)-C(2A)	1.469(5)	C(17A)-H(17A)	0.9500
C(2A)-C(3A)	1.377(7)	C(18A)-C(19A)	1.408(7)
C(2A)-H(2A)	0.9500	C(18A)-H(18A)	0.9500
C(3A)-C(4A)	1.462(6)	C(19A)-N(24A)	1.358(5)
C(3A)-H(3A)	0.9500	C(19A)-C(20A)	1.393(6)
C(4A)-N(21A)	1.339(6)	C(20A)-C(27A)	1.483(6)

C(25A)-C(26A)	1.204(7)	C(52A)-H(52A)	0.9500
C(26A)-C(70A)	1.451(7)	C(53A)-C(54A)	1.391(7)
C(27A)-C(28A)	1.175(6)	C(53A)-C(60A)	1.515(7)
C(28A)-C(80A)	1.434(7)	C(54A)-C(55A)	1.376(7)
C(31A)-C(36A)	1.383(8)	C(54A)-H(54A)	0.9500
C(31A)-C(32A)	1.470(7)	C(55A)-C(56A)	1.382(6)
C(32A)-C(33A)	1.372(6)	C(55A)-C(65A)	1.482(8)
C(32A)-H(32A)	0.9500	C(56A)-H(56A)	0.9500
C(33A)-C(34A)	1.367(8)	C(60A)-O(61A)	1.214(7)
C(33A)-C(40A)	1.483(7)	C(60A)-O(62A)	1.308(5)
C(34A)-C(35A)	1.384(7)	O(62A)-C(63A)	1.457(6)
C(34A)-H(34A)	0.9500	C(63A)-C(64A)	1.524(8)
C(35A)-C(36A)	1.428(6)	C(63A)-H(63A)	0.9900
C(35A)-C(45A)	1.478(8)	C(63A)-H(63B)	0.9900
C(36A)-H(36A)	0.9500	C(64A)-H(64A)	0.9800
C(40A)-O(41A)	1.220(7)	C(64A)-H(64B)	0.9800
C(40A)-O(42A)	1.353(5)	C(64A)-H(64C)	0.9800
O(42A)-C(43A)	1.443(6)	C(65A)-O(66A)	1.199(5)
C(43A)-C(44A)	1.496(8)	C(65A)-O(67A)	1.348(6)
C(43A)-H(43A)	0.9900	O(67A)-C(68A)	1.473(8)
C(43A)-H(43B)	0.9900	C(68A)-C(69A)	1.414(7)
C(44A)-H(44A)	0.9800	C(68A)-H(68A)	0.9900
C(44A)-H(44B)	0.9800	C(68A)-H(68B)	0.9900
C(44A)-H(44C)	0.9800	C(69A)-H(69A)	0.9800
C(45A)-O(46A)	1.226(5)	C(69A)-H(69B)	0.9800
C(45A)-O(47A)	1.327(5)	C(69A)-H(69C)	0.9800
O(47A)-C(48A)	1.457(7)	C(70A)-C(74A)	1.373(6)
C(48A)-C(49A)	1.520(8)	C(70A)-C(71A)	1.412(7)
C(48A)-H(48A)	0.9900	C(71A)-C(72A)	1.383(7)
C(48A)-H(48B)	0.9900	C(71A)-H(71A)	0.9500
C(49A)-H(49A)	0.9800	C(72A)-C(73A)	1.421(9)
C(49A)-H(49B)	0.9800	C(72A)-H(72A)	0.9500
C(49A)-H(49C)	0.9800	C(73A)-C(74A)	1.463(9)
C(51A)-C(56A)	1.342(8)	C(73A)-H(73A)	0.9500
C(51A)-C(52A)	1.406(7)	C(74A)-H(74A)	0.9500
C(52A)-C(53A)	1.460(6)	C(75A)-C(79A)	1.293(10)

C(75A)-C(76A)	1.397(12)	C(73A)-Fe(2A)-C(74A)	42.6(3)
C(75A)-H(75A)	0.9500	C(71A)-Fe(2A)-C(74A)	66.6(2)
C(76A)-C(77A)	1.499(11)	C(73A)-Fe(2A)-C(78A)	112.6(3)
C(76A)-H(76A)	0.9500	C(71A)-Fe(2A)-C(78A)	165.4(3)
C(77A)-C(78A)	1.388(12)	C(74A)-Fe(2A)-C(78A)	123.9(3)
C(77A)-H(77A)	0.9500	C(73A)-Fe(2A)-C(79A)	131.8(3)
C(78A)-C(79A)	1.415(12)	C(71A)-Fe(2A)-C(79A)	150.1(3)
C(78A)-H(78A)	0.9500	C(74A)-Fe(2A)-C(79A)	110.0(3)
C(79A)-H(79A)	0.9500	C(78A)-Fe(2A)-C(79A)	40.8(3)
C(80A)-C(84A)	1.446(7)	C(73A)-Fe(2A)-C(75A)	167.0(3)
C(80A)-C(81A)	1.485(7)	C(71A)-Fe(2A)-C(75A)	119.6(2)
C(81A)-C(82A)	1.368(9)	C(74A)-Fe(2A)-C(75A)	127.6(3)
C(81A)-H(81A)	0.9500	C(78A)-Fe(2A)-C(75A)	63.8(3)
C(82A)-C(83A)	1.377(9)	C(79A)-Fe(2A)-C(75A)	37.1(3)
C(82A)-H(82A)	0.9500	C(73A)-Fe(2A)-C(70A)	69.6(2)
C(83A)-C(84A)	1.447(7)	C(71A)-Fe(2A)-C(70A)	40.7(2)
C(83A)-H(83A)	0.9500	C(74A)-Fe(2A)-C(70A)	39.55(18)
C(84A)-H(84A)	0.9500	C(78A)-Fe(2A)-C(70A)	153.8(3)
C(85A)-C(86A)	1.403(10)	C(79A)-Fe(2A)-C(70A)	117.1(3)
C(85A)-C(89A)	1.447(12)	C(75A)-Fe(2A)-C(70A)	107.8(3)
C(85A)-H(85A)	1.0000	C(73A)-Fe(2A)-C(77A)	121.4(3)
C(86A)-C(87A)	1.373(11)	C(71A)-Fe(2A)-C(77A)	126.7(3)
C(86A)-H(86A)	0.9500	C(74A)-Fe(2A)-C(77A)	157.9(2)
C(87A)-C(88A)	1.341(11)	C(78A)-Fe(2A)-C(77A)	39.8(3)
C(87A)-H(87A)	0.9500	C(79A)-Fe(2A)-C(77A)	67.8(4)
C(88A)-C(89A)	1.464(10)	C(75A)-Fe(2A)-C(77A)	64.7(3)
C(88A)-H(88A)	1.0000	C(70A)-Fe(2A)-C(77A)	162.0(2)
C(89A)-H(89A)	0.9500	C(73A)-Fe(2A)-C(72A)	40.9(3)
		C(71A)-Fe(2A)-C(72A)	39.7(2)
N(23A)-Zn(1A)-N(22A)	90.11(15)	C(74A)-Fe(2A)-C(72A)	69.3(2)
N(23A)-Zn(1A)-N(24A)	89.35(14)	C(78A)-Fe(2A)-C(72A)	130.5(3)
N(22A)-Zn(1A)-N(24A)	179.41(15)	C(79A)-Fe(2A)-C(72A)	169.7(3)
N(23A)-Zn(1A)-N(21A)	179.67(18)	C(75A)-Fe(2A)-C(72A)	151.3(3)
N(22A)-Zn(1A)-N(21A)	89.95(15)	C(70A)-Fe(2A)-C(72A)	69.4(3)
N(24A)-Zn(1A)-N(21A)	90.58(14)	C(77A)-Fe(2A)-C(72A)	108.7(3)
C(73A)-Fe(2A)-C(71A)	67.3(2)	C(73A)-Fe(2A)-C(76A)	153.1(3)

C(71A)-Fe(2A)-C(76A)	104.0(3)	C(89A)-Fe(3A)-C(87A)	69.2(3)
C(74A)-Fe(2A)-C(76A)	159.3(3)	C(85A)-Fe(3A)-C(87A)	65.9(3)
C(78A)-Fe(2A)-C(76A)	69.2(3)	C(88A)-Fe(3A)-C(87A)	38.6(3)
C(79A)-Fe(2A)-C(76A)	68.2(3)	C(84A)-Fe(3A)-C(87A)	169.4(3)
C(75A)-Fe(2A)-C(76A)	39.3(3)	C(83A)-Fe(3A)-C(87A)	130.3(3)
C(70A)-Fe(2A)-C(76A)	121.4(3)	C(86A)-Fe(3A)-C(87A)	39.1(3)
C(77A)-Fe(2A)-C(76A)	42.2(3)	C(82A)-Fe(3A)-C(87A)	108.2(3)
C(72A)-Fe(2A)-C(76A)	116.2(3)	C(81A)-Fe(3A)-C(87A)	114.2(3)
C(89A)-Fe(3A)-C(85A)	42.6(4)	C(89A)-Fe(3A)-C(80A)	130.1(3)
C(89A)-Fe(3A)-C(88A)	43.0(3)	C(85A)-Fe(3A)-C(80A)	109.2(3)
C(85A)-Fe(3A)-C(88A)	68.4(3)	C(88A)-Fe(3A)-C(80A)	172.1(2)
C(89A)-Fe(3A)-C(84A)	107.4(3)	C(84A)-Fe(3A)-C(80A)	41.4(2)
C(85A)-Fe(3A)-C(84A)	118.9(2)	C(83A)-Fe(3A)-C(80A)	67.6(2)
C(88A)-Fe(3A)-C(84A)	132.4(3)	C(86A)-Fe(3A)-C(80A)	116.0(3)
C(89A)-Fe(3A)-C(83A)	119.1(3)	C(82A)-Fe(3A)-C(80A)	67.8(2)
C(85A)-Fe(3A)-C(83A)	154.9(3)	C(81A)-Fe(3A)-C(80A)	42.33(19)
C(88A)-Fe(3A)-C(83A)	111.1(3)	C(87A)-Fe(3A)-C(80A)	148.2(3)
C(84A)-Fe(3A)-C(83A)	41.7(2)	N(21A)-C(1A)-C(20A)	126.9(3)
C(89A)-Fe(3A)-C(86A)	71.4(4)	N(21A)-C(1A)-C(2A)	109.4(4)
C(85A)-Fe(3A)-C(86A)	40.6(3)	C(20A)-C(1A)-C(2A)	123.5(4)
C(88A)-Fe(3A)-C(86A)	67.5(3)	C(3A)-C(2A)-C(1A)	105.7(4)
C(84A)-Fe(3A)-C(86A)	150.5(2)	C(3A)-C(2A)-H(2A)	127.1
C(83A)-Fe(3A)-C(86A)	164.2(2)	C(1A)-C(2A)-H(2A)	127.2
C(89A)-Fe(3A)-C(82A)	150.8(3)	C(2A)-C(3A)-C(4A)	106.0(4)
C(85A)-Fe(3A)-C(82A)	164.7(3)	C(2A)-C(3A)-H(3A)	127.0
C(88A)-Fe(3A)-C(82A)	116.6(3)	C(4A)-C(3A)-H(3A)	127.0
C(84A)-Fe(3A)-C(82A)	69.6(2)	N(21A)-C(4A)-C(5A)	127.7(4)
C(83A)-Fe(3A)-C(82A)	39.4(3)	N(21A)-C(4A)-C(3A)	109.5(4)
C(86A)-Fe(3A)-C(82A)	125.9(3)	C(5A)-C(4A)-C(3A)	122.8(4)
C(89A)-Fe(3A)-C(81A)	169.7(3)	C(4A)-C(5A)-C(6A)	124.8(4)
C(85A)-Fe(3A)-C(81A)	128.7(3)	C(4A)-C(5A)-C(31A)	118.5(3)
C(88A)-Fe(3A)-C(81A)	145.1(2)	C(6A)-C(5A)-C(31A)	116.5(4)
C(84A)-Fe(3A)-C(81A)	71.0(2)	N(22A)-C(6A)-C(7A)	111.3(3)
C(83A)-Fe(3A)-C(81A)	66.9(3)	N(22A)-C(6A)-C(5A)	123.5(4)
C(86A)-Fe(3A)-C(81A)	104.7(3)	C(7A)-C(6A)-C(5A)	125.1(4)
C(82A)-Fe(3A)-C(81A)	39.0(3)	C(8A)-C(7A)-C(6A)	106.8(4)

C(8A)-C(7A)-H(7A)	126.6	N(24A)-C(19A)-C(18A)	108.5(3)
C(6A)-C(7A)-H(7A)	126.6	C(20A)-C(19A)-C(18A)	125.7(4)
C(7A)-C(8A)-C(9A)	106.2(4)	C(19A)-C(20A)-C(1A)	126.1(4)
C(7A)-C(8A)-H(8A)	126.9	C(19A)-C(20A)-C(27A)	118.3(4)
C(9A)-C(8A)-H(8A)	126.9	C(1A)-C(20A)-C(27A)	115.7(4)
C(10A)-C(9A)-N(22A)	123.1(4)	C(1A)-N(21A)-C(4A)	109.0(3)
C(10A)-C(9A)-C(8A)	125.4(4)	C(1A)-N(21A)-Zn(1A)	125.1(3)
N(22A)-C(9A)-C(8A)	111.5(3)	C(4A)-N(21A)-Zn(1A)	125.8(3)
C(9A)-C(10A)-C(25A)	114.5(4)	C(6A)-N(22A)-C(9A)	104.2(4)
C(9A)-C(10A)-C(11A)	128.9(4)	C(6A)-N(22A)-Zn(1A)	127.9(3)
C(25A)-C(10A)-C(11A)	116.5(3)	C(9A)-N(22A)-Zn(1A)	127.6(3)
C(12A)-C(11A)-N(23A)	112.1(4)	C(14A)-N(23A)-C(11A)	103.5(3)
C(12A)-C(11A)-C(10A)	126.5(4)	C(14A)-N(23A)-Zn(1A)	127.8(3)
N(23A)-C(11A)-C(10A)	121.4(4)	C(11A)-N(23A)-Zn(1A)	128.7(3)
C(13A)-C(12A)-C(11A)	107.0(4)	C(19A)-N(24A)-C(16A)	108.0(4)
C(13A)-C(12A)-H(12A)	126.5	C(19A)-N(24A)-Zn(1A)	125.5(3)
C(11A)-C(12A)-H(12A)	126.5	C(16A)-N(24A)-Zn(1A)	126.5(3)
C(12A)-C(13A)-C(14A)	108.2(3)	C(26A)-C(25A)-C(10A)	178.5(6)
C(12A)-C(13A)-H(13A)	125.9	C(25A)-C(26A)-C(70A)	172.7(6)
C(14A)-C(13A)-H(13A)	125.9	C(28A)-C(27A)-C(20A)	173.1(5)
N(23A)-C(14A)-C(15A)	123.7(3)	C(27A)-C(28A)-C(80A)	177.6(5)
N(23A)-C(14A)-C(13A)	109.2(4)	C(36A)-C(31A)-C(32A)	116.3(4)
C(15A)-C(14A)-C(13A)	127.2(4)	C(36A)-C(31A)-C(5A)	123.0(4)
C(16A)-C(15A)-C(14A)	126.7(4)	C(32A)-C(31A)-C(5A)	120.6(5)
C(16A)-C(15A)-C(51A)	118.9(4)	C(33A)-C(32A)-C(31A)	120.3(5)
C(14A)-C(15A)-C(51A)	114.3(3)	C(33A)-C(32A)-H(32A)	119.8
C(15A)-C(16A)-N(24A)	125.7(5)	C(31A)-C(32A)-H(32A)	119.8
C(15A)-C(16A)-C(17A)	125.7(4)	C(34A)-C(33A)-C(32A)	122.3(5)
N(24A)-C(16A)-C(17A)	108.0(3)	C(34A)-C(33A)-C(40A)	122.2(4)
C(18A)-C(17A)-C(16A)	105.5(4)	C(32A)-C(33A)-C(40A)	115.5(5)
C(18A)-C(17A)-H(17A)	127.3	C(33A)-C(34A)-C(35A)	119.2(4)
C(16A)-C(17A)-H(17A)	127.3	C(33A)-C(34A)-H(34A)	120.4
C(17A)-C(18A)-C(19A)	109.9(4)	C(35A)-C(34A)-H(34A)	120.4
C(17A)-C(18A)-H(18A)	125.1	C(34A)-C(35A)-C(36A)	120.6(5)
C(19A)-C(18A)-H(18A)	125.1	C(34A)-C(35A)-C(45A)	119.7(4)
N(24A)-C(19A)-C(20A)	125.8(4)	C(36A)-C(35A)-C(45A)	119.6(4)

C(31A)-C(36A)-C(35A)	121.1(4)	C(56A)-C(51A)-C(15A)	123.7(4)
C(31A)-C(36A)-H(36A)	119.4	C(52A)-C(51A)-C(15A)	117.1(5)
C(35A)-C(36A)-H(36A)	119.4	C(51A)-C(52A)-C(53A)	119.0(5)
O(41A)-C(40A)-O(42A)	121.9(4)	C(51A)-C(52A)-H(52A)	120.5
O(41A)-C(40A)-C(33A)	126.7(4)	C(53A)-C(52A)-H(52A)	120.5
O(42A)-C(40A)-C(33A)	111.4(4)	C(54A)-C(53A)-C(52A)	117.6(4)
C(40A)-O(42A)-C(43A)	117.9(4)	C(54A)-C(53A)-C(60A)	123.7(4)
O(42A)-C(43A)-C(44A)	108.3(5)	C(52A)-C(53A)-C(60A)	118.8(5)
O(42A)-C(43A)-H(43A)	110.0	C(55A)-C(54A)-C(53A)	122.0(4)
C(44A)-C(43A)-H(43A)	110.0	C(55A)-C(54A)-H(54A)	119.0
O(42A)-C(43A)-H(43B)	110.0	C(53A)-C(54A)-H(54A)	119.0
C(44A)-C(43A)-H(43B)	110.0	C(54A)-C(55A)-C(56A)	118.4(5)
H(43A)-C(43A)-H(43B)	108.4	C(54A)-C(55A)-C(65A)	118.5(4)
C(43A)-C(44A)-H(44A)	109.5	C(56A)-C(55A)-C(65A)	123.1(4)
C(43A)-C(44A)-H(44B)	109.5	C(51A)-C(56A)-C(55A)	123.9(5)
H(44A)-C(44A)-H(44B)	109.5	C(51A)-C(56A)-H(56A)	118.1
C(43A)-C(44A)-H(44C)	109.5	C(55A)-C(56A)-H(56A)	118.1
H(44A)-C(44A)-H(44C)	109.5	O(61A)-C(60A)-O(62A)	125.7(4)
H(44B)-C(44A)-H(44C)	109.5	O(61A)-C(60A)-C(53A)	122.0(4)
O(46A)-C(45A)-O(47A)	124.0(5)	O(62A)-C(60A)-C(53A)	112.3(4)
O(46A)-C(45A)-C(35A)	121.8(4)	C(60A)-O(62A)-C(63A)	116.1(4)
O(47A)-C(45A)-C(35A)	114.2(4)	O(62A)-C(63A)-C(64A)	105.8(5)
C(45A)-O(47A)-C(48A)	116.6(3)	O(62A)-C(63A)-H(63A)	110.6
O(47A)-C(48A)-C(49A)	106.2(4)	C(64A)-C(63A)-H(63A)	110.6
O(47A)-C(48A)-H(48A)	110.5	O(62A)-C(63A)-H(63B)	110.6
C(49A)-C(48A)-H(48A)	110.5	C(64A)-C(63A)-H(63B)	110.6
O(47A)-C(48A)-H(48B)	110.5	H(63A)-C(63A)-H(63B)	108.7
C(49A)-C(48A)-H(48B)	110.5	C(63A)-C(64A)-H(64A)	109.5
H(48A)-C(48A)-H(48B)	108.7	C(63A)-C(64A)-H(64B)	109.5
C(48A)-C(49A)-H(49A)	109.5	H(64A)-C(64A)-H(64B)	109.5
C(48A)-C(49A)-H(49B)	109.5	C(63A)-C(64A)-H(64C)	109.5
H(49A)-C(49A)-H(49B)	109.5	H(64A)-C(64A)-H(64C)	109.5
C(48A)-C(49A)-H(49C)	109.5	H(64B)-C(64A)-H(64C)	109.5
H(49A)-C(49A)-H(49C)	109.5	O(66A)-C(65A)-O(67A)	123.9(5)
H(49B)-C(49A)-H(49C)	109.5	O(66A)-C(65A)-C(55A)	123.9(4)
C(56A)-C(51A)-C(52A)	119.1(4)	O(67A)-C(65A)-C(55A)	112.3(4)

C(65A)-O(67A)-C(68A)	116.3(4)	Fe(2A)-C(73A)-H(73A)	125.0
C(69A)-C(68A)-O(67A)	107.6(4)	C(70A)-C(74A)-C(73A)	109.4(5)
C(69A)-C(68A)-H(68A)	110.2	C(70A)-C(74A)-Fe(2A)	71.2(3)
O(67A)-C(68A)-H(68A)	110.2	C(73A)-C(74A)-Fe(2A)	68.5(3)
C(69A)-C(68A)-H(68B)	110.2	C(70A)-C(74A)-H(74A)	125.3
O(67A)-C(68A)-H(68B)	110.2	C(73A)-C(74A)-H(74A)	125.3
H(68A)-C(68A)-H(68B)	108.5	Fe(2A)-C(74A)-H(74A)	126.6
C(68A)-C(69A)-H(69A)	109.5	C(79A)-C(75A)-C(76A)	119.7(7)
C(68A)-C(69A)-H(69B)	109.5	C(79A)-C(75A)-Fe(2A)	71.3(5)
H(69A)-C(69A)-H(69B)	109.5	C(76A)-C(75A)-Fe(2A)	73.3(5)
C(68A)-C(69A)-H(69C)	109.5	C(79A)-C(75A)-H(75A)	120.2
H(69A)-C(69A)-H(69C)	109.5	C(76A)-C(75A)-H(75A)	120.2
H(69B)-C(69A)-H(69C)	109.5	Fe(2A)-C(75A)-H(75A)	127.2
C(74A)-C(70A)-C(71A)	105.4(4)	C(75A)-C(76A)-C(77A)	97.9(6)
C(74A)-C(70A)-C(26A)	130.7(5)	C(75A)-C(76A)-Fe(2A)	67.4(4)
C(71A)-C(70A)-C(26A)	123.9(4)	C(77A)-C(76A)-Fe(2A)	66.5(4)
C(74A)-C(70A)-Fe(2A)	69.3(3)	C(75A)-C(76A)-H(76A)	131.0
C(71A)-C(70A)-Fe(2A)	68.6(3)	C(77A)-C(76A)-H(76A)	131.0
C(26A)-C(70A)-Fe(2A)	123.9(4)	Fe(2A)-C(76A)-H(76A)	126.6
C(72A)-C(71A)-C(70A)	112.9(4)	C(78A)-C(77A)-C(76A)	109.0(8)
C(72A)-C(71A)-Fe(2A)	71.6(4)	C(78A)-C(77A)-Fe(2A)	69.3(5)
C(70A)-C(71A)-Fe(2A)	70.6(3)	C(76A)-C(77A)-Fe(2A)	71.3(5)
C(72A)-C(71A)-H(71A)	123.5	C(78A)-C(77A)-H(77A)	125.5
C(70A)-C(71A)-H(71A)	123.5	C(76A)-C(77A)-H(77A)	125.5
Fe(2A)-C(71A)-H(71A)	125.9	Fe(2A)-C(77A)-H(77A)	125.6
C(71A)-C(72A)-C(73A)	105.6(6)	C(77A)-C(78A)-C(79A)	108.5(7)
C(71A)-C(72A)-Fe(2A)	68.7(4)	C(77A)-C(78A)-Fe(2A)	70.9(5)
C(73A)-C(72A)-Fe(2A)	68.0(4)	C(79A)-C(78A)-Fe(2A)	69.8(5)
C(71A)-C(72A)-H(72A)	127.2	C(77A)-C(78A)-H(78A)	125.8
C(73A)-C(72A)-H(72A)	127.2	C(79A)-C(78A)-H(78A)	125.8
Fe(2A)-C(72A)-H(72A)	127.6	Fe(2A)-C(78A)-H(78A)	125.1
C(72A)-C(73A)-C(74A)	106.8(5)	C(75A)-C(79A)-C(78A)	104.7(8)
C(72A)-C(73A)-Fe(2A)	71.1(4)	C(75A)-C(79A)-Fe(2A)	71.6(6)
C(74A)-C(73A)-Fe(2A)	68.9(4)	C(78A)-C(79A)-Fe(2A)	69.4(5)
C(72A)-C(73A)-H(73A)	126.6	C(75A)-C(79A)-H(79A)	127.6
C(74A)-C(73A)-H(73A)	126.6	C(78A)-C(79A)-H(79A)	127.6

Fe(2A)-C(79A)-H(79A)	123.1	C(86A)-C(85A)-C(89A)	111.5(7)
C(28A)-C(80A)-C(84A)	126.5(4)	C(86A)-C(85A)-Fe(3A)	71.7(5)
C(28A)-C(80A)-C(81A)	124.8(5)	C(89A)-C(85A)-Fe(3A)	68.4(5)
C(84A)-C(80A)-C(81A)	108.0(4)	C(86A)-C(85A)-H(85A)	124.2
C(28A)-C(80A)-Fe(3A)	121.0(4)	C(89A)-C(85A)-H(85A)	124.2
C(84A)-C(80A)-Fe(3A)	68.2(3)	Fe(3A)-C(85A)-H(85A)	124.2
C(81A)-C(80A)-Fe(3A)	68.7(3)	C(87A)-C(86A)-C(85A)	105.2(7)
C(82A)-C(81A)-C(80A)	106.7(5)	C(87A)-C(86A)-Fe(3A)	70.8(5)
C(82A)-C(81A)-Fe(3A)	70.3(4)	C(85A)-C(86A)-Fe(3A)	67.8(5)
C(80A)-C(81A)-Fe(3A)	69.0(3)	C(87A)-C(86A)-H(86A)	127.4
C(82A)-C(81A)-H(81A)	126.7	C(85A)-C(86A)-H(86A)	127.4
C(80A)-C(81A)-H(81A)	126.7	Fe(3A)-C(86A)-H(86A)	125.6
Fe(3A)-C(81A)-H(81A)	125.6	C(88A)-C(87A)-C(86A)	112.0(6)
C(81A)-C(82A)-C(83A)	110.3(5)	C(88A)-C(87A)-Fe(3A)	68.5(5)
C(81A)-C(82A)-Fe(3A)	70.7(4)	C(86A)-C(87A)-Fe(3A)	70.1(5)
C(83A)-C(82A)-Fe(3A)	69.7(4)	C(88A)-C(87A)-H(87A)	124.0
C(81A)-C(82A)-H(82A)	124.9	C(86A)-C(87A)-H(87A)	124.0
C(83A)-C(82A)-H(82A)	124.9	Fe(3A)-C(87A)-H(87A)	129.2
Fe(3A)-C(82A)-H(82A)	126.4	C(87A)-C(88A)-C(89A)	109.9(7)
C(82A)-C(83A)-C(84A)	111.1(6)	C(87A)-C(88A)-Fe(3A)	72.9(5)
C(82A)-C(83A)-Fe(3A)	70.9(4)	C(89A)-C(88A)-Fe(3A)	68.1(4)
C(84A)-C(83A)-Fe(3A)	69.0(4)	C(87A)-C(88A)-H(88A)	125.0
C(82A)-C(83A)-H(83A)	124.5	C(89A)-C(88A)-H(88A)	125.0
C(84A)-C(83A)-H(83A)	124.5	Fe(3A)-C(88A)-H(88A)	125.0
Fe(3A)-C(83A)-H(83A)	127.2	C(85A)-C(89A)-C(88A)	101.2(7)
C(83A)-C(84A)-C(80A)	103.8(4)	C(85A)-C(89A)-Fe(3A)	69.0(5)
C(83A)-C(84A)-Fe(3A)	69.3(4)	C(88A)-C(89A)-Fe(3A)	68.9(4)
C(80A)-C(84A)-Fe(3A)	70.4(3)	C(85A)-C(89A)-H(89A)	129.4
C(83A)-C(84A)-H(84A)	128.1	C(88A)-C(89A)-H(89A)	129.4
C(80A)-C(84A)-H(84A)	128.1	Fe(3A)-C(89A)-H(89A)	124.5
Fe(3A)-C(84A)-H(84A)	124.0		

Symmetry transformations used to generate equivalent atoms:

#1 -x+1,-y+1,-z+1 #2 -x,-y+1,-z+1

A1.4. Table of selected bond lengths [Å] and angles [°] for (4) – $2H^+$.

Fe(1)-C(70)	2.053(5)	C(25)-C(31)	1.498(10)
Fe(1)-C(71)	2.066(7)	C(31)-C(32)	1.398(12)
Fe(1)-C(72)	2.032(7)	C(31)-C(36)	1.389(11)
Fe(1)-C(73)	1.998(7)	C(32)-H(32)	0.9500
Fe(1)-C(74)	2.011(7)	C(32)-C(33)	1.372(11)
Fe(1)-C(75)	2.045(17)	C(33)-C(34)	1.391(12)
Fe(1)-C(78)	2.02(2)	C(33)-C(40)	1.492(13)
Fe(1)-C(79)	1.99(2)	C(34)-H(34)	0.9500
Fe(1)-C(76A)	1.94(2)	C(34)-C(35)	1.350(12)
Fe(1)-C(77A)	1.94(3)	C(35)-C(36)	1.406(11)
Fe(1)-C(78B)	2.048(14)	C(35)-C(45)	1.517(12)
Fe(1)-C(79B)	2.049(15)	C(36)-H(36)	0.9500
C(1)-C(2)	1.434(11)	C(40)-O(41)	1.196(11)
C(1)-N(21)	1.352(10)	C(40)-O(42)	1.364(11)
C(1)-C(25)#1	1.431(10)	O(42)-C(43)	1.446(11)
C(2)-H(2)	0.9500	C(43)-H(43a)	0.9900
C(2)-C(3)	1.343(11)	C(43)-H(43b)	0.9900
C(3)-H(3)	0.9500	C(43)-C(44)	1.509(12)
C(3)-C(4)	1.433(12)	C(44)-H(44a)	0.9800
C(4)-C(5)	1.420(11)	C(44)-H(44b)	0.9800
C(4)-N(21)	1.386(11)	C(44)-H(44c)	0.9800
C(5)-C(6)	1.398(11)	C(45)-O(46)	1.218(12)
C(5)-C(70)	1.497(9)	C(45)-O(47)	1.307(11)
C(6)-C(7)	1.435(12)	O(47)-C(48B)	1.476(14)
C(6)-N(22)	1.373(10)	O(47)-C(48B)	1.487(13)
C(7)-H(7)	0.9500	C(48B)-H(48a)	0.9900
C(7)-C(8)	1.365(15)	C(48B)-H(48b)	0.9900
C(8)-H(8)	0.9500	C(48B)-H(48c)	0.9900
C(8)-C(9)	1.451(13)	C(48B)-H(48d)	0.9900
C(9)-N(22)	1.365(11)	C(48B)-C(49A)	1.47(4)
C(9)-C(25)	1.371(12)	C(48B)-C(49B)	1.63(3)
C(25)-C(1)#1	1.431(10)	C(49A)-H(49a)	0.9800

C(49A)-H(49b)	0.9800	C(75B)-C(79B)	1.4200
C(49A)-H(49c)	0.9800	C(76B)-H(76B)	0.9500
C(49B)-H(49d)	0.9800	C(76B)-C(77B)	1.4200
C(49B)-H(49e)	0.9800	C(77B)-H(77B)	0.9500
C(49B)-H(49f)	0.9800	C(77B)-C(78B)	1.4200
C(70)-C(71)	1.4200	C(78B)-H(78B)	0.9500
C(70)-C(74)	1.4200	C(78B)-C(79B)	1.4200
C(71)-H(71)	0.9500	C(79B)-H(79B)	0.9500
C(71)-C(72)	1.4200		
C(72)-H(72)	0.9500	C(70)-Fe(1)-C(71)	40.33(10)
C(72)-C(73)	1.4200	C(72)-Fe(1)-C(70)	68.44(14)
C(73)-H(73)	0.9500	C(72)-Fe(1)-C(71)	40.54(13)
C(73)-C(74)	1.4200	C(72)-Fe(1)-C(75)	156.7(12)
C(74)-H(74)	0.9500	C(72)-Fe(1)-C(78B)	115.9(5)
C(75)-H(75)	0.9500	C(72)-Fe(1)-C(79B)	137.2(6)
C(75)-C(76)	1.4200	C(73)-Fe(1)-C(70)	69.09(14)
C(75)-C(79)	1.4200	C(73)-Fe(1)-C(71)	68.84(16)
C(76)-H(76)	0.9500	C(73)-Fe(1)-C(72)	41.25(13)
C(76)-C(77)	1.4200	C(73)-Fe(1)-C(74)	41.48(13)
C(77)-H(77)	0.9500	C(73)-Fe(1)-C(75)	162.0(12)
C(77)-C(78)	1.4200	C(73)-Fe(1)-C(78)	104.2(7)
C(78)-H(78)	0.9500	C(73)-Fe(1)-C(78B)	117.6(5)
C(78)-C(79)	1.4200	C(73)-Fe(1)-C(79B)	158.1(4)
C(79)-H(79)	0.9500	C(74)-Fe(1)-C(70)	40.88(11)
C(75A)-H(75A)	0.9500	C(74)-Fe(1)-C(71)	68.59(13)
C(75A)-C(76A)	1.4200	C(74)-Fe(1)-C(72)	69.25(16)
C(75A)-C(79A)	1.4200	C(74)-Fe(1)-C(75)	127.3(9)
C(76A)-H(76A)	0.9500	C(74)-Fe(1)-C(78)	122.7(10)
C(76A)-C(77A)	1.4200	C(74)-Fe(1)-C(78B)	144.4(6)
C(77A)-H(77A)	0.9500	C(74)-Fe(1)-C(79B)	153.1(6)
C(77A)-C(78A)	1.4200	C(75)-Fe(1)-C(70)	111.9(4)
C(78A)-H(78A)	0.9500	C(75)-Fe(1)-C(71)	124.4(9)
C(78A)-C(79A)	1.4200	C(75)-Fe(1)-C(78B)	62.0(6)
C(79A)-H(79A)	0.9500	C(75)-Fe(1)-C(79B)	26.5(7)
C(75B)-H(75B)	0.9500	C(78)-Fe(1)-C(70)	161.2(11)
C(75B)-C(76B)	1.4200	C(78)-Fe(1)-C(71)	155.3(8)

C(78)-Fe(1)-C(72)	118.8(6)	C(78B)-Fe(1)-C(79B)	40.6(3)
C(78)-Fe(1)-C(75)	68.9(4)	C(79B)-Fe(1)-C(70)	132.8(4)
C(78)-Fe(1)-C(78B)	22.1(8)	C(79B)-Fe(1)-C(71)	125.8(6)
C(78)-Fe(1)-C(79B)	55.3(8)	N(21)-C(1)-C(2)	111.9(7)
C(79)-Fe(1)-C(70)	126.5(8)	N(21)-C(1)-C(25)#1	124.9(7)
C(79)-Fe(1)-C(71)	161.7(6)	C(25)#1-C(1)-C(2)	123.3(7)
C(79)-Fe(1)-C(72)	157.4(7)	C(1)-C(2)-H(2)	126.9
C(79)-Fe(1)-C(73)	122.8(11)	C(3)-C(2)-C(1)	106.2(8)
C(79)-Fe(1)-C(74)	109.7(11)	C(3)-C(2)-H(2)	126.9
C(79)-Fe(1)-C(75)	41.1(3)	C(2)-C(3)-H(3)	126.5
C(79)-Fe(1)-C(78)	41.4(4)	C(2)-C(3)-C(4)	107.0(8)
C(79)-Fe(1)-C(78B)	51.2(7)	C(4)-C(3)-H(3)	126.5
C(79)-Fe(1)-C(79B)	48.7(9)	C(5)-C(4)-C(3)	124.0(8)
C(76A)-Fe(1)-C(70)	129.7(7)	N(21)-C(4)-C(3)	110.3(7)
C(76A)-Fe(1)-C(71)	152.4(11)	N(21)-C(4)-C(5)	125.6(8)
C(76A)-Fe(1)-C(72)	161.9(7)	C(4)-C(5)-C(70)	116.9(7)
C(76A)-Fe(1)-C(73)	137.5(12)	C(6)-C(5)-C(4)	123.4(7)
C(76A)-Fe(1)-C(74)	122.8(10)	C(6)-C(5)-C(70)	119.7(6)
C(76A)-Fe(1)-C(75)	28.0(8)	C(5)-C(6)-C(7)	126.4(8)
C(76A)-Fe(1)-C(78)	44.2(10)	N(22)-C(6)-C(5)	126.5(7)
C(76A)-Fe(1)-C(79)	15.3(8)	N(22)-C(6)-C(7)	107.1(7)
C(76A)-Fe(1)-C(78B)	46.1(8)	C(6)-C(7)-H(7)	126.4
C(76A)-Fe(1)-C(79B)	33.8(11)	C(8)-C(7)-C(6)	107.2(9)
C(77A)-Fe(1)-C(70)	170.2(9)	C(8)-C(7)-H(7)	126.4
C(77A)-Fe(1)-C(71)	149.5(9)	C(7)-C(8)-H(8)	125.6
C(77A)-Fe(1)-C(72)	119.0(8)	C(7)-C(8)-C(9)	108.9(9)
C(77A)-Fe(1)-C(73)	111.7(9)	C(9)-C(8)-H(8)	125.6
C(77A)-Fe(1)-C(74)	133.4(10)	N(22)-C(9)-C(8)	105.6(8)
C(77A)-Fe(1)-C(75)	64.0(9)	N(22)-C(9)-C(25)	129.0(8)
C(77A)-Fe(1)-C(78)	10.7(12)	C(25)-C(9)-C(8)	125.1(8)
C(77A)-Fe(1)-C(79)	44.3(12)	C(1)-N(21)-C(4)	104.5(6)
C(77A)-Fe(1)-C(76A)	43.0(5)	C(9)-N(22)-C(6)	111.1(6)
C(77A)-Fe(1)-C(78B)	11.5(11)	C(1)#1-C(25)-C(31)	117.5(7)
C(77A)-Fe(1)-C(79B)	46.9(9)	C(9)-C(25)-C(1)#1	126.0(7)
C(78B)-Fe(1)-C(70)	173.3(5)	C(9)-C(25)-C(31)	116.5(7)
C(78B)-Fe(1)-C(71)	139.8(6)	C(32)-C(31)-C(25)	121.1(7)

C(36)-C(31)-C(25)	120.8(7)	C(45)-O(47)-C(48B)	120.3(14)
C(36)-C(31)-C(32)	118.1(7)	C(45)-O(47)-C(48B)	113.7(11)
C(31)-C(32)-H(32)	119.7	C(48B)-O(47)-C(48B)	13.2(16)
C(33)-C(32)-C(31)	120.6(8)	O(47)-C(48B)-H(48a)	109.3
C(33)-C(32)-H(32)	119.7	O(47)-C(48B)-H(48b)	109.3
C(32)-C(33)-C(34)	121.5(8)	O(47)-C(48B)-H(48c)	112.2
C(32)-C(33)-C(40)	121.6(8)	O(47)-C(48B)-H(48d)	112.2
C(34)-C(33)-C(40)	117.0(8)	O(47)-C(48B)-C(49B)	97.9(15)
C(33)-C(34)-H(34)	121.0	H(48a)-C(48B)-H(48b)	108.0
C(35)-C(34)-C(33)	118.1(8)	H(48c)-C(48B)-H(48d)	109.8
C(35)-C(34)-H(34)	121.0	C(49A)-C(48B)-O(47)	111.4(19)
C(34)-C(35)-C(36)	122.1(8)	C(49A)-C(48B)-H(48a)	109.3
C(34)-C(35)-C(45)	121.5(8)	C(49A)-C(48B)-H(48b)	109.3
C(36)-C(35)-C(45)	116.4(8)	C(49B)-C(48B)-H(48c)	112.2
C(31)-C(36)-C(35)	119.7(8)	C(49B)-C(48B)-H(48d)	112.2
C(31)-C(36)-H(36)	120.2	C(48B)-C(49A)-H(49a)	109.5
C(35)-C(36)-H(36)	120.2	C(48B)-C(49A)-H(49b)	109.5
O(41)-C(40)-C(33)	125.8(9)	C(48B)-C(49A)-H(49c)	109.5
O(41)-C(40)-O(42)	123.5(9)	H(49a)-C(49A)-H(49b)	109.5
O(42)-C(40)-C(33)	110.7(7)	H(49a)-C(49A)-H(49c)	109.5
C(40)-O(42)-C(43)	115.1(7)	H(49b)-C(49A)-H(49c)	109.5
O(42)-C(43)-H(43a)	110.5	C(48B)-C(49B)-H(49d)	109.5
O(42)-C(43)-H(43b)	110.5	C(48B)-C(49B)-H(49e)	109.5
O(42)-C(43)-C(44)	106.2(7)	C(48B)-C(49B)-H(49f)	109.5
H(43a)-C(43)-H(43b)	108.7	H(49d)-C(49B)-H(49e)	109.5
C(44)-C(43)-H(43a)	110.5	H(49d)-C(49B)-H(49f)	109.5
C(44)-C(43)-H(43b)	110.5	H(49e)-C(49B)-H(49f)	109.5
C(43)-C(44)-H(44a)	109.5	C(5)-C(70)-Fe(1)	133.0(5)
C(43)-C(44)-H(44b)	109.5	C(71)-C(70)-Fe(1)	70.3(3)
C(43)-C(44)-H(44c)	109.5	C(71)-C(70)-C(5)	126.6(5)
H(44a)-C(44)-H(44b)	109.5	C(71)-C(70)-C(74)	108.0
H(44a)-C(44)-H(44c)	109.5	C(74)-C(70)-Fe(1)	68.0(3)
H(44b)-C(44)-H(44c)	109.5	C(74)-C(70)-C(5)	124.9(5)
O(46)-C(45)-C(35)	123.6(8)	Fe(1)-C(71)-H(71)	127.8
O(46)-C(45)-O(47)	124.5(9)	C(70)-C(71)-Fe(1)	69.4(2)
O(47)-C(45)-C(35)	111.8(8)	C(70)-C(71)-H(71)	126.0

C(72)-C(71)-Fe(1)	68.5(2)	C(76)-C(77)-C(78)	108.0
C(72)-C(71)-C(70)	108.0	C(78)-C(77)-Fe(1)	67.3(9)
C(72)-C(71)-H(71)	126.0	C(78)-C(77)-H(77)	126.0
Fe(1)-C(72)-H(72)	126.5	Fe(1)-C(78)-H(78)	125.0
C(71)-C(72)-Fe(1)	71.0(2)	C(77)-C(78)-Fe(1)	72.2(9)
C(71)-C(72)-H(72)	126.0	C(77)-C(78)-H(78)	126.0
C(71)-C(72)-C(73)	108.0	C(79)-C(78)-Fe(1)	68.3(8)
C(73)-C(72)-Fe(1)	68.1(3)	C(79)-C(78)-C(77)	108.0
C(73)-C(72)-H(72)	126.0	C(79)-C(78)-H(78)	126.0
Fe(1)-C(73)-H(73)	125.2	Fe(1)-C(79)-H(79)	124.0
C(72)-C(73)-Fe(1)	70.7(3)	C(75)-C(79)-Fe(1)	71.3(8)
C(72)-C(73)-H(73)	126.0	C(75)-C(79)-H(79)	126.0
C(72)-C(73)-C(74)	108.0	C(78)-C(79)-Fe(1)	70.2(8)
C(74)-C(73)-Fe(1)	69.8(2)	C(78)-C(79)-C(75)	108.0
C(74)-C(73)-H(73)	126.0	C(78)-C(79)-H(79)	126.0
Fe(1)-C(74)-H(74)	125.7	Fe(1)-C(75A)-H(75A)	127.6
C(70)-C(74)-Fe(1)	71.1(2)	C(76A)-C(75A)-Fe(1)	62.6(10)
C(70)-C(74)-H(74)	126.0	C(76A)-C(75A)-H(75A)	126.0
C(73)-C(74)-Fe(1)	68.8(2)	C(76A)-C(75A)-C(79A)	108.0
C(73)-C(74)-C(70)	108.0	C(79A)-C(75A)-Fe(1)	75.1(10)
C(73)-C(74)-H(74)	126.0	C(79A)-C(75A)-H(75A)	126.0
Fe(1)-C(75)-H(75)	126.0	Fe(1)-C(76A)-H(76A)	120.4
C(76)-C(75)-Fe(1)	72.1(9)	C(75A)-C(76A)-Fe(1)	76.9(11)
C(76)-C(75)-H(75)	126.0	C(75A)-C(76A)-H(76A)	126.0
C(76)-C(75)-C(79)	108.0	C(77A)-C(76A)-Fe(1)	68.4(10)
C(79)-C(75)-Fe(1)	67.5(9)	C(77A)-C(76A)-C(75A)	108.0
C(79)-C(75)-H(75)	126.0	C(77A)-C(76A)-H(76A)	126.0
Fe(1)-C(76)-H(76)	128.1	Fe(1)-C(77A)-H(77A)	120.3
C(75)-C(76)-Fe(1)	67.9(8)	C(76A)-C(77A)-Fe(1)	68.6(10)
C(75)-C(76)-H(76)	126.0	C(76A)-C(77A)-H(77A)	126.0
C(77)-C(76)-Fe(1)	69.6(8)	C(78A)-C(77A)-Fe(1)	76.8(11)
C(77)-C(76)-C(75)	108.0	C(78A)-C(77A)-C(76A)	108.0
C(77)-C(76)-H(76)	126.0	C(78A)-C(77A)-H(77A)	126.0
Fe(1)-C(77)-H(77)	127.5	Fe(1)-C(78A)-H(78A)	127.4
C(76)-C(77)-Fe(1)	70.7(7)	C(77A)-C(78A)-Fe(1)	62.6(10)
C(76)-C(77)-H(77)	126.0	C(77A)-C(78A)-H(78A)	126.0

C(77A)-C(78A)-C(79A)	108.0	C(77B)-C(76B)-H(76B)	126.0
C(79A)-C(78A)-Fe(1)	75.2(9)	Fe(1)-C(77B)-H(77B)	125.8
C(79A)-C(78A)-H(78A)	126.0	C(76B)-C(77B)-Fe(1)	72.7(6)
Fe(1)-C(79A)-H(79A)	131.8	C(76B)-C(77B)-H(77B)	126.0
C(75A)-C(79A)-Fe(1)	67.0(9)	C(78B)-C(77B)-Fe(1)	67.0(6)
C(75A)-C(79A)-H(79A)	126.0	C(78B)-C(77B)-C(76B)	108.0
C(78A)-C(79A)-Fe(1)	66.8(9)	C(78B)-C(77B)-H(77B)	126.0
C(78A)-C(79A)-C(75A)	108.0	Fe(1)-C(78B)-H(78B)	122.6
C(78A)-C(79A)-H(79A)	126.0	C(77B)-C(78B)-Fe(1)	73.3(6)
Fe(1)-C(75B)-H(75B)	125.9	C(77B)-C(78B)-H(78B)	126.0
C(76B)-C(75B)-Fe(1)	72.6(6)	C(77B)-C(78B)-C(79B)	108.0
C(76B)-C(75B)-H(75B)	126.0	C(79B)-C(78B)-Fe(1)	69.8(6)
C(76B)-C(75B)-C(79B)	108.0	C(79B)-C(78B)-H(78B)	126.0
C(79B)-C(75B)-Fe(1)	67.0(6)	Fe(1)-C(79B)-H(79B)	122.6
C(79B)-C(75B)-H(75B)	126.0	C(75B)-C(79B)-Fe(1)	73.3(6)
Fe(1)-C(76B)-H(76B)	127.8	C(75B)-C(79B)-H(79B)	126.0
C(75B)-C(76B)-Fe(1)	68.9(5)	C(78B)-C(79B)-Fe(1)	69.7(6)
C(75B)-C(76B)-H(76B)	126.0	C(78B)-C(79B)-C(75B)	108.0
C(77B)-C(76B)-Fe(1)	68.8(5)	C(78B)-C(79B)-H(79B)	126.0
C(77B)-C(76B)-C(75B)	108.0		

A1.5. Table of selected bond lengths [Å] and angles [°] for (15).

C(1)-N(21)	1.358(4)	C(35)-C(36)	1.393(4)
C(1)-C(25)#1	1.410(4)	C(35)-C(45)	1.494(4)
C(1)-C(2)	1.439(4)	C(36)-H(36)	0.9500
C(2)-C(3)	1.353(4)	C(40)-O(41)	1.202(3)
C(2)-H(2)	0.9500	C(40)-O(42)	1.336(4)
C(3)-C(4)	1.438(4)	O(42)-C(43)	1.454(3)
C(3)-H(3)	0.9500	C(43)-C(44)	1.504(4)
C(4)-N(21)	1.377(3)	C(43)-H(43A)	0.9900
C(4)-C(5)	1.399(4)	C(43)-H(43B)	0.9900
C(5)-C(6)	1.399(4)	C(44)-H(44A)	0.9800
C(5)-C(31)	1.499(4)	C(44)-H(44B)	0.9800
C(6)-N(22)	1.377(3)	C(44)-H(44C)	0.9800
C(6)-C(7)	1.441(4)	C(45)-O(46)	1.205(4)
C(7)-C(8)	1.353(4)	C(45)-O(47)	1.333(3)
C(7)-H(7)	0.9500	O(47)-C(48)	1.457(4)
C(8)-C(9)	1.440(4)	C(48)-C(49)	1.507(5)
C(8)-H(8)	0.9500	C(48)-H(48A)	0.9900
C(9)-N(22)	1.359(4)	C(48)-H(48B)	0.9900
C(9)-C(25)	1.413(4)	C(49)-H(49A)	0.9800
N(21)-H(21)	0.8800	C(49)-H(49B)	0.9800
N(22)-H(22)	0.8800	C(49)-H(49C)	0.9800
C(25)-C(1)#1	1.410(4)	Fe(1)-C(79)	2.018(5)
C(25)-C(26)	1.425(4)	Fe(1)-C(75)	2.021(4)
C(26)-C(27)	1.197(4)	Fe(1)-C(78)	2.031(4)
C(27)-C(70)	1.423(4)	Fe(1)-C(70)	2.035(3)
C(31)-C(36)	1.393(4)	Fe(1)-C(74)	2.035(3)
C(31)-C(32)	1.399(4)	Fe(1)-C(72)	2.038(4)
C(32)-C(33)	1.393(4)	Fe(1)-C(73)	2.041(3)
C(32)-H(32)	0.9500	Fe(1)-C(77)	2.041(4)
C(33)-C(34)	1.394(4)	Fe(1)-C(71)	2.044(4)
C(33)-C(40)	1.496(4)	Fe(1)-C(76)	2.046(4)
C(34)-C(35)	1.393(4)	C(70)-C(71)	1.429(4)
C(34)-H(34)	0.9500	C(70)-C(74)	1.432(4)

C(71)-C(72)	1.417(5)	C(8)-C(7)-C(6)	107.4(2)
C(71)-H(71)	0.9500	C(8)-C(7)-H(7)	126.3
C(72)-C(73)	1.417(6)	C(6)-C(7)-H(7)	126.3
C(72)-H(72)	0.9500	C(7)-C(8)-C(9)	106.7(2)
C(73)-C(74)	1.415(5)	C(7)-C(8)-H(8)	126.6
C(73)-H(73)	0.9500	C(9)-C(8)-H(8)	126.6
C(74)-H(74)	0.9500	N(22)-C(9)-C(25)	126.2(2)
C(75)-C(79)	1.393(7)	N(22)-C(9)-C(8)	109.9(2)
C(75)-C(76)	1.404(7)	C(25)-C(9)-C(8)	123.8(3)
C(75)-H(75)	1.0000	C(1)-N(21)-C(4)	108.1(2)
C(76)-C(77)	1.373(7)	C(1)-N(21)-H(21)	126.0
C(76)-H(76)	0.9500	C(4)-N(21)-H(21)	126.0
C(77)-C(78)	1.376(8)	C(9)-N(22)-C(6)	106.9(2)
C(77)-H(77)	0.9500	C(9)-N(22)-H(22)	126.5
C(78)-C(79)	1.470(9)	C(6)-N(22)-H(22)	126.5
C(78)-H(78)	0.9500	C(1)#1-C(25)-C(9)	125.9(3)
C(79)-H(79)	0.9500	C(1)#1-C(25)-C(26)	116.5(2)
		C(9)-C(25)-C(26)	117.5(2)
N(21)-C(1)-C(25)#1	126.5(2)	C(27)-C(26)-C(25)	176.7(3)
N(21)-C(1)-C(2)	109.0(2)	C(26)-C(27)-C(70)	176.7(3)
C(25)#1-C(1)-C(2)	124.5(3)	C(36)-C(31)-C(32)	118.7(2)
C(3)-C(2)-C(1)	107.2(2)	C(36)-C(31)-C(5)	120.2(2)
C(3)-C(2)-H(2)	126.4	C(32)-C(31)-C(5)	121.0(2)
C(1)-C(2)-H(2)	126.4	C(33)-C(32)-C(31)	120.2(3)
C(2)-C(3)-C(4)	107.7(2)	C(33)-C(32)-H(32)	119.9
C(2)-C(3)-H(3)	126.2	C(31)-C(32)-H(32)	119.9
C(4)-C(3)-H(3)	126.2	C(32)-C(33)-C(34)	120.8(3)
N(21)-C(4)-C(5)	125.1(2)	C(32)-C(33)-C(40)	121.5(2)
N(21)-C(4)-C(3)	108.1(2)	C(34)-C(33)-C(40)	117.7(2)
C(5)-C(4)-C(3)	126.7(2)	C(35)-C(34)-C(33)	119.0(2)
C(4)-C(5)-C(6)	125.7(2)	C(35)-C(34)-H(34)	120.5
C(4)-C(5)-C(31)	117.3(2)	C(33)-C(34)-H(34)	120.5
C(6)-C(5)-C(31)	117.0(2)	C(36)-C(35)-C(34)	120.2(3)
N(22)-C(6)-C(5)	125.4(2)	C(36)-C(35)-C(45)	118.2(2)
N(22)-C(6)-C(7)	109.0(2)	C(34)-C(35)-C(45)	121.5(2)
C(5)-C(6)-C(7)	125.6(2)	C(35)-C(36)-C(31)	121.0(3)

C(35)-C(36)-H(36)	119.5	C(75)-Fe(1)-C(78)	67.9(2)
C(31)-C(36)-H(36)	119.5	C(79)-Fe(1)-C(70)	126.6(2)
O(41)-C(40)-O(42)	124.0(3)	C(75)-Fe(1)-C(70)	107.22(16)
O(41)-C(40)-C(33)	124.0(3)	C(78)-Fe(1)-C(70)	167.9(2)
O(42)-C(40)-C(33)	112.0(2)	C(79)-Fe(1)-C(74)	106.8(2)
C(40)-O(42)-C(43)	115.5(2)	C(75)-Fe(1)-C(74)	117.72(18)
O(42)-C(43)-C(44)	106.7(2)	C(78)-Fe(1)-C(74)	130.0(2)
O(42)-C(43)-H(43A)	110.4	C(70)-Fe(1)-C(74)	41.19(12)
C(44)-C(43)-H(43A)	110.4	C(79)-Fe(1)-C(72)	152.6(2)
O(42)-C(43)-H(43B)	110.4	C(75)-Fe(1)-C(72)	166.19(19)
C(44)-C(43)-H(43B)	110.4	C(78)-Fe(1)-C(72)	118.8(2)
H(43A)-C(43)-H(43B)	108.6	C(70)-Fe(1)-C(72)	68.58(13)
C(43)-C(44)-H(44A)	109.5	C(74)-Fe(1)-C(72)	68.43(14)
C(43)-C(44)-H(44B)	109.5	C(79)-Fe(1)-C(73)	118.1(2)
H(44A)-C(44)-H(44B)	109.5	C(75)-Fe(1)-C(73)	151.60(19)
C(43)-C(44)-H(44C)	109.5	C(78)-Fe(1)-C(73)	109.73(17)
H(44A)-C(44)-H(44C)	109.5	C(70)-Fe(1)-C(73)	68.85(12)
H(44B)-C(44)-H(44C)	109.5	C(74)-Fe(1)-C(73)	40.64(13)
O(46)-C(45)-O(47)	124.1(3)	C(72)-Fe(1)-C(73)	40.66(16)
O(46)-C(45)-C(35)	123.7(3)	C(79)-Fe(1)-C(77)	68.3(3)
O(47)-C(45)-C(35)	112.2(2)	C(75)-Fe(1)-C(77)	65.9(2)
C(45)-O(47)-C(48)	116.8(2)	C(78)-Fe(1)-C(77)	39.5(2)
O(47)-C(48)-C(49)	106.4(3)	C(70)-Fe(1)-C(77)	150.08(18)
O(47)-C(48)-H(48A)	110.4	C(74)-Fe(1)-C(77)	168.49(18)
C(49)-C(48)-H(48A)	110.4	C(72)-Fe(1)-C(77)	110.7(2)
O(47)-C(48)-H(48B)	110.4	C(73)-Fe(1)-C(77)	131.35(18)
C(49)-C(48)-H(48B)	110.4	C(79)-Fe(1)-C(71)	165.1(2)
H(48A)-C(48)-H(48B)	108.6	C(75)-Fe(1)-C(71)	127.75(17)
C(48)-C(49)-H(49A)	109.5	C(78)-Fe(1)-C(71)	150.7(2)
C(48)-C(49)-H(49B)	109.5	C(70)-Fe(1)-C(71)	41.01(12)
H(49A)-C(49)-H(49B)	109.5	C(74)-Fe(1)-C(71)	69.00(13)
C(48)-C(49)-H(49C)	109.5	C(72)-Fe(1)-C(71)	40.63(15)
H(49A)-C(49)-H(49C)	109.5	C(73)-Fe(1)-C(71)	68.73(14)
H(49B)-C(49)-H(49C)	109.5	C(77)-Fe(1)-C(71)	118.4(2)
C(79)-Fe(1)-C(75)	40.3(2)	C(79)-Fe(1)-C(76)	69.3(2)
C(79)-Fe(1)-C(78)	42.6(3)	C(75)-Fe(1)-C(76)	40.4(2)

C(78)-Fe(1)-C(76)	67.98(19)	C(73)-C(74)-H(74)	126.0
C(70)-Fe(1)-C(76)	116.14(15)	C(70)-C(74)-H(74)	126.0
C(74)-Fe(1)-C(76)	150.29(16)	Fe(1)-C(74)-H(74)	126.3
C(72)-Fe(1)-C(76)	128.43(19)	C(79)-C(75)-C(76)	111.5(5)
C(73)-Fe(1)-C(76)	167.29(18)	C(79)-C(75)-Fe(1)	69.7(3)
C(77)-Fe(1)-C(76)	39.27(19)	C(76)-C(75)-Fe(1)	70.8(2)
C(71)-Fe(1)-C(76)	106.78(17)	C(79)-C(75)-H(75)	124.2
C(27)-C(70)-C(71)	127.2(3)	C(76)-C(75)-H(75)	124.2
C(27)-C(70)-C(74)	124.9(3)	Fe(1)-C(75)-H(75)	124.2
C(71)-C(70)-C(74)	107.8(3)	C(77)-C(76)-C(75)	105.4(5)
C(27)-C(70)-Fe(1)	123.0(2)	C(77)-C(76)-Fe(1)	70.2(3)
C(71)-C(70)-Fe(1)	69.9(2)	C(75)-C(76)-Fe(1)	68.8(2)
C(74)-C(70)-Fe(1)	69.41(17)	C(77)-C(76)-H(76)	127.3
C(72)-C(71)-C(70)	107.4(3)	C(75)-C(76)-H(76)	127.3
C(72)-C(71)-Fe(1)	69.4(2)	Fe(1)-C(76)-H(76)	125.3
C(70)-C(71)-Fe(1)	69.13(19)	C(76)-C(77)-C(78)	112.0(6)
C(72)-C(71)-H(71)	126.3	C(76)-C(77)-Fe(1)	70.5(2)
C(70)-C(71)-H(71)	126.3	C(78)-C(77)-Fe(1)	69.9(3)
Fe(1)-C(71)-H(71)	126.7	C(76)-C(77)-H(77)	124.0
C(73)-C(72)-C(71)	108.9(3)	C(78)-C(77)-H(77)	124.0
C(73)-C(72)-Fe(1)	69.8(2)	Fe(1)-C(77)-H(77)	127.3
C(71)-C(72)-Fe(1)	69.9(2)	C(77)-C(78)-C(79)	106.5(4)
C(73)-C(72)-H(72)	125.6	C(77)-C(78)-Fe(1)	70.6(3)
C(71)-C(72)-H(72)	125.6	C(79)-C(78)-Fe(1)	68.2(3)
Fe(1)-C(72)-H(72)	126.3	C(77)-C(78)-H(78)	126.8
C(74)-C(73)-C(72)	107.9(3)	C(79)-C(78)-H(78)	126.8
C(74)-C(73)-Fe(1)	69.45(18)	Fe(1)-C(78)-H(78)	125.9
C(72)-C(73)-Fe(1)	69.6(2)	C(75)-C(79)-C(78)	104.5(5)
C(74)-C(73)-H(73)	126.1	C(75)-C(79)-Fe(1)	69.9(3)
C(72)-C(73)-H(73)	126.1	C(78)-C(79)-Fe(1)	69.2(3)
Fe(1)-C(73)-H(73)	126.5	C(75)-C(79)-H(79)	127.7
C(73)-C(74)-C(70)	108.0(3)	C(78)-C(79)-H(79)	127.7
C(73)-C(74)-Fe(1)	69.91(18)	Fe(1)-C(79)-H(79)	124.8
C(70)-C(74)-Fe(1)	69.39(17)		

Symmetry transformations used to generate equivalent atoms: #1 -x+1,-y,-z+1

Appendix 2. Crystallographic data of structures discussed in Chapter 4

A2.1. Table of selected bond lengths [Å] and angles [^{o}] for (7)

Fe(1)-N(11A)	1.958(13)	Fe(4)-C(44C)	2.015(15)
Fe(1)-N(21A)	1.978(13)	Fe(4)-C(45C)	2.020(15)
Fe(1)-N(11B)	1.996(13)	Fe(4)-C(51C)	1.991(15)
Fe(1)-N(21B)	1.955(13)	Fe(4)-C(52C)	2.019(15)
Fe(1)-N(11C)	1.978(13)	Fe(4)-C(53C)	2.074(16)
Fe(1)-N(21C)	1.946(13)	Fe(4)-C(54C)	2.081(16)
Fe(2)-C(41A)	2.038(15)	Fe(4)-C(55C)	2.030(16)
Fe(2)-C(42A)	2.040(15)	N(11A)-C(12A)	1.391(14)
Fe(2)-C(43A)	2.050(16)	N(11A)-C(15A)	1.337(14)
Fe(2)-C(44A)	2.054(16)	C(12A)-C(13A)	1.430(15)
Fe(2)-C(45A)	2.047(16)	C(12A)-C(31A)	1.391(14)
Fe(2)-C(51A)	2.072(17)	C(13A)-H(13A)	0.9500
Fe(2)-C(52A)	2.063(16)	C(13A)-C(14A)	1.331(15)
Fe(2)-C(53A)	2.053(16)	C(14A)-H(14A)	0.9500
Fe(2)-C(54A)	2.055(16)	C(14A)-C(15A)	1.392(15)
Fe(2)-C(55A)	2.067(17)	C(15A)-H(15A)	0.9500
Fe(3)-C(41B)	2.042(16)	N(21A)-C(22A)	1.420(14)
Fe(3)-C(42B)	2.051(17)	N(21A)-C(25A)	1.360(14)
Fe(3)-C(43B)	2.058(17)	C(22A)-C(23A)	1.391(15)
Fe(3)-C(44B)	2.053(16)	C(22A)-C(31A)	1.411(14)
Fe(3)-C(45B)	2.043(16)	C(23A)-H(23A)	0.9500
Fe(3)-C(51B)	2.011(15)	C(23A)-C(24A)	1.384(15)
Fe(3)-C(52B)	2.030(15)	C(24A)-H(24A)	0.9500
Fe(3)-C(53B)	2.069(16)	C(24A)-C(25A)	1.399(16)
Fe(3)-C(54B)	2.075(16)	C(25A)-H(25A)	0.9500
Fe(3)-C(55B)	2.039(17)	C(31A)-C(32A)	1.430(15)
Fe(4)-C(41C)	2.037(14)	C(32A)-C(33A)	1.194(14)
Fe(4)-C(42C)	2.043(16)	C(33A)-C(41A)	1.434(14)
Fe(4)-C(43C)	2.030(15)	C(41A)-C(42A)	1.4200

C(41A)-C(45A)	1.4200	C(31B)-C(32B)	1.425(15)
C(42A)-H(42A)	1.0000	C(32B)-C(33B)	1.188(14)
C(42A)-C(43A)	1.4200	C(33B)-C(41B)	1.448(15)
C(43A)-H(43A)	1.0000	C(41B)-C(42B)	1.4200
C(43A)-C(44A)	1.4200	C(41B)-C(45B)	1.4200
C(44A)-H(44A)	1.0000	C(42B)-H(42B)	1.0000
C(44A)-C(45A)	1.4200	C(42B)-C(43B)	1.4200
C(45A)-H(45A)	1.0000	C(43B)-H(43B)	1.0000
C(51A)-H(51A)	1.0000	C(43B)-C(44B)	1.4200
C(51A)-C(52A)	1.4200	C(44B)-H(44B)	1.0000
C(51A)-C(55A)	1.4200	C(44B)-C(45B)	1.4200
C(52A)-H(52A)	1.0000	C(45B)-H(45B)	1.0000
C(52A)-C(53A)	1.4200	C(51B)-H(51B)	1.0000
C(53A)-H(53A)	1.0000	C(51B)-C(52B)	1.4200
C(53A)-C(54A)	1.4200	C(51B)-C(55B)	1.4200
C(54A)-H(54A)	1.0000	C(52B)-H(52B)	1.0000
C(54A)-C(55A)	1.4200	C(52B)-C(53B)	1.4200
C(55A)-H(55A)	1.0000	C(53B)-H(53B)	1.0000
N(11B)-C(12B)	1.378(14)	C(53B)-C(54B)	1.4200
N(11B)-C(15B)	1.344(14)	C(54B)-H(54B)	1.0000
C(12B)-C(13B)	1.429(15)	C(54B)-C(55B)	1.4200
C(12B)-C(31B)	1.395(14)	C(55B)-H(55B)	1.0000
C(13B)-H(13B)	0.9500	N(11C)-C(12C)	1.391(15)
C(13B)-C(14B)	1.337(15)	N(11C)-C(15C)	1.336(14)
C(14B)-H(14B)	0.9500	C(12C)-C(13C)	1.433(15)
C(14B)-C(15B)	1.395(16)	C(12C)-C(31C)	1.376(14)
C(15B)-H(15B)	0.9500	C(13C)-H(13C)	0.9500
N(21B)-C(22B)	1.398(14)	C(13C)-C(14C)	1.346(15)
N(21B)-C(25B)	1.359(14)	C(14C)-H(14C)	0.9500
C(22B)-C(23B)	1.408(15)	C(14C)-C(15C)	1.403(16)
C(22B)-C(31B)	1.420(14)	C(15C)-H(15C)	0.9500
C(23B)-H(23B)	0.9500	N(21C)-C(22C)	1.424(15)
C(23B)-C(24B)	1.391(16)	N(21C)-C(25C)	1.358(14)
C(24B)-H(24B)	0.9500	C(22C)-C(23C)	1.391(15)
C(24B)-C(25B)	1.401(16)	C(22C)-C(31C)	1.416(15)
C(25B)-H(25B)	0.9500	C(23C)-H(23C)	0.9500

C(23C)-C(24C)	1.380(16)	N(11C)-Fe(1)-N(11B)	90.1(6)
C(24C)-H(24C)	0.9500	N(21C)-Fe(1)-N(11A)	177.1(6)
C(24C)-C(25C)	1.405(16)	N(21C)-Fe(1)-N(21A)	92.3(6)
C(25C)-H(25C)	0.9500	N(21C)-Fe(1)-N(11B)	84.7(6)
C(31C)-C(32C)	1.424(16)	N(21C)-Fe(1)-N(21B)	89.9(6)
C(32C)-C(33C)	1.200(15)	N(21C)-Fe(1)-N(11C)	90.1(5)
C(33C)-C(41C)	1.433(15)	C(41A)-Fe(2)-C(42A)	40.8(3)
C(41C)-C(42C)	1.4200	C(41A)-Fe(2)-C(43A)	68.4(3)
C(41C)-C(45C)	1.4200	C(41A)-Fe(2)-C(44A)	68.3(4)
C(42C)-H(42C)	1.0000	C(41A)-Fe(2)-C(45A)	40.7(3)
C(42C)-C(43C)	1.4200	C(41A)-Fe(2)-C(51A)	110.1(5)
C(43C)-H(43C)	1.0000	C(41A)-Fe(2)-C(52A)	121.3(6)
C(43C)-C(44C)	1.4200	C(41A)-Fe(2)-C(53A)	154.6(6)
C(44C)-H(44C)	1.0000	C(41A)-Fe(2)-C(54A)	164.3(6)
C(44C)-C(45C)	1.4200	C(41A)-Fe(2)-C(55A)	128.0(6)
C(45C)-H(45C)	1.0000	C(42A)-Fe(2)-C(43A)	40.6(3)
C(51C)-H(51C)	1.0000	C(42A)-Fe(2)-C(44A)	68.3(4)
C(51C)-C(52C)	1.4200	C(42A)-Fe(2)-C(45A)	68.4(4)
C(51C)-C(55C)	1.4200	C(42A)-Fe(2)-C(51A)	126.4(6)
C(52C)-H(52C)	1.0000	C(42A)-Fe(2)-C(52A)	107.1(6)
C(52C)-C(53C)	1.4200	C(42A)-Fe(2)-C(53A)	118.5(6)
C(53C)-H(53C)	1.0000	C(42A)-Fe(2)-C(54A)	153.3(6)
C(53C)-C(54C)	1.4200	C(42A)-Fe(2)-C(55A)	164.2(6)
C(54C)-H(54C)	1.0000	C(43A)-Fe(2)-C(44A)	40.5(3)
C(54C)-C(55C)	1.4200	C(43A)-Fe(2)-C(51A)	161.8(6)
C(55C)-H(55C)	1.0000	C(43A)-Fe(2)-C(52A)	123.9(6)
		C(43A)-Fe(2)-C(53A)	105.4(5)
N(11A)-Fe(1)-N(21A)	90.3(5)	C(43A)-Fe(2)-C(54A)	118.8(6)
N(11A)-Fe(1)-N(11B)	92.7(5)	C(43A)-Fe(2)-C(55A)	154.8(6)
N(11A)-Fe(1)-N(11C)	91.2(6)	C(44A)-Fe(2)-C(51A)	157.3(6)
N(21A)-Fe(1)-N(11B)	176.4(5)	C(44A)-Fe(2)-C(52A)	160.6(6)
N(21A)-Fe(1)-N(11C)	87.9(6)	C(44A)-Fe(2)-C(54A)	107.4(6)
N(21B)-Fe(1)-N(11A)	88.7(6)	C(44A)-Fe(2)-C(55A)	121.7(6)
N(21B)-Fe(1)-N(21A)	92.6(6)	C(45A)-Fe(2)-C(43A)	68.2(4)
N(21B)-Fe(1)-N(11B)	89.4(5)	C(45A)-Fe(2)-C(44A)	40.5(3)
N(21B)-Fe(1)-N(11C)	179.4(6)	C(45A)-Fe(2)-C(51A)	123.3(6)

C(45A)-Fe(2)-C(52A)	157.1(6)	C(51B)-Fe(3)-C(42B)	117.4(6)
C(45A)-Fe(2)-C(53A)	161.9(6)	C(51B)-Fe(3)-C(43B)	149.5(7)
C(45A)-Fe(2)-C(54A)	126.4(6)	C(51B)-Fe(3)-C(44B)	169.4(7)
C(45A)-Fe(2)-C(55A)	110.3(5)	C(51B)-Fe(3)-C(45B)	131.1(6)
C(52A)-Fe(2)-C(51A)	40.2(3)	C(51B)-Fe(3)-C(52B)	41.1(3)
C(52A)-Fe(2)-C(55A)	67.6(4)	C(51B)-Fe(3)-C(53B)	68.5(4)
C(53A)-Fe(2)-C(44A)	123.9(6)	C(51B)-Fe(3)-C(54B)	68.4(4)
C(53A)-Fe(2)-C(51A)	67.7(4)	C(51B)-Fe(3)-C(55B)	41.0(3)
C(53A)-Fe(2)-C(52A)	40.4(3)	C(52B)-Fe(3)-C(41B)	128.5(6)
C(53A)-Fe(2)-C(54A)	40.4(3)	C(52B)-Fe(3)-C(42B)	106.2(6)
C(53A)-Fe(2)-C(55A)	67.8(4)	C(52B)-Fe(3)-C(43B)	114.9(6)
C(54A)-Fe(2)-C(51A)	67.7(4)	C(52B)-Fe(3)-C(44B)	148.4(7)
C(54A)-Fe(2)-C(52A)	67.8(4)	C(52B)-Fe(3)-C(45B)	168.2(7)
C(54A)-Fe(2)-C(55A)	40.3(3)	C(52B)-Fe(3)-C(53B)	40.5(3)
C(55A)-Fe(2)-C(51A)	40.1(3)	C(52B)-Fe(3)-C(54B)	68.1(3)
C(41B)-Fe(3)-C(42B)	40.6(3)	C(52B)-Fe(3)-C(55B)	68.8(3)
C(41B)-Fe(3)-C(43B)	68.2(4)	C(53B)-Fe(3)-C(54B)	40.1(3)
C(41B)-Fe(3)-C(44B)	68.3(4)	C(55B)-Fe(3)-C(41B)	120.7(6)
C(41B)-Fe(3)-C(45B)	40.7(3)	C(55B)-Fe(3)-C(42B)	152.8(7)
C(41B)-Fe(3)-C(53B)	165.4(7)	C(55B)-Fe(3)-C(43B)	166.6(7)
C(41B)-Fe(3)-C(54B)	153.9(7)	C(55B)-Fe(3)-C(44B)	130.4(7)
C(42B)-Fe(3)-C(43B)	40.4(3)	C(55B)-Fe(3)-C(45B)	111.1(6)
C(42B)-Fe(3)-C(44B)	68.1(4)	C(55B)-Fe(3)-C(53B)	68.0(3)
C(42B)-Fe(3)-C(53B)	126.4(6)	C(55B)-Fe(3)-C(54B)	40.4(3)
C(42B)-Fe(3)-C(54B)	164.5(7)	C(41C)-Fe(4)-C(42C)	40.7(3)
C(43B)-Fe(3)-C(53B)	105.8(6)	C(41C)-Fe(4)-C(53C)	153.8(6)
C(43B)-Fe(3)-C(54B)	127.4(7)	C(41C)-Fe(4)-C(54C)	164.6(6)
C(44B)-Fe(3)-C(43B)	40.4(3)	C(42C)-Fe(4)-C(53C)	119.6(6)
C(44B)-Fe(3)-C(53B)	116.4(6)	C(42C)-Fe(4)-C(54C)	153.8(6)
C(44B)-Fe(3)-C(54B)	108.8(6)	C(43C)-Fe(4)-C(41C)	68.8(4)
C(45B)-Fe(3)-C(42B)	68.3(4)	C(43C)-Fe(4)-C(42C)	40.8(3)
C(45B)-Fe(3)-C(43B)	68.1(4)	C(43C)-Fe(4)-C(53C)	107.8(5)
C(45B)-Fe(3)-C(44B)	40.6(3)	C(43C)-Fe(4)-C(54C)	119.6(6)
C(45B)-Fe(3)-C(53B)	151.1(7)	C(43C)-Fe(4)-C(55C)	153.6(6)
C(45B)-Fe(3)-C(54B)	120.0(6)	C(44C)-Fe(4)-C(41C)	69.1(4)
C(51B)-Fe(3)-C(41B)	109.4(6)	C(44C)-Fe(4)-C(42C)	69.0(3)

C(44C)-Fe(4)-C(43C)	41.1(3)	C(31A)-C(12A)-C(13A)	126.4(12)
C(44C)-Fe(4)-C(45C)	41.2(3)	C(12A)-C(13A)-H(13A)	126.5
C(44C)-Fe(4)-C(52C)	163.6(6)	C(14A)-C(13A)-C(12A)	107.1(12)
C(44C)-Fe(4)-C(53C)	126.4(6)	C(14A)-C(13A)-H(13A)	126.5
C(44C)-Fe(4)-C(54C)	108.0(6)	C(13A)-C(14A)-H(14A)	126.3
C(44C)-Fe(4)-C(55C)	119.0(6)	C(13A)-C(14A)-C(15A)	107.4(12)
C(45C)-Fe(4)-C(41C)	41.0(3)	C(15A)-C(14A)-H(14A)	126.3
C(45C)-Fe(4)-C(42C)	68.9(3)	N(11A)-C(15A)-C(14A)	111.8(12)
C(45C)-Fe(4)-C(43C)	69.1(3)	N(11A)-C(15A)-H(15A)	124.1
C(45C)-Fe(4)-C(53C)	164.2(6)	C(14A)-C(15A)-H(15A)	124.1
C(45C)-Fe(4)-C(54C)	127.0(6)	C(22A)-N(21A)-Fe(1)	129.1(8)
C(45C)-Fe(4)-C(55C)	107.4(5)	C(25A)-N(21A)-Fe(1)	126.1(9)
C(51C)-Fe(4)-C(41C)	106.8(6)	C(25A)-N(21A)-C(22A)	104.8(10)
C(51C)-Fe(4)-C(42C)	125.9(6)	C(23A)-C(22A)-N(21A)	109.4(10)
C(51C)-Fe(4)-C(43C)	163.7(6)	C(23A)-C(22A)-C(31A)	128.8(12)
C(51C)-Fe(4)-C(44C)	153.6(6)	C(31A)-C(22A)-N(21A)	121.8(11)
C(51C)-Fe(4)-C(45C)	118.6(6)	C(22A)-C(23A)-H(23A)	126.2
C(51C)-Fe(4)-C(52C)	41.5(3)	C(24A)-C(23A)-C(22A)	107.7(12)
C(51C)-Fe(4)-C(53C)	68.8(3)	C(24A)-C(23A)-H(23A)	126.2
C(51C)-Fe(4)-C(54C)	68.7(4)	C(23A)-C(24A)-H(24A)	126.8
C(51C)-Fe(4)-C(55C)	41.3(3)	C(23A)-C(24A)-C(25A)	106.5(12)
C(52C)-Fe(4)-C(41C)	119.0(6)	C(25A)-C(24A)-H(24A)	126.8
C(52C)-Fe(4)-C(42C)	107.1(5)	N(21A)-C(25A)-C(24A)	111.6(12)
C(52C)-Fe(4)-C(43C)	125.7(6)	N(21A)-C(25A)-H(25A)	124.2
C(52C)-Fe(4)-C(45C)	153.7(6)	C(24A)-C(25A)-H(25A)	124.2
C(52C)-Fe(4)-C(53C)	40.6(3)	C(12A)-C(31A)-C(22A)	125.3(12)
C(52C)-Fe(4)-C(54C)	68.1(4)	C(12A)-C(31A)-C(32A)	117.2(12)
C(52C)-Fe(4)-C(55C)	69.1(3)	C(22A)-C(31A)-C(32A)	117.4(12)
C(53C)-Fe(4)-C(54C)	40.0(3)	C(33A)-C(32A)-C(31A)	170.1(19)
C(55C)-Fe(4)-C(41C)	126.7(6)	C(32A)-C(33A)-C(41A)	177(2)
C(55C)-Fe(4)-C(42C)	164.3(6)	C(33A)-C(41A)-Fe(2)	119.4(12)
C(55C)-Fe(4)-C(53C)	68.1(4)	C(42A)-C(41A)-Fe(2)	69.7(6)
C(55C)-Fe(4)-C(54C)	40.4(3)	C(42A)-C(41A)-C(33A)	124.1(12)
C(15A)-N(11A)-C(12A)	105.3(11)	C(42A)-C(41A)-C(45A)	108.0
N(11A)-C(12A)-C(13A)	108.4(11)	C(45A)-C(41A)-Fe(2)	70.0(6)
C(31A)-C(12A)-N(11A)	125.3(12)	C(45A)-C(41A)-C(33A)	127.4(12)

Fe(2)-C(42A)-H(42A)	126.0	Fe(2)-C(53A)-H(53A)	126.0
C(41A)-C(42A)-Fe(2)	69.5(6)	C(52A)-C(53A)-Fe(2)	70.2(6)
C(41A)-C(42A)-H(42A)	126.0	C(52A)-C(53A)-H(53A)	126.0
C(43A)-C(42A)-Fe(2)	70.1(6)	C(54A)-C(53A)-Fe(2)	69.9(6)
C(43A)-C(42A)-C(41A)	108.0	C(54A)-C(53A)-C(52A)	108.0
C(43A)-C(42A)-H(42A)	126.0	C(54A)-C(53A)-H(53A)	126.0
Fe(2)-C(43A)-H(43A)	126.0	Fe(2)-C(54A)-H(54A)	126.0
C(42A)-C(43A)-Fe(2)	69.3(6)	C(53A)-C(54A)-Fe(2)	69.7(6)
C(42A)-C(43A)-H(43A)	126.0	C(53A)-C(54A)-H(54A)	126.0
C(42A)-C(43A)-C(44A)	108.0	C(53A)-C(54A)-C(55A)	108.0
C(44A)-C(43A)-Fe(2)	69.9(6)	C(55A)-C(54A)-Fe(2)	70.3(6)
C(44A)-C(43A)-H(43A)	126.0	C(55A)-C(54A)-H(54A)	126.0
Fe(2)-C(44A)-H(44A)	126.0	Fe(2)-C(55A)-H(55A)	126.0
C(43A)-C(44A)-Fe(2)	69.6(6)	C(51A)-C(55A)-Fe(2)	70.1(6)
C(43A)-C(44A)-H(44A)	126.0	C(51A)-C(55A)-C(54A)	108.0
C(43A)-C(44A)-C(45A)	108.0	C(51A)-C(55A)-H(55A)	126.0
C(45A)-C(44A)-Fe(2)	69.5(6)	C(54A)-C(55A)-Fe(2)	69.4(6)
C(45A)-C(44A)-H(44A)	126.0	C(54A)-C(55A)-H(55A)	126.0
Fe(2)-C(45A)-H(45A)	126.0	C(12B)-N(11B)-Fe(1)	126.7(9)
C(41A)-C(45A)-Fe(2)	69.3(6)	C(15B)-N(11B)-Fe(1)	126.3(10)
C(41A)-C(45A)-C(44A)	108.0	C(15B)-N(11B)-C(12B)	106.5(11)
C(41A)-C(45A)-H(45A)	126.0	N(11B)-C(12B)-C(13B)	107.8(11)
C(44A)-C(45A)-Fe(2)	70.0(6)	N(11B)-C(12B)-C(31B)	124.4(12)
C(44A)-C(45A)-H(45A)	126.0	C(31B)-C(12B)-C(13B)	127.7(13)
Fe(2)-C(51A)-H(51A)	126.0	C(12B)-C(13B)-H(13B)	126.2
C(52A)-C(51A)-Fe(2)	69.6(6)	C(14B)-C(13B)-C(12B)	107.7(13)
C(52A)-C(51A)-H(51A)	126.0	C(14B)-C(13B)-H(13B)	126.2
C(55A)-C(51A)-Fe(2)	69.8(6)	C(13B)-C(14B)-H(14B)	126.4
C(55A)-C(51A)-H(51A)	126.0	C(13B)-C(14B)-C(15B)	107.1(13)
C(55A)-C(51A)-C(52A)	108.0	C(15B)-C(14B)-H(14B)	126.4
Fe(2)-C(52A)-H(52A)	126.0	N(11B)-C(15B)-C(14B)	110.9(12)
C(51A)-C(52A)-Fe(2)	70.2(6)	N(11B)-C(15B)-H(15B)	124.6
C(51A)-C(52A)-H(52A)	126.0	C(14B)-C(15B)-H(15B)	124.6
C(53A)-C(52A)-Fe(2)	69.4(6)	C(22B)-N(21B)-Fe(1)	128.5(9)
C(53A)-C(52A)-C(51A)	108.0	C(25B)-N(21B)-Fe(1)	124.3(10)
C(53A)-C(52A)-H(52A)	126.0	C(25B)-N(21B)-C(22B)	106.3(11)

N(21B)-C(22B)-C(23B)	108.8(11)	C(43B)-C(44B)-Fe(3)	70.0(6)
N(21B)-C(22B)-C(31B)	122.6(12)	C(43B)-C(44B)-H(44B)	126.0
C(23B)-C(22B)-C(31B)	128.5(12)	C(45B)-C(44B)-Fe(3)	69.3(6)
C(22B)-C(23B)-H(23B)	126.3	C(45B)-C(44B)-C(43B)	108.0
C(24B)-C(23B)-C(22B)	107.4(12)	C(45B)-C(44B)-H(44B)	126.0
C(24B)-C(23B)-H(23B)	126.3	Fe(3)-C(45B)-H(45B)	126.0
C(23B)-C(24B)-H(24B)	126.9	C(41B)-C(45B)-Fe(3)	69.6(6)
C(23B)-C(24B)-C(25B)	106.3(13)	C(41B)-C(45B)-H(45B)	126.0
C(25B)-C(24B)-H(24B)	126.9	C(44B)-C(45B)-Fe(3)	70.1(6)
N(21B)-C(25B)-C(24B)	111.1(12)	C(44B)-C(45B)-C(41B)	108.0
N(21B)-C(25B)-H(25B)	124.5	C(44B)-C(45B)-H(45B)	126.0
C(24B)-C(25B)-H(25B)	124.5	Fe(3)-C(51B)-H(51B)	126.0
C(12B)-C(31B)-C(22B)	124.5(12)	C(52B)-C(51B)-Fe(3)	70.1(6)
C(12B)-C(31B)-C(32B)	118.9(12)	C(52B)-C(51B)-H(51B)	126.0
C(22B)-C(31B)-C(32B)	116.5(12)	C(52B)-C(51B)-C(55B)	108.0
C(33B)-C(32B)-C(31B)	175.0(19)	C(55B)-C(51B)-Fe(3)	70.6(6)
C(32B)-C(33B)-C(41B)	177(2)	C(55B)-C(51B)-H(51B)	126.0
C(33B)-C(41B)-Fe(3)	127.1(12)	Fe(3)-C(52B)-H(52B)	126.0
C(42B)-C(41B)-Fe(3)	70.0(6)	C(51B)-C(52B)-Fe(3)	68.7(6)
C(42B)-C(41B)-C(33B)	125.9(14)	C(51B)-C(52B)-H(52B)	126.0
C(42B)-C(41B)-C(45B)	108.0	C(51B)-C(52B)-C(53B)	108.0
C(45B)-C(41B)-Fe(3)	69.7(6)	C(53B)-C(52B)-Fe(3)	71.2(6)
C(45B)-C(41B)-C(33B)	126.1(14)	C(53B)-C(52B)-H(52B)	126.0
Fe(3)-C(42B)-H(42B)	126.0	Fe(3)-C(53B)-H(53B)	126.0
C(41B)-C(42B)-Fe(3)	69.4(6)	C(52B)-C(53B)-Fe(3)	68.2(6)
C(41B)-C(42B)-H(42B)	126.0	C(52B)-C(53B)-H(53B)	126.0
C(43B)-C(42B)-Fe(3)	70.1(6)	C(52B)-C(53B)-C(54B)	108.0
C(43B)-C(42B)-C(41B)	108.0	C(54B)-C(53B)-Fe(3)	70.2(6)
C(43B)-C(42B)-H(42B)	126.0	C(54B)-C(53B)-H(53B)	126.0
Fe(3)-C(43B)-H(43B)	126.0	Fe(3)-C(54B)-H(54B)	126.0
C(42B)-C(43B)-Fe(3)	69.5(6)	C(53B)-C(54B)-Fe(3)	69.7(6)
C(42B)-C(43B)-H(43B)	126.0	C(53B)-C(54B)-H(54B)	126.0
C(42B)-C(43B)-C(44B)	108.0	C(55B)-C(54B)-Fe(3)	68.5(6)
C(44B)-C(43B)-Fe(3)	69.6(6)	C(55B)-C(54B)-C(53B)	108.0
C(44B)-C(43B)-H(43B)	126.0	C(55B)-C(54B)-H(54B)	126.0
Fe(3)-C(44B)-H(44B)	126.0	Fe(3)-C(55B)-H(55B)	126.0

C(51B)-C(55B)-Fe(3)	68.4(6)	C(12C)-C(31C)-C(32C)	118.8(12)
C(51B)-C(55B)-H(55B)	126.0	C(22C)-C(31C)-C(32C)	116.1(12)
C(54B)-C(55B)-Fe(3)	71.2(6)	C(33C)-C(32C)-C(31C)	172(2)
C(54B)-C(55B)-C(51B)	108.0	C(32C)-C(33C)-C(41C)	178(2)
C(54B)-C(55B)-H(55B)	126.0	C(33C)-C(41C)-Fe(4)	124.2(11)
C(12C)-N(11C)-Fe(1)	125.9(9)	C(42C)-C(41C)-Fe(4)	69.9(6)
C(15C)-N(11C)-Fe(1)	126.3(10)	C(42C)-C(41C)-C(33C)	128.2(13)
C(15C)-N(11C)-C(12C)	106.8(11)	C(45C)-C(41C)-Fe(4)	68.8(6)
N(11C)-C(12C)-C(13C)	107.7(10)	C(45C)-C(41C)-C(33C)	123.7(13)
C(31C)-C(12C)-N(11C)	125.4(12)	C(45C)-C(41C)-C(42C)	108.0
C(31C)-C(12C)-C(13C)	126.9(12)	Fe(4)-C(42C)-H(42C)	126.0
C(12C)-C(13C)-H(13C)	126.4	C(41C)-C(42C)-Fe(4)	69.4(5)
C(14C)-C(13C)-C(12C)	107.3(12)	C(41C)-C(42C)-H(42C)	126.0
C(14C)-C(13C)-H(13C)	126.4	C(43C)-C(42C)-Fe(4)	69.1(5)
C(13C)-C(14C)-H(14C)	126.3	C(43C)-C(42C)-C(41C)	108.0
C(13C)-C(14C)-C(15C)	107.3(13)	C(43C)-C(42C)-H(42C)	126.0
C(15C)-C(14C)-H(14C)	126.3	Fe(4)-C(43C)-H(43C)	126.0
N(11C)-C(15C)-C(14C)	110.9(12)	C(42C)-C(43C)-Fe(4)	70.1(6)
N(11C)-C(15C)-H(15C)	124.6	C(42C)-C(43C)-H(43C)	126.0
C(14C)-C(15C)-H(15C)	124.6	C(42C)-C(43C)-C(44C)	108.0
C(22C)-N(21C)-Fe(1)	127.9(9)	C(44C)-C(43C)-Fe(4)	68.9(6)
C(25C)-N(21C)-Fe(1)	127.0(10)	C(44C)-C(43C)-H(43C)	126.0
C(25C)-N(21C)-C(22C)	104.6(11)	Fe(4)-C(44C)-H(44C)	126.0
C(23C)-C(22C)-N(21C)	109.5(11)	C(43C)-C(44C)-Fe(4)	70.0(6)
C(23C)-C(22C)-C(31C)	128.7(13)	C(43C)-C(44C)-H(44C)	126.0
C(31C)-C(22C)-N(21C)	121.4(12)	C(43C)-C(44C)-C(45C)	108.0
C(22C)-C(23C)-H(23C)	126.2	C(45C)-C(44C)-Fe(4)	69.6(6)
C(24C)-C(23C)-C(22C)	107.5(12)	C(45C)-C(44C)-H(44C)	126.0
C(24C)-C(23C)-H(23C)	126.2	Fe(4)-C(45C)-H(45C)	126.0
C(23C)-C(24C)-H(24C)	126.7	C(41C)-C(45C)-Fe(4)	70.2(6)
C(23C)-C(24C)-C(25C)	106.5(12)	C(41C)-C(45C)-C(44C)	108.0
C(25C)-C(24C)-H(24C)	126.7	C(41C)-C(45C)-H(45C)	126.0
N(21C)-C(25C)-C(24C)	111.4(12)	C(44C)-C(45C)-Fe(4)	69.2(6)
N(21C)-C(25C)-H(25C)	124.3	C(44C)-C(45C)-H(45C)	126.0
C(24C)-C(25C)-H(25C)	124.3	Fe(4)-C(51C)-H(51C)	126.0
C(12C)-C(31C)-C(22C)	125.1(12)	C(52C)-C(51C)-Fe(4)	70.3(6)

C(52C)-C(51C)-H(51C)	126.0	C(54C)-C(53C)-Fe(4)	70.3(6)
C(52C)-C(51C)-C(55C)	108.0	C(54C)-C(53C)-H(53C)	126.0
C(55C)-C(51C)-Fe(4)	70.8(6)	Fe(4)-C(54C)-H(54C)	126.0
C(55C)-C(51C)-H(51C)	126.0	C(53C)-C(54C)-Fe(4)	69.8(6)
Fe(4)-C(52C)-H(52C)	126.0	C(53C)-C(54C)-H(54C)	126.0
C(51C)-C(52C)-Fe(4)	68.2(6)	C(55C)-C(54C)-Fe(4)	67.9(6)
C(51C)-C(52C)-H(52C)	126.0	C(55C)-C(54C)-C(53C)	108.0
C(53C)-C(52C)-Fe(4)	71.8(6)	C(55C)-C(54C)-H(54C)	126.0
C(53C)-C(52C)-C(51C)	108.0	Fe(4)-C(55C)-H(55C)	126.0
C(53C)-C(52C)-H(52C)	126.0	C(51C)-C(55C)-Fe(4)	67.9(6)
Fe(4)-C(53C)-H(53C)	126.0	C(51C)-C(55C)-H(55C)	126.0
C(52C)-C(53C)-Fe(4)	67.6(6)	C(54C)-C(55C)-Fe(4)	71.7(6)
C(52C)-C(53C)-H(53C)	126.0	C(54C)-C(55C)-C(51C)	108.0
C(52C)-C(53C)-C(54C)	108.0	C(54C)-C(55C)-H(55C)	126.0

A2.2. Table of selected bond lengths [Å] and angles [°] for (6)

Cu(1)-N(21B)	1.951(6)	Fe(2A)-C(51A)	2.035(7)
Cu(1)-N(21A)	1.952(6)	Fe(2A)-C(43A)	2.047(7)
Cu(1)-N(11A)	1.952(6)	Fe(2A)-C(44A)	2.048(7)
Cu(1)-N(11B)	1.960(6)	C(41A)-C(42A)	1.424(9)
N(11A)-C(15A)	1.331(9)	C(41A)-C(45A)	1.451(9)
N(11A)-C(12A)	1.386(9)	C(42A)-C(43A)	1.400(10)
C(12A)-C(31A)	1.411(10)	C(42A)-H(42A)	0.9500
C(12A)-C(13A)	1.419(11)	C(43A)-C(44A)	1.430(11)
C(13A)-C(14A)	1.358(11)	C(43A)-H(43A)	0.9500
C(13A)-H(13A)	0.9500	C(44A)-C(45A)	1.402(10)
C(14A)-C(15A)	1.421(11)	C(44A)-H(44A)	0.9500
C(14A)-H(14A)	0.9500	C(45A)-H(45A)	0.9500
C(15A)-H(15A)	0.9500	C(51A)-C(52A)	1.405(10)
N(21A)-C(25A)	1.341(9)	C(51A)-C(55A)	1.419(12)
N(21A)-C(22A)	1.383(9)	C(51A)-H(51A)	0.9500
C(22A)-C(31A)	1.386(10)	C(52A)-C(53A)	1.414(13)
C(22A)-C(23A)	1.437(10)	C(52A)-H(52A)	0.9500
C(23A)-C(24A)	1.357(11)	C(53A)-C(54A)	1.398(14)
C(23A)-H(23A)	0.9500	C(53A)-H(53A)	0.9500
C(24A)-C(25A)	1.415(10)	C(54A)-C(55A)	1.399(13)
C(24A)-H(24A)	0.9500	C(54A)-H(54A)	0.9500
C(25A)-H(25A)	0.9500	C(55A)-H(55A)	0.9500
C(31A)-C(32A)	1.437(9)	N(11B)-C(15B)	1.355(9)
C(32A)-C(33A)	1.200(10)	N(11B)-C(12B)	1.371(9)
C(33A)-C(41A)	1.420(10)	C(12B)-C(31B)	1.412(9)
Fe(2A)-C(53A)	2.015(9)	C(12B)-C(13B)	1.427(9)
Fe(2A)-C(54A)	2.027(8)	C(13B)-C(14B)	1.368(10)
Fe(2A)-C(45A)	2.027(8)	C(13B)-H(13B)	0.9500
Fe(2A)-C(42A)	2.028(7)	C(14B)-C(15B)	1.405(10)
Fe(2A)-C(55A)	2.028(8)	C(14B)-H(14B)	0.9500
Fe(2A)-C(52A)	2.032(8)	C(15B)-H(15B)	0.9500
Fe(2A)-C(41A)	2.035(7)	N(21B)-C(25B)	1.343(9)

N(21B)-C(22B)	1.372(9)	C(53B)-H(53B)	0.9500
C(22B)-C(31B)	1.404(9)	C(54B)-C(55B)	1.380(12)
C(22B)-C(23B)	1.437(9)	C(54B)-H(54B)	0.9500
C(23B)-C(24B)	1.362(10)	C(55B)-H(55B)	0.9500
C(23B)-H(23B)	0.9500		
C(24B)-C(25B)	1.394(10)	N(21B)-Cu(1)-N(21A)	145.6(3)
C(24B)-H(24B)	0.9500	N(21B)-Cu(1)-N(11A)	97.3(2)
C(25B)-H(25B)	0.9500	N(21A)-Cu(1)-N(11A)	91.6(2)
C(31B)-C(32B)	1.424(10)	N(21B)-Cu(1)-N(11B)	92.4(2)
C(32B)-C(33B)	1.186(10)	N(21A)-Cu(1)-N(11B)	97.6(2)
C(33B)-C(41B)	1.431(10)	N(11A)-Cu(1)-N(11B)	147.6(3)
Fe(3B)-C(42B)	2.029(8)	C(15A)-N(11A)-C(12A)	105.6(6)
Fe(3B)-C(53B)	2.036(7)	C(15A)-N(11A)-Cu(1)	126.8(5)
Fe(3B)-C(52B)	2.037(7)	C(12A)-N(11A)-Cu(1)	127.4(5)
Fe(3B)-C(41B)	2.038(7)	N(11A)-C(12A)-C(31A)	123.1(7)
Fe(3B)-C(55B)	2.041(8)	N(11A)-C(12A)-C(13A)	109.5(7)
Fe(3B)-C(51B)	2.041(7)	C(31A)-C(12A)-C(13A)	127.4(7)
Fe(3B)-C(54B)	2.042(8)	C(14A)-C(13A)-C(12A)	107.0(7)
Fe(3B)-C(43B)	2.053(8)	C(14A)-C(13A)-H(13A)	126.5
Fe(3B)-C(45B)	2.056(7)	C(12A)-C(13A)-H(13A)	126.5
Fe(3B)-C(44B)	2.065(7)	C(13A)-C(14A)-C(15A)	106.0(7)
C(41B)-C(42B)	1.422(10)	C(13A)-C(14A)-H(14A)	127.0
C(41B)-C(45B)	1.452(10)	C(15A)-C(14A)-H(14A)	127.0
C(42B)-C(43B)	1.389(11)	N(11A)-C(15A)-C(14A)	111.8(7)
C(42B)-H(42B)	0.9500	N(11A)-C(15A)-H(15A)	124.1
C(43B)-C(44B)	1.436(11)	C(14A)-C(15A)-H(15A)	124.1
C(43B)-H(43B)	0.9500	C(25A)-N(21A)-C(22A)	106.6(6)
C(44B)-C(45B)	1.404(10)	C(25A)-N(21A)-Cu(1)	125.6(5)
C(44B)-H(44B)	0.9500	C(22A)-N(21A)-Cu(1)	127.8(5)
C(45B)-H(45B)	0.9500	N(21A)-C(22A)-C(31A)	123.4(7)
C(51B)-C(52B)	1.407(11)	N(21A)-C(22A)-C(23A)	108.9(6)
C(51B)-C(55B)	1.416(11)	C(31A)-C(22A)-C(23A)	127.6(7)
C(51B)-H(51B)	0.9500	C(24A)-C(23A)-C(22A)	106.4(6)
C(52B)-C(53B)	1.407(12)	C(24A)-C(23A)-H(23A)	126.8
C(52B)-H(52B)	0.9500	C(22A)-C(23A)-H(23A)	126.8
C(53B)-C(54B)	1.436(13)	C(23A)-C(24A)-C(25A)	107.3(7)

C(23A)-C(24A)-H(24A)	126.3	C(52A)-Fe(2A)-C(51A)	40.4(3)
C(25A)-C(24A)-H(24A)	126.3	C(41A)-Fe(2A)-C(51A)	106.3(3)
N(21A)-C(25A)-C(24A)	110.7(7)	C(53A)-Fe(2A)-C(43A)	108.2(3)
N(21A)-C(25A)-H(25A)	124.7	C(54A)-Fe(2A)-C(43A)	124.5(3)
C(24A)-C(25A)-H(25A)	124.7	C(45A)-Fe(2A)-C(43A)	68.7(3)
C(22A)-C(31A)-C(12A)	126.2(6)	C(42A)-Fe(2A)-C(43A)	40.2(3)
C(22A)-C(31A)-C(32A)	117.5(6)	C(55A)-Fe(2A)-C(43A)	160.6(3)
C(12A)-C(31A)-C(32A)	116.3(6)	C(52A)-Fe(2A)-C(43A)	122.2(3)
C(33A)-C(32A)-C(31A)	175.7(7)	C(41A)-Fe(2A)-C(43A)	68.4(3)
C(32A)-C(33A)-C(41A)	178.2(8)	C(51A)-Fe(2A)-C(43A)	157.3(3)
C(53A)-Fe(2A)-C(54A)	40.5(4)	C(53A)-Fe(2A)-C(44A)	123.2(3)
C(53A)-Fe(2A)-C(45A)	158.0(4)	C(54A)-Fe(2A)-C(44A)	108.6(3)
C(54A)-Fe(2A)-C(45A)	122.1(4)	C(45A)-Fe(2A)-C(44A)	40.3(3)
C(53A)-Fe(2A)-C(42A)	123.1(3)	C(42A)-Fe(2A)-C(44A)	68.4(3)
C(54A)-Fe(2A)-C(42A)	159.7(4)	C(55A)-Fe(2A)-C(44A)	124.0(3)
C(45A)-Fe(2A)-C(42A)	69.5(3)	C(52A)-Fe(2A)-C(44A)	158.8(3)
C(53A)-Fe(2A)-C(55A)	68.0(4)	C(41A)-Fe(2A)-C(44A)	68.7(3)
C(54A)-Fe(2A)-C(55A)	40.4(4)	C(51A)-Fe(2A)-C(44A)	159.9(3)
C(45A)-Fe(2A)-C(55A)	107.4(3)	C(43A)-Fe(2A)-C(44A)	40.9(3)
C(42A)-Fe(2A)-C(55A)	158.0(3)	C(33A)-C(41A)-C(42A)	125.9(7)
C(53A)-Fe(2A)-C(52A)	40.9(4)	C(33A)-C(41A)-C(45A)	127.0(6)
C(54A)-Fe(2A)-C(52A)	68.4(4)	C(42A)-C(41A)-C(45A)	106.9(6)
C(45A)-Fe(2A)-C(52A)	159.4(3)	C(33A)-C(41A)-Fe(2A)	123.5(5)
C(42A)-Fe(2A)-C(52A)	106.7(3)	C(42A)-C(41A)-Fe(2A)	69.2(4)
C(55A)-Fe(2A)-C(52A)	68.2(3)	C(45A)-C(41A)-Fe(2A)	68.8(4)
C(53A)-Fe(2A)-C(41A)	159.1(4)	C(43A)-C(42A)-C(41A)	108.7(6)
C(54A)-Fe(2A)-C(41A)	158.4(4)	C(43A)-C(42A)-Fe(2A)	70.6(4)
C(45A)-Fe(2A)-C(41A)	41.8(3)	C(41A)-C(42A)-Fe(2A)	69.7(4)
C(42A)-Fe(2A)-C(41A)	41.0(3)	C(43A)-C(42A)-H(42A)	125.6
C(55A)-Fe(2A)-C(41A)	122.1(3)	C(41A)-C(42A)-H(42A)	125.6
C(52A)-Fe(2A)-C(41A)	122.1(3)	Fe(2A)-C(42A)-H(42A)	125.6
C(53A)-Fe(2A)-C(51A)	68.4(3)	C(42A)-C(43A)-C(44A)	108.2(6)
C(54A)-Fe(2A)-C(51A)	68.5(3)	C(42A)-C(43A)-Fe(2A)	69.2(4)
C(45A)-Fe(2A)-C(51A)	123.1(3)	C(44A)-C(43A)-Fe(2A)	69.6(4)
C(42A)-Fe(2A)-C(51A)	121.4(3)	C(42A)-C(43A)-H(43A)	125.9
C(55A)-Fe(2A)-C(51A)	40.9(3)	C(44A)-C(43A)-H(43A)	125.9

Fe(2A)-C(43A)-H(43A)	126.9	Fe(2A)-C(54A)-H(54A)	126.3
C(45A)-C(44A)-C(43A)	108.4(6)	C(54A)-C(55A)-C(51A)	108.4(8)
C(45A)-C(44A)-Fe(2A)	69.1(4)	C(54A)-C(55A)-Fe(2A)	69.8(5)
C(43A)-C(44A)-Fe(2A)	69.5(4)	C(51A)-C(55A)-Fe(2A)	69.8(4)
C(45A)-C(44A)-H(44A)	125.8	C(54A)-C(55A)-H(55A)	125.8
C(43A)-C(44A)-H(44A)	125.8	C(51A)-C(55A)-H(55A)	125.8
Fe(2A)-C(44A)-H(44A)	127.2	Fe(2A)-C(55A)-H(55A)	126.2
C(44A)-C(45A)-C(41A)	107.7(6)	C(15B)-N(11B)-C(12B)	105.9(6)
C(44A)-C(45A)-Fe(2A)	70.7(4)	C(15B)-N(11B)-Cu(1)	127.4(5)
C(41A)-C(45A)-Fe(2A)	69.4(4)	C(12B)-N(11B)-Cu(1)	126.4(4)
C(44A)-C(45A)-H(45A)	126.1	N(11B)-C(12B)-C(31B)	124.2(6)
C(41A)-C(45A)-H(45A)	126.1	N(11B)-C(12B)-C(13B)	109.7(6)
Fe(2A)-C(45A)-H(45A)	125.4	C(31B)-C(12B)-C(13B)	126.0(6)
C(52A)-C(51A)-C(55A)	107.5(7)	C(14B)-C(13B)-C(12B)	106.4(6)
C(52A)-C(51A)-Fe(2A)	69.7(4)	C(14B)-C(13B)-H(13B)	126.8
C(55A)-C(51A)-Fe(2A)	69.3(4)	C(12B)-C(13B)-H(13B)	126.8
C(52A)-C(51A)-H(51A)	126.3	C(13B)-C(14B)-C(15B)	106.7(6)
C(55A)-C(51A)-H(51A)	126.3	C(13B)-C(14B)-H(14B)	126.6
Fe(2A)-C(51A)-H(51A)	126.3	C(15B)-C(14B)-H(14B)	126.6
C(51A)-C(52A)-C(53A)	107.7(7)	N(11B)-C(15B)-C(14B)	111.2(7)
C(51A)-C(52A)-Fe(2A)	69.9(4)	N(11B)-C(15B)-H(15B)	124.4
C(53A)-C(52A)-Fe(2A)	68.9(5)	C(14B)-C(15B)-H(15B)	124.4
C(51A)-C(52A)-H(52A)	126.1	C(25B)-N(21B)-C(22B)	106.7(6)
C(53A)-C(52A)-H(52A)	126.1	C(25B)-N(21B)-Cu(1)	126.4(5)
Fe(2A)-C(52A)-H(52A)	126.6	C(22B)-N(21B)-Cu(1)	126.7(4)
C(54A)-C(53A)-C(52A)	108.5(7)	N(21B)-C(22B)-C(31B)	124.6(6)
C(54A)-C(53A)-Fe(2A)	70.2(5)	N(21B)-C(22B)-C(23B)	109.0(6)
C(52A)-C(53A)-Fe(2A)	70.2(5)	C(31B)-C(22B)-C(23B)	126.3(6)
C(54A)-C(53A)-H(53A)	125.7	C(24B)-C(23B)-C(22B)	105.6(6)
C(52A)-C(53A)-H(53A)	125.7	C(24B)-C(23B)-H(23B)	127.2
Fe(2A)-C(53A)-H(53A)	125.4	C(22B)-C(23B)-H(23B)	127.2
C(53A)-C(54A)-C(55A)	107.9(8)	C(23B)-C(24B)-C(25B)	107.9(6)
C(53A)-C(54A)-Fe(2A)	69.3(5)	C(23B)-C(24B)-H(24B)	126.1
C(55A)-C(54A)-Fe(2A)	69.9(5)	C(25B)-C(24B)-H(24B)	126.1
C(53A)-C(54A)-H(54A)	126.0	N(21B)-C(25B)-C(24B)	110.7(6)
C(55A)-C(54A)-H(54A)	126.0	N(21B)-C(25B)-H(25B)	124.6

C(24B)-C(25B)-H(25B)	124.6	C(52B)-Fe(3B)-C(45B)	152.6(3)
C(22B)-C(31B)-C(12B)	124.7(6)	C(41B)-Fe(3B)-C(45B)	41.5(3)
C(22B)-C(31B)-C(32B)	117.9(6)	C(55B)-Fe(3B)-C(45B)	108.6(3)
C(12B)-C(31B)-C(32B)	117.3(6)	C(51B)-Fe(3B)-C(45B)	118.9(3)
C(33B)-C(32B)-C(31B)	176.0(8)	C(54B)-Fe(3B)-C(45B)	127.2(3)
C(32B)-C(33B)-C(41B)	178.1(7)	C(43B)-Fe(3B)-C(45B)	68.2(3)
C(42B)-Fe(3B)-C(53B)	118.6(3)	C(42B)-Fe(3B)-C(44B)	67.7(3)
C(42B)-Fe(3B)-C(52B)	107.6(3)	C(53B)-Fe(3B)-C(44B)	128.8(3)
C(53B)-Fe(3B)-C(52B)	40.4(3)	C(52B)-Fe(3B)-C(44B)	165.9(3)
C(42B)-Fe(3B)-C(41B)	40.9(3)	C(41B)-Fe(3B)-C(44B)	68.4(3)
C(53B)-Fe(3B)-C(41B)	151.7(3)	C(55B)-Fe(3B)-C(44B)	119.9(3)
C(52B)-Fe(3B)-C(41B)	117.5(3)	C(51B)-Fe(3B)-C(44B)	153.0(3)
C(42B)-Fe(3B)-C(55B)	165.4(3)	C(54B)-Fe(3B)-C(44B)	109.3(3)
C(53B)-Fe(3B)-C(55B)	67.7(3)	C(43B)-Fe(3B)-C(44B)	40.8(3)
C(52B)-Fe(3B)-C(55B)	67.9(3)	C(45B)-Fe(3B)-C(44B)	39.8(3)
C(41B)-Fe(3B)-C(55B)	127.5(3)	C(42B)-C(41B)-C(33B)	128.1(7)
C(42B)-Fe(3B)-C(51B)	127.2(3)	C(42B)-C(41B)-C(45B)	106.4(6)
C(53B)-Fe(3B)-C(51B)	67.9(3)	C(33B)-C(41B)-C(45B)	125.4(7)
C(52B)-Fe(3B)-C(51B)	40.4(3)	C(42B)-C(41B)-Fe(3B)	69.2(4)
C(41B)-Fe(3B)-C(51B)	107.0(3)	C(33B)-C(41B)-Fe(3B)	127.0(5)
C(55B)-Fe(3B)-C(51B)	40.6(3)	C(45B)-C(41B)-Fe(3B)	69.9(4)
C(42B)-Fe(3B)-C(54B)	153.4(3)	C(43B)-C(42B)-C(41B)	109.8(7)
C(53B)-Fe(3B)-C(54B)	41.3(4)	C(43B)-C(42B)-Fe(3B)	71.0(5)
C(52B)-Fe(3B)-C(54B)	68.5(3)	C(41B)-C(42B)-Fe(3B)	69.9(4)
C(41B)-Fe(3B)-C(54B)	164.9(3)	C(43B)-C(42B)-H(42B)	125.1
C(55B)-Fe(3B)-C(54B)	39.5(3)	C(41B)-C(42B)-H(42B)	125.1
C(51B)-Fe(3B)-C(54B)	67.9(3)	Fe(3B)-C(42B)-H(42B)	125.5
C(42B)-Fe(3B)-C(43B)	39.8(3)	C(42B)-C(43B)-C(44B)	107.7(6)
C(53B)-Fe(3B)-C(43B)	108.6(3)	C(42B)-C(43B)-Fe(3B)	69.2(4)
C(52B)-Fe(3B)-C(43B)	127.2(3)	C(44B)-C(43B)-Fe(3B)	70.0(4)
C(41B)-Fe(3B)-C(43B)	68.4(3)	C(42B)-C(43B)-H(43B)	126.2
C(55B)-Fe(3B)-C(43B)	153.8(3)	C(44B)-C(43B)-H(43B)	126.2
C(51B)-Fe(3B)-C(43B)	164.4(3)	Fe(3B)-C(43B)-H(43B)	126.2
C(54B)-Fe(3B)-C(43B)	120.4(3)	C(45B)-C(44B)-C(43B)	108.4(6)
C(42B)-Fe(3B)-C(45B)	68.6(3)	C(45B)-C(44B)-Fe(3B)	69.8(4)
C(53B)-Fe(3B)-C(45B)	165.7(3)	C(43B)-C(44B)-Fe(3B)	69.1(4)

C(45B)-C(44B)-H(44B)	125.8	Fe(3B)-C(52B)-H(52B)	125.9
C(43B)-C(44B)-H(44B)	125.8	C(52B)-C(53B)-C(54B)	107.6(7)
Fe(3B)-C(44B)-H(44B)	126.9	C(52B)-C(53B)-Fe(3B)	69.8(4)
C(44B)-C(45B)-C(41B)	107.7(6)	C(54B)-C(53B)-Fe(3B)	69.6(4)
C(44B)-C(45B)-Fe(3B)	70.4(4)	C(52B)-C(53B)-H(53B)	126.2
C(41B)-C(45B)-Fe(3B)	68.6(4)	C(54B)-C(53B)-H(53B)	126.2
C(44B)-C(45B)-H(45B)	126.2	Fe(3B)-C(53B)-H(53B)	125.9
C(41B)-C(45B)-H(45B)	126.2	C(55B)-C(54B)-C(53B)	107.5(7)
Fe(3B)-C(45B)-H(45B)	126.4	C(55B)-C(54B)-Fe(3B)	70.2(4)
C(52B)-C(51B)-C(55B)	107.5(7)	C(53B)-C(54B)-Fe(3B)	69.2(4)
C(52B)-C(51B)-Fe(3B)	69.7(4)	C(55B)-C(54B)-H(54B)	126.3
C(55B)-C(51B)-Fe(3B)	69.7(4)	C(53B)-C(54B)-H(54B)	126.3
C(52B)-C(51B)-H(51B)	126.2	Fe(3B)-C(54B)-H(54B)	125.9
C(55B)-C(51B)-H(51B)	126.2	C(54B)-C(55B)-C(51B)	109.2(7)
Fe(3B)-C(51B)-H(51B)	126.0	C(54B)-C(55B)-Fe(3B)	70.3(5)
C(51B)-C(52B)-C(53B)	108.1(7)	C(51B)-C(55B)-Fe(3B)	69.7(4)
C(51B)-C(52B)-Fe(3B)	70.0(4)	C(54B)-C(55B)-H(55B)	125.4
C(53B)-C(52B)-Fe(3B)	69.7(4)	C(51B)-C(55B)-H(55B)	125.4
C(51B)-C(52B)-H(52B)	125.9	Fe(3B)-C(55B)-H(55B)	126.2
C(53B)-C(52B)-H(52B)	125.9		